



## 저작자표시-비영리-변경금지 2.0 대한민국

이용자는 아래의 조건을 따르는 경우에 한하여 자유롭게

- 이 저작물을 복제, 배포, 전송, 전시, 공연 및 방송할 수 있습니다.

다음과 같은 조건을 따라야 합니다:



저작자표시. 귀하는 원저작자를 표시하여야 합니다.



비영리. 귀하는 이 저작물을 영리 목적으로 이용할 수 없습니다.



변경금지. 귀하는 이 저작물을 개작, 변형 또는 가공할 수 없습니다.

- 귀하는, 이 저작물의 재이용이나 배포의 경우, 이 저작물에 적용된 이용허락조건을 명확하게 나타내어야 합니다.
- 저작권자로부터 별도의 허가를 받으면 이러한 조건들은 적용되지 않습니다.

저작권법에 따른 이용자의 권리는 위의 내용에 의하여 영향을 받지 않습니다.

이것은 [이용허락규약\(Legal Code\)](#)을 이해하기 쉽게 요약한 것입니다.

[Disclaimer](#)

이학박사 학위논문

**Cyclopolymerization of 1,6-Heptadiyne  
Derivatives using Ru-based Grubbs Catalysts  
: Synthesis, Analysis, and Applications**

루테늄 기반의 그럽스 촉매를 이용한  
1,6-헵타다이하인 유도체의 고리화 중합

2016 년 2 월

서울대학교 대학원

화학부 유기화학 전공

강 은 혜

**Cyclopolymerization of 1,6-Heptadiyne**  
**Derivatives using Ru-based Grubbs Catalysts**  
**: Synthesis, Analysis, and Applications**

지도 교수 최 태 립

이 논문을 이학박사 학위논문으로 제출함  
2016 년 2월

서울대학교 대학원  
화학부 유기화학 전공  
강 은 혜

강은혜의 이학박사 학위논문을 인준함  
2016 년 2 월

위 원 장 \_\_\_\_\_ 이 동 환 \_\_\_\_\_ (인)

부위원장 \_\_\_\_\_ 최 태 립 \_\_\_\_\_ (인)

위 원 \_\_\_\_\_ 손 병 혁 \_\_\_\_\_ (인)

위 원 \_\_\_\_\_ 홍 순 혁 \_\_\_\_\_ (인)

위 원 \_\_\_\_\_ 김 정 곤 \_\_\_\_\_ (인)

## **Abstract**

# **Cyclopolymerization of 1,6-Heptadiyne Derivatives using Ru-based Grubbs Catalysts : Synthesis, Analysis, and Applications**

Eun-Hye Kang

Department of Chemistry

The Graduate School

Seoul National University

Cyclopolymerization of 1,6-heptadiyne based on the olefin metathesis reaction is one of the useful methods to prepare polyacetylene derivatives. The polyacetylene backbone from cyclopolymerization is stable enough under the ambient condition. The solubility of this conjugated polymer is easily regulated by the substituent manipulation. Therefore, it is expected as a versatile candidate for studies of conducting and conjugated polymers. However, the catalytic system to control the polymer structure and molecular weight was limited to air- and moisture-sensitive metal catalysts, which made a high entry barrier for applications in a wide range.

This dissertation describes the development and applications of cyclopolymerization mediated by Ru-based Grubbs catalysts. Ru-alkylidenes have been known as less reactive toward the cyclopolymerization than Mo- or W-alkylidenes. In this study, however, it was disclosed that coordinating solvents and other sufficient reaction conditions notably enhanced the efficiency of CP using Grubbs catalysts. The discovery provided an important clue to understand the low efficiency of CP catalyzed by Grubbs catalysts; furthermore, it led in-depth studies



on the ligand effect on the CP. First, weakly coordinating agents, such as THF or pyridines, showed a critical role in preventing the rapid decomposition of the propagating carbene during the reaction. Low temperature or steric effect near carbene also increased the lifetime of propagating carbene in a similar manner. Second, the ligand-free condition resulted in dimerization and trimerization of 1,6-heptadiynes, rather than CP. This side reaction was catalyzed by decomposed Ru-species due to the lack of weakly-coordinating agents, lowering the efficiency of CP. These observations supported the strategy of effective living CP, which was achieved by the fast-initiating Grubbs catalyst in the presence of weakly coordinating agents.

The living CP by Grubbs catalyst widened the area of application, such as the construction of complex macromolecules or self-assembled structures based on the block copolymer synthesis. With the aim of single molecular wires, defect-free dendronized polymers and molecular brushes were synthesized in high yield by CP. An interesting conformational transition in those giant molecules led the further investigation on the polymer structure. Poly(cyclopentenylene-vinylene) (PCPV) synthesized by CP showed a spontaneous *cis*-to-*trans* isomerization of olefin. This local change of chemical structure induced straight change in the macromolecular structure, as coil-to-rod transition. Atomic force microscopy (AFM) visualized afforded polymers in extended and rod-like shape.

Lastly, the *in situ* self-assembly of block copolymers prepared by the combination of ROMP-CP was investigated, resulting in spherical micelles. The isomerization of PCPV was readily applicable to alter the micelle structure, followed by the structural evolution into higher dimensional nanostructures.

**Keyword :** Cyclopolymerization, Living polymerization, Polyacetylene, Ru catalyst (Ru-alkylidene), Single molecular wire, Polymer structure, Self-assembly

**Student Number :** 2010-20262

# Table of Contents

<b>Abstract .....</b>	<b>i</b>
<b>Table of Contents .....</b>	<b>iii</b>
<b>List of Figures .....</b>	<b>vii</b>
<b>List of Schemes .....</b>	<b>xii</b>
<b>List of Tables .....</b>	<b>xiv</b>

## **Chapter 1. Introduction**

1.1. Research background .....	2
1.2. Thesis research .....	9
1.3. References .....	11

## **Chapter 2. Living Cyclopolymerization of 1,6-Heptadiynes by Ru-based Grubbs catalyst**

2.1. Abstract .....	15
2.2. Introduction .....	16
2.3. Results and Discussion .....	18
2.3.1. Living Cyclopolymerization using Grubb Catalyst .....	18
2.3.2. Improvement of Living Cyclopolymerization using Additives ...	25
2.4. Conclusion .....	32
2.5. Experimental Section .....	33
2.6. References and Notes .....	41

### **Chapter 3. Decomposition of Ru-alkylidene in Cyclopolymerization of 1,6-Heptadiynes**

3.1. Abstract .....	44
3.2. Introduction .....	45
3.3. Results and Discussion .....	47
3.3.1. Detection of Carbene Decomposition during CP.....	47
3.3.2. Steric Effect on Carbene Decomposition.....	53
3.4. Conclusion .....	55
3.5. Experimental Section .....	56
3.6. Supporting Information.....	58
3.7. References and Notes.....	63

### **Chapter 4. Mechanistic Investigations on Cyclopolymerization vs. [2+2+2] Cycloaddition of 1,6-Heptadiynes**

4.1. Abstract .....	65
4.2. Introduction.....	66
4.3. Results and Discussion .....	68
4.3.1. Mechanism of Dimerization and Trimerization of 1,6-Heptadiyne Derivatives during Cyclopolymerization.....	68
4.3.2. Substituent Effect on Cyclopolymerization and [2+2+2] Cycloaddition.....	79
4.4. Conclusion .....	85
4.5. Experimental Section .....	86
4.6. Supporting Information.....	93
4.7. References and Notes.....	97

## Chapter 5. Grafting-Through Synthesis of Dendronized Polymers and Brush Polymers by Cyclopolymerization of 1,6-Heptadiynes

5.1. Abstract .....	100
5.2. Introduction.....	101
5.3. Results and Discussion .....	103
5.3.1. Synthesis of Dendronized Polymers .....	103
5.3.2. Synthesis of Brush Polymers .....	107
5.4. Conclusion .....	115
5.5. Experimental Section .....	116
5.6. References and Notes.....	122

## Chapter 6. Coil-to-Rod Transition of Conjugated Polymers Prepared by Cyclopolymerization of 1,6-Heptadiynes

6.1. Abstract .....	125
6.2. Introduction.....	126
6.3. Results and Discussion .....	128
6.3.1. Coil-to-rod Conformational Transition of Brush Polymer.....	128
6.3.2. General Features on Conformational Change of PCPV .....	132
6.3.3. Cis-to-trans isomerization of PCPV and Conformational Change ..	
.....	137
6.4. Conclusion .....	142
6.5. Experimental Section .....	143
6.6. Supporting Infomation.....	146
6.7. References and Notes.....	150

## Chapter 7. Light-driven Evolution of Nanostructures Prepared from Cyclopolymerization of 1,6-Heptadiynes

7.1. Abstract .....	153
7.2. Introductions .....	154
7.3. Results and Discussion .....	156
7.3.1. Structural Evolution of Poly(NB)- <i>b</i> -poly(MA-1,6-heptadiyne)	156
7.3.2. One-shot Copolymerization of Poly(TD)- <i>g</i> -poly(MA-1,6- heptadiyne) and Structural Evolution .....	164
7.4. Conclusion .....	171
7.5. Experimental Section .....	172
7.6. Supporting Information.....	176
7.7. References and Notes.....	178
<b>Abstract (Korean).....</b>	<b>180</b>

# List of Figures

## Chapter 1.

<b>Figure 1.1.</b> Mo-based Schrock alkylidenes promoting CP. ....	4
<b>Figure 1.2.</b> Ru-based Grubbs catalysts for the olefin metathesis reaction. ....	6
<b>Figure 1.3.</b> In situ nanoparticlization of block copolymer containing PA.....	8

## Chapter 2.

<b>Figure 2.1.</b> Common NHC-containing Grubbs catalysts .....	17
<b>Figure 2.2.</b> Electron withdrawing group modified Ru-alkylidenes.....	17
<b>Figure 2.3.</b> Structures of initiator ( <b>G3-Cl</b> ) and monomers <b>1–5</b> .....	18
<b>Figure 2.4.</b> $^{13}\text{C}$ NMR spectra of poly( <b>2</b> ).....	19
<b>Figure 2.5.</b> UV–vis spectra of poly( <b>2</b> ).....	20
<b>Figure 2.6.</b> Reaction kinetics of <b>2</b> observed by in situ $^1\text{H}$ NMR spectroscopy .....	20
<b>Figure 2.7.</b> Plots of $M_n$ vs. $M/I$ and corresponding PDI values for poly( <b>2</b> ) through poly( <b>5</b> ). ....	23
<b>Figure 2.8.</b> SEC traces for poly( <b>2</b> ) <sub>25</sub> and poly( <b>2</b> ) <sub>25</sub> - <i>b</i> -poly( <b>3</b> ) <sub>50</sub> .....	24
<b>Figure 2.9.</b> Structures of monomers used for controlled polymerization in DCM .....	27
<b>Figure 2.10.</b> Plots of $M_n$ vs. $M/I$ and corresponding PDI values for poly( <b>1</b> ), poly( <b>6</b> ), poly( <b>7</b> ), and poly( <b>8</b> ).....	28
<b>Figure 2.11.</b> SEC traces of poly( <b>1</b> ), poly( <b>6</b> ), poly( <b>7</b> ), and poly( <b>8</b> ).....	30
<b>Figure 2.12.</b> SEC traces for poly( <b>7</b> ) <sub>50</sub> (black, solid; $M_n = 17.5$ k, PDI = 1.11) and poly( <b>7</b> ) <sub>50</sub> - <i>b</i> -poly( <b>7</b> ) <sub>92</sub> .....	31

## Chapter 3.

<b>Figure 3.1.</b> Structures of model compound ( <b>1</b> ) and catalyst ( <b>G3-Cl</b> ) .....	48
<b>Figure 3.2.</b> $^1\text{H}$ NMR spectra of the propagating carbene and decrease in the	

carbene signal over time during CP .....	48
<b>Figure 3.3.</b> Plots of carbene% and monomer conversion (%) vs. time for the CP of <b>1</b> .....	49
<b>Figure 3.4.</b> Plots of $-\ln[M]$ vs. time for CP of <b>1</b> .....	51
<b>Figure S3.1.</b> $^1\text{H}$ NMR spectra of initial and propagating carbenes from the polymerization of <b>1-a</b> in $\text{DCM-}d_2$ .....	59
<b>Figure S3.2.</b> Plots of monomer conversion (%) and carbene% vs. time for the CP of <b>1-a</b> .....	60
<b>Figure S3.3.</b> Linear plot of $-\ln[M]$ vs. time for the cyclopolymerization of <b>1-a</b> .....	60

## Chapter 4.

<b>Figure 4.1.</b> Structures of common Grubbs catalysts .....	67
<b>Figure 4.2.</b> Reaction of 1,7-octadiyne derivatives using <b>HG2</b> .....	76
<b>Figure 4.3.</b> Cycloaddition of <b>1a</b> using the residue of 1,6-heptadiyne and <b>HG2</b> reaction mixture .....	77
<b>Figure 4.4.</b> (a) Poorly occurred cycloaddition in the reaction of <b>G3-Cl</b> and <b>1a</b> . (b) Monitoring reaction profile change before and after the addition of pyridine in the middle of the reaction of <b>HG2</b> and <b>1a</b> . .....	78
<b>Figure 4.5.</b> Structures of 1,6-heptadiyne derivatives screened using <b>HG2</b> ..	79
<b>Figure 4.6.</b> Comparison of remaining carbene% after the CP of <b>1e–1h</b> .....	81
<b>Figure 4.7.</b> Addition of diethyl malonate to the CP of <b>1h</b> .....	83
<b>Figure S4.1.</b> $^1\text{H}$ NMR spectra of copolymer (poly( <b>1a</b> )- <i>ran</i> -poly( <b>1d</b> )), polymer (I), and polymer (II) .....	93
<b>Figure S4.2.</b> $^1\text{H}$ NMR spectra of filtrate from reaction (I), <b>3a</b> , and <b>4a</b> .....	94
<b>Figure S4.3.</b> $^1\text{H}$ NMR spectra of filtrate from reaction (II), <b>3d</b> , and <b>4d</b> .....	94
<b>Figure S4.4.</b> $^1\text{H}$ NMR spectrum of the mixture of <b>3a'-i</b> and <b>3a'-ii</b> .....	95
<b>Figure S4.5.</b> COSY of the mixture of <b>3a'-i</b> and <b>3a'-ii</b> (aromatic signals)....	95
<b>Figure S4.6.</b> NOESY of the mixture of <b>3a'-i</b> and <b>3a'-ii</b> .....	96

<b>Figure S4.7.</b> Gas chromatography of <b>3a'-i</b> and <b>3a'-ii</b> mixture.....	97
---------------------------------------------------------------------------------------	----

## Chapter 5.

<b>Figure 5.1.</b> Synthetic schemes of dendronized and brush polymers .....	102
<b>Figure 5.2.</b> Plots of $M_n$ vs. $M/I$ and corresponding PDI values for poly( <b>3</b> ) and poly( <b>4</b> ) .....	105
<b>Figure 5.3.</b> AFM image (height) of poly( <b>4</b> ) .....	106
<b>Figure 5.4.</b> $^1\text{H}$ NMR spectra of PLLA ( <b>5</b> ) and PCL ( <b>6</b> ).....	108
<b>Figure 5.5.</b> MALDI-TOF spectra of PLLA ( <b>5</b> ) and PCL ( <b>6</b> ) .....	109
<b>Figure 5.6.</b> SEC traces of the macromonomer <b>5</b> and crude sample of poly( <b>5</b> ) <sub>90</sub> .....	111
<b>Figure 5.7.</b> DSC thermograms of macromonomers ( <b>5</b> and <b>6</b> ) and brush polymers (poly( <b>5</b> ) and poly( <b>6</b> )).....	113
<b>Figure 5.8.</b> AFM image (height) of poly( <b>5</b> ) .....	114

## Chapter 6.

<b>Figure 6.1.</b> Time-dependent UV-vis spectra of poly(PLLA) <sub>190</sub> aged in THF solution and decrease of Huang-Rhys factor ( $S$ ) over time.....	129
<b>Figure 6.2.</b> Time-dependent Mark-Houwink-Sakurada plots of poly(PLLA) <sub>190</sub> in THF and correlation between Huang-Rhys factor $S$ and shape parameter $\alpha$ .....	130
<b>Figure 6.3.</b> UV-vis spectra of poly(PLLA) obtained from the polymerization with various reaction times and temperatures.....	131
<b>Figure 6.4.</b> (a) Change in the absorption spectrum of PDHDPM (b) Time-dependent change of $S$ by aging in THF (c) Linear correlation between $S$ - $\alpha$ and (d) $S$ - $R_h$ (e) SEC trace shift after aging (f) Hydrodynamic diameter change as $S$ decreased .....	133
<b>Figure 6.5.</b> Time-dependent changes of $S$ of PDHDPM in various organic solvents .....	135
<b>Figure 6.6.</b> Time-dependent changes of $S$ with different concentrations of	



PDHDPM solution in chloroform and THF .....	135
<b>Figure 6.7.</b> Changes in absorption spectra of PDHDPM under fluorescent lighting and dark at room temperature, and dark at 0 °C .....	136
<b>Figure 6.8.</b> Light source effect on the isomerization of PDHDPM.....	136
<b>Figure 6.9.</b> <sup>1</sup> H NMR spectrum of PDHDPM with the protons assigned by 2D NMR spectroscopy.....	138
<b>Figure 6.10.</b> Change in the <sup>1</sup> H NMR spectrum for a PDHDPM aged by blue LED light and a plot of <i>S</i> and the corresponding integration ratios of <sup>1</sup> H NMR spectra .....	139
<b>Figure 6.11.</b> Change in the UV–vis spectra by I <sub>2</sub> vapor, BHT and TEMPO addition in chloroform .....	140
<b>Figure S6.1.</b> Changes in absorption spectra of PCPV derivatives. ....	147
<b>Figure S6.2.</b> COSY of PDHDPM.....	148
<b>Figure S6.3.</b> NOESY of PDHDPM.....	149

## Chapter 7.

<b>Figure 7.1.</b> DLS profiles of aged nanostructures ( <b>BCP-II</b> ) and plot of size ( <i>D<sub>h</sub></i> ) vs. aging time .....	158
<b>Figure 7.2.</b> Changes in UV-vis absorption spectra of <b>BCP-II</b> by aging in chlorobenzene and chloroform.....	159
<b>Figure 7.3.</b> Changes of UV-vis absorption spectra and DLS profiles of <b>BCP-II</b> by aging under the dark condition and light in chlorobenzene .....	159
<b>Figure 7.4.</b> Growth of spherical micelles into 1D and branched structures .....	161
<b>Figure 7.5.</b> Change in UV-vis absorption spectra and increase in <i>D<sub>h</sub></i> of <b>BCP-II</b> induced by aging under a blue LED.....	163
<b>Figure 7.6.</b> AFM image of <b>BCP-II</b> after 48 h of aging in chloroform under a blue LED .....	163
<b>Figure 7.7.</b> Plots of monomer conversion vs. time and -ln([ <i>M</i> ]/[ <i>M</i> ] <sub>0</sub> ) vs. time	

for one-shot copolymerization of <b>2</b> and <b>4</b> .....	165
<b>Figure 7.8.</b> Time-dependent increase in $D_h$ by aging <b>GCP-50-30</b> under a blue LED and change in the UV–Vis spectra. ....	167
<b>Figure 7.9.</b> AFM and TEM images of <b>GCP-50-30</b> aged in chloroform.....	168
<b>Figure 7.10.</b> Schematic illustration for the spontaneous macroscopic evolution of nanostructures by aging .....	170
<b>Figure S7.1.</b> DLS profiles ( $D_h$ ) of <b>BCP-I</b> and <b>BCP-II</b> after blue LED aging in chloroform .....	176
<b>Figure S7.2.</b> Identical $^1\text{H}$ NMR spectra of poly( <b>3</b> ) and the crude of poly( <b>3</b> )- <i>b</i> -poly( <b>2</b> ) ( <b>BCP-II</b> ).....	176
<b>Figure S7.3.</b> Statistics of the length distribution of <b>BCP-II</b> aged in chlorobenzene under the fluorescent light .....	177

# List of Schemes

## Chapter 1.

<b>Scheme 1.1.</b> Olefin metathesis and chain growth metathesis polymerizations .....	3
<b>Scheme 1.2.</b> Mechanism and regioselectivity of CP of 1,6-heptadiyne .....	4
<b>Scheme 1.3.</b> Synthesis of soluble polyacetylenes.....	7

## Chapter 2.

<b>Scheme 2.1.</b> Cyclopolymerization of 1,6-heptadiyne.....	16
<b>Scheme 2.2.</b> Block copolymerization of <b>2</b> and <b>3</b> .....	24
<b>Scheme 2.3.</b> Block copolymerization of <b>7</b> and <b>6</b> in DCM.....	31

## Chapter 3.

<b>Scheme 3.1.</b> Cyclopolymerization of 1,6-heptadiyne and propagating carbene intermediate.....	46
<b>Scheme 3.2.</b> Proposed scheme for the effects of weakly coordinating ligands .....	52
<b>Scheme 3.3.</b> <sup>1</sup> H NMR spectroscopic measurement of the propagating carbene during polymerization of <b>1-a</b> .....	54
<b>Scheme 3.4.</b> Cyclopolymerization of <b>1-a</b> in DCM at room temperature.....	54

## Chapter 4.

<b>Scheme 4.1.</b> Cyclopolymerization using Ru-alkylidene and the formation of dimer and trimer.....	67
<b>Scheme 4.2.</b> Mechanism of dimerization based on the olefin metathesis reaction ( <b>Cycle I</b> ).....	70
<b>Scheme 4.3.</b> Mechanism of dimerization based on Ru-catalyzed [2+2+2] cycloaddition mechanism ( <b>Cycle II</b> ) .....	72
<b>Scheme 4.4.</b> Reaction of propagating carbene on poly( <b>1d</b> ) and <b>1a</b> .....	73

<b>Scheme 4.5.</b> Cyclopolymerization and cycloaddition of 3,3-dimethyl substituted analog of <b>1a</b> ( <b>1a'</b> ) .....	74
<b>Scheme 4.6.</b> Plausible mechanisms of dimerization of <b>1a'</b> and structures of dimers .....	75
<b>Scheme 4.7.</b> Proposed model showing how substituents effect by intramolecular coordination influenced the reactions .....	84

## Chapter 5.

<b>Scheme 5.1.</b> Synthesis of macromonomers ( <b>3</b> and <b>4</b> ) for dendronized polymerization .....	104
<b>Scheme 5.2.</b> Synthesis of polymer-substituted macromonomers ( <b>5</b> and <b>6</b> ).....	107
<b>Scheme 5.3.</b> Cyclopolymerization of macromonomers ( <b>5</b> and <b>6</b> ) using <b>HG2</b> for the synthesis of molecular brushes.....	110

## Chapter 6.

<b>Scheme 6.1.</b> Repeat unit structures produced by CP of 1,6-heptadiynes ...	127
<b>Scheme 6.2.</b> Synthesis and chemical structure of poly(PLLA) .....	129
<b>Scheme 6.3.</b> Synthesis and chemical structure of PDHDPM .....	132

## Chapter 7.

<b>Scheme 7.1.</b> Synthesis of block copolymer using living ROMP and cyclopolymerization.....	155
<b>Scheme 7.2.</b> Synthesis of block copolymer containing modified NB derivative ( <b>3</b> ) and MA-containing 1,6-heptadiyne ( <b>2</b> ) .....	157
<b>Scheme 7.3.</b> One-shot gradient copolymerization of MA-1,6-heptadiyne ( <b>2</b> ) and TD derivative ( <b>4</b> ).....	164

# List of Tables

## Chapter 2.

Table 2.1. Cyclopolymerization of 2-5 .....	21
Table 2.2. Additive screening for polymerization of 1 .....	26
Table 2.3. Cyclopolymerization of 1 and 6–10.....	29

## Chapter 3.

Table S3.1. Partial data from Table 2.2 for the comparison of additive effect .....	58
-------------------------------------------------------------------------------------	----

## Chapter 4.

Table 4.1. Cyclopolymerization of 1a and 1b varied by reaction conditions .....	69
Table 4.2. Monomer screening in CP using HG2.....	80
Table 4.3. Enhancement of CP under low temperature .....	82

## Chapter 5.

Table 5.1. CP of 3 and 4 using G3-Cl.....	105
Table 5.2. CP of 5 and 6 by HG2 at 50 °C .....	111

## Chapter 7.

Table 7.1. One-shot copolymerization of 2 and 4 .....	165
-------------------------------------------------------	-----

# **Chapter 1. Introduction**

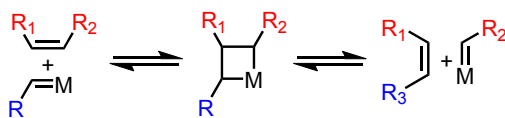
## 1.1. Research background

### Living polymerization and olefin metathesis polymerizations

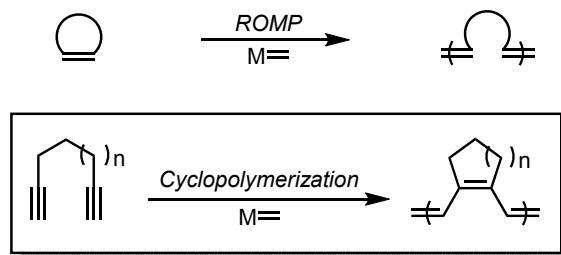
Living polymerization is one of the most important topics in chain growth polymerizations, regarding high degree of control over polymer chain architecture.<sup>1</sup> Swarc defined the living polymerization as the process “without chain transfer or termination”.<sup>2</sup> However, many cases involve side reactions disturbing an actual “living” chain end. Thus, the practical definition of living polymerization has described and ranked the polymerization system.<sup>3</sup> General requirements for living polymerization are (i) fast initiation (large  $k_i/k_p$ ), (ii) a linear relationship between the degree of polymerization and number-average molecular weight ( $M_n$ ), and (iii) narrow polydispersity index (PDI) lower than 1.5. By controlling the molecular weight and its distribution in a narrow range within those specific conditions, many living polymerizations achieved precise control of complex polymer structures, including telechelic polymers, block copolymers, graft polymers, star, ladder, and cyclic polymers.<sup>1</sup> Nowadays, the importance of those control of polymer composite has risen for complicated self-assembled morphologies of materials.<sup>4</sup>

Olefin metathesis polymerizations have revolutionized the field of synthetic polymer chemistry because of the efficient living polymerization, as well as producing various functional materials.<sup>5</sup> Ring-opening metathesis polymerization (ROMP) is a prominent representative of the chain growth metathesis polymerization (Scheme 1.1). Living ROMP enabled a variety of synthetic and applicable approaches in polymer science based on well-defined catalysts and mechanism, and excellent reactivity, lying in needs of contemporary science.<sup>6</sup> Cyclopolymerization (CP) of diyne derivatives, either based on the metathesis mechanism, is another attractive polymerization because it converts alkynes into conjugated polyenes.<sup>7</sup> However, compared to ROMP, CP is far less investigated due to the lack of catalytic systems promoting well-controlled polymerization.

### Mechanism of olefin metathesis



### Chain growth metathesis polymerizations



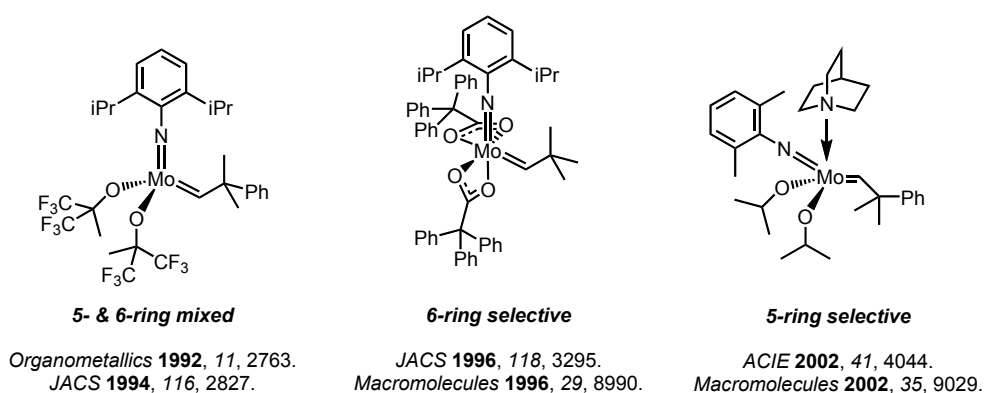
**Scheme 1.1.** Olefin metathesis and chain growth metathesis polymerizations

## Cyclopolymerization of 1,6-heptadiyne derivatives

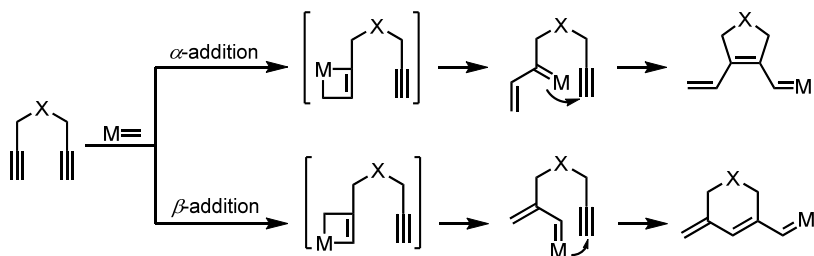
CP of 1,6-heptadiyne derivatives is one of the powerful methods for synthesizing substituted polyacetylenes (PAs). The conjugated polymers by CP are highly stable in air and soluble in common organic solvents depending on their side chains, making the polymers potential materials for use in organic electronics and optics.<sup>8-16</sup> Over the past three decades, many catalyst systems based on transition metals have been applied to the CP. Early studies of CP were carried out using ill-defined classical catalysts, including Ziegler-type,<sup>8,17-19</sup>  $\text{MoCl}_5/\text{WCl}_6$ ,<sup>12,20-26</sup> anionic polymerization,<sup>11,27</sup> and thus provided little understanding of the CP mechanism. However, recent work by Schrock and colleagues using well-defined Schrock catalysts (Figure 1.1) has provided a better understanding of the mechanism by examining the effects of catalyst regioselectivity on the structure of the polymer backbone. As shown in Scheme 1.2,  $\alpha$ - or  $\beta$ -addition occurs, depending on the orientation of the metal carbene reacting with the terminal alkyne.<sup>28</sup> This results in two different ring-closing modes that form microstructures consisting of a mixture of both five- and six-membered rings as a repeat unit (cyclopentenylene-vinylene and methyldiene-cyclohexene). Despite this nonselective addition mode, Schrock



and coworkers demonstrated the first example of the promotion of living CP of 1,6-heptadiyne derivatives.<sup>28,29</sup> Later, using a modified Schrock catalyst, they reported selective CP with  $\beta$ -addition to give conjugated polymers with six-membered rings only.<sup>30-32</sup> Subsequently, Buchmeiser and co-workers succeeded in the selective synthesis of polyenes consisting of a five-membered ring structure in a living manner, using Mo alkylidene with quinuclidine.<sup>33,34</sup> This result is more useful because the polymer with a five-membered ring unit contains a coplanar polymer backbone, resulting in a longer conjugation length.<sup>35</sup>



**Figure 1.1.** Mo-based Schrock alkylidenes promoting CP.

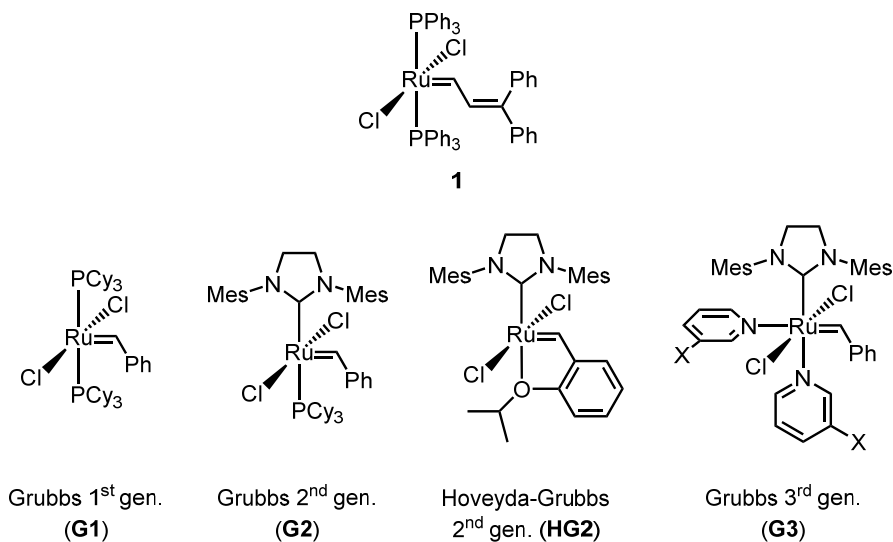


**Scheme 1.2.** Mechanism and regioselectivity of CP of 1,6-heptadiyne

## Ru-based olefin metathesis catalysts

Ru-based Grubbs catalysts are another series of olefin metathesis catalysts (Figure 1.2). From ill-defined traditional catalytic systems (e.g.  $\text{WCl}_6/\text{EtAlCl}_2$ ,  $\text{WCl}_6/\text{BuSn}_4$ ) to well-defined Ti, W, Mo-based alkylidenes, olefin metathesis

catalysts of early transition metals had been developed for higher activity and variety of utilities.<sup>36</sup> However, their sensitivity toward oxygen and moisture and low functional group tolerance provided limited use in many cases. Comparing to Mo or W catalysts, the inherent stability of Ru due to the low oxophilicity and high selectivity toward olefin brought fairly practical synthesis of complex molecules and polymers.<sup>6,37</sup> The first Ru-alkylidene was prepared from  $\text{RuCl}_2(\text{PPh}_3)_3$  and a diphenylcyclopropene (**1**) by Grubbs and his colleagues.<sup>38</sup> It was active for ROMP of norbornene and was very stable in the water and alcohols, and exchanging  $\text{PPh}_3$  to more basic  $\text{PCy}_3$  enhanced the catalytic activity of this complex.<sup>39</sup> For practical synthesis, alternative benzylidene catalyst, known as the first generation Grubbs catalyst (**G1**), was finally designed. This catalyst even showed better initiation rate than that of the diphenylvinyl derivative.<sup>40</sup> N-heterocyclic carbene (NHC) ligand provided another breakthrough, the second generation catalyst series (**G2**).<sup>41</sup> In particular, phosphine-free catalysts (**HG1** and **HG2**) developed by Hoveyda showed reusability and higher thermal stability.<sup>42</sup> Those NHC-containing catalysts greatly enhanced the catalytic activity as comparable to early transition metal catalysts, based on the stronger  $\sigma$  donor ability of NHC than that of the phosphine. Consequently, the utilization of Grubbs catalysts became much widened by achieving several challenging reactions, such as ROMP of low-strain cyclic monomers,<sup>43</sup> and cross-metathesis of trisubstituted olefins and electron-deficient olefins.<sup>40a,44</sup> One of the most useful and intriguing developments was the fast-initiating third generation Grubbs catalyst (**G3**),<sup>45</sup> which achieved living ROMP with very narrow PDI ( $< 1.10$ ).<sup>46</sup> Despite those valuable utilizations, CP had been excluded from the applications using Grubbs catalysts without a clear understanding of low efficiency.



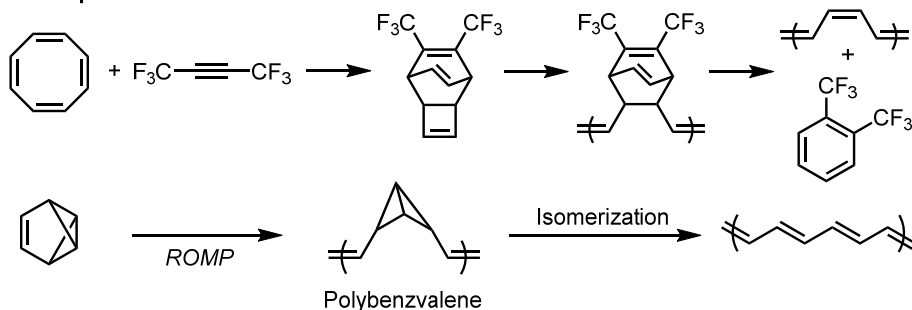
**Figure 1.2.** Ru-based Grubbs catalysts for the olefin metathesis reaction.

## Synthesis of polyacetylenes

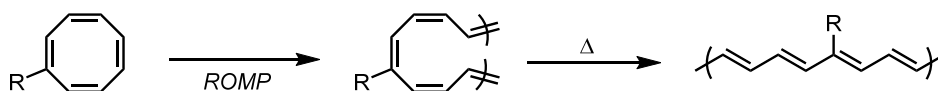
High electrical conductivity of polyacetylene (PA), close to metals, attracted researchers to develop “conductive plastic”.<sup>47</sup> PA is usually denoted by  $(\text{CH})_x$ , or  $[-(\text{CH}=\text{CH})-]$ , typically consisting of *cis* and *trans* vinylenes. The alternating chemical structure of single and double bonds usually presents the semiconducting properties; however, the doped PA by halogen or  $\text{AsF}_5$  showed a remarkable increase of conductivity up to  $10^5 \text{ S/cm}$ . Unfortunately, the original PA film synthesized from acetylene gas and Ziegler-Natta catalysts was insoluble due to strong  $\pi$ - $\pi$  interactions of backbones. Thus, the solution process based fabrication was impossible. For overcoming the limitation, there have been several attempts to prepare soluble polyacetylenes or block copolymers with desirable electrical properties (Scheme 1.3).<sup>48</sup> However, it was still challenging improve the instability of PA under ambient conditions, maintaining its useful physical properties. In addition, too much substituted PAs suffer from steric hindrance, resulting in the distorted conjugated backbone and the loss of the highly conjugated system. Poly(cyclopentenylene-vinylene) (PCPV) synthesized by CP of 1,6-heptadiyne derivatives is now expected to satisfy those requirements as a PA

derivative, providing a stable and highly conjugated backbone with excellent solubility.

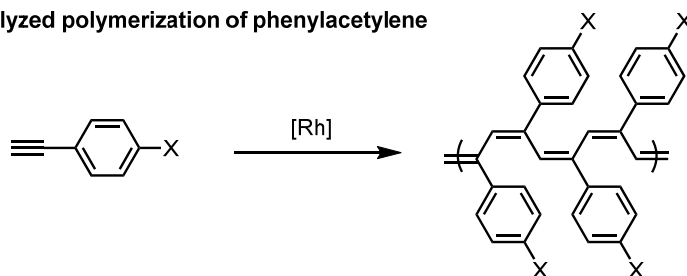
#### Soluble precursors of PA



#### ROMP - Substituted cyclooctatetraene



#### Rh-catalyzed polymerization of phenylacetylene

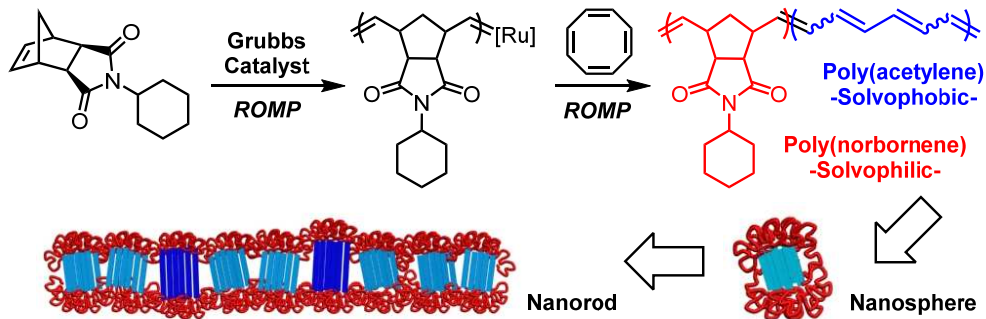


**Scheme 1.3.** Synthesis of soluble polyacetylenes

### *In situ* self-assembly of block copolymers

As one of the synthetic methods of PA derivatives, ROMP of substituted cyclooctatetraenes had been studied from the late 1980s (Scheme 1.3).<sup>48b</sup> It was originally intended to prepare substituted PA for better solubility; however, there was an interesting case that utilized 1,3,5,7-cyclooctatetraene (COT) without any substituent to prepare PA as a fragment of a block copolymer. Because of the insolubility of PA, the block copolymer of poly(norbornene) (PNB) derivative and PA synthesized by ROMP formed micelles as *in situ* during the polymerization (Figure 1.3).<sup>49</sup> In fact, efficient preparation and mass production of polymeric

nanomaterials by self-assembly have been significant challenges, because the procedures for preparing them in large quantities are very difficult. Therefore, researchers have attempted to develop more economical and convenient *in situ* self-assembly strategies for nanomaterial production by avoiding post-synthetic treatment on the purified BCP; these strategies include dialysis, use of selective solvents or additives, and change in temperature or pH. Polymerization-induced self-assembly (PISA), for example, provided a simpler route to the nanostructures by allowing the preparation of amphiphilic BCPs using selective solvents as the reaction media, thereby inducing *in situ* self-assembly.<sup>50</sup> Therefore, *in situ* self-assembly of PA-containing block copolymer became another potential strategy to achieve spontaneous formation of nanostructures during polymerization.<sup>49</sup> Similar to the conventional self-assembly process,<sup>51</sup> the composition of the solvophobic conjugated polymers and their degree of polymerization (DP) determined the type of nanostructure formed, from spherical micelles (zero-dimensional; 0D), nanocaterpillars (one-dimensional; 1D), and branched networks to three-dimensional (3D) microaggregates. Also, because of the strong  $\pi$ - $\pi$  interaction, there was no exchange or equilibrium among the unimers of the conjugated BCPs, thereby making them stable nanoadducts against heat and mechanical force.



**Figure 1.3.** In situ nanoparticlization of block copolymer containing PA.

## 1.2. Thesis Research

Although cyclopolymerization of 1,6-heptadiyne is an attractive candidate as a polyacetylene derivative, the synthetic constraint of limited catalytic system impeded its wide utilization. This research describes the development of the effective cyclopolymerization (CP) of 1,6-heptadiyne derivatives using Ru-based Grubbs catalysts and the applications.

Chapter 2 describes the living CP of 1,6-heptadiynes using Grubbs catalyst. Based on a severe solvent effect, the fast-initiating Grubbs catalyst achieved the living CP by controlling molecular weights with narrow PDIs. Further systematic development arose from the solvent effect, thereby the livingness of the CP was improved by using weakly coordinating ligands as additives.

Chapter 3 demonstrates in depth how weakly coordinating solvents or ligands enhanced the efficiency of CP of 1,6-heptadiynes. The observation of the propagating carbene proved that coordinating agents facilitated the CP using Grubbs catalysts by suppressing the decomposition of the metal carbene. This approach elucidated the influence of temperature and steric effects on CP as well.

Chapter 4 addresses a detailed investigation on the side reaction in CP by Grubbs catalysts. In a ligand-free condition, the formation of dimers and trimers of 1,6-heptadiynes was dominant instead of the polymerization. Several mechanistic studies revealed that decomposed metal carbene catalyzed this side reaction and how the substituent of 1,6-heptadiyne and reaction conditions affected it.

In Chapter 5, the preparation of single molecular wires in the formation of dendronized polymers and brush polymers is reported. The efficient CP developed in Chapter 2 easily promoted a grafting-through (macromonomer) approach to construct those graft polymers, which are potential insulating molecular wires. Additional discovery of the conformational change of large molecules provided a clue of the coil-to-rod transition.

Chapter 6 explores the origin of the conformational change found in Chapter 5. The demonstration on the composition of *cis* and *trans* vinylenes and the isomerization addressed macroscopic structural change of the conjugated polymer. Consequently, chemical and physical analyses clearly examined the general spontaneous coil-to-rod transition in the polyene prepared by CP.

Chapter 7 shows the total application of this research on CP, from *in situ* nanoparticlization of conjugated polymers (INCP) to the morphological change of self-assembled structures. The combination of living ROMP and CP provided INCP of block copolymer resulting in stable micelles. The coil-to-rod transition shown in previous chapters finally provided a new strategy to fabricate those pre-formed micelles, achieving a structural evolution to higher dimensional nanostructures through hierarchical self-assembly.

### 1.3. References

- (1) Webster, O. W. *Science* **1991**, 251, 887-893.
- (2) Szwarc, M. *Nature* **1956**, 178, 1168-1169.
- (3) Matyjaszewski, K. *Macromolecules* **1993**, 26, 1787-1788.
- (4) Hawker, C. J. *Acc. Chem. Res.* **1997**, 30, 373-382.
- (5) (a) Schrock, R. R. *Acc. Chem. Res.* **1990**, 23, 158-165. (b) Buchmeiser, M. R. *Chem. Rev.* **2000**, 100, 1565-1604. (c) Leitgeb, A.; Wappel, J.; Slugovc, C. *Polymer* **2010**, 51, 2927-2946. (d) Sutthira, S.; Shiotsuki, M.; Sanda, F. *Polym. J.* **2010**, 42, 905-915. (e) Mutlu, H.; de Espinosa, L. M.; Meier, M. A. R. *Chem. Soc. Rev.* **2011**, 40, 1404-1445. (f) Martinez, H.; Ren, N.; Matta, M. E.; Hillmyer, M. A. *Polym. Chem.* **2014**, 5, 3507-3532. (g) Sauty, N. F.; da Silva, L. C.; Schulz, M. D.; Few, C. S.; Wagener, K. B. *Appl. Petrochem. Res.* **2014**, 4, 225-233. (h) Haque, T.; Nomura, K. *Catalysis* **2015**, 5, 500-517.
- (6) Bielawski, C. W.; Grubbs, R. H. *Prog. Polym. Sci.* **2007**, 32, 1-29.
- (7) Choi, S.-K.; Gal, Y.-S.; Jin, S.-H.; Kim, H. K. *Chem. Rev.* **2000**, 100, 1645-1681.
- (8) Gibson, H. W.; Bailey, F. C.; Epstein, A. J.; Rommelmann, H.; Kaplan, S.; Harbour, J.; Yang, X.-Q.; Tanner, D. B.; Pochan, J. M. *J. Am. Chem. Soc.* **1983**, 105, 4417-4431.
- (9) Zhang, N.; Wu, R.; Li, Q.; Pakbaz, K.; Yoon, C. O.; Wudl, F. *Chem. Mater.* **1993**, 5, 1598-1599.
- (10) Samuel, I. D. W.; Ledoux, I.; Dhenaut, C.; Zyss, J.; Fox, H. H.; Schrock, R. R.; Silbey, R. J. *Science* **1994**, 265, 1070-1072.
- (11) Sivakumar, C.; Vasudevan, T.; Gopalan, A.; Wen, T.-C. *Polymer* **2002**, 43, 1781-1787.
- (12) Gal, Y. S.; Jin, S. H.; Choi, S. K. *J. Mol. Catal. A: Chem.* **2004**, 213, 115-121.
- (13) Vygodskii, Y. S.; Shaplov, A.; Lozinskaya, E. I.; Vlasov, P. S.; Malyshkina,



- I. A.; Gavrilova, N. D.; Kumar, P. S.; Buchmeiser, M. R. *Macromolecules* **2008**, *41*, 1919-1928.
- (14) Sudheendran, M.; Horecha, M.; Kiriy, A.; Gevorgyan, S. A.; Krebs, F. C.; Buchmeiser, M. R. *Polym. Chem.* **2013**, *4*, 1590-1599.
- (15) Song, W.; Han, H.; Wu, J.; Xie, M. *Chem. Commun.* **2014**, *50*, 12899-12902.
- (16) Guo, M.; Sun, R.; Han, H.; Wu, J.; Xie, M.; Liao, X. *Macromolecules* **2015**, *48*, 2378-2387.
- (17) Stille, J. K.; Frey, D. A. *J. Am. Chem. Soc.* **1961**, *83*, 1697-1701.
- (18) Gibson, H. W.; Bailey, F. C.; Epstein, A. J.; Rommelmann, H.; Pochan, J. M. *J. Chem. Soc., Chem. Commun.* **1980**, 426.
- (19) Gibson, H. W.; Epstein, A. J.; Rommelmann, H.; Tanner, D. B.; Yang, X.-Q.; Pochan, J. M. *J. Phys. (Paris) Colloq. C-3* **1983**, *44*, 651-656.
- (20) Kim, Y.-H.; Gal, Y.-S.; Kim, U.-Y.; Choi, S.-K. *Macromolecules* **1988**, *21*, 1991-1995.
- (21) Ryoo, M.-S.; Lee, W.-C.; Choi, S.-K. *Macromolecules* **1990**, *23*, 3029-3031.
- (22) Jang, M.-S.; Kwon, S.-K.; Choi, S.-K. *Macromolecules* **1990**, *23*, 4135-4140.
- (23) Koo, K.-M.; Han, S.-H.; Kang, Y.-S.; Kim, U.-Y.; Choi, S.-K. *Macromolecules* **1993**, *26*, 2485-2488.
- (24) Kang, K.-L.; Kim, S.-H.; Cho, H.-N.; Choi, K.-Y.; Choi, S.-K. *Macromolecules* **1993**, *26*, 4539-4543.
- (25) Kim, S.-H.; Kim, Y.-H.; Cho, H.-N.; Kwon, S.-K.; Kim, H.-K.; Choi, S.-K. *Macromolecules* **1996**, *29*, 5422-5426.
- (26) Anders, U.; Wagner, M.; Nuyken, O.; Buchmeiser, M. R. *Macromolecules* **2003**, *36*, 2668-2673.
- (27) Sivakumar, C.; Gopalan, A.; Vasudevan, T. *Polymer* **1999**, *40*, 7472-7431.
- (28) Fox, H. H.; Schrock, R. R. *Organometallics* **1992**, *11*, 2763-2765.

- (29) Fox, H. H.; Wolf, M. O.; O'Dell, R.; Lin, B. L.; Schrock, R. R.; Wrighton, M. S. *J. Am. Chem. Soc.* **1994**, *116*, 2827-2843.
- (30) Schattenmann, F. J.; Schrock, R. R.; Davis, W. M. *J. Am. Chem. Soc.* **1996**, *118*, 3295-3296.
- (31) Schattenmann, F. J.; Schrock, R. R. *Macromolecules* **1996**, *29*, 8990-8991.
- (32) Schrock, R. R.; Tonzetich, Z. J.; Lichtscheidl, A. G.; Muller, P. *Organometallics* **2008**, *27*, 3986.
- (33) Anders, U.; Nuyken, O.; Buchmeiser, M. R.; Wurst, K. *Angew. Chem., Int. Ed.* **2002**, *41*, 4044-4047.
- (34) Anders, U.; Nuyken, O.; Buchmeiser, M. R.; Wurst, K. *Macromolecules* **2002**, *35*, 9029-9038.
- (35) Anders, U.; Nuyken, O.; Buchmeiser, M. R. *Des. Monomers Polym.* **2003**, *6*, 135-143.
- (36) Schrock, R. R. *Chem. Rev.* **2002**, *102*, 145-179.
- (37) Trnka, T. M.; Grubbs, R. H. *Acc. Chem. Res.* **2001**, *34*, 18-29.
- (38) Nguyen, S. T.; Johnson, L. K.; Grubbs, R. H.; Ziller, J. W. *J. Am. Chem. Soc.* **1992**, *114*, 3974-3975.
- (39) Nguyen, S. T.; Grubbs, R. H. *J. Am. Chem. Soc.* **1993**, *115*, 9858-9859.
- (40) (a) Schwab, P.; France, M. B.; Ziller, J. W.; Grubbs, R. H. *Angew. Chem., Int. Ed.* **1995**, *34*, 2039-2041. (b) Schwab, P.; Grubbs, R. H.; Ziller, J. W. *J. Am. Chem. Soc.* **1996**, *118*, 100-110.
- (41) (a) Scholl, M.; Ding, S.; Lee, C. W.; Grubbs, R. H. *Org. Lett.* **1999**, *1*, 953-956. (b) Scholl, M.; Trnka, T. M.; Morgan, J. P.; Grubbs, R. H. *Tetrahedron Lett.* **1999**, *40*, 2247-2250. (c) Vougioukalakis, G. C.; Grubbs, R. H. *Chem. Rev.* **2010**, *110*, 1746-1787.
- (42) (a) Kingbury, J. S.; Harrity, J. P. A.; Bonitatebus, Jr, P. J.; Hoveyda, A. H. *J. Am. Chem. Soc.* **1999**, *121*, 791-799. (b) Garber, S. B.; Kingsbury, J. S.; Gray, B. L.; Hoveyda, A. H. *J. Am. Chem. Soc.* **2000**, *122*, 8168-8179.
- (43) Bielawski, C. W.; Grubbs, R. H. *Angew. Chem., Int. Ed.* **2000**, *39*, 2903-

2906.

- (44) Chatterjee, A. K. Choi, T.-L.; Sanders, D. P.; Grubbs, R. H. *J. Am. Chem. Soc.* **2003**, *125*, 11360-11370.
- (45) Love, J. A.; Morgan, J. P.; Trnka, T. M.; Grubbs, R. H. *Angew. Chem., Int. Ed.* **2002**, *41*, 4035-4037.
- (46) Choi, T.-L.; Grubbs, R. H. *Angew. Chem., Int. Ed.* **2003**, *42*, 1743-1746.
- (47) (a) Shirakawa, H. Synthesis of Polyacetylene. *Handbook of Conducting Polymers*. 2<sup>nd</sup> Ed.; Marcel Dekker, Inc.; New York, 1998; pp 197-208. (b) Shirakawa, H. *Angew. Chem., Int. Ed.* **2001**, *40*, 2574.
- (48) (a) Edwards, J. H.; Feast, W. J. *Polymer* **1980**, *21*, 595-596. (b) Swager, T. M.; Dougherty, D. A.; Grubbs, R. H. *J. Am. Chem. Soc.* **1988**, *110*, 2973-2974. (c) Ginsberg, E. J.; Gorman, C. B.; Marder, S. R.; Grubbs, R. H. *J. Am. Chem. Soc.* **1989**, *111*, 7621-7622. (d) Moore, J. S.; Gorman, C. B.; Grubbs, R. H. *J. Am. Chem. Soc.* **1991**, *113*, 1704-1712. (e) Kishimoto, Y.; Eckerle, P.; Miyatake, T.; Ikariya, T.; Noyori, R. *J. Am. Chem. Soc.* **1994**, *116*, 12131-12132.
- (49) Yoon, K.-Y.; Lee, I.-H.; Kim, K. O.; Jang, J.; Lee, E.; Choi, T.-L. *J. Am. Chem. Soc.* **2012**, *134*, 14291-14294.
- (50) (a) Sun, J.-T.; Hong, C.-Y.; Pan, C.-Y. *Soft Matter* **2012**, *8*, 7753-7767. (b) Sugihara, S.; Blanz, A.; Armes, S. P.; Ryan, A. J.; Lewis, A. L. *J. Am. Chem. Soc.* **2011**, *133*, 15707-15713.
- (51) Zhang, L.; Yu, K.; Eisenberg, A. *Science* **1996**, *272*, 1777-1779.

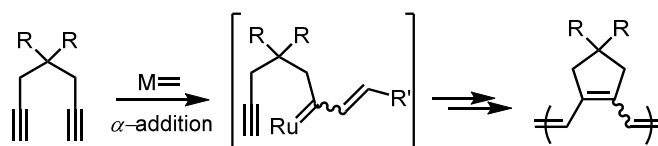
## Chapter 2. Living Cyclopolymerization of 1,6-Heptadiynes by Ru-based Grubbs Catalyst

### 2.1. Abstract

Cyclopolymerization (CP) of 1,6-heptadiyne derivatives using the Grubbs catalysts has been known to afford conjugated polyenes in low yields. Based on a discovery of a solvent effect, the ultrafast CP of 1,6-heptadiyne derivatives was achieved by a third generation Grubbs catalyst in tetrahydrofuran. After optimization, this superior catalyst selectively produced conjugated polymers having a five-membered ring structure with excellent molecular weight control and narrow polydispersity index (PDI). This living polymerization allowed us to prepare fully conjugated diblock copolymers with narrow PDIs. Further investigation from this living CP constructed a new polymerization system using weakly coordinating additives in dichloromethane. These new reaction conditions not only expand the monomer scope by resolving the solubility concerns of conjugated polymers but also more efficiently reduced the chain transfer.

## 2.2. Introduction

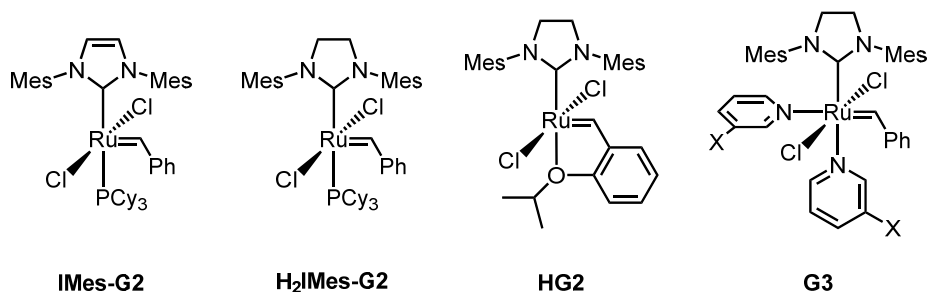
Cyclopolymerization (CP) of 1,6-heptadiyne derivatives via olefin metathesis provides a powerful and easy method for the synthesis of polyacetylene derivatives,<sup>1</sup> whose utility has increased with recent developments of living polymerization (Scheme 2.1). Although the early studies achieved mechanistic understandings and living polymerization using Mo-based Schrock alkylidenes,<sup>2</sup> a major drawback of air- and moisture-sensitive catalysts and low functional group tolerance limited the broad utilization of CP.



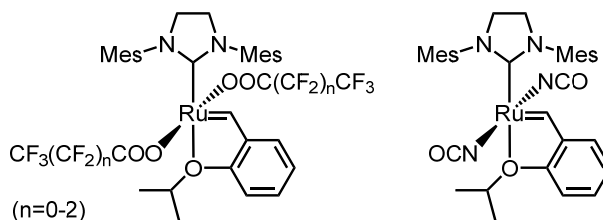
**Scheme 2.1.** Cyclopolymerization of 1,6-heptadiyne

Ru-based Grubbs catalysts, particularly N-heterocyclic carbene (NHC)-Ru complexes, are widely used in synthesis, because they are not only highly active but also highly tolerant to air, moisture, and many functional groups (Figure 2.1).<sup>3-6</sup> Despite their superior reactivity in various metathesis reactions,<sup>7</sup> initial attempts to use well-known Ru-alkylidenes, such as second generation Grubbs catalyst (**G2**) or Hoveyda-Grubbs catalyst (**HG2**), did not bring any CP. It became a well-accepted fact that the Grubbs catalysts were not active enough for CP.<sup>8</sup> In fact, it has been known that the reactivity of Grubbs catalysts for alkyne polymerization was much lower than that of Mo- or W-based catalysts,<sup>9</sup> thus people have focused on enhancing the reactivity of catalyst itself. Buchmeiser and his colleagues disclosed groundbreaking results on CP using modified Ru initiators (Figure 2.2).<sup>8,10-15</sup> They substituted a chloride ligand on the **HG2** with trifluoroacetate or isocyanate for increasing the polarizability of Ru-alkylidene, and succeeded in achieving CP with controlled molecular weights. They also found that these modified Ru catalysts underwent selective  $\alpha$ -addition to produce conjugated polymers with only five-

membered rings. However, the drawback was that the prepared polymers had broad PDIs because many of the modified catalysts had large  $k_p/k_i$  values of 1000, implying slow initiation.<sup>8</sup> Therefore, a more rapidly initiating catalyst would be desirable to achieve more precisely controlled polymerization.<sup>16</sup>



**Figure 2.1.** Common NHC-containing Grubbs catalysts.



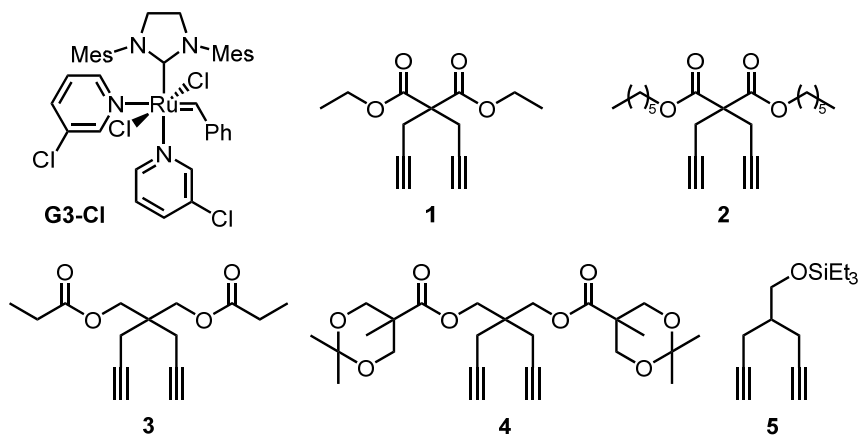
**Figure 2.2.** Electron withdrawing group modified Ru-alkylidenes.

In this chapter, we investigate living CP of 1,6-heptadiyne derivatives for the selective preparation of conjugated polymers with five-membered ring backbones and narrow PDIs using a third generation Grubbs catalyst (**G3**). First, the breakthrough of living CP using a fast-initiating **G3** was observed with dramatic coordinating solvent effect and temperature effect. Second, based on this observation, we designed improved CP in a non-coordinating solvent by introducing weakly coordinating reagents as an additive. Thereby, the CP efficiency increased for various monomers to afford polyenes with controlled molecular weights and narrow PDIs that had been insoluble in THF.

## 2.3. Results and Discussion

### 2.3.1. Living Cyclopolymerization using Grubb Catalyst

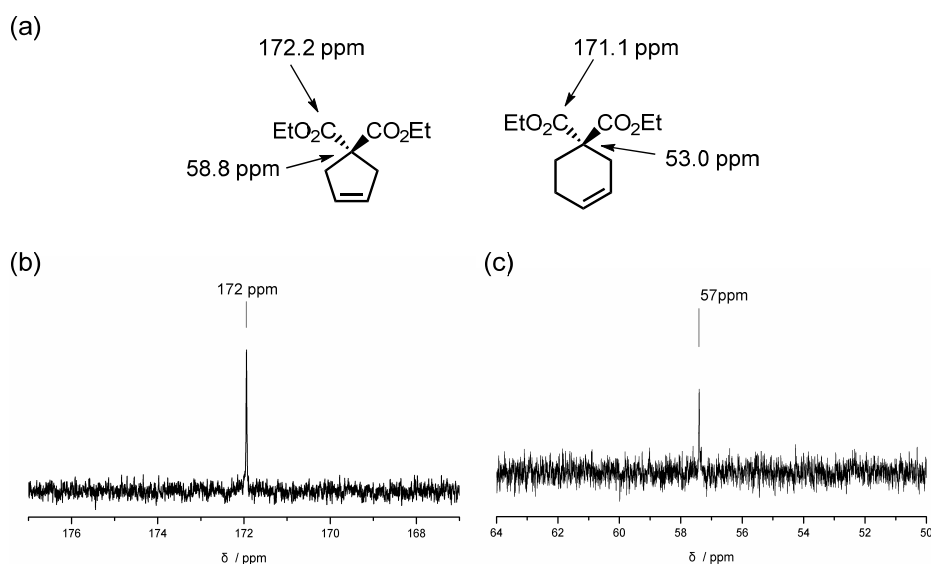
Our investigations began with tests to determine whether CP would be possible with a highly active and fast-initiating third generation Grubbs catalyst<sup>6</sup> (**G3-Cl**, Figure 2.3), which has been found to promote living ring-opening metathesis polymerization (ROMP) of norbornene derivatives with high functional group tolerance.<sup>17</sup> Initially, the most common monomer, diethyl dipropargylmalonate (**1**), was tested for CP in dichloromethane (DCM), a common solvent for this reaction. However, only low conversion of **1** was observed, similar to the previous report that used **G2** or **HG2**.<sup>8</sup> To improve the conversion, several solvents were screened, and this CP showed a remarkable solvent effect. When tetrahydrofuran (THF) was used instead of DCM, a huge enhancement of the monomer conversion up to 92% occurred in a short reaction time; however, poly(**1**) precipitated out from the solution because of its low solubility in THF.



**Figure 2.3.** Structures of initiator (**G3-Cl**) and monomers **1–5**.

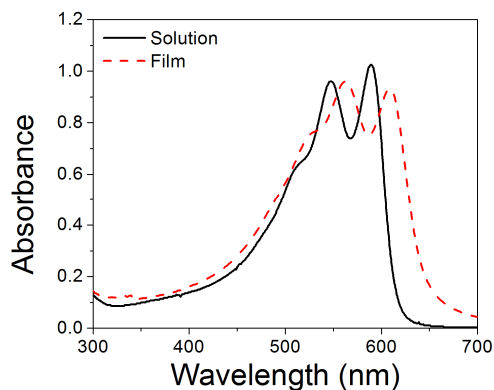
With the partial success of the CP in THF, we changed the monomer to dihexyl dipropargylmalonate (**2**, Figure 2.3) to improve the solubility. Indeed, the CP by **G3-Cl** produced readily soluble poly(**2**) with high conversion in a short reaction time. Just like the previous report, **G3-Cl** also produced highly

regioregular poly(**1**) by selective  $\alpha$ -addition. This uniform polymer microstructure having a five-membered ring as the repeat unit was confirmed by the reported  $^{13}\text{C}$  NMR spectroscopic analysis (Figure 2.4). The  $^{13}\text{C}$  NMR spectrum showed only one signal for the carbonyl carbon of malonate at 172 ppm and a signal for the quaternary C4 atom at 57 ppm.<sup>2b,18</sup> In addition, UV-vis analysis showed well-resolved absorption spectra of two peaks with  $\lambda_{\text{max}} = 548$  and 590 nm (Figure 2.5), providing another indication of a planar five-membered ring structure in the regioregular polymer.<sup>19</sup>



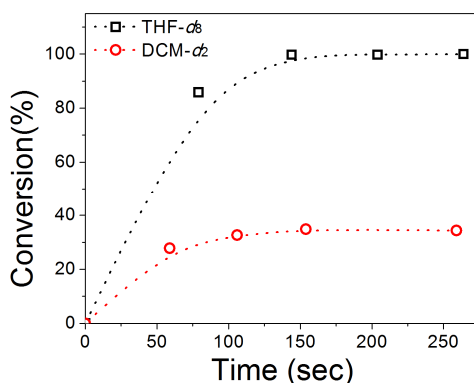
**Figure 2.4.** (a) Reference chemical shifts for  $^{13}\text{C}$  NMR spectroscopy of carbonyl carbon and quaternary carbon of five-membered ring and six-membered ring taken from the literature.<sup>18</sup> Signals of a  $^{13}\text{C}$  NMR spectrum for (b) carbonyl carbon of malonate and (c) quaternary carbon (C4 of heptadiyne) of poly(**2**).





**Figure 2.5.** UV-vis spectra of poly(**2**)<sub>50</sub> in chloroform (0.01 g/L) and film of poly(**2**)<sub>50</sub> (spin-coated on glass, 1 g/L chloroform solution, 2000 rpm, 30 s). Optical band gaps are 2.0 eV (solution) and 1.9 eV (film).

Prompted by the accelerated CP in THF, we monitored the polymerization kinetics in an NMR tube. Amazingly, <sup>1</sup>H NMR analysis in deuterated THF (THF-*d*<sub>8</sub>) revealed that greater than 95% of **2** was consumed within 2 min after the addition of 2 mol % **G3-Cl**, whereas the reaction in deuterated DCM (DCM-*d*<sub>2</sub>) showed much slower propagation (Figure 2.6). Our preliminary study suggested that using a weakly coordinating solvent (e.g., THF or diethyl ether) greatly improved the catalyst lifetime by stabilizing the propagating species through solvent coordination.<sup>20</sup>



**Figure 2.6.** Reaction kinetics of **2** observed by in situ <sup>1</sup>H NMR spectroscopy (M/I = 50).

**Table 2.1. Cyclopolymerization of 2-5**

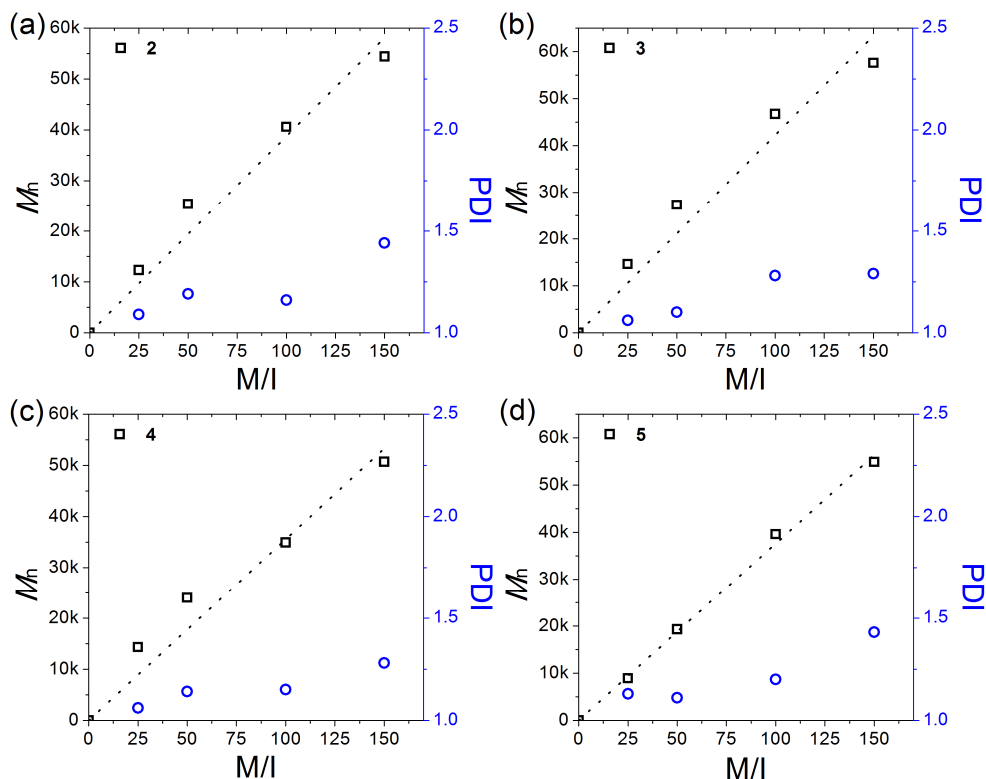
Reaction scheme: Monomer (with substituents R and R') reacts with G3-Cl in THF (0.5 M) for 20-60 min to form a cyclopolymer (with a five-membered ring and a double bond).

entry	monomer	M/I	temp (°C)	$M_n^a$ (kDa)	PDI <sup>a</sup>	yield <sup>b</sup> (%)
1	2	100	RT	41.7	1.81	87
2	2	25	0	12.3	1.09	>99
3	2	50	0	25.4	1.19	81
4	2	100	0	40.6	1.16	97
5	2	150	0	54.4	1.44	94
6	3	25	0	14.6	1.06	93
7	3	50	0	27.3	1.10	93
8	3	100	0	46.7	1.28	96
9	3	150	0	57.6	1.29	>99
10	4	25	0	14.3	1.06	85
11	4	50	0	24.0	1.14	80
12	4	100	0	34.9	1.15	>99
13	4	150	0	50.7	1.28	87
14	5	25	-10	8.9	1.13	97
15	5	50	-10	19.3	1.11	79
16	5	100	-10	39.6	1.20	89
17	5	150	-5	54.9	1.43	87

<sup>a</sup>Determined by THF SEC calibrated by PS standards. <sup>b</sup>Isolated yields after purification. Monomer conversions of all entries were above 95% except entry 1 (94%).

Even with the fast-initiating catalyst, the PDI of the polymer from **2** was still broad (Table 2.1, entry 1). With the enhanced activity of the catalyst in THF, it seemed that a chain transfer reaction caused PDI broadening. Therefore, the reaction temperature was lowered to 0 °C to suppress this reaction.<sup>17</sup> Indeed, the CP of **2** produced a polymer having a narrow PDI of 1.1 with complete consumption of the monomer. With this narrow PDI, the molecular weight of poly(**2**) was linearly controlled by changing the monomer-to-initiator (M/I) ratio from 25:1 to 150:1 (Table 2.1, entries 2–5; Figure 2.7a). The reactions reached completion within 30 min to 1 h, despite the low reaction temperature. To understand the origin of the narrow PDI, we measured the  $k_i/k_p$  value by <sup>1</sup>H NMR analysis<sup>21</sup> at 0 °C and obtained a value of 0.84. It was the highest  $k_i/k_p$  value reported to date, indicating that the initiation was fast enough to show much narrower PDIs than those in the previous reports.<sup>2e,8,12</sup>

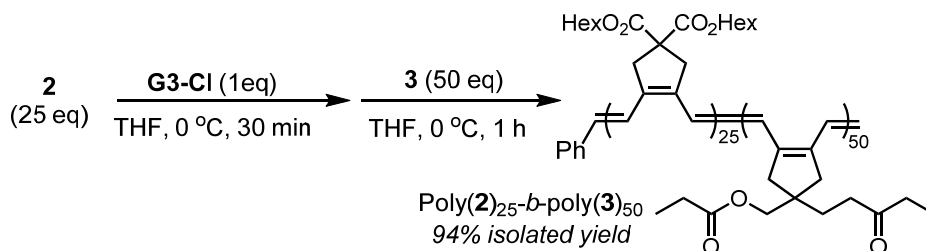
The monomer scope for CP was broadened to various mono- and bis-substituted 1,6-heptadiyne derivatives (**3–5**, Figure 2.3). Those ester- and ether-containing monomers also underwent fast and efficient cyclopolymerization to form five-membered ring structures that were confirmed by <sup>13</sup>C NMR analysis. As in the CP of **2**, the polymers obtained from monomers **3–5** also shared the characteristics of living polymerization, with narrow PDIs and controlled molecular weights (Table 2.1, entries 6–17; Figure 2.7). In particular, the mono-substituted monomer **5** underwent even faster CP than **2** with greater than 95% conversion in 1 min in an NMR tube at room temperature (M/I = 50). It was presumed that mono-substitution was more free from the steric hindrance, thereby promoting faster complexation of the catalyst and monomer. However, for the same reason, poly(**5**) was more vulnerable to the chain transfer reaction than were the bis-substituted polymers, and as a result, its PDI broadened even at 0 °C. Lowering the temperature further to –10 °C solved this problem, where polymers with narrow PDIs and controlled molecular weights were obtained (Table 2.1, entries 14–17).



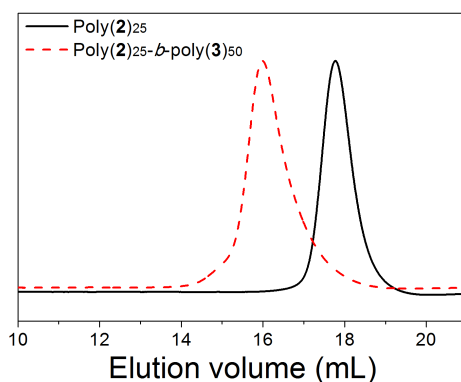
**Figure 2.7.** Plots of  $M_n$  vs.  $M/I$  and corresponding PDI values for poly(**2**) through poly(**5**) ((a) – (d)).

Previously, Schrock reported the synthesis of the diblock copolymer poly(**1**)-*b*-poly(norbornene), which contains a mixture of five- and six-membered rings, via CP followed by ROMP of norbornene derivatives.<sup>2b</sup> However, there has been no report of true block copolymers with fully conjugated backbones obtained by CP. If **G3-Cl** could promote living CP, one should be able to prepare a block copolymer having a fully conjugated backbone with a narrow PDI. Indeed, the diblock copolymer was synthesized by the addition of the first monomer **2** followed by the sequential addition of the second monomer **3** ( $[2]:[3]:[G3-Cl] = 25:50:1$ ). Size-exclusion chromatography (SEC) traces showed the complete shift from the initial block of **2** to a higher molecular weight. Thus, the validity of the block copolymerization was confirmed as well as the living character of this CP by **G3-Cl** (Scheme 2.2 and Figure 2.8,  $M_n = 33.9$  k, PDI = 1.14, yield = 94%). This is

the first example of block copolymerization between two different 1,6-heptadiyne derivatives with a narrow PDI and a regioregular microstructure. It shows the potential of using fully conjugated block copolymers having a polyene backbone for the study of controlling various nanostructure morphologies by phase separation.



**Scheme 2.2.** Block copolymerization of **2** and **3**



**Figure 2.8.** THF SEC traces for poly(**2**)<sub>25</sub> ( $M_n = 13.6$  k, PDI = 1.09) and poly(**2**)<sub>25</sub>-*b*-poly(**3**)<sub>50</sub> ( $M_n = 33.9$  k, PDI = 1.14). PS standards were used for calibration.

### 2.3.2. Improvement of Living Cyclopolymerization using Additives

Despite the advantages of using THF, DCM is still a preferred solvent for CP, because conjugated polymers are usually much more soluble in chlorinated solvents. Therefore, the utility and monomer scope of CP would be further broadened if conditions could be developed to achieve living polymerization in DCM. However, with a monomer-to-initiator ratio (M/I) of 100, conversion of **1** was only 18% in DCM, but 92% in THF. In fact, solvents with high dielectric constants ( $\epsilon$ ) are known to stabilize four-coordinate, 14 electron-metal complexes after ligand dissociation.<sup>22</sup> However, in our preliminary experiments, diethyl ether ( $\epsilon = 4.34$ ), a less polar solvent than DCM ( $\epsilon = 8.9$ ), was also an effective solvent for the polymerization of **2**. Therefore, we proposed that the major role of THF and diethyl ether in the polymerization of **2** be to act as a weakly coordinating ligand.

To investigate the coordination effect more extensively, we ran several CP experiments of **1** using **G3-Cl** and compared the CP efficiency of various external ligands in DCM while holding the M/I ratio fixed at 50. As a control experiment, **1** was polymerized without any additive, resulting in 68% conversion at room temperature (Table 2.2, entry 1). On the other hand, monomer conversion at room temperature increased to 90% by adding 40 mol % THF (Table 2.2, entry 3). Because it was difficult to handle very small amounts of liquid THF, we screened solid reagents as alternative additives. The first candidate was benzoquinone because it is known to inhibit the decomposition of Grubbs catalyst.<sup>23</sup> Adding 20 mol % of 2,6-dichlorobenzoquinone (2,6-Cl<sub>2</sub>BQ) increased the conversion to 89% (Table 2.2, entry 4). However, in all the preceding cases, the PDIs of the resulting polymers were still very broad ( $> 2$ ), leading us to speculate that the high catalyst activity resulted in an extensive chain transfer reaction. Lowering the reaction temperature to 0 °C to suppress the chain transfer reaction, was proved largely ineffective (Table 2.2, entry 5). Interestingly, we found that lowering the reaction temperature could also increase the monomer conversion (Table 2.2, entry 1 vs. 2

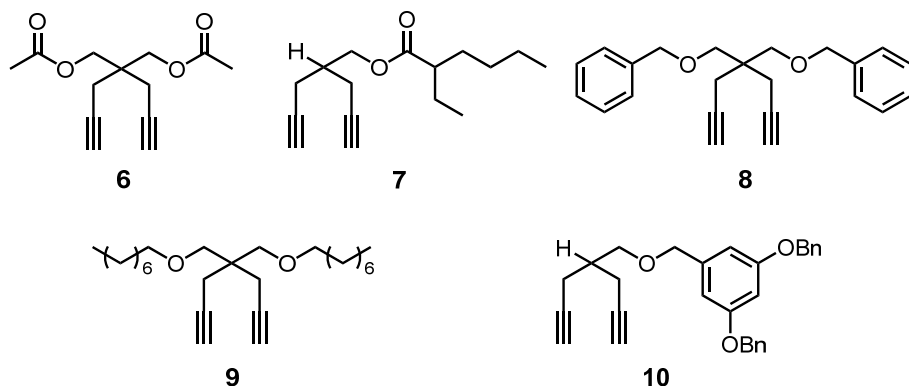
and entry 4 vs. 5), a counterintuitive finding given how temperature increase generally results in better activity for olefin metathesis. This observation will be discussed further when we review our findings from the kinetic analysis in Chapter 3.

Assuming that the weakly coordinating ketone functionality of 2,6-Cl<sub>2</sub>BQ might be responsible for the observed improvement in polymerization, we tested another solid reagent, 3,5-dichloropyridine (3,5-Cl<sub>2</sub>Py), as a substitute for liquid 3-chloropyridine, a labile ligand already bound to **G3-Cl**. Adding 20 mol % of 3,5-Cl<sub>2</sub>Py led to the full conversion of **1** to polymer in 1 h at room temperature, with a surprisingly narrow PDI of 1.13 (Table 2.2, entry 6). Increasing M/I to 100 led to the high conversion of **1** at room temperature, along with significantly broadening the PDI. Lowering the reaction temperature to 10 °C suppressed the chain transfer and successfully reduced the PDI from 1.62 to 1.16 (Table 2.2, entries 7 and 8). It demonstrated that the appropriate additive in the DCM solvent system not only improved the conversion but also achieved the controlled polymerization.

**Table 2.2. Additive screening for polymerization of 1**

entry	additive	M/I/Add	temp (°C)	time (h)	$M_n^a$ (kDa)	PDI <sup>a</sup>	conv <sup>b</sup> (%)
1	-	50/1/-	RT	1	12.6	2.56	68
2	-	50/1/-	0	1	21.5	2.38	90
3	THF	50/1/20	RT	1	10.5	2.00	91
4	2,6-Cl <sub>2</sub> BQ	50/1/10	RT	1	19.4	2.41	89
5	2,6-Cl <sub>2</sub> BQ	50/1/10	0	1	16.4	2.11	98
6	3,5-Cl <sub>2</sub> Py	50/1/10	RT	1	26.4	1.13	>99
7	3,5-Cl <sub>2</sub> Py	100/1/20	RT	1	39.7	1.62	90
8	3,5-Cl <sub>2</sub> Py	100/1/20	10	3	49.9	1.16	91

<sup>a</sup>Determined by CHCl<sub>3</sub> SEC calibrated using polystyrene (PS) standards. <sup>b</sup>Calculated from <sup>1</sup>H NMR spectra.

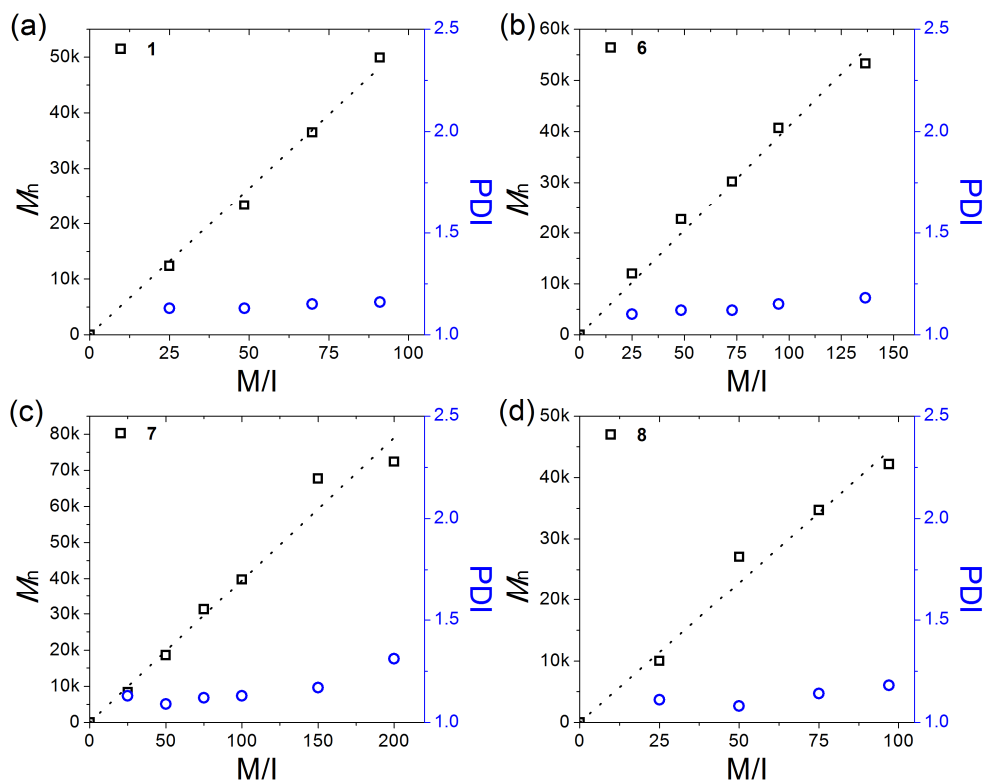


**Figure 2.9.** Structures of monomers used for controlled polymerization in DCM.

**1** and several other 1,6-heptadiyne derivatives were tested for controlled CP under the optimized reaction conditions (20 mol % of 3,5-Cl<sub>2</sub>Py) (Figure 2.9). Various monomers (**1**, **6–8**) were successfully polymerized in a controlled manner to afford polymers with molecular weights directly proportional to the M/I ratio and with narrow PDIs in the range 1.08–1.31 (Table 2.3, Figure 2.10 and Figure 2.11). In THF, we could only use monomers containing long alkyl groups or bulky moieties to overcome the solubility problems of conjugated polyenes. Now, with the improved solubility in DCM, monomers containing short side chains (**1** and **6**) could yield polymers with high  $M_n$  values (up to 50 k) and narrow PDIs (Table 2.3, entries 1–9). Polymerization of mono-substituted ester **7** in THF (M/I = 100) resulted in a broad PDI (2.23), even at –10 °C, because a relatively small side-chain could not effectively suppress the chain transfer. In contrast, with 20 mol % of the pyridine additive, CP of **7** in DCM at 0 °C produced polymers with a high degree of polymerization (DP) of 200 and narrow PDIs (Table 2.3, entries 10–15). This result demonstrated that the new DCM reaction conditions with the appropriate additive could provide better control than the THF conditions. Controlled polymerization was also possible with ether-containing **8**, demonstrating an even greater monomer scope (Table 2.3, entries 16–19). Meanwhile, **9**, which had previously been polymerized using Schrock catalysts to yield polymers with a broad PDI (2.4),<sup>15</sup> yielded polymers with a much narrower



PDI (1.26) using the new DCM system (Table 2.3, entry 20). The new conditions were even capable of polymerizing **10** to yield low-PDI polymer containing first-generation Fréchet-type dendron,<sup>24</sup> which, while soluble in DCM, exhibited low solubility in THF (Table 2.3, entry 21). In brief, the use of coordinating additives in DCM has significantly expanded the monomer scope of the controlled CP.

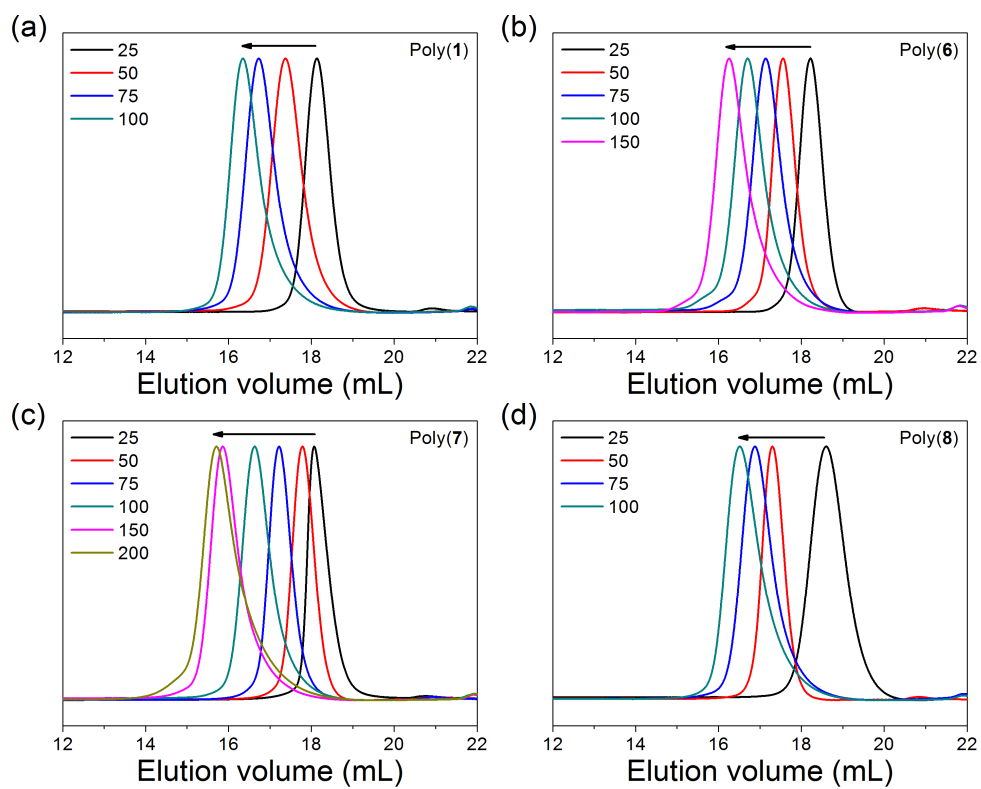


**Figure 2.10.** Plots of  $M_n$  vs.  $M/I$  and corresponding PDI values for (a) poly(**1**), (b) poly(**6**), (c) poly(**7**), and (d) poly(**8**). The actual  $M/I$  values were calculated from the initial feeding ratios and the final conversions.

**Table 2.3. Cyclopolymerization of 1 and 6–10**

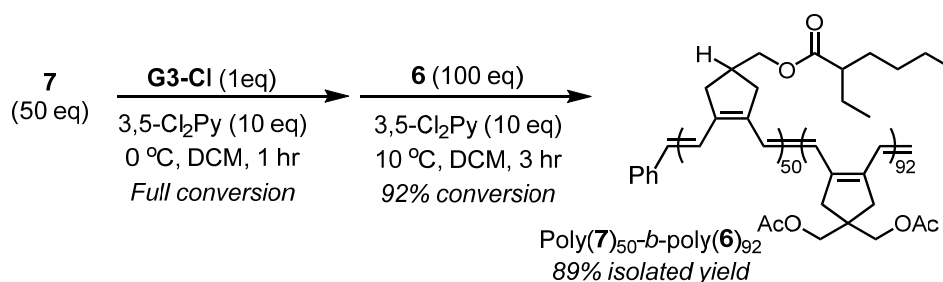
entry	monomer	M/I/Add	temp (°C)	time (h)	$M_n^a$ (kDa)	PDI <sup>a</sup>	conv <sup>b</sup> (%)
1	<b>1</b>	25/1/5	10	3	12.4	1.13	>99
2	<b>1</b>	50/1/10	10	3	23.4	1.13	97
3	<b>1</b>	75/1/15	10	3	36.5	1.15	93
4	<b>1</b>	100/1/20	10	3	49.9	1.16	91
5	<b>6</b>	25/1/5	10	3	12.0	1.10	>99
6	<b>6</b>	50/1/10	10	3	22.7	1.12	97
7	<b>6</b>	75/1/15	10	3	30.2	1.12	97
8	<b>6</b>	100/1/20	10	3	40.7	1.15	95
9	<b>6</b>	150/1/30	10	3	53.3	1.18	91
10	<b>7</b>	25/1/5	0	0.5	8.4	1.13	>99
11	<b>7</b>	50/1/10	0	1	18.6	1.09	>99
12	<b>7</b>	75/1/15	0	1.3	31.3	1.12	>99
13	<b>7</b>	100/1/20	0	3	39.8	1.13	>99
14	<b>7</b>	150/1/30	0	3	67.7	1.17	>99
15	<b>7</b>	200/1/40	0	3	72.4	1.31	>99
16	<b>8</b>	25/1/5	10	1.5	10.0	1.11	>99
17	<b>8</b>	50/1/10	10	2	27.1	1.08	>99
18	<b>8</b>	75/1/15	10	2.5	34.	1.14	>99
19	<b>8</b>	100/1/20	10	3	42.2	1.18	97
20	<b>9</b>	50/1/10	10	3	28.3	1.26	>99
21	<b>10</b>	50/1/10	10	3	28.5	1.17	99

<sup>a</sup>Determined by CHCl<sub>3</sub> SEC calibrated using polystyrene (PS) standards. <sup>b</sup>Calculated from <sup>1</sup>H NMR spectra.

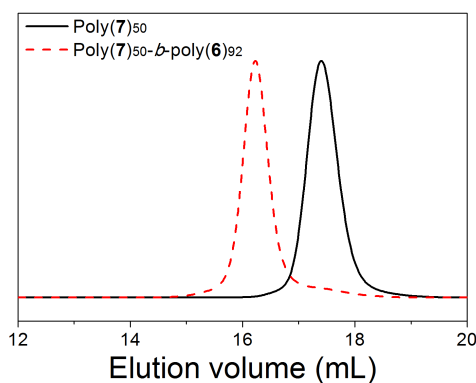


**Figure 2.11.** SEC traces of (a) poly(1), (b) poly(6), (c) poly(7), and (d) poly(8) (Table 2.3, entries 1–19).

Block copolymerization was attempted as similar in the case of THF to show that living CP is possible in DCM. Fully conjugated diblock copolymer was successfully prepared from 50 equiv of **7** (to catalyst loading) in DCM at 0 °C followed by the addition of 100 equiv of **6** at 10 °C to produce poly(**7**)-*b*-poly(**6**) in 89% isolated yield (Scheme 2.3). Block copolymerization was confirmed using SEC, which showed an increase in  $M_n$  from 17.5 k to 56.2 k upon adding a second monomer; narrow PDIs (< 1.3) were successfully retained throughout the process (Figure 2.12). These conditions were more efficient than those of in Scheme 2.2, resulting in the doubling of the DP for each block.



**Scheme 2.3.** Block copolymerization of **7** and **6** in DCM



**Figure 2.12.** SEC traces for poly(**7**)<sub>50</sub> (black, solid;  $M_n$  = 17.5 k, PDI = 1.11) and poly(**7**)<sub>50</sub>-*b*-poly(**7**)<sub>92</sub> (red, dashed;  $M_n$  = 56.2 k, PDI = 1.29).

## 2.4. Conclusion

We have used a third generation Grubbs catalyst to achieve living CP of 1,6-heptadiyne derivatives to produce semiconducting polymers with controlled molecular weights and narrow PDIs. The microstructure of resulted polymer showed sole five-membered ring structure, making planar conjugated backbone. Coordinating solvent (THF) overcame a poor reactivity of Grubbs catalysts in CP, and this solvent effect led to a new additive strategy for enhanced CP in non-coordinating solvents. This improvement greatly expanded the monomer scope and utility of the reaction. The living CP finally allowed the synthesis of diblock copolymers with narrow PDIs from several different 1,6-heptadiyne derivatives, forming fully conjugated polymer in chain growth manner.

## 2.5. Experimental Section

### Characterization

$^1\text{H}$  NMR and  $^{13}\text{C}$  NMR spectra were recorded by Varian/Oxford As-500 (500 MHz for  $^1\text{H}$  and 125 MHz for  $^{13}\text{C}$ ) spectrometer and Agilent 400-MR (400 MHz for  $^1\text{H}$  and 100 MHz for  $^{13}\text{C}$ ). THF-based size exclusion chromatography (SEC) for polymer analysis was carried out with Waters system (1515 pump, 2414 refractive index detector) and Shodex GPC LF-804 column.  $\text{CHCl}_3$ -based SEC analyses were carried out with Waters system (515 pump, 2410 refractive index detector), Viscotek 270 dual detector, and Shodex GPC LF-804 column. Samples were diluted in 0.001-0.003 wt% by THF (GPC grade, Honeywell Burdick & Jackson®) or chloroform (HPLC grade, J. T. Baker®), and passed through a 0.20- $\mu\text{m}$  PTFE filter (Whatman®). Flow rate was 1.0 mL/min and temperature of column was maintained at 35 °C. The SEC data were analyzed using Breeze (for THF SEC) and OmniSEC 4.2 (Viscotek, for  $\text{CHCl}_3$ ). High resolution mass spectroscopy (HRMS) analyses were performed by the National Center for Inter-University Research Facility.

### Materials

All reactions were carried out under dry argon atmospheres using standard Schlenk-line techniques. All reagents which are commercially available from Sigma-Aldrich®, Tokyo Chemical Industry Co. Ltd., Acros Organics, Alfa Aesar®, without additional notes, were used without further purification. **1**,<sup>25</sup> **6**,<sup>26</sup> **8**,<sup>27</sup> and **9**<sup>15</sup> were prepared by literature methods. For polymerization, THF was distilled from sodium and benzophenone, and DCM was purified by Glass Contour Organic Solvent Purification System. Both solvents were degassed further by Ar bubbling for 10 minutes before performing reactions.  $\text{CDCl}_3$  (99.50% D),  $\text{DCM-}d_2$  (99.90% D, 0.75mL) and  $\text{THF-}d_8$  (99.50% D, 0.75 mL) were purchased from Cambridge Isotope Laboratories, Inc. and used without further purification. Thin-layer

chromatography (TLC) was carried out on MERCK TLC silica gel 60 F254 and flash column chromatography was performed using MERCK silica gel 60 (0.040–0.063 mm).

## Synthesis

### Dihexyl dipropargylmalonate (**2**)

A mixture of sodium hydride (60%, dispersion in mineral oil) (359 mg, 8.98 mmol) and THF (10 mL) was prepared at 0 °C in a round bottomed flask under argon atmosphere. Dihexyl malonate (1.063 g, 3.90 mmol) was added to the mixture by dropwise then the temperature was raised to 25 °C. After 30 min, propargyl bromide (80 wt%, in toluene) (0.93 mL, 8.39 mmol) was added and stirred for 2 h. The reaction was quenched by adding NH<sub>4</sub>Cl aqueous solution and extracted with ethyl acetate (75 mL\*2). The organic layer was dried over MgSO<sub>4</sub> and concentrated to give a yellow colored liquid. It was purified by flash column chromatography on silica gel (EtOAc:hexane = 1:30) to afford compound **2** as a colorless liquid (1.169 g, 85.9%). <sup>1</sup>H NMR (500 MHz, CDCl<sub>3</sub>): δ 0.89 (t, 6 H), 1.30 (m, 12 H), 1.61 (qui, 4 H), 3.00 (d, 4 H), 4.16 (t, 4H); <sup>13</sup>C NMR (125 MHz, CDCl<sub>3</sub>): δ 14.2, 22.7, 22.8, 25.6, 28.6, 31.5, 56.6, 66.4, 71.9, 78.7, 168.9; HRMS (CI+): calcd. for C<sub>21</sub>H<sub>33</sub>O<sub>4</sub>, 349.2379, found, 349.2375.

### 4,4-Bis[(propionyloxy)methyl]-1,6-heptadiyne (**3**)

To a mixture solution of 4,4-bis(hydroxymethyl)-1,6-heptadiyne<sup>2b</sup> (191.2 mg, 1.25 mmol), triethylamine (632.4 mg, 6.25 mmol) and 4-dimethylaminopyridine (DMAP) (7.6 mg, 0.0625 mmol) in dichloromethane (3 mL) was added propionic anhydride (488.0 mg, 3.75 mmol). The reaction mixture was stirred for 3 h at room temperature. The reaction was quenched by adding saturated NaHCO<sub>3</sub> aqueous solution and stirred for a few minutes. The mixture was washed with saturated NH<sub>4</sub>Cl solution and extracted by ethyl acetate (75 mL\*2). The organic layer was

dried over  $\text{MgSO}_4$  and concentrated to give a yellow colored liquid. It was purified by flash column chromatography on silica gel ( $\text{EtOAc}:\text{hexane} = 1:10$ ) to afford compound **3** as a colorless liquid (301.1 mg, 91%).  $^1\text{H}$  NMR (500 MHz,  $\text{CDCl}_3$ ):  $\delta$  1.15 (t, 6 H), 2.04 (t, 2 H), 2.36 (q, 4 H), 2.42 (d, 4 H), 4.13 (s, 4 H);  $^{13}\text{C}$  NMR (125 MHz,  $\text{CDCl}_3$ ):  $\delta$  9.3, 22.4, 27.7, 40.3, 65.0, 71.9, 79.1, 174.2; HRMS ( $\text{CI}^+$ ): calcd. for  $\text{C}_{15}\text{H}_{21}\text{O}_4$ , 265.1440, found, 265.1439.

#### **4,4-Bis[(isopropylidene-2,2-(bis(methoxy)propionyloxy)methyl)-1,6-heptadiyne (4)**

To a mixture solution of 4,4-bis(hydroxymethyl)-1,6-heptadiyne<sup>2b</sup> (186.6 mg, 1.22 mmol) triethylamine (0.85 mL, 6.1 mmol) and 4-dimethylaminopyridine (DMAP) (7 mg, 0.061 mmol) in dichloromethane (3 mL) was added isopropylidene-2,2-bis(oxymethyl)propionic anhydride<sup>28</sup> (1.0 g, 3.05 mmol). The mixture was stirred for 3 h at room temperature. Saturated  $\text{NaHCO}_3$  aqueous solution was added to the mixture, followed by more stirring for 1 h. The mixture was washed with saturated  $\text{NH}_4\text{Cl}$  solution, then the organic layer was extracted by ethyl acetate (75 mL\*2). It was washed by  $\text{NaHCO}_3$  solution twice and extracted by ethyl acetate. The organic layer was dried over  $\text{MgSO}_4$  and concentrated. It was purified by flash column chromatography on silica gel ( $\text{EtOAc}:\text{hexane} = 1:3$ ) to afford compound **4** as a white solid (542.3 mg, 95%).  $^1\text{H}$  NMR (500 MHz,  $\text{CDCl}_3$ ):  $\delta$  1.16 (s, 6 H), 1.38, 1.43 (s, s, 12 H), 2.06 (t, 2 H), 2.47 (s, 4 H), 3.65 (d, 4 H,  $J = 11.5$  Hz), 4.18 (d, 4 H,  $J = 12$  Hz), 4.24 (s, 4 H);  $^{13}\text{C}$  NMR (125 MHz,  $\text{CDCl}_3$ ):  $\delta$  18.7, 22.4, 25.8, 41.0, 42.4, 65.2, 66.3, 72.0, 79.0, 98.4, 173.9; HRMS ( $\text{CI}^+$ ): calcd. for  $\text{C}_{25}\text{H}_{37}\text{O}_8$ , 465.2488, found, 465.2492.

#### **4-(Triethylsiloxy)-methyl-1,6-heptadiyne (5)**

Chlorotriethylsilane (388 mg, 2.57 mmol) was added to the mixture of 4-hydroxymethyl-1,6-heptadiyne<sup>29</sup> (290.5 mg, 2.24 mmol), pyridine (442.7 mg, 5.60 mmol), and DMAP (13.7 mg, 0.112 mmol) in dichloromethane (6 mL) at 0 °C. The mixture was stirred for 7 h at room temperature then saturated  $\text{NaHCO}_3$  aqueous





To a 50-mL round bottom flask was added 4-hydroxymethyl-1,6-heptadiyne (98.3 mg, 1.72 mmol). After purging the flask with argon, 4 mL of DMF was added and the mixture was cooled to 0 °C. Sodium hydride (60% dispersion in mineral oil, 94.0 mg, 2.35 mmol) was added, and the reaction mixture was stirred for 30 min at room temperature. The solution of dendritic bromide (**A**)<sup>30</sup> (600 mg, 1.57 mmol) dissolved in anhydrous THF (2 mL) was added dropwise. The mixture was stirred for 1 h at room temperature then saturated NH<sub>4</sub>Cl aqueous solution was added. The organic layer was washed with brine and extracted with diethyl ether (50 mL\*3), dried over MgSO<sub>4</sub>, and concentrated. Product was purified by column chromatography on silica gel (EtOAc:hexane = 1:10) to afford compound **10** as a colorless and viscous liquid (527.3 mg, 79.1%). <sup>1</sup>H NMR (500 MHz, CDCl<sub>3</sub>): δ 1.97 (t, *J* = 2.7 Hz, 2 H), 2.08 (hept, *J* = 2.7 Hz, 1 H), 2.38 (m, 4 H), 3.51 (d, *J* = 6.1 Hz, 2 H), 4.46 (s, 2 H), 5.04 (s, 4 H), 6.54 (t, *J* = 2.3 Hz, 1 H), 6.58 (d, *J* = 2.3 Hz, 2 H), 7.31-7.43 (m, 10 H); <sup>13</sup>C NMR (125MHz, CDCl<sub>3</sub>): δ 20.2, 37.7, 70.2, 70.4, 71.5, 73.4, 82.2, 101.6, 106.7, 127.8, 128.3, 128.9, 137.3, 141.2, 160.4; HRMS (EI<sup>+</sup>): calcd. for C<sub>29</sub>H<sub>28</sub>O<sub>3</sub>, 424.2038, found, 424.2038.

### Preparation of G3-Cl

**G2** (51.8 mg, 0.0610 mmol) and 3-chloropyridine (0.5 mL) were mixed in 4-mL sized vial for 2 minutes. It was precipitated in n-pentane with vigorous stirring, and the precipitate was filtered and washed with pentane. The green solid (39.1 mg, 0.0491 mmol, 80.5%) was vacuum dried for 10 min and stored in a desiccator.

### General procedure for CP

To a flamed-dried 5-mL vial with a septum containing PTFE-silicon were added the monomer and a magnetic bar. The vial was purged with Ar four times, and dry solvent was added. The initiator (and additive in the case of DCM reaction) was dissolved in the given reaction solvent under the inert atmosphere, and then this solution was rapidly injected into the monomer solution using a microsyringe at an

experimental temperature ( $-10\text{ }^{\circ}\text{C}$  –  $10\text{ }^{\circ}\text{C}$ ) under vigorous stirring. The low reaction temperature was regulated by the fuzzy control system with refrigerated bath circulators (Wisecircu<sup>®</sup>). Excess ethyl vinyl ether quenched the reaction after desired reaction time and the mixture was partially precipitated in methanol, except 5 – 10% of the aliquot. Obtained solid was filtered and dried *in vacuo*. Monomer conversion was calculated from the  $^1\text{H}$  NMR spectrum of the aliquot.

### **Preparation of diblock copolymer poly(2)-*b*-poly(3)**

To a flamed-dried 5-mL vial with a septum containing PTFE-silicon were added **2** (25 eq) and a magnetic bar. The vial was purged with argon four times, and dry THF was added. After purging with Ar, **G3-Cl** (1 eq) in another flame dried 5-mL vial was dissolved in THF, then rapidly injected into the solution of **2** at  $0\text{ }^{\circ}\text{C}$  under vigorous stirring. After 30 min, **3** in THF (50 eq) was injected. Excess ethyl vinyl ether quenched the reaction after 1 h, and the mixture was partially precipitated in methanol, except 5% of the aliquot. Obtained solid was filtered and dried *in vacuo*. Monomer conversion was calculated from the  $^1\text{H}$  NMR spectrum of the aliquot.

### **Preparation of diblock copolymer poly(7)-*b*-poly(6)**

To a flamed-dried 5-mL vial with a septum containing PTFE-silicon were added **7** (50 eq) and a magnetic bar. The vial was purged with Ar four times and degassed anhydrous DCM was added. After purging the air with Ar, the mixture of **G3-Cl** (1 eq) and 3,5-dichloropyridine (10 eq) in another flame dried 5-mL vial was dissolved in DCM, then the solution was rapidly injected to the solution of **7** at  $0\text{ }^{\circ}\text{C}$  under vigorous stirring. After 1 h, the reaction temperature was elevated to  $10\text{ }^{\circ}\text{C}$ , and then the mixed solution of **6** (100 eq) and 3,5-dichloropyridine (20 eq), prepared similarly to the solution of **7**, was injected. Excess ethyl vinyl ether quenched the reaction after 3 h, and the mixture was precipitated in methanol

except 5% of the aliquot. Obtained solid was filtered and dried *in vacuo*. Monomer conversion was calculated from the  $^1\text{H}$  NMR spectrum of the aliquot.

### Reaction kinetics monitored by $^1\text{H}$ NMR

To a screw-cap NMR tube (Wilmad-Labglass, screw-cap tube, 500 MHz, 5 mm) with a septum containing PTFE-silicon was added the monomer, purged with Ar, and a deuterated solvent (ampoule) (500  $\mu\text{L}$ ) was added. Concentrations were set to 0.30 M. After obtaining the NMR spectrum of the monomer, 100  $\mu\text{L}$  of initiator solution was added to monomer solution and  $^1\text{H}$  NMR measurement was recorded over time. The conversion was calculated by integration value of the distinguished signal of the monomer versus that of the monomer-polymer sharing signal as an internal standard.

### $^1\text{H}$ and $^{13}\text{C}$ NMR characterization of polymers

The  $^1\text{H}$  NMR and  $^{13}\text{C}$  NMR spectrum of poly(**1**) is described in the literature.<sup>31</sup>

**Poly(2)**  $^1\text{H}$  NMR (500 MHz,  $\text{CDCl}_3$ )  $\delta$  0.88 (br m, 6 H), 1.30 (br m, 12 H), 1.60-1.75 (br m, 4 H), 3.17-3.42 (br m, 4H), 4.05-4.23 (br m, 4 H), 6.30-6.67 (br m, 2 H);  $^{13}\text{C}$  NMR (75 MHz,  $\text{CD}_2\text{Cl}_2$ ):  $\delta$  13.8, 22.5, 25.4, 28.4, 31.4, 41.4, 57.3, 65.9, 123.1, 137.1, 171.6

**Poly(3)**  $^1\text{H}$  NMR (500 MHz,  $\text{CDCl}_3$ ):  $\delta$  1.15 (br m, 6 H), 2.37-2.39 (br m, 4 H), 2.57-2.71 (br m, 4 H), 4.06-4.29 (br m, 4 H), 6.64-6.29 (br m, 2 H);  $^{13}\text{C}$  NMR (125 MHz,  $\text{CD}_2\text{Cl}_2$ ):  $\delta$  9.1, 27.6, 39.8, 43.3, 67.2, 123.5, 138.1, 174.3

**Poly(4)**  $^1\text{H}$  NMR (500 MHz,  $\text{CDCl}_3$ ):  $\delta$  1.15 (br s, 6 H), 1.33-1.42 (br m, 12 H), 2.71 (br s, 4 H), 3.65-3.67 (br d, 4 H), 4.17-4.20 (br m, 8 H), 6.60 (br s, 2 H);  $^{13}\text{C}$  NMR (125 MHz,  $\text{CDCl}_3$ ):  $\delta$  18.9, 22.0, 26.2, 40.0, 42.6, 44.2, 66.6, 67.9, 98.4, 123.9, 138.4, 174.5

**Poly(5)**  $^1\text{H}$  NMR (500 MHz,  $\text{CDCl}_3$ ):  $\delta$  0.61-0.66 (br m, 6 H), 0.98-1.01 (br m, 9 H), 2.45-2.60 (br m, 3 H), 2.74-2.92 (br m, 2 H), 3.57 (br s, 2 H), 6.50-6.85 (br s, 2 H);  $^{13}\text{C}$  NMR (75 MHz,  $\text{CD}_2\text{Cl}_2$ ):  $\delta$  4.4, 6.6, 36.5, 38.0, 66.8, 123.2, 139.1

**Poly(6)**  $^1\text{H}$  NMR (400 MHz,  $\text{CDCl}_3$ ):  $\delta$  1.94-2.16 (br m, 6 H), 2.33-2.84 (br m, 4 H), 3.83-4.24 (br m, 4 H), 6.10-6.80 (br m, 2 H);  $^{13}\text{C}$  NMR (100 MHz,  $\text{CDCl}_3$ ):  $\delta$  21.3, 40.0, 43.4, 67.6, 123.7, 138.0, 171.3

**Poly(7)**  $^1\text{H}$  NMR (500 MHz,  $\text{CDCl}_3$ ):  $\delta$  0.74-1.00 (br m, 6 H), 1.09-1.39 (br m, 4 H), 1.39-1.74 (br m, 4 H), 2.10-3.09 (br m, 6 H), 3.82-4.30 (br m, 2 H), 6.10-6.90 (br m, 2 H);  $^{13}\text{C}$  NMR (125 MHz,  $\text{CDCl}_3$ ):  $\delta$  12.3, 14.4, 23.0, 25.9, 30.0, 32.2, 35.0, 37.2, 47.7, 67.8, 123.5, 139.0, 176.8

**Poly(8)**  $^1\text{H}$  NMR (500 MHz,  $\text{CDCl}_3$ ):  $\delta$  2.25-2.90 (br m, 4 H), 3.19-3.70 (br m, 4 H), 4.26-4.74 (br m, 4 H), 6.12-6.83 (br m, 2 H), 7.09-7.44 (m, 10 H);  $^{13}\text{C}$  NMR (125 MHz,  $\text{CDCl}_3$ ):  $\delta$  40.6, 45.2, 73.7, 74.4, 123.6, 127.7, 128.0, 128.6, 138.6, 139.0

**Poly(9)**  $^1\text{H}$  NMR (400 MHz,  $\text{CDCl}_3$ ):  $\delta$  0.83-0.91 (br m, 6 H), 1.18-1.40 (br m, 20 H), 1.47-1.67 (br m, 4 H), 2.19-2.80 (br m, 4 H), 3.07-3.60 (br m, 8 H), 5.92-6.90 (br m, 2 H);  $^{13}\text{C}$  NMR (100 MHz,  $\text{CDCl}_3$ ):  $\delta$  14.5, 23.0, 26.5, 29.7, 29.86, 29.89, 32.3, 40.6, 45.1, 71.9, 74.7, 123.7, 138.8

**Poly(10)**  $^1\text{H}$  NMR (500 MHz,  $\text{CDCl}_3$ ):  $\delta$  2.21-3.08 (br m, 5 H), 3.16-3.55 (br m, 2 H), 4.26-4.65 (br m, 2 H), 4.80-5.09 (br m, 4 H), 6.38-6.83 (br m, 5 H), 7.11-7.55 (br m, 10 H);  $^{13}\text{C}$  NMR (125 MHz,  $\text{CDCl}_3$ ):  $\delta$  35.6, 37.5, 70.4, 73.4, 74.8, 101.7, 106.8, 123.6, 127.8, 128.2, 128.8, 137.2, 139.3, 141.4, 160.4

**Poly(M3)<sub>50</sub>-b-poly(M2)<sub>92</sub>**  $^1\text{H}$  NMR (400 MHz,  $\text{CDCl}_3$ ):  $\delta$  0.74-0.96 (br m, 6 H), 1.09-1.38 (br m, 4 H), 1.38-1.69 (br m, 4 H), 1.83-2.18 (br m, 11 H), 2.18-3.09 (br m, 13 H), 3.80-4.31 (br m, 9 H), 6.00-6.90 (br m, 6 H);  $^{13}\text{C}$  NMR (100 MHz,  $\text{CDCl}_3$ ):  $\delta$  12.3, 14.4, 21.3, 23.0, 25.8, 30.0, 32.2, 34.9, 37.1, 40.0, 43.4, 47.7, 67.6, 67.8, 123.5, 123.7, 138.0, 139.0, 171.3, 176.7

## 2.6. References and Notes

- <sup>†</sup> Portions of this chapter have been previously reported, see: (a) Kang, E.-H.; Lee, I. S.; Choi, T.-L. *J. Am. Chem. Soc.* **2011**, *133*, 11904-11907. (b) Kang, E.-H.; Yu, S. Y.; Lee, I. S.; Park, S. E.; Choi, T.-L. *J. Am. Chem. Soc.* **2014**, *136*, 10508-10514.
- (1) Choi, S.-K.; Gal, Y.-S.; Jin, S.-H.; Kim, H.-K. *Chem. Rev.* **2000**, *100*, 1645-1681.
- (2) (a) Fox, H. H.; Schrock, R. R. *Organometallics* **1992**, *11*, 2763-2765. (b) Fox, H. H.; Wolf, M. O.; O'Dell, R.; Lin, B. L.; Schrock, R. R.; Wrighton, M. S. *J. Am. Chem. Soc.* **1994**, *116*, 2827-2843. (c) Schattenmann, F. J.; Schrock, R. R.; Davis, W. M. *J. Am. Chem. Soc.* **1996**, *118*, 3295-3296. (d) Schattenmann, F. J.; Schrock, R. R. *Macromolecules* **1996**, *29*, 8990-8991. (e) Anders, U.; Nuyken, O.; Buchmeiser, M. R.; Wurst, K. *Angew. Chem., Int. Ed.* **2002**, *41*, 4044-4047.
- (3) Huang, J.; Stevens, E. D.; Nolan, S. P.; Petersen, J. L. *J. Am. Chem. Soc.* **1999**, *121*, 2674-2678.
- (4) Scholl, M.; Ding, S.; Lee, C. W.; Grubbs, R. H. *Org. Lett.* **1999**, *1*, 953-956.
- (5) Kingbury, J. S.; Harrity, J. P. A.; Bonitatebus, Jr, P. J.; Hoveyda, A. H. *J. Am. Chem. Soc.* **1999**, *121*, 791-799.
- (6) Love, J. A.; Morgan, J. P.; Trnka, T. M.; Grubbs, R. H. *Angew. Chem., Int. Ed.* **2002**, *41*, 4035-4037.
- (7) (a) Vougioukalakis, G. C.; Grubbs, R. H. *Chem. Rev.* **2010**, *110*, 1746-1787. (b) Diver, S. T. *J. Mol. Catal. A: Chem.* **2006**, *254*, 29-42.
- (8) Krause, J. O.; Zarka, M. T.; Anders, U.; Weberskirch, R.; Nuyken, O.; Buchmeiser, M. R. *Angew. Chem., Int. Ed.* **2003**, *42*, 5965-5969.
- (9) Koltzenburg, S.; Eder, E.; Stelzer, F.; Nuyken, O. *Macromolecules*, **1999**, *32*, 21-26.
- (10) Krauze, J. O.; Nuyken, O.; Buchmeiser, M. R. *Chem. Eur. J.* **2004**, *10*,

2029-2035.

- (11) Halbach, T. S.; Krause, J. O.; Nuyken, O.; Buchmeiser, M. R. *Macromol. Rapid. Commun.* **2005**, *26*, 784-790.
- (12) Mayershofer, M. G.; Nuyken, O.; Buchmeiser, M. R. *Macromolecules* **2006**, *39*, 3484-3493.
- (13) Vygodskii, Y. S.; Shaplov, A. S.; Lozinskaya, E. I.; Vlasov, P. S.; Malyshkina, I. A.; Gavrilova, N. D.; Kumar, P. S.; Buchmeiser, M. R. *Macromolecules* **2008**, *41*, 1919-1928.
- (14) Kumar, P. S.; Wurst, K.; Buchmeiser, M. R. *J. Am. Chem. Soc.* **2009**, *131*, 387-395.
- (15) Sudheendran, M.; Horecha, M.; Kiriy, A.; Gevorgyan, S. A.; Krebs, F. C.; Buchmeiser, M. R. *Polym. Chem.* **2013**, *4*, 1590-1599.
- (16) Matyjaszewski, K. *Macromolecules* **1993**, *26*, 1787-1788.
- (17) Choi, T.-L.; Grubbs, R. H. *Angew. Chem., Int. Ed.* **2003**, *42*, 1743-1746.
- (18) Anders, U.; Nuyken, O.; Buchmeiser, M. R.; Wurst, K. *Macromolecules* **2002**, *35*, 9029-9038.
- (19) Anders, U.; Nuyken, O.; Buchmeiser, M. R. *Des. Monomers Polym.* **2003**, *6*, 135-143.
- (20) Fox, H. H.; Lee, J.-K.; Park, L. Y.; Schrock, R. R. *Organometallics* **1993**, *12*, 759-758.
- (21) Bazan, G. C.; Khosravi, E.; Schrock, R. R.; Feast, W. J.; Gibson, V. C.; O'Regan, M. B.; Thomas, J. K.; Davis, W. M. *J. Am. Chem. Soc.* **1990**, *112*, 8378-8387.
- (22) Sanford, M. S.; Love, J. A.; Grubbs, R. H. *J. Am. Chem. Soc.* **2001**, *123*, 6543-6554.
- (23) Hong, S. H.; Day, M. W.; Grubbs, R. H. *J. Am. Chem. Soc.* **2004**, *126*, 7414-7415.
- (24) Fréchet, J. M. *Proc. Natl. Acad. Sci. U. S. A.* **2002**, *99*, 4782-4787.
- (25) Eglinton, G.; Galbraith, A. R. *J. Chem. Soc.* **1959**, 889-896.

- (26) Kim, S.-H.; Kim, Y.-H.; Cho, H.-N.; Kwon, S.-K.; Kim, H.-K.; Choi, S.-K. *Macromolecules* **1996**, *29*, 5422-5426.
- (27) Madine, J. W.; Wang, X.; Widenhoefer, R. A. *Org. Lett.* **2001**, *3*, 385-388.
- (28) Gillies, E. T.; Fréchet, J. M. J. *J. Am. Chem. Soc.* **2002**, *124*, 14137-14146.
- (29) Carney, J. M.; Donoghue, P. J.; Wuest, W. M.; Wiest, O.; Helquist, P. *Org. Lett.* **2008**, *10*, 3903-3906.
- (30) Freeman, A. W.; Chrisstoffels, L. A. J.; Fréchet, J. M. J. *J. Org. Chem.* **2000**, *65*, 7612-7617.
- (31) Anders, U.; Wagner, M.; Nuyken, O.; Buchmeiser, M. R. *Macromolecules* **2003**, *36*, 2668-2673.



## **Chapter 3. Decomposition of Ru-alkylidene in Cyclopolymerization of 1,6-Heptadiynes**

### **3.1. Abstract**

Kinetic analysis has revealed that low efficiency of cyclopolymerization (CP) in dichloromethane (DCM) resulted from the rapid decomposition of the propagating carbene. This decomposition was effectively suppressed by both pyridine additives and tetrahydrofuran (THF), suggesting that weakly coordinating additives stabilize the living chain end. Furthermore, the turnover number of CP was higher at lower temperatures than at ambient temperatures, consistent with the understanding that the lifetime of a propagating carbene is greater at lower temperatures. Steric protection was also shown to increase the stability of the propagating carbene, as demonstrated by a higher turnover number for the 3,3-dimethylsubstituted 1,6-heptadiyne compared to the non-functionalized monomer.

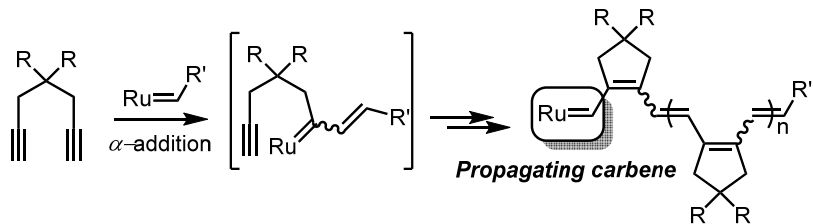
### 3.2. Introduction

In Chapter 2, it was reported that reactivity in the cyclopolymerization (CP) of 1,6-heptadiyne derivatives using the third generation Grubbs catalyst was greatly enhanced by simply using coordinating solvents (THF). This solvent effect was ironic because dichloromethane (DCM) was the most conventional solvents in olefin metathesis reactions using Ru-complexes, particularly in ROMP. Furthermore, huge solvent effect on the metathesis polymerization was less common with exceptions of a few reports on ROMP, demonstrating that solvents affected the control of tacticities,<sup>1</sup> propagation rate,<sup>2</sup> inhibition of secondary metathesis reaction,<sup>3</sup> and even some cases showed reverse solvent effect (DCM  $\gg$  THF).<sup>4</sup>

In our preliminary experiments, the low efficiency of CP in DCM seemed that the conversion stopped in the early stage of the reaction, and further conversion was impossible. It is indicative of the propagating carbene may be altered in any other form, and the catalytic activity decreased. Sanford and Grubbs reported that solvents with high dielectric constant, especially dichloromethane (DCM), stabilized the active 14-electron species.<sup>5</sup> Another suggestion was that the stabilization of 14-electron species also may involve the coordination of solvents (THF or diethyl ether); however, the detection of solvent-adduct was impossible by NMR spectroscopy. Even though previous studies cannot explain this solvent effect in CP, it is still valuable to focus on the behavior of the propagating carbene during CP. Since there has been no attempt to observe and analyze the carbene species in CP, this is an interesting examination to show the relation between reaction efficiency and chain end stability.

In this chapter, we demonstrate how the additive, reaction temperature, and substituents on the monomer affect the lifetime of the active propagating carbene on the growing polymer chain end by kinetic analysis of CP. The propagating carbene was monitored by NMR spectroscopy during the

polymerization, and the lifetime of it in several reaction conditions was compared (Scheme 3.1). Furthermore, a new strategy to suppress the carbene decomposition was suggested to improve the CP efficiency.

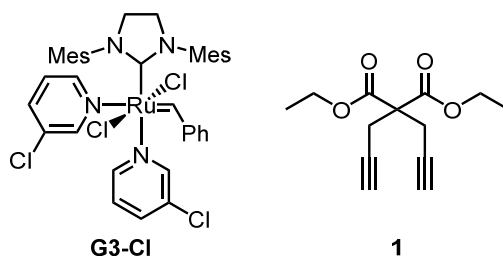


**Scheme 3.1.** Cyclopolymerization of 1,6-heptadiyne and propagating carbene intermediate

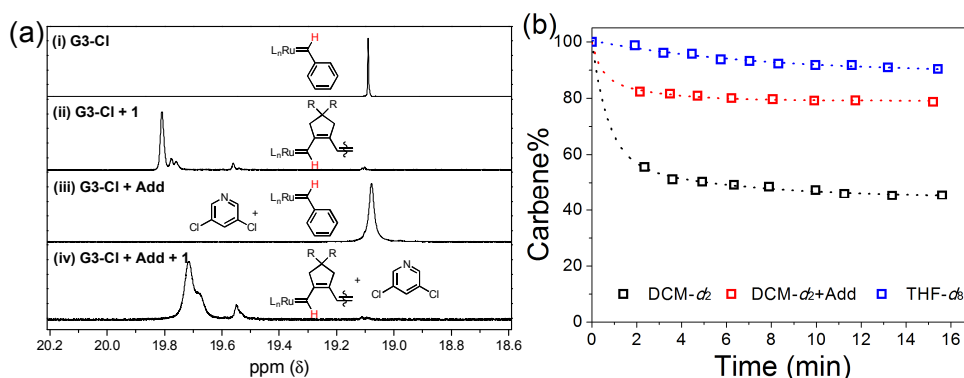
### 3.3. Results and Discussion

#### 3.3.1. Detection of Carbene Decomposition during CP

To understand the coordination effect of THF or additives revealed in Chapter 2 (Table S3.1), we designed  $^1\text{H}$  NMR experiments to observe how additives affect the propagating carbene and overall conversion. Diethyl dipropargylmalonate (**1**) and the third generation Grubbs catalyst (**G3-Cl**) was chosen as model compounds for the kinetic studies (Figure 3.1). We began by determining the chemical shift of the propagating carbene, mixing a 10:1 ratio of **1** and **G3-Cl** in deuterated DCM ( $\text{DCM-}d_2$ ) and obtaining the  $^1\text{H}$  NMR spectra after full conversion (Figure 3.2a, (i) and (ii)). The initial benzyldiene moiety in **G3-Cl** appeared at 19.1 ppm; upon adding **1**, new propagating carbenes began to appear at 19.8 ppm. Similarly, with the pyridine additive, the chemical shift for the carbene changed from 19.1 to 19.7 ppm upon the addition of **1** (Figure 3.2a, (iii) and (iv)). Based on these assignments, it becomes possible to monitor changes in the total propagating carbene signals over time by plotting time vs. percentage of the remaining propagating carbene (carbene%). Initially, we monitored the carbene signals for the CP of **1** with M/I = 10 at room temperature without additives; as shown in Figure 3.2b, carbene% drastically declined early in the reaction before leveling out at less than 50% of the initial carbene concentration (black line). However, we observed much higher carbene% of up to 80% remaining for an otherwise identical reaction with 3,5- $\text{Cl}_2\text{Py}$  added (red line). Moreover, almost no change in carbene% occurred during the reaction in deuterated THF ( $\text{THF-}d_8$ ) (blue line). At this point, it is unclear how the propagating carbene decomposes, but it does appear as though weakly coordinating species such as pyridine additives or THF suppress or retard this process.



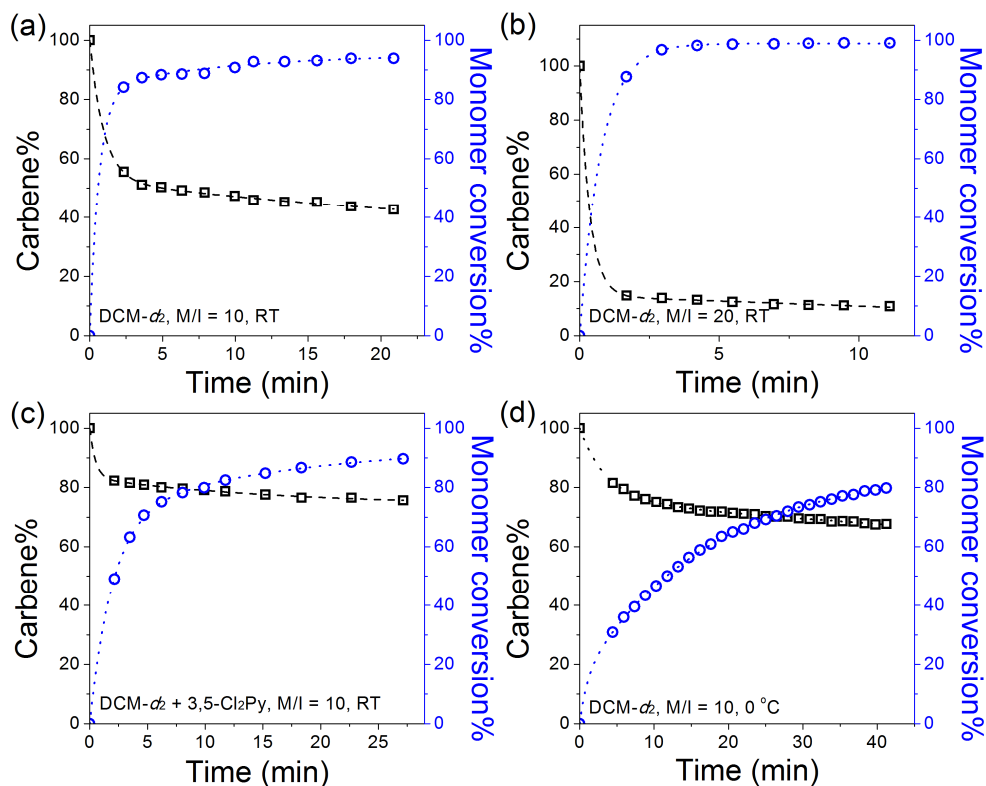
**Figure 3.1.** Structures of model compound (**1**) and catalyst (**G3-Cl**).



**Figure 3.2.** (a) <sup>1</sup>H NMR spectra of the initial and propagating carbene of [**G3-Cl**] and [**G3-Cl** + additive] in DCM-*d*<sub>2</sub>. (b) Decrease in the carbene signal over time during CP (M/I = 10). Remaining carbene% was calculated from <sup>1</sup>H NMR spectra using hexamethyl disilane as an internal standard.

To understand how the decay of the signals for the propagating carbenes affects the CP, we monitored both the carbene% and monomer conversion (**1**) by <sup>1</sup>H NMR spectroscopy under different reaction conditions in DCM-*d*<sub>2</sub>. For CP with M/I = 10 in DCM-*d*<sub>2</sub> at room temperature, monomer conversion was quite fast (90% after 5 min) even though only half of the propagating carbenes remained (Figure 3.3a). When the M/I ratio increased to 20, only 10% of carbene remained, despite full conversion (Figure 3.3b). Unfortunately, further comparison using higher M/I ratios was challenging, as monitoring the signal with such a low concentration of propagating carbenes by <sup>1</sup>H NMR spectroscopy became more difficult; nevertheless, the data in Figures 3.3a and 3.3b suggest that faster decay of

the propagating carbene would be observed for higher M/I ratios. This might explain the low conversions of **1** discussed previously (68% for M/I = 50 and 18% for M/I = 100). On the other hand, carbene% was far greater when 3,5-Cl<sub>2</sub>Py was added to a reaction where M/I = 10 (Figure 3.3a vs. 3.3c). Although the addition of the external ligand slowed the propagation (90% conversion after 25 min), consistent with how Grubbs catalyst follows a dissociative mechanism,<sup>5</sup> the lifetime of the propagating carbene greatly increased.

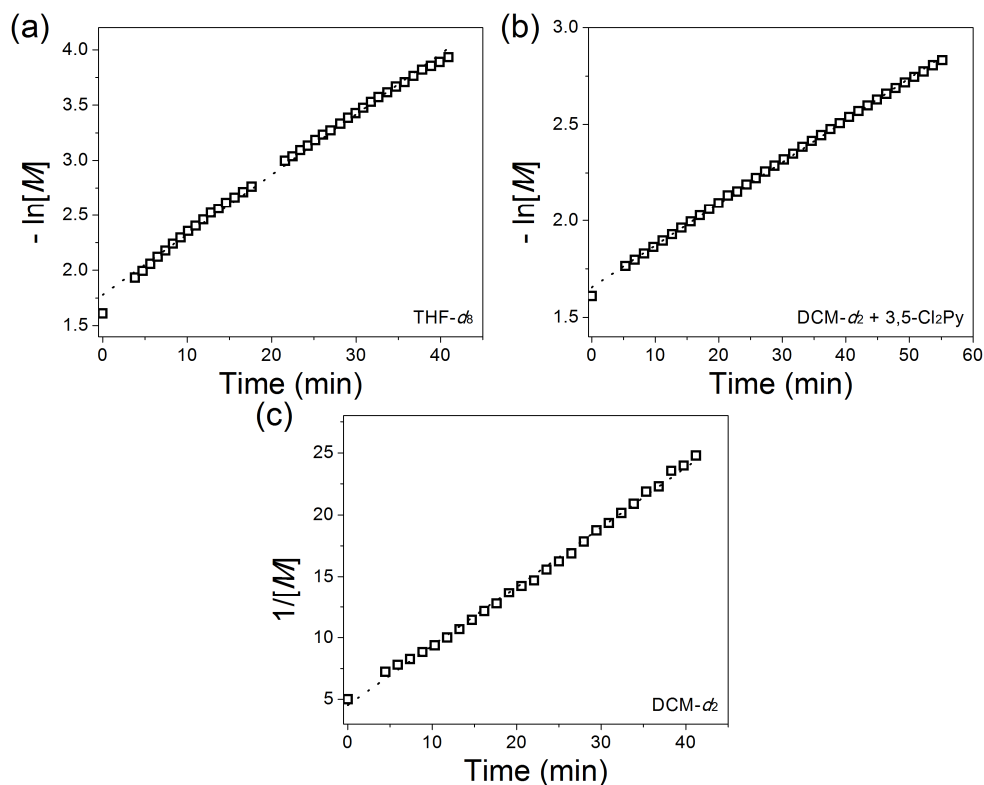


**Figure 3.3.** Plots of carbene% and monomer conversion (%) vs. time for the CP of **1** at room temperature for (a) M/I = 10 in DCM-*d*<sub>2</sub>, (b) M/I = 20 in DCM-*d*<sub>2</sub>, and (c) M/I = 10 in DCM-*d*<sub>2</sub> with the pyridine additive (5 equiv to **G3-Cl**). (d) Plot for the CP of **1** for M/I = 10 in DCM-*d*<sub>2</sub> at 0 °C. Conversions and carbene% were calculated from <sup>1</sup>H NMR spectra.

While optimizing the reaction conditions, we observed an interesting temperature effect whereby the CP of **1** proceeded more efficiently at 0°C than at room temperature (Table S3.1, entry 1 vs. entry 2). For a better understanding of this effect, an additional kinetic analysis was performed at 0 °C (M/I = 10 in DCM-*d*<sub>2</sub>). Indeed, the propagation rate decreased (80% conversion after 40 min) because of the lower catalytic activity at the lower temperature, but carbene decay slowed to a greater extent (Figure 3.3d), accounting for the unusual effect observed. As a result, this increased carbene stability overwhelmed the lower propagation rate, thereby leading to the higher conversion. These kinetic analyses explain why the Grubbs catalysts have not been utilized for the CP of 1,6-heptadiynes; because the propagating carbenes were not stable enough in DCM at ambient temperature to perform the efficient CP.

Because conversion occurred more slowly at 0 °C, more reliable and insightful kinetic analysis became possible by analyzing the data at the early stages of polymerization. We compared the reaction orders on the concentration of monomer (*[M]*) under various polymerization conditions; according to Eq 1, any change in *[C]* (concentration of the initial or propagating carbenes) would strongly affect the order of monomer conversion. Data from the polymerization reactions of **1** in DCM-*d*<sub>2</sub>, DCM-*d*<sub>2</sub> + additive, and THF-*d*<sub>8</sub> at 0 °C reveal that the reaction in THF-*d*<sub>8</sub> and the reaction in DCM-*d*<sub>2</sub> with additive follow the first-order kinetics for *[M]*, suggesting ideal living polymerization (Figure 3.4a and b). However, monomer conversion for the reaction in DCM-*d*<sub>2</sub> without additive followed, at least, second-order kinetics, implying a deviation from living polymerization because of significant catalyst decomposition (Figure 3.4c). These results are also in agreement with the data of Table S3.1.

$$-\frac{d[M]}{dt} = k_{obs}[M][C] \quad (1)$$

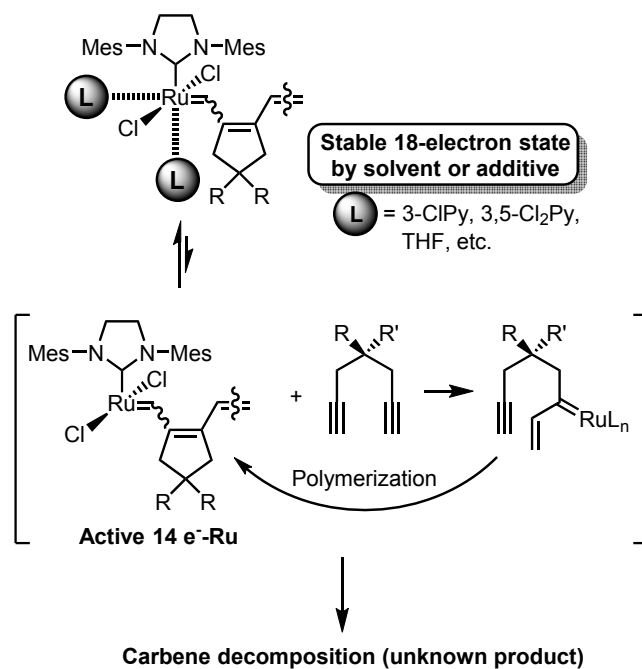


**Figure 3.4.** Plots of  $-\ln[M]$  vs. time for (a) THF- $d_8$  and (b) DCM- $d_2$  + additive and (c)  $1/[M]$  vs. time for DCM- $d_2$  for CP of **1** with  $M/I = 10$  at  $0^\circ\text{C}$ .

The use of transition-metal catalysts such as W, Mo, Nb, Ta, and Rh for the synthesis of substituted polyacetylenes from alkynes has been well studied.<sup>6</sup> However, there are far fewer examples of Ru-based Grubbs catalysts being used for this purpose,<sup>7-10</sup> largely because the activity of Grubbs catalysts toward alkyne polymerization (including for CP) has traditionally been believed to be low.<sup>11</sup> Now, it is clear from our mechanistic analysis that the major drawback in the CP of 1,6-heptadiynes is not the lack of intrinsic reactivity between Ru alkylidenes and alkynes, but rather facile carbene decomposition of the 14-electron Ru-based propagating species that occurs in the absence of external ligands (Scheme 3.2).<sup>12</sup> However, the weakly coordinating external ligands would increase the population of the more stable 18-electron state and the lifetime of the propagating species. Unsurprisingly, several additives (THF, 2,6- $\text{Cl}_2\text{BQ}$ , 3,5- $\text{Cl}_2\text{Py}$ ) demonstrated this



stabilizing effect, as evidenced by the increased monomer conversion.

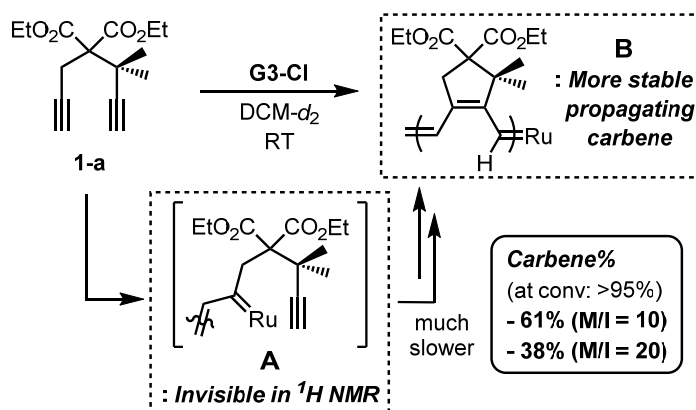


**Scheme 3.2.** Proposed scheme for the effects of weakly coordinating ligands

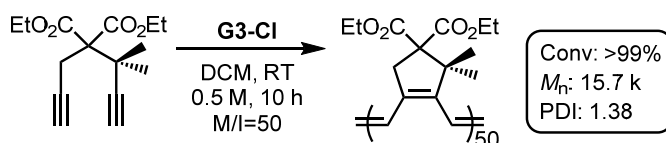
### 3.3.2. Steric Effect on Carbene Decomposition

Our discovery on the stability of propagating carbenes gave an alternative strategy to design new monomers which could be polymerized via more stable propagating carbenes. Ru-alkylidenes are reported to undergo decomposition through the formation of bimolecular complexes.<sup>13-15</sup> In particular, recent work by the Lee group demonstrated that *gem*-dimethyl groups at the propargyl carbon stabilize alkyne-chelated Ru-alkylidene complexes.<sup>16</sup> To investigate how this dimethyl group could affect the stability of the propagating carbene during CP, we prepared a new monomer, **1-a**, an analog of **1**, and performed the same kinetic analysis in DCM-*d*<sub>2</sub> at room temperature (Scheme 3.3). This polymerization proceeded much more slowly than for **1**, especially initially, because the *gem*-dimethyl substituent significantly retarded both ring closing and propagation (Scheme 3.3 and Figures S3.1 and S3.2). Although benzylidene efficiently underwent the initiation by reacting with the sterically less demanding terminal alkyne, it was difficult to monitor the carbene concentration during the initial stages of propagation because the disubstituted carbene intermediate **A** without any proton was invisible in <sup>1</sup>H NMR spectrum and was the major species at the initial stage because of the much slower ring-closure. With increasing conversion, the carbene peak (corresponding to the actual propagating species **B**) grew, and the carbene% was monitored by <sup>1</sup>H NMR spectroscopy. The remaining carbene% was measured after 95% monomer conversion and was found to be 61% (M/I = 10, after 3 h) and 38% (M/I = 20, after 5 h). As expected, these values were higher than the corresponding carbene% of **1** in the previous kinetic analysis (Figure 3.3, 43% for M/I = 10 and 13% for M/I = 20). This result suggests that the sterically hindered dimethyl group near the propagating carbene provided some shielding effect or protection, thereby increasing the carbene lifetime. Finally, we conducted the CP of **1-a** with M/I = 50 at room temperature in DCM; even without the additive, full conversion was achieved, although it required a much longer reaction time (10 h) because of much slower cyclization and propagation owing to the 3,3-dimethyl group. This again

showed that higher conversion of **1-a** (compared to **1**; Table S3.1, entry 1) was possible because of greater stabilization of the propagating carbene (Scheme 3.4). Moreover, PDI value of the polymer produced at room temperature was quite narrow (1.38), suggesting that chain transfer is also suppressed by the steric effects of dimethyl substitution (compared to a PDI of 2.56; Table S3.1, entry 1). With a lower M/I=25, the polymer having  $M_n$  of 7.9 k and PDI of 1.13 was obtained after 7 h. These experiments provide significant insights into CP, as the quantitative carbene analysis could predict polymerization efficiency. It is expected that this strategy will be helpful in investigating other CP systems.



**Scheme 3.3.**  $^1\text{H}$  NMR spectroscopic measurement of the propagating carbene during polymerization of **1-a**



**Scheme 3.4.** Cyclopolymerization of **1-a** in DCM at room temperature

### 3.4. Conclusion

Mechanistic studies using  $^1\text{H}$  NMR spectroscopy revealed that weakly coordinating reagents (THF and 3,5- $\text{Cl}_2\text{Py}$ ) suppressed the decomposition of the propagating carbene (a 14-electron state) and increased the turnover numbers of the reactions. Kinetic analyses of the reaction order showed that living polymerization was possible in the presence of weakly coordinating reagents at lower temperatures because the propagating carbenes were stabilized and chain transfer was suppressed. As an alternative strategy to stabilizing the propagating carbene, we introduced *gem*-dimethyl substituents into the 3-position on the 1,6-heptadiyne derivative. This steric protection effectively increased the carbene lifetime of the new monomer, improving the turnover number.

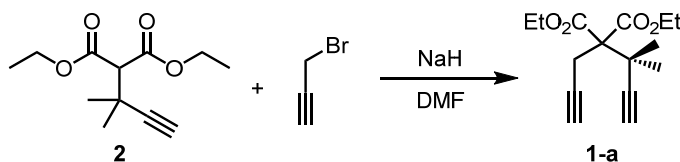
### 3.5. Experimental Section

#### Characterization

$^1\text{H}$  NMR and  $^{13}\text{C}$  NMR spectra were recorded by Varian/Oxford As-500 (500 MHz for  $^1\text{H}$  and 125 MHz for  $^{13}\text{C}$ ) spectrometer and Agilent 400-MR (400 MHz for  $^1\text{H}$  and 100 MHz for  $^{13}\text{C}$ ). For the  $^1\text{H}$  NMR spectroscopic measurement at low temperature (0 °C), Avance 500 (Bruker, 500 MHz for  $^1\text{H}$ ) system was utilized at National Center for Inter-University Research Facilities (NCIRF). High resolution mass spectroscopy (HRMS) analyses were performed by NCIRF.

#### Synthesis

##### Diethyl-2-(propargyl)-2-(dimethylpropargyl)malonate (**1-a**)



To a 50-mL round bottom flask was added **2**<sup>17</sup> (589.3 mg, 2.60 mmol). After purging the flask with argon, 10 mL of DMF was added, and the mixture was cooled down to 0 °C. Sodium hydride (60% dispersion in mineral oil, 160 mg, 4.00 mmol) was added, and the reaction mixture was stirred for 30 minutes at room temperature. Propargyl bromide (80 wt% in toluene, 0.3 mL, 3.4 mmol) was added dropwise, and the mixture was stirred for 1 h at room temperature. The reaction was quenched with saturated  $\text{NH}_4\text{Cl}$  aqueous solution, and the organic layer was washed with water and extracted with diethyl ether (50 mL\*3), dried with  $\text{MgSO}_4$ , and concentrated. The product was purified by flash column chromatography on silica gel (EtOAc:hexane = 1:10) to afford compound **1-a** as a pale yellow liquid (483.4 mg, 1.83 mmol, 70%).  $^1\text{H}$  NMR (500 MHz,  $\text{CDCl}_3$ ):  $\delta$  1.29 (t,  $J$  = 7.5 Hz, 6 H), 1.52 (s, 6 H), 2.00 (t,  $J$  = 2.7 Hz, 1 H), 2.24 (s, 1 H), 3.05 (d,  $J$  = 3.0 Hz, 2 H), 4.25 (q,  $J$  = 7.0 Hz, 4 H);  $^{13}\text{C}$  NMR (100MHz,  $\text{CDCl}_3$ ):  $\delta$  14.3, 23.8, 27.1, 37.4,

61.8, 63.0, 70.9, 71.1, 81.1, 88.8, 169.0; HRMS (EI+): calcd. for  $C_{15}H_{20}O_4$ , 264.1361, found, 264.1368.

### Procedure for polymerization of 1-a

The procedure is same with the description in Chapter 2, except the reaction temperature (25 °C). **Poly(1-a)**  $^1H$  NMR (500 MHz,  $CDCl_3$ ):  $\delta$  1.13-1.29 (br m, 6 H), 1.29-1.47 (br m, 6 H), 2.90-3.24 (br m, 2 H), 3.98-4.32 (br m, 4 H), 6.17-6.54 (br m, 1 H), 6.59-6.99 (br m, 1 H);  $^{13}C$  NMR (125 MHz,  $CDCl_3$ ):  $\delta$  14.4, 24.2, 38.0, 52.1, 61.3, 66.8, 122.5, 124.6, 135.7, 145.2, 170.9; see Figure S3.4 for 2D NMR analysis of conjugated backbone.

### General procedure for kinetic experiments

To a screw-cap NMR tube (Wilmad-Labglass, screw-cap tube, 500 MHz, 5 mm) was added the monomer (0.12 mmol, 10 eq). The tube was purged with argon, and deuterated solvent (400  $\mu$ L) was added to dissolve the monomer. The solution of initiator (0.012 mmol, 1 eq) (and 5 eq of additive) was prepared under argon atmosphere and one drop of hexamethyl disilane was added as an internal standard. The total amount of initiator and additive was 5/4 of original value; after dissolving those using deuterated solvent (250  $\mu$ L), 1/5 (50  $\mu$ L) of it was diluted in another NMR tube and used for checking the ratio between initial carbene and internal standard. After obtaining the NMR spectrum of monomer, 200  $\mu$ L of initiator solution was added to monomer solution and  $^1H$  NMR measurement was recorded over time. In 0 °C experiment, only 1 equiv of additive was used because the propagation was much slower at a lower temperature.

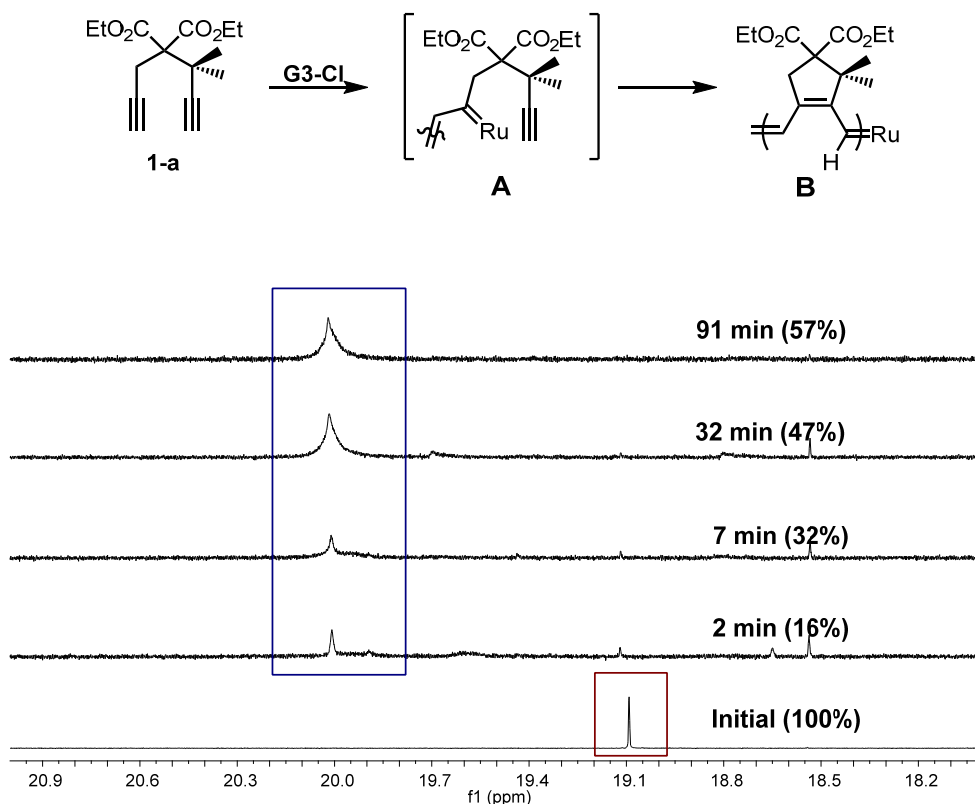
### 3.6. Supporting Information

**Table S3.1. Partial data from Table 2.2 for the comparison of additive effect**

Reaction scheme: Monomer **1** (1,1-dimethacrylate derivative) reacts with **G3-Cl** in **DCM, 0.5 M** with an **Additive** to form a polymer product.

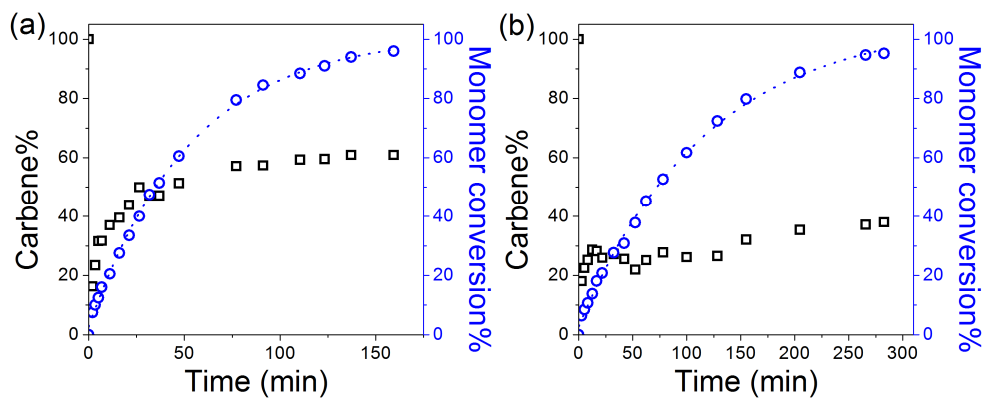
entry	additive	M/I/Add	temp (°C)	time (h)	$M_n^a$ (kDa)	PDI <sup>a</sup>	conv <sup>b</sup> (%)
1	-	50/1/-	RT	1	12.6	2.56	68
2	-	50/1/-	0	1	21.5	2.38	90
3	THF	50/1/20	RT	1	10.5	2.00	91
4	2,6-Cl <sub>2</sub> BQ	50/1/10	RT	1	19.4	2.41	89
5	3,5-Cl <sub>2</sub> Py	50/1/10	RT	1	26.4	1.13	>99

<sup>a</sup>Determined by CHCl<sub>3</sub> SEC calibrated using polystyrene (PS) standards. <sup>b</sup>Calculated from <sup>1</sup>H NMR spectra.

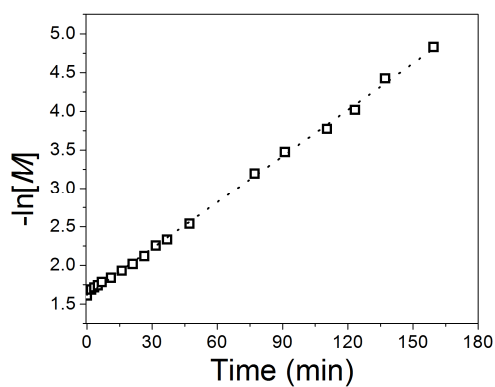


**Figure S3.1.** <sup>1</sup>H NMR spectra of initial and propagating carbenes from the polymerization of **1-a** in DCM-*d*<sub>2</sub>. (M/I = 10) The percentage in brackets is relative carbene% compared with the initial amount of the carbene. Due to the intermediate (**A**) having no carbene proton, only small portion of the propagating carbene was shown in the early stage of the polymerization; it increased continuously with the monomer conversion because the actual propagating species (**B**) having a carbene proton were formed.



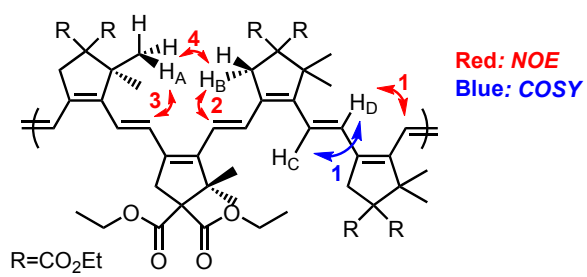


**Figure S3.2.** Plots of monomer conversion (%) and carbene% vs. time for the CP of **1-a** with (a)  $M/I = 10$  and (b)  $M/I = 20$  in  $\text{DCM-}d_2$  at room temperature. Low carbene% during the initial stage is described in Figure S3.1.

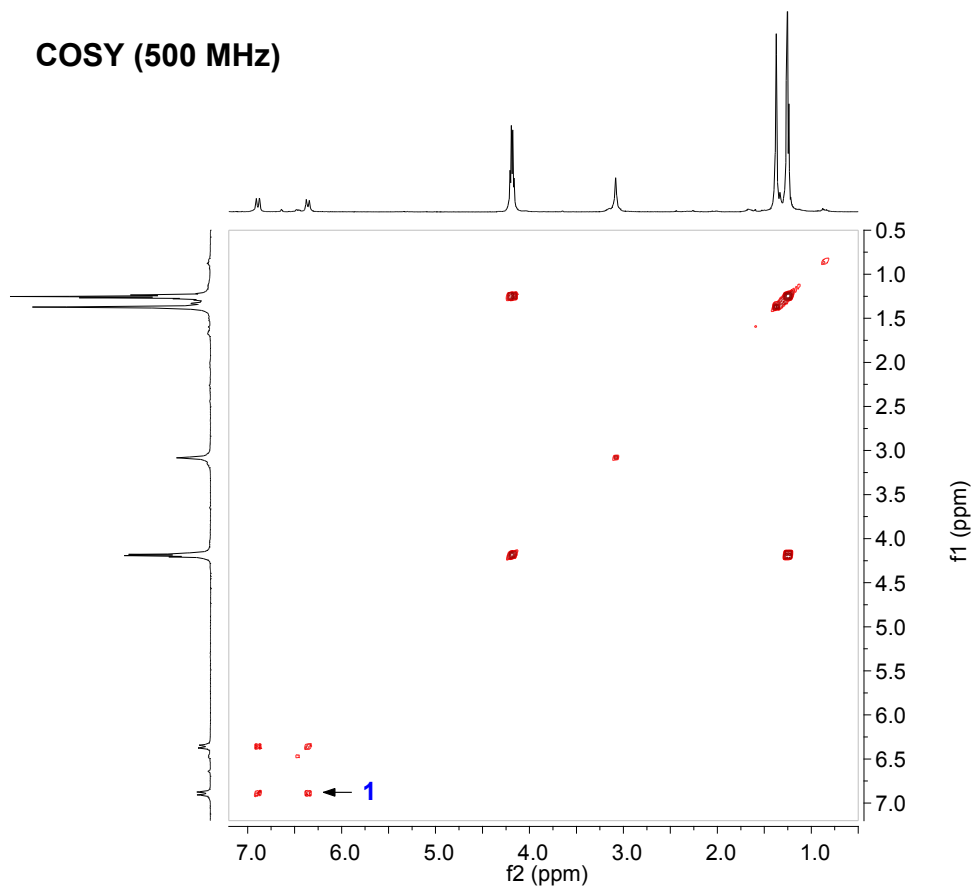


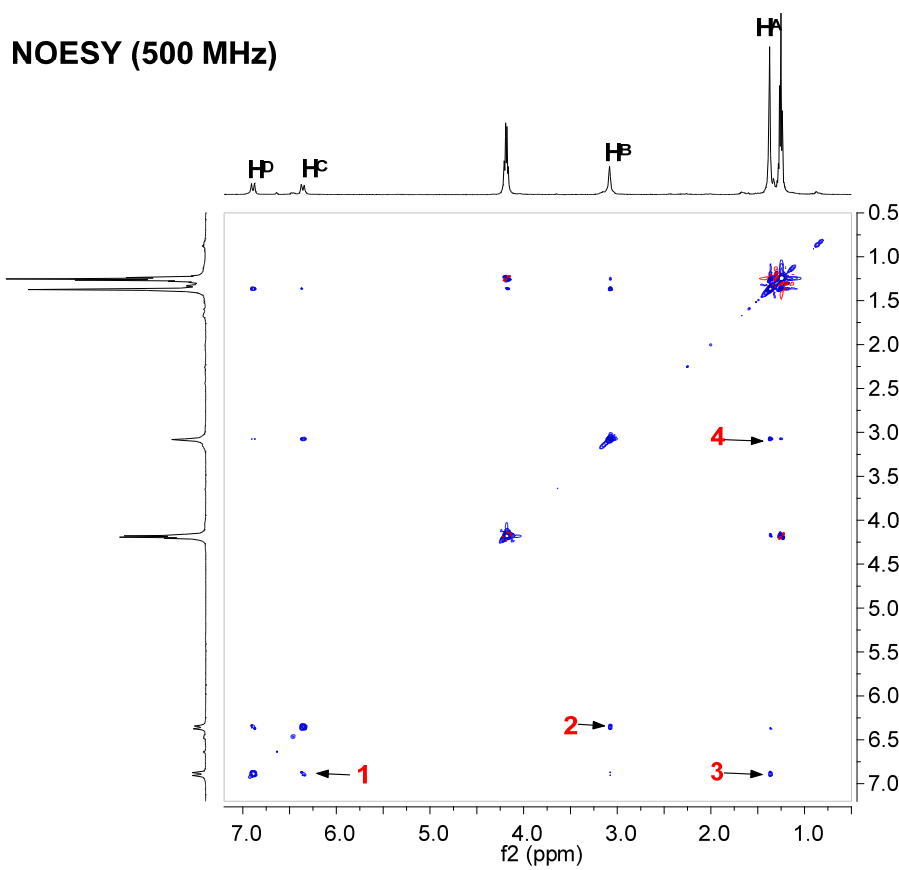
**Figure S3.3.** Linear plot of  $-\ln[M]$  vs. time for the cyclopolymerization of **1-a** with  $M/I = 10$  in  $\text{DCM-}d_2$  at room temperature.

## 2D NMR (COSY and NOESY) assignment of poly(1-a)



### COSY (500 MHz)





### 3.7. References and Notes

- <sup>†</sup> Portions of this chapter have been previously reported, see: Kang, E.-H.; Yu, S. Y.; Lee, I. S.; Park, S. E.; Choi, T.-L. *J. Am. Chem. Soc.* **2014**, *136*, 10508-10514.
- (1) Samak, B. A.; Amir-Ebrahimi, V.; Corry, D. G.; Hamilton, J. G.; Rigby, S.; Rooney, J. J.; Thompson, J. M. *J. Mol. Catal. A: Chem.* **2000**, *160*, 13-21.
  - (2) Slugovc, C. *Macromol. Rapid Commun.* **2004**, *25*, 1283-1297.
  - (3) Walker, R.; Conrad, R. M.; Grubbs, R. H. *Macromolecules* **2009**, *42*, 599-605.
  - (4) Schulz, M. D.; Wagener, K. B. *ACS Macro Lett.* **2012**, *1*, 449-451.
  - (5) Sanford, M. S.; Love, J. A.; Grubbs, R. H. *J. Am. Chem. Soc.* **2001**, *123*, 6543-6554.
  - (6) Masuda, T. *J. Polym. Sci. Part A: Polym. Chem.* **2007**, *45*, 165-180.
  - (7) Schuehler, D. E.; Williams, J. E.; Sponsler, M. B. *Macromolecules* **2004**, *37*, 6255-6257.
  - (8) Katsumata, T.; Shiotsuki, M.; Kuroki, S.; Ando, I.; Masuda, T. *Polym. J.* **2005**, *37*, 608-616.
  - (9) Katsumata, T.; Shiotsuki, M.; Masuda, T. *Macromol. Chem. Phys.* **2006**, *207*, 1244-1252.
  - (10) Katsumata, T.; Shiotsuki, M.; Sanda, F.; Sauvage, X.; Delaude, L.; Masuda, T. *Macromol. Chem. Phys.* **2009**, *210*, 1891-1902.
  - (11) Naumov, S.; Buchmeiser, M. R. *Organometallics* **2012**, *31*, 847-856.
  - (12) It is not clear how propagating carbene is deactivated, but there are some reports about decomposition or deactivation during reactions of Ru-catalysts and alkynes.; See (i) Wolf, J.; Stürer, W.; Grünwald, C.; Gevert, O.; Laubender, M.; Werner, H. *Eur. J. Inorg. Chem.* **1998**, 1827-1834 for vinylidene formation, (ii) for carbene consumption by cyclodimerization; see: Diver, S. T.; Kulkarni, A. A.; Clark, D. A.; Peppers, B. P. *J. Am. Chem. Soc.* **2007**, *129*, 5832-5833.

- (13) Hong, S. H.; Day, M. W.; Grubbs, R. H. *J. Am. Chem. Soc.* **2004**, *126*, 7414-7415.
- (14) Hong, S. H.; Wenzel, A. G.; Salguero, T. T.; Day, M. W.; Grubbs, R. H. *J. Am. Chem. Soc.* **2007**, *129*, 7961-7968.
- (15) Leitao, E. M.; Dubberley, S. R.; Piers, W. E.; Wu, Q.; MacDonald, R. *Chem. Eur. J.* **2008**, *14*, 11565-11572.
- (16) Wang, K.-P.; Yun, S. Y.; Lee, D.; Wink, D. J. *J. Am. Chem. Soc.* **2009**, *131*, 15114-15115.
- (17) Stulgies, B.; Prinz, P.; Magull, J.; Rauch, K.; Meindl, K.; Ruhl, S.; Meijere, A. *Chem. Eur. J.* **2005**, *11*, 308-320.

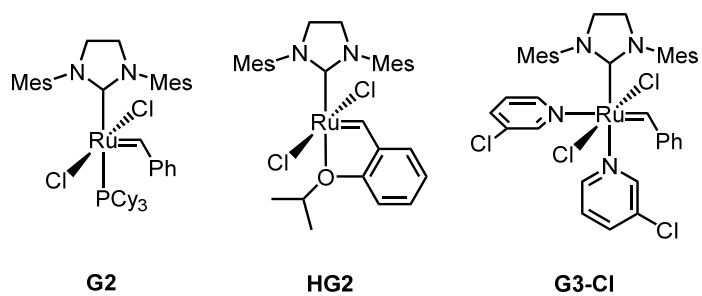
## **Chapter 4. Mechanistic Investigations on Cyclopolymerization vs. [2+2+2] Cycloaddition of 1,6-Heptadiynes**

### **4.1. Abstract**

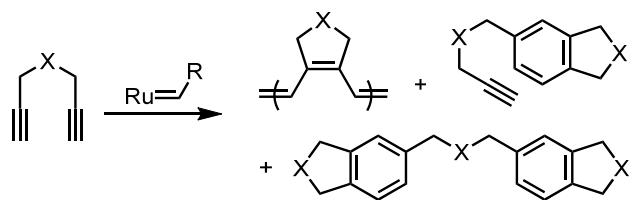
It was found that second generation Grubbs catalyst or Hoveyda-Grubbs catalyst in dichloromethane (DCM) dominantly formed side products, dimers and trimers of 1,6-heptadiyne derivatives, instead of producing conjugated polymers. Further mechanistic studies disclosed that [2+2+2] cycloaddition by the decomposed Grubbs catalyst was responsible for these side products, not commonly believed olefin metathesis pathway. Furthermore, a control experiment revealed that pyridine not only stabilized the propagating carbene, but also suppressed the dimer formation by poisoning the newly generated catalytic species that would promote [2+2+2] cycloaddition. Another observation was that depending on the nature of substituents of the 1,6-heptadiyne, different ratios of polymer and the side-products were obtained as a result of competition between CP and cycloaddition. Monomers containing more coordinating substituents favored the undesired cycloaddition products as a consequence of slower polymerization and faster decomposition of carbene, while weakly chelating monomers strongly favored CP. Finally, with good understanding on what factors contributed to the CP propagation and decomposition on the Grubbs catalysts, the efficiency of CP was maximized by modifying the monomer structure, lowering the reaction temperature, or adding the stabilizing ligands.

## 4.2. Introduction

Cyclopolymerization (CP) of 1,6-heptadiyne derivatives using Grubbs catalysts had been unsuccessful, and this led to misbelief that they were just inactive. However, in Chapter 2 and 3, it was investigated that the weakly coordinating ligands such as tetrahydrofuran (THF) and pyridine greatly enhanced the efficiency of CP using Grubbs catalysts by suppressing the decomposition of active propagating metal carbene species during the polymerization. With this valuable lesson regarding the crucial ligand effect, we turned our focus to reasons why previous attempts of CP using second generation Grubbs catalyst (**G2**) and Hoveyda-Grubbs catalyst (**HG2**) (Figure 4.1) were unsuccessful. Interestingly, we produced brush polymers via macromonomer approach using **HG2** in THF (see Chapter 5).<sup>1</sup> This observation puzzled us why the CP had been impossible using **G2** or **HG2**. In this chapter, we rationalize the previous failures of CP by addressing on a competing reaction pathway of 1,6-heptadiyne derivatives. This reaction produced their dimer and even trimers as major side products (Scheme 4.1) when a ligand-free catalyst (**HG2**) was used under various reaction conditions. Also, we concluded that this major side reaction, whose mechanism had been in dispute, was [2+2+2] cycloaddition of alkynes catalyzed by decomposed Ru-alkylidene from numerous mechanistic investigations. Lastly, this study revealed which factors influenced the competition between CP and cycloaddition, and how to understand the structure-reactivity relationship to maximize the efficiency of CP. Therefore, we successfully cyclopolymerized 1,6-heptadiynes using **HG2** and suggest a general guideline for successful CP using Grubbs catalysts.



**Figure 4.1.** Structures of common Grubbs catalysts.



**Scheme 4.1.** Cyclopolymerization using Ru-alkylidene and the formation of dimer and trimer



### 4.3. Results and Discussion

#### 4.3.1. Mechanism of Dimerization and Trimerization of 1,6-Heptadiyne Derivatives during Cyclopolymerization

We first screened various cyclopolymerization conditions to examine what happened during the typical polymerization of the most common monomer, dipropargyl malonate esters, **1a** and **1b**, by various Grubbs catalysts and compared their efficiencies (Table 4.1). Tetrahydrofuran (THF) and dichloromethane (DCM) were selected as coordinating and non-coordinating solvents respectively, and three different Grubbs catalysts in Figure 4.1 were tested. Reactions using **G2** or **HG2** in DCM afforded just dimer (**3**) or trimer (**4**) almost exclusively at room temperature (Table 4.1, entries 1, 2 and 4). On the other hand, reactions using pyridine-containing **G3-Cl** in DCM (Table 4.1, entry 3) or **HG2** in THF (Table 4.1, entry 5) did not produce **3** or **4** and underwent CP dominantly instead. However, repeating the same reaction using **HG2** in THF at elevated temperature (50 °C) resulted in an increment of the dimer formation and decrease in CP (Table 4.1, entry 6). Instead of using **G3-Cl** (entry 3), adding pyridines, such as 3-chloropyridine (3-ClPy) and 3,5-dichloropyridine (3,5-Cl<sub>2</sub>Py), to ligand-free **HG2** also selectively promoted CP with higher conversion (Table 4.1, entries 7 and 8). However, adding a benzoquinone derivative as a weaker ligand increased the conversion of CP only slightly while maintaining the high yield of **3** and **4** (Table 4.1, entry 4 vs. entry 9). These dimerization and trimerization of 1,6-heptadiynes were previously reported by Buchmeiser group when modified Grubbs catalysts containing trifluoroacetate or isocyanate reacted with 1,6-heptadiyne derivatives containing nitrogen and ethers (Scheme 4.1).<sup>2,3</sup> As a mechanism of the dimer formation, they proposed an intramolecular backbiting reaction via olefin metathesis mechanism (**Cycle I** in Scheme 4.2). Due to this side reaction, lower conversion to polymer was inevitable. Initially, we assumed that the mechanism of dimerization by Grubbs catalysts should be very similar to the previous reports from Buchmeiser group although the catalysts were different.

**Table 4.1. Cyclopolymerization of 1a and 1b varied by reaction conditions**

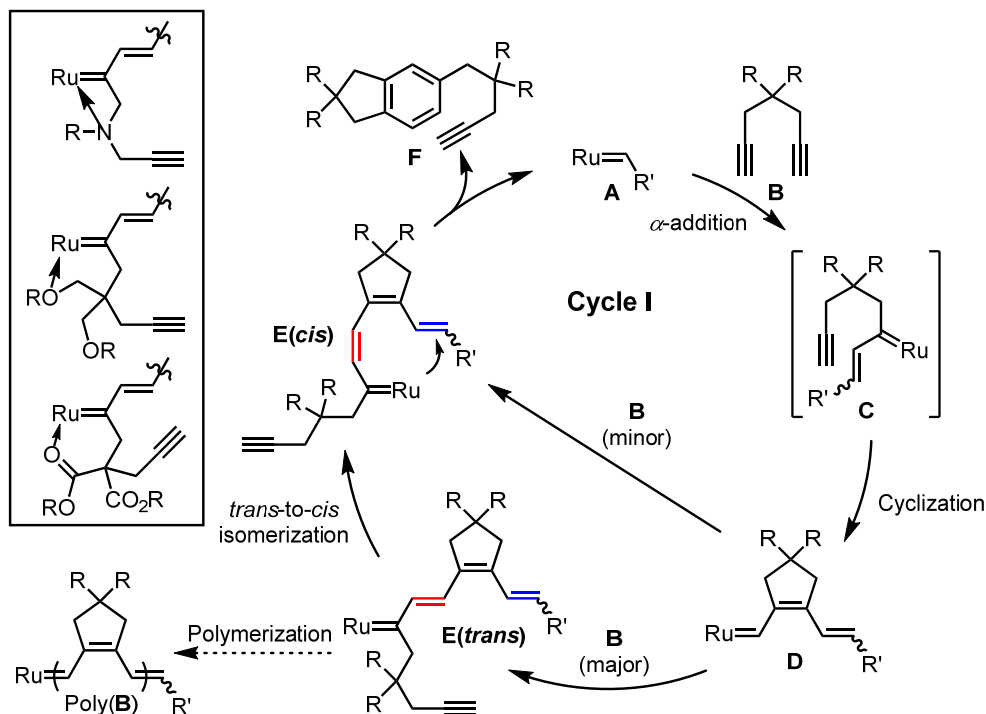
$\text{1a: R=CO}_2\text{Et}$   
 $\text{1b: R=CO}_2\text{Hex}$

entry	cat	monomer	solvent	additive <sup>a</sup>	<b>2</b> <sup>b</sup> (%)	<b>3</b> <sup>b</sup> (%)	<b>4</b> <sup>b</sup> (%)	conv <sup>b</sup> (%)
1	<b>HG2</b>	<b>1a</b>	DCM	-	2	47	6	60
2	<b>G2</b>	<b>1a</b>	DCM	-	3	24	trace	33
3	<b>G3-Cl</b>	<b>1a</b>	DCM	-	55	trace	0	65
4	<b>HG2</b>	<b>1b</b>	DCM	-	5	47	9	81
5	<b>HG2</b>	<b>1b</b>	THF	-	79	0	0	99
6 <sup>c</sup>	<b>HG2</b>	<b>1b</b>	THF	-	49	27	0	93
7	<b>HG2</b>	<b>1b</b>	DCM	3-ClPy	73	0	0	75
8	<b>HG2</b>	<b>1b</b>	DCM	3,5-Cl <sub>2</sub> Py	94	0	0	97
9	<b>HG2</b>	<b>1b</b>	DCM	2,6-Cl <sub>2</sub> BQ	13	52	17	88

<sup>a</sup>10 mol % of monomer was added. <sup>b</sup>Calculated from <sup>1</sup>H NMR spectra. <sup>c</sup>The reaction was performed at 50 °C.

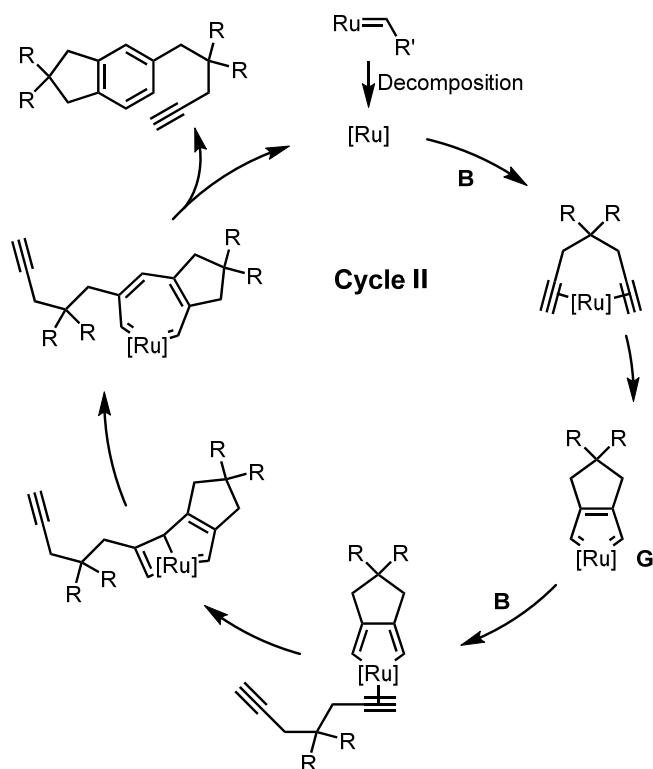
Buchmeiser group reported that the coordination of heteroatoms on the monomers or 2-PrO-styrene ligand to metal center promoted the backbiting side reaction, particularly with the emphasis on the release-return mechanism of the chelating styrene. They further explained that the pyridine impeded the backbiting reaction because the pyridine competed with the alkenes of the polymer backbone for the coordination to the Ru metal. As a result, they proposed a scheme, **Cycle I**, to describe the backbiting mechanism and coordination models via olefin metathesis pathway (Scheme 4.2). After Ru-alkylidene (**A**) reacted with a 1,6-heptadiyne derivative (**B**) by  $\alpha$ -addition to produce **C**, it undergoes rapid cyclization to form the initial propagating carbene **D**. Reacting with another **B**, **D** makes the second intermediate **E**, which should cyclize onto the alkyne and polymerize. Instead, **E** undergoes backbiting side reaction by cyclizing onto the

olefin (blue) of the backbone to generate an aromatic dimer (**F**). However, there is one issue with this proposed mechanism because this process requires **E** to be *cis*-dienes for successful cyclization to produce aromatic compound **F**. Therefore, they proposed *trans*-to-*cis* isomerization to explain the production of **F**. However, as well as reports from Buchmeiser group, we showed that the CP mediated by Ru catalysts predominantly formed *trans*-vinylene PCPV, and even a small amount of *cis*-vinylene spontaneously isomerized into thermodynamically stable *trans*-vinylene (see Chapter 6).<sup>4</sup> Therefore, it was highly unlikely that the non-spontaneous *trans*-to-*cis* isomerization would rapidly occur and promote the dimer formation.



**Scheme 4.2.** Mechanism of dimerization based on the olefin metathesis reaction (**Cycle I**)

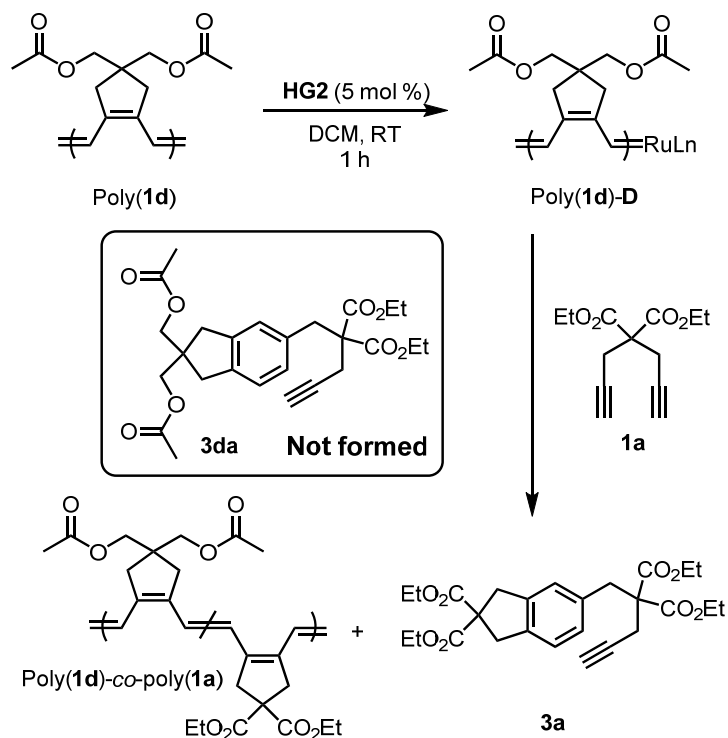
Instead, we turned to an alternative pathway, a well-investigated transition metal-catalyzed [2+2+2] cycloaddition reaction to produce **3** and **4**.<sup>5-7</sup> The mechanism of Ru-catalyzed cycloaddition involves ruthenacyclopentatriene intermediate (**G**) (Scheme 4.3, **Cycle II**).<sup>6a,8</sup> Interestingly, Blechert group reported the first intramolecular trimerization or cyclization of triyne using the first generation Grubbs catalyst (**G1**) by proposing a mechanism of the cascade olefin metathesis reaction,<sup>9</sup> just like Buchmeiser group. Furthermore, Witulski and coworkers adopted this olefin metathesis pathway to explain their regioselectivity issues during the cycloaddition between diynes and terminal alkynes.<sup>10</sup> On the other hand, more reactive Grubbs catalysts, **G2** and **HG2**, were recently investigated for various cycloaddition reactions by Pérez-Castells group who proposed a [2+2+2] cycloaddition mechanism catalyzed by some Ru-species, as a result of the decomposed Grubbs catalysts under the harsh reaction condition (> 60 °C).<sup>5</sup> However, even there remained some ambiguities for the [2+2+2] cycloaddition mechanism catalyzed by decomposed Ru species via metallacyclopentatriene intermediate, because they also observed another olefin metathesis reaction still operative at room temperature.<sup>5d</sup> Summing up all the previous observations, these seemed to be still a dispute on exactly which mechanism produced dimers of 1,6-heptadiyne derivatives during CP.



**Scheme 4.3.** Mechanism of dimerization based on Ru-catalyzed [2+2+2] cycloaddition mechanism (**Cycle II**)

Although the **Cycle II** seemed to be more plausible mechanism than the **Cycle I** which required unfavorable *trans*-to-*cis* isomerization, more systematic investigations and evidence were necessary. Therefore, we designed following control experiments to confirm the right mechanism. Firstly, we conducted a cross-over experiment to check if the **Cycle I** was operative. To a purified poly(**1d**), **HG2** was added to generate propagating carbene by chain transfer reaction (intermediate **D** in Scheme 4.2), and **1a** was sequentially added (Scheme 4.4, Figure S4.1 and Figure S4.2). According to the **Cycle I**, the reaction between a propagating carbene on poly(**1d**) (poly(**1d**)-**D**) and **1a** should produce a hetero-cycloaddition product (**3da**) through intermediate **E** by the backbiting mechanism (Scheme 4.4). As a result of the generation of poly(**1d**)-**D**, one could isolate the copolymer of poly(**1d**)-*co*-poly(**1a**). However, we could not detect **3da** at all, but only dimer and

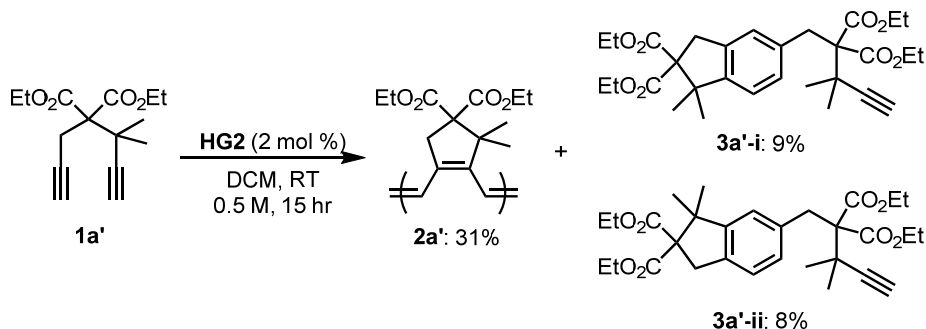
trimer of **1a** (**3a** and **4a**) were confirmed. As a counter experiment, the reaction between poly(**1a**) and **1d** was repeated, but it also produced homodimer of **1d** only and no cross-over product at all, supporting against **Cycle I** (Figure S4.3).



**Scheme 4.4.** Reaction of propagating carbene on poly(**1d**) and **1a**

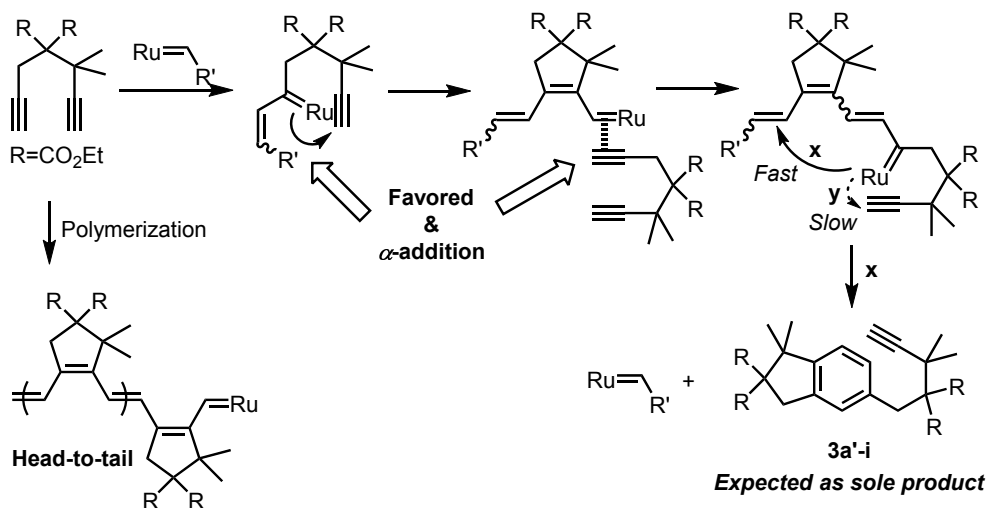
To provide a more support for the **Cycle II** over **Cycle I**, we attempted the same dimerization using an asymmetric monomer, 3,3-dimethyl substituted diyne (**1a'**, Scheme 4.5). If the steric effects were negligible, **1a'** would produce all four isomers (Scheme 4.6, **3a'**; **i-iv**). However, dimethyl group on **1a'** provided such a large steric effect which would make the biased catalysis. For example, it was revealed that the propagating carbene only reacted with the sterically less hindered alkyne, thereby producing highly regular head-to-tail microstructure, **2a'**, via cyclopolymerization (see Chapter 3). Therefore, if the **Cycle I** were valid, the dimerization by olefin metathesis mechanism would produce **3a'-i** as a sole product. In contrast, **Cycle II** would produce two isomers, **3a'-i** and **3a'-ii**, because

a steric effect on the alkyne having dimethyl group would suppress its binding to the metallacyclopentatriene intermediates (Scheme 4.6, not forming **3a'-iii** and **3a'-iv**). Interestingly, the actual reaction of **1a'** using **HG2** produced not only the expected regioregular **2a'** (31%), but also a mixture of the isomers of **3a'**. From two-dimensional NMR analyses (COSY and NOESY) and GC/MS analyses on the mixture of isomers (Figure S4.4–S4.7), we concluded that these isomers were **3a'-i** and **3a'-ii** in the ratio of almost 1:1 (9% and 8%). Furthermore, the much higher CP efficiency of **1a'** (33%) than that of **1a** (2%, Table 4.1) supported more favorable **Cycle II** mechanism. CP of **1a'** should have been suppressed because *gem*-dimethyl on the 3-position of diyne slowed down the intramolecular cyclization, thereby favoring the backbiting process (**x**) according to the **Cycle I** than the polymerization (**y**); however, the reaction of **1a'** produced more polymer than **1a**. Lastly, this higher yield of the polymer from **1a'** also makes sense because the dimethyl group significantly suppresses carbene decomposition. Therefore, when compared to the analogous reaction with **1a**, the carbene survived longer to continue cyclopolymerization to give a higher yield of **2a'**, while dimerization was greatly retarded as a result of slower decomposition of the propagating carbene.

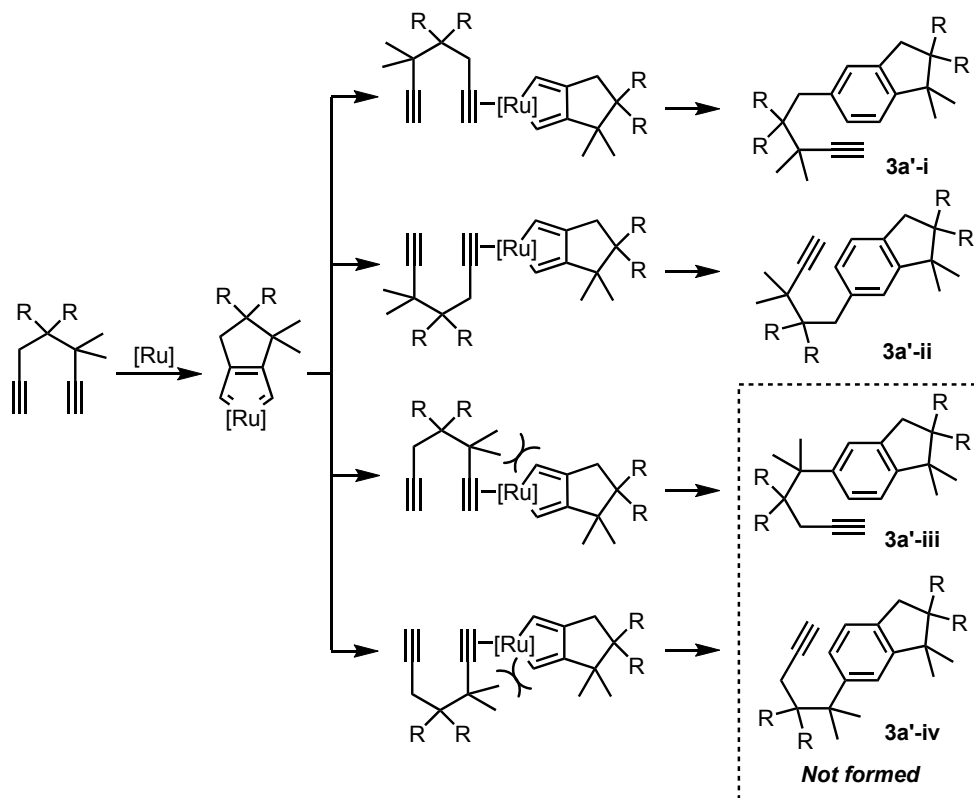


**Scheme 4.5.** Cyclopolymerization and cycloaddition of 3,3-dimethyl substituted analog of **1a** (**1a'**)

### Metathesis-pathway (Cycle I)



### Non-Metathesis-pathway (Cycle II)

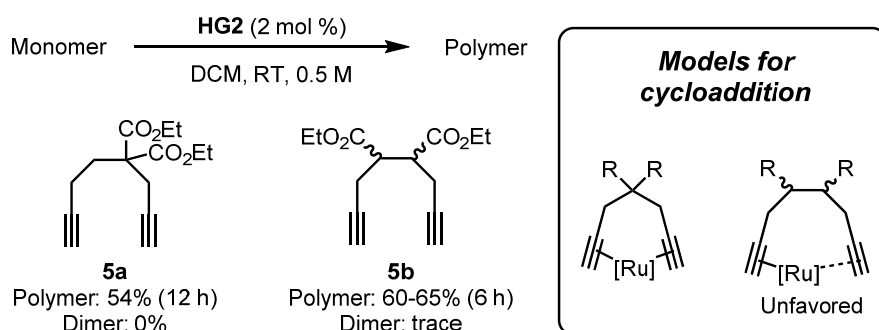


**Scheme 4.6.** Plausible mechanisms of dimerization of **1a'** and structures of dimers

Previously, we reported that CP of 1,7-octadiyne derivatives was much slower than that of 1,6-heptadiyne derivatives due to longer distance between two



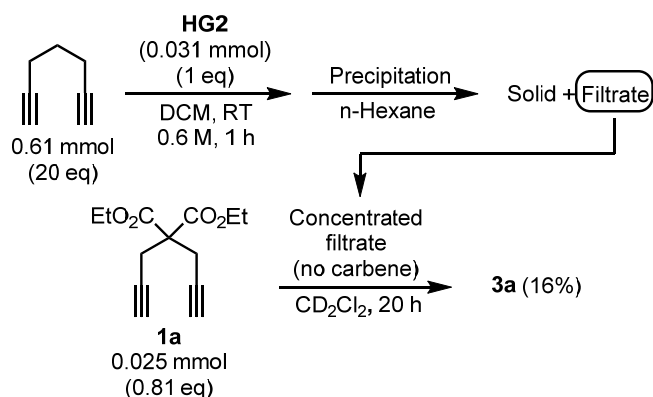
alkynes, thereby leading to slower cyclization.<sup>11</sup> Therefore, if **Cycle I** were operative, the backbiting reaction should dominate over the CP, just like the **Cycle I** in Scheme 4.6. However, from the reactions of **5a** and **5b**, we could observe good conversion to the corresponding polymer but find almost no dimer (Figure 4.2). Furthermore, it was reported that [2+2+2] cycloaddition of 1,7-octadiynes was less efficient than that of 1,6-heptadiynes because the longer tether disfavored the formation of metallacyclopentatriene intermediate (Figure 4.2),<sup>8b,12</sup> and this result further supported **Cycle II**.



**Figure 4.2.** Reaction of 1,7-octadiyne derivatives using **HG2**.

To confirm that the decomposed product of Ru-alkylidene catalyzed the cycloaddition to produce dimers, we designed a reaction by taking a residue from the reaction mixture of **HG2** and 1,6-heptadiyne, and reusing it for the catalysis of cycloaddition. First, the reaction of 1,6-heptadiyne<sup>13</sup> and **HG2** produced the oligomer which was easily removed after the precipitation and filtration (Figure 4.3). Then, the filtrate solution containing the decomposed Ru-species and the dimer product of 1,6-heptadiyne was recovered and analyzed by <sup>1</sup>H NMR spectroscopy to confirm that the residue contained no remaining carbene. Gratifyingly, the reaction of this residue and **1a** produced **3a** in 16% conversion and this final result concluded that the decomposed Ru-species promoted the cycloaddition via **Cycle II** to produce the side products. After confirming the correct pathway as **Cycle II**, we could explain all the data in Table 4.1. First, using

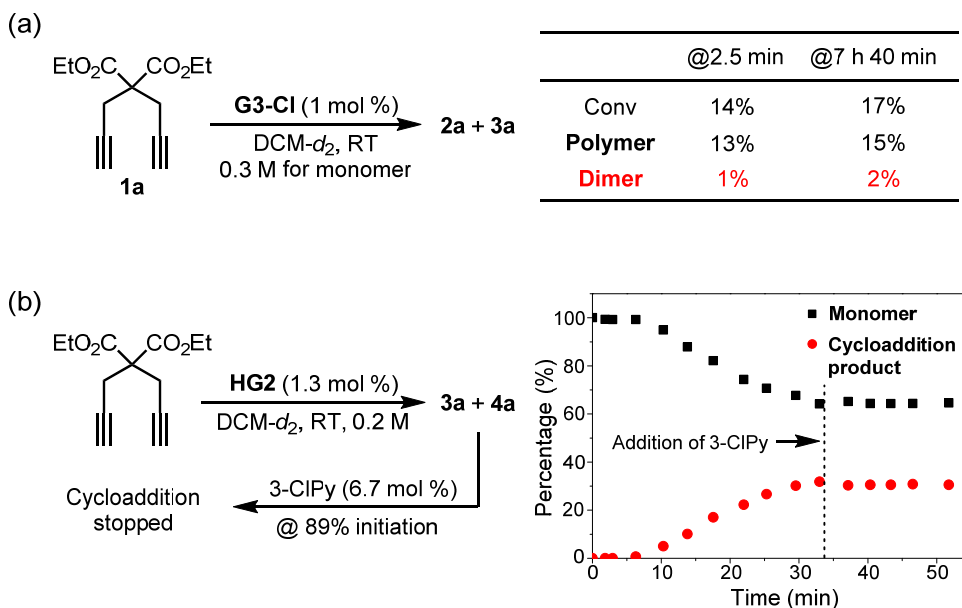
coordinating solvents, such as THF, or pyridine-type additives in non-coordinating solvents effectively suppressed the decomposition of carbene and promoted the efficient polymerization (Table 4.1, entries 1, 4, 5, 7 and 8). Also, the addition of 2,6-Cl<sub>2</sub>BQ, very weakly coordinating or less stabilizing ligand, improved the CP only slightly (Table 4.1, entry 9). Lastly the reaction at a higher temperature in THF induced more dimerization because of more facile decomposition of the catalyst (Table 4.1, entry 6).



**Figure 4.3.** Cycloaddition of **1a** using the residue of 1,6-heptadiyne and **HG2** reaction mixture.

Then we became curious why the dimerization was not observed for the same CP by **G3-Cl**. The CP of **1a** using **G3-Cl** in DCM was more efficient than using **G2** or **HG2**, because **G3-Cl** already contained stabilizing pyridine ligands. However, without additional ligand or coordinating solvent, we did observe the significant decomposition of propagating carbene from **G3-Cl**, resulting in very low conversion (17%, Figure 4.4a). Interestingly, even with long reaction time over 7 h, the decomposed Ru-species, which should promote cycloaddition reaction, poorly produced the dimer from the remaining **1a** (only 2%). In contrast, the same reactions using **HG2** in THF at high temperature (Table 4.1, entry 6) or with the addition of 2,6-Cl<sub>2</sub>BQ in DCM at room temperature (Table 4.1, entry 9) produced large amount of the cycloaddition products, suggesting that the pyridine played a

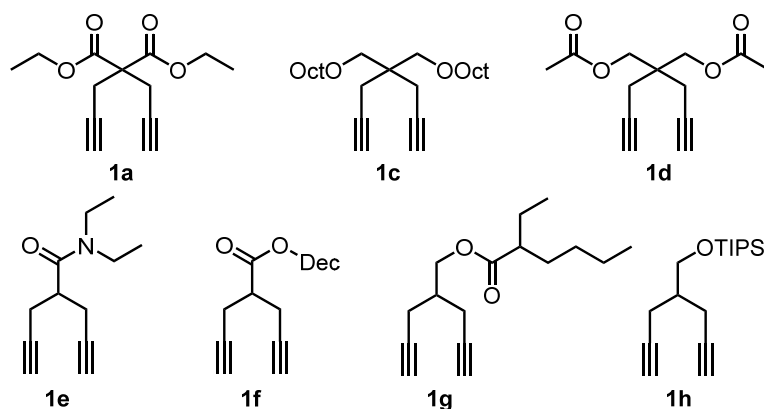
major role in cycloaddition. To confirm this, we monitored the reaction of **1a** and **HG2** in deuterated dichloromethane (DCM- $d_2$ ) before and after adding 3-chloropyridine (3-ClPy) by  $^1\text{H}$  NMR spectroscopy (Figure 4.4b). As the reaction progressed, **1a** was converted to **3a** (and a small amount of **4a**), showing that cycloaddition was dominant. After 35 minutes when 89% of **HG2** initiated, five equiv of 3-ClPy to the catalyst was added to the NMR tube. Then, the cycloaddition immediately stopped, implying that pyridines poisoned or strongly coordinated to the decomposed Ru catalyst that was responsible for the cycloaddition, whereas weakly coordinating THF or 2,6-Cl $_2$ BQ could not. In short, pyridine ligand was essential not only to stabilize the propagating carbene intermediate for CP, but also to suppress the major side reaction, the cycloaddition pathway.



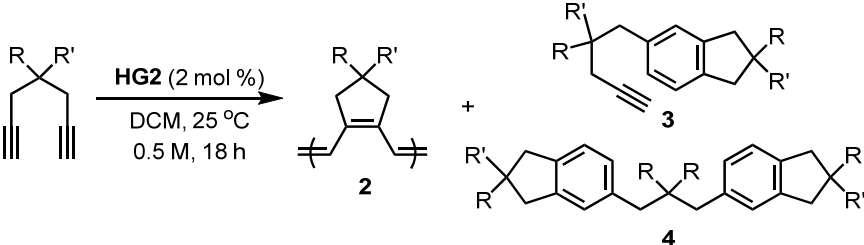
**Figure 4.4.** (a) Poorly occurred cycloaddition in the reaction of **G3-Cl** and **1a**. Conversion and the composition of products were monitored by  $^1\text{H}$  NMR spectroscopy. (b) Monitoring reaction profile change before and after the addition of pyridine in the middle of the reaction.

### 4.3.2. Substituent Effect on Cyclopolymerization and [2+2+2] Cycloaddition

Buchmeiser group reported that using the modified Ru catalysts, monomers containing heteroatoms (nitrogen or oxygen), which would coordinate to the metal, facilitated the dimerization.<sup>2,3</sup> This observation led us to hypothesize that the structure of the monomer and its coordination to a metal would affect both the decomposition of Ru-species and the cycloaddition. Therefore, we screened several 1,6-heptadiyne derivatives containing different substituents to monitor structure-reactivity relationship by altering electronic and steric nature of substituents (Figure 4.5, **1a–1h**). Similar to the entry 1 in Table 4.1, reactions of **HG2** and these monomers in DCM were investigated with an extended reaction time of 18 h (Table 4.2).



**Figure 4.5.** Structures of 1,6-heptadiyne derivatives (**1a–1h**) screened using **HG2**.

**Table 4.2. Monomer screening in CP using HG2**


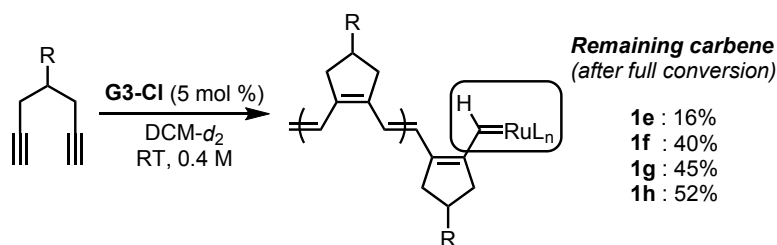
entry	monomer	<b>2</b> <sup>a</sup> (%)	<b>3</b> <sup>a</sup> (%)	<b>4</b> <sup>a</sup> (%)	conv <sup>a</sup>
1	<b>1a</b>	2	51	39	>99
2	<b>1c</b>	5	19	0	33
3	<b>1d</b>	7	44	0	66
4	<b>1e</b>	14	42	44	>99
5	<b>1f</b>	37	32	22	>99
6	<b>1g</b>	>99	0	0	>99
7	<b>1h</b>	>99	0	0	>99

<sup>a</sup> Calculated from <sup>1</sup>H NMR spectra.

In general, bis-substituted compounds (**1a**, **1c**, **1d**) showed poor efficiencies in CP, favoring the cycloaddition (Table 4.2, entries 1–3). However, the efficiencies slightly increased (**1d** (7%) > **1c** (5%) > **1a** (2%)) with inverse proportional to donating ability of the lone pair of oxygen. Indeed, the carbonyl oxygen on  $\alpha$ -position of **1a** has stronger coordinating ability than other monomers, whereas the carbonyl oxygen on the  $\delta$ -position (**1d**) is far from the metal center, thereby weakening the coordination. Surprisingly, mono-substituted monomers (**1e–1h**) resulted in much more efficient CP than bis-substituted monomers (Table 4.2, entries 4–7). The strongest coordinating amide produced the least amount of **2e** (14%) and large amounts of **3e** (42%) and **4e** (44%) (Table 4.2, entry 4). Then, CP of less coordinating **1f** improved to 37%, and its cycloaddition products relatively decreased (32% for **3f**; 22% for **4f**) (Table 4.2, entry 5). Remarkably, **1g** containing a distant carbonyl group and **1h** containing a sterically hindered triisopropyl silyl (TIPS) protecting group were exclusively cyclopolymerized with no side product (Table 4.2, entries 6 and 7). It was notable that these were the first examples of the

successful CP catalyzed by **HG2** in DCM. Through in-depth investigation of coordinating substituents, we concluded that the cycloaddition was favored with the increase in strength and the number of the coordinating group.

To understand how the coordination affected the efficiency of CP, we quantified the remaining percentages of the propagating carbenes for each monomer (Figure 4.6, **1e–1h**). The fast-initiating **G3-Cl** was used instead of **HG2**, because signals from the propagating 14-electron Ru-alkylidenes from **HG2** were undetectable in  $^1\text{H}$  NMR spectroscopy.<sup>14</sup> The remaining carbene% in DCM- $d_2$  after full monomer conversion was lowest for **1e**, and increased according to the efficiency of CP in Table 4.2. This showed that the functional groups on the monomers indeed affected the decomposition of the propagating carbene, thereby decreasing the efficiency of CP and increasing the preference for cycloaddition.



**Figure 4.6.** Comparison of remaining carbene% after the CP of **1e–1h**.

Now, it became clear that suppressing the carbene decomposition was the most important factor to enhance the CP and reduce the cycloaddition. For the improvement of CP under the ligand-free system, the temperature was lowered to 0 °C, and the TON of **1c** for CP increased from 2.5 at room temperature to 22.5 to give a polymer with  $M_n = 8.6$  k (Table 4.3, entry 1 and entry 2). Among the mono-substituted monomers, the CP of **1f** which originally preferred cycloaddition products at room temperature, now produced high molecular weight polymer exclusively with TON of at least 48 at 0 °C, or even up to TON at least 95 (Table 4.3, entries 5 and 6).<sup>15</sup> These results address that reaction conditions could be

optimized to maximize the CP even with **HG2** in DCM.

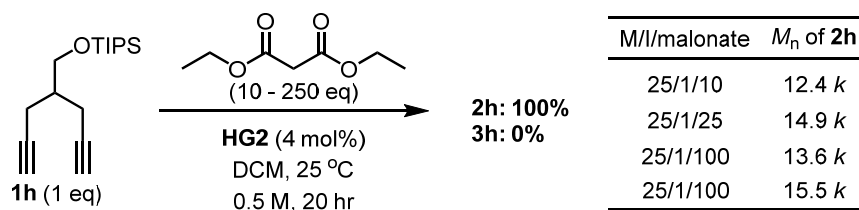
**Table 4.3. Enhancement of CP under low temperature**

entry	mono- mer	M/I	temp (°C)	time (h)	<b>2</b> <sup>a</sup> (%)	<b>3</b> <sup>a</sup> (%)	<b>4</b> <sup>a</sup> (%)	TON of <b>2</b>	<i>M<sub>n</sub></i> of <b>2</b> (kDa) (PDI) <sup>b</sup>	conv <sup>a</sup> (%)
1 <sup>c</sup>	<b>1c</b>	50	RT	18	5	19	0	2.5	-	33
2	<b>1c</b>	50	0	8	45	17	0	22.5	8.6 (2.84)	77
3 <sup>d</sup>	<b>1f</b>	50	RT	18	37	32	22	18.5	-	>99
4	<b>1f</b>	50	0	5	≥95	0	0	≥48	17.6 (4.80)	>99
5	<b>1f</b>	100	0	5	≥95	0	0	≥95	15.1 (4.82)	>99

<sup>a</sup>Calculated from <sup>1</sup>H NMR spectra. <sup>b</sup>Determined by CHCl<sub>3</sub> SEC calibrated using polystyrene (PS) standards. <sup>c</sup>Result of entry 2 of Table 4.2. <sup>d</sup>Result of entry 5 of Table 4.2.

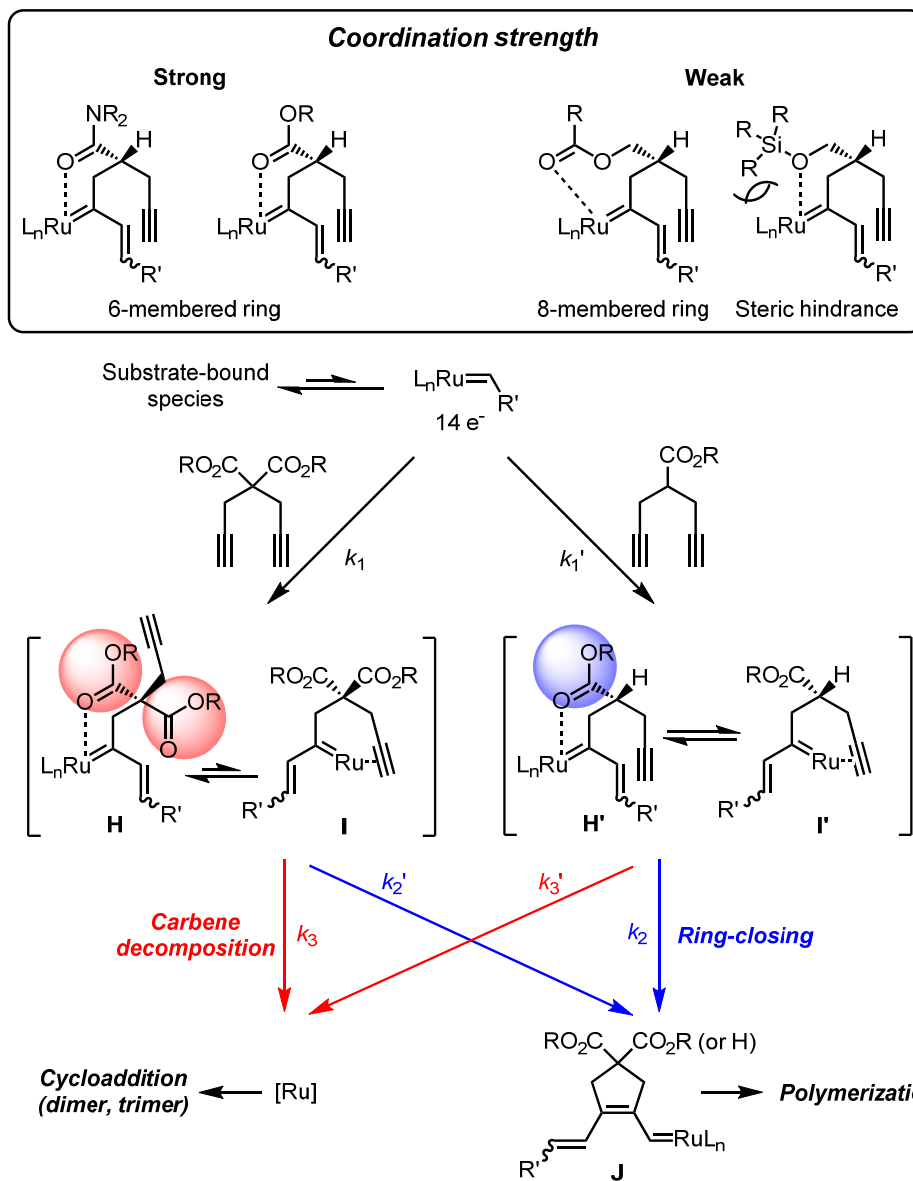
We became curious how electronic and steric properties of the substituents influenced the carbene decomposition. The first hypothesis was the possibility of intermolecular coordination of the substituents to the metal carbene, and this was easily checked by adding 10 to 250 equivalent of diethyl malonate (DEM) to the **HG2** during CP of **1h**, the most productive monomer (Figure 4.7). However, the ratio of the products and molecular weights of **2h** did not decrease even with increasing amount of DEM, so we could rule out the poisoning the catalyst by intermolecular coordination of the carbonyl group. Alternatively, an intramolecular coordination or chelation in the intermediate states (**H** or **H'**, Scheme 4.7) might facilitate the decomposition of the carbenes. For instance, for propagation, a ring closing reaction should occur from 1,1-disubstituted Ru-carbene intermediate by binding to the other alkyne (**I** or **I'**), but this step would be retarded for the monomers containing carbonyl groups, which could form a stable chelate of the six-membered ring (**H** or **H'**). Therefore, the longer the intermediates

were trapped as the chelated **H** or **H'**, the slower the propagation and the faster catalyst decomposition occurred. For the bis-substituted monomers (**1a–1d**), chelation state (**H**) could be more dominant, retarding the ring closing of **I** to **J**, while the mono-substituted monomers would have less chelation, thereby promoting faster propagation ( $k_2'$ ). In addition, the stronger chelation of electron-rich carbonyl groups (**1e** and **1f**) could favor chelation, while an eight-membered chelation for **1g** and sterically bulky ether in **1h** would disfavor the chelation, thereby enhancing the CP pathway ( $k_2'$ ). This also explains why we could achieve successful CP by **HG2** for the first time in THF because that monomer resembled **1g** in Figure 4.5 (see Chapter 5).<sup>1</sup> In short, the chelation of the carbonyl vs. alkyne coordination determined the competition between the propagation of CP ( $k_2$  or  $k_2'$ ) and the carbene decomposition ( $k_3$  or  $k_3'$ ) leading to the cycloaddition pathway. This model gives an insight into the correlation between the monomer structure and the carbene decomposition, and explains why the cycloaddition pathway was favored over CP in cases of the strong chelation such as **1a**. Now we can finally understand why the previous CP of 1,6-heptadiynes was unsuccessful using **HG2**, and what actually happened, especially for the most common monomer, **1a**.



**Figure 4.7.** Addition of diethyl malonate to the CP of **1h**.





**Scheme 4.7.** Proposed model showing how substituents effect by intramolecular coordination influenced the reactions

## 4.4. Conclusion

It was investigated what happened during the intended CP of 1,6-heptadiyne derivatives catalyzed by Grubbs catalysts and how the cycloaddition, the major side reaction producing dimers and trimers of the monomers occurred. Conclusions of these studies shed a light on why **G2** or **HG2** could not cyclopolymerize 1,6-heptadiyne derivatives, and, indeed, the actual products of the attempted reactions were dimers and trimers of diynes instead of polymers. The structure of monomers, catalysts, solvents, temperature, and additives influenced the two competing pathway of CP and cycloaddition to give the different ratio of conjugated polymers and the side products. Based on these observations, detailed mechanistic studies disclosed that, in fact, the decomposed Ru-carbene catalyzed the critical dimerization by [2+2+2] cycloaddition of alkynes, rather than the previously proposed olefin metathesis pathway. Therefore, minimizing the carbene decomposition from **HG2** using weakly coordinating agents, such as pyridine ligands in DCM, could suppress the cycloaddition, thereby leading to successful cyclopolymerization of the various 1,6-heptadiynes, especially **1a** and **1b**, which had been known to be failed. In addition, pyridine was such an excellent additive because it suppressed not only the carbene decomposition, but also the cycloaddition pathway. Therefore, why CP using **G3-Cl** containing pyridine ligand did not produce dimers even in non-stabilizing solvents like DCM was rationalized. Furthermore, the efficiency of CP was highly dependent on the substituents of 1,6-heptadiyne monomers, because the degree of coordination of those substituents or chelation retarded polymerization, thus, led to the decomposition of the active carbenes. Although these studies clarified why **HG2** was a poor catalyst for the CP of 1,6-heptadiynes in non-coordinating solvents, by understanding the detailed mechanism, one could modify the experimental conditions or monomer structures to minimize the side-reaction and maximize the efficiency of CP.

## 4.5. Experimental Section

### Characterization

$^1\text{H}$  NMR and  $^{13}\text{C}$  NMR spectra were recorded by Varian/Oxford As-500 (500 MHz for  $^1\text{H}$  and 125 MHz for  $^{13}\text{C}$ ) spectrometer and Agilent 400-MR (400 MHz for  $^1\text{H}$ ). Chloroform size exclusion chromatography (SEC) analyses were carried out with Waters system (515 pump, 2410 refractive index detector), Viscotek 270 dual detector, and Shodex GPC LF-804 column on samples diluted in chloroform (0.001-0.003 wt%; HPLC grade, J. T. Baker<sup>®</sup>) and filtered with a 0.2  $\mu\text{m}$  PTFE filter (Whatman<sup>®</sup>). Flow rate was 1.0 mL/min and temperature of column was maintained at 35 °C. The SEC data were analyzed using OmniSEC 4.2 (Viscotek).

### Materials

All reactions were carried out under dry argon atmospheres using standard Schlenk-line techniques. All reagents which are commercially available from Sigma-Aldrich<sup>®</sup>, Tokyo Chemical Industry Co. Ltd., Acros Organics, and Alfa Aesar<sup>®</sup>, without additional notes, were used without further purification. **1a**,<sup>16</sup> **1c**,<sup>3</sup> **1d**,<sup>17</sup> **5a**,<sup>18</sup> and **5b**,<sup>19</sup> were prepared by literature methods, and **1a'**, **1b**, **1g**, and **G3-Cl** was prepared as described in Chapter 2. Dichloromethane (DCM) for the polymerization was purified by Glass Contour Organic Solvent Purification System, and tetrahydrofuran (THF) for the polymerization was distilled from sodium and benzophenone. Both were degassed further by Ar bubbling for 10 minutes before performing reactions. Thin-layer chromatography (TLC) was carried out on MERCK TLC silica gel 60 F254 and flash column chromatography was performed using MERCK silica gel 60 (0.040~0.063 mm). For SEC analysis, HPLC grade chloroform was purchased from J. T. Baker<sup>®</sup>.  $\text{CDCl}_3$  (99.50% D) and  $\text{DCM-}d_2$  (99.90% D, 0.75mL) were purchased from Euriso-top<sup>®</sup> and used without further purification.

## Synthesis

### 4-(1,6-Heptadiyne)-*N,N*-diethylformamide (1e)

4-Carboxy-1,6-heptadiyne<sup>20</sup> (441.8 mg, 3.25 mmol) was added to a 50-mL round-bottom flask containing a magnetic stirring bar, and the flask was purged with argon. DCM (10 mL) was added and the mixture was cooled down to 0 °C. A solution of oxalyl chloride (2.0 M in DCM, 2.43 mL, 4.87 mmol) was added, and 2 drops of DMF was added under the control of atmospheric pressure. Generated CO<sub>2</sub> gas was trapped by a balloon. The reaction mixture was stirred for 2 hours at room temperature, and concentrated to give yellow colored liquid. After this flask was filled with argon, DCM (10 mL), diethylamine (0.41 mL, 3.99 mmol) and triethylamine (0.56 mL, 3.99 mmol) were added. After stirring 2 h at room temperature, the reaction was quenched by saturated NaHCO<sub>3</sub> aqueous solution. The organic layer was washed with water and extracted by ethyl acetate, dried over MgSO<sub>4</sub>, and concentrated. The product was purified by flash column chromatography on silica gel (gradient elution: EtOAc:hexane = 1:10 to 1:5) to afford the compound as colorless liquid (569.6 mg, 2.98 mmol, 91.8%). <sup>1</sup>H NMR (500 MHz, CDCl<sub>3</sub>) δ 3.43 (dq, *J* = 9.4, 7.2 Hz, 4H), 3.10 – 3.02 (m, 1H), 2.55 – 2.44 (m, 4H), 1.99 (t, *J* = 2.7 Hz, 2H), 1.24 (t, *J* = 7.2 Hz, 3H), 1.13 (t, *J* = 7.1 Hz, 3H); <sup>13</sup>C NMR (125 MHz, CDCl<sub>3</sub>) δ 171.92, 171.90, 81.53, 70.17, 42.40, 40.93, 39.81, 21.97, 15.10, 13.17; HRMS (ESI): *m/z* for C<sub>12</sub>H<sub>17</sub>NNaO [M+Na]<sup>+</sup>, calcd. 214.1202, found: 214.1201.

### 4-(Decylcarboxy)-1,6-heptadiyne (1f)

4-Carboxy-1,6-heptadiyne<sup>20</sup> (305.0 mg, 2.24 mmol) was added to a 50-mL round-bottom flask containing a magnetic stirring bar, and the flask was purged with argon. DCM (8 mL) was added and the mixture was cooled down to 0 °C. A solution of oxalyl chloride (2.0 M in DCM, 1.46 mL, 2.91 mmol) was added, and 2 drops of DMF was added under the control of atmospheric pressure. Generated CO<sub>2</sub> gas was trapped by a balloon. The reaction mixture was stirred for 2 h at room

temperature, and concentrated to give a yellow colored liquid. After this flask was filled with argon, DCM (8 mL), n-decanol (0.56 mL, 2.91 mmol) and triethylamine (0.81 mL, 5.82 mmol) were added. After stirring overnight at room temperature, the reaction was quenched with saturated NaHCO<sub>3</sub> aqueous solution. The organic layer was washed with water and extracted with ethyl acetate, dried with MgSO<sub>4</sub>, and concentrated. The product was purified by flash column chromatography on silica gel (ethyl acetate:hexane = 1:50) to afford the compound as colorless liquid (536.7 mg, 1.94 mmol, 86.7%) <sup>1</sup>H NMR (400 MHz, CDCl<sub>3</sub>) δ 4.13 (t, *J* = 6.7 Hz, 2H), 2.76 (m, 1H), 2.70 – 2.58 (m, 4H), 2.01 (t, *J* = 2.6 Hz, 2H), 1.68 – 1.60 (m, 2H), 1.40 – 1.18 (m, 14H), 0.88 (t, *J* = 6.9 Hz, 3H); <sup>13</sup>C NMR (125 MHz, CDCl<sub>3</sub>) δ 172.51, 80.65, 70.60, 65.39, 43.20, 32.03, 29.67, 29.67, 29.45, 29.35, 28.73, 26.01, 22.82, 20.05, 14.26; HRMS (ESI): *m/z* for C<sub>18</sub>H<sub>28</sub>NaO<sub>2</sub> [M+Na]<sup>+</sup>, calcd. 299.1982, found: 299.1983.

#### **4-(Triisopropylsilyloxy)-methyl-1,6-heptadiyne (1h)**

Triisopropylsilyl trifluoromethanesulfonate (2.43 mL, 9.02 mmol) was added to the mixture of 4-hydroxymethyl-1,6-heptadiyne<sup>21</sup> (919 mg, 7.52 mmol), TEA (3.14 mL, 22.6 mmol), and DMAP (45.9 mg, 0.376 mmol) dissolved by DCM (24 mL) in 100-mL round-bottom flask at 0°C. The mixture was stirred for 5 hours at room temperature then saturated NaHCO<sub>3</sub> aqueous solution was added. The mixture was washed with NH<sub>4</sub>Cl aqueous solution and extracted by ethyl acetate. The organic layer was dried with MgSO<sub>4</sub> and concentrated. It was purified by flash column chromatography on silica gel (hexane only) to afford compound as a colorless liquid (1.94 mg, 6.96 mmol, 92.5%). <sup>1</sup>H NMR (400 MHz, CDCl<sub>3</sub>) δ 3.76 (d, *J* = 5.5 Hz, 2H), 2.43 – 2.31 (m, 4H), 1.97 (t, *J* = 2.7 Hz, 2H), 1.95 (m, 1H), 1.13 – 1.03 (m, 21H); <sup>13</sup>C NMR (125 MHz, CDCl<sub>3</sub>) δ 82.47, 69.73, 64.11, 40.06, 19.70, 18.15, 12.12; HRMS (ESI):

## General procedure for the reaction of 1,6-heptadiyne derivatives and Grubbs catalysts

Monomer (0.100 mmol) and a magnetic bar were added to a 4-mL vial with a cap containing PTFE-silicon septum. Dry solvent (0.10 mL) was added after the vial was purged with argon three times, and the solution of catalyst (0.1 mL) prepared from the inert atmosphere was rapidly injected at given temperature. The reaction was quenched by excess ethyl vinyl ether (0.2 mL) after desired reaction time, and dried under vacuum. The ratio of products was calculated from crude  $^1\text{H}$  NMR, and then, the mixture was precipitated in methanol (10 mL). The polymer was filtered, and dimer and trimer were purified from the filtrate by flash column chromatography on silica gel.

## Characterization of polymers

The spectroscopic data of **2a**,<sup>22</sup> poly(**5a**)<sup>11</sup> and poly(**5b**)<sup>19</sup> were reported in the literature. For **2a'**, **2b**, **2c**, **2d**, **2g**; see Chapter 2.

**2e**:  $^1\text{H}$  NMR (500 MHz,  $\text{CD}_2\text{Cl}_2$ )  $\delta$  6.90 – 6.07 (br, 2H), 3.42 (br, 5H), 3.15 – 2.52 (br, 4H), 1.39 – 0.94 (br, 6H);  $^{13}\text{C}$  NMR (125 MHz,  $\text{CD}_2\text{Cl}_2$ )  $\delta$  174.61, 138.96, 123.57, 42.62, 40.91, 38.66, 38.22, 15.23, 13.46.

**2f**:  $^1\text{H}$  NMR (500 MHz,  $\text{CDCl}_3$ )  $\delta$  7.13 – 5.83 (br, 2H), 4.34 – 3.69 (br, 2H), 3.14 (br, 4H), 1.71 (br, 2H), 1.27 (br, 14H), 0.87 (d,  $J = 6.6$  Hz, 3H);  $^{13}\text{C}$  NMR (125 MHz,  $\text{CDCl}_3$ )  $\delta$  175.86, 138.30, 123.28, 65.19, 40.43, 37.37, 32.02, 29.68, 29.43, 29.40, 28.81, 26.03, 22.80, 14.23.

**2h**:  $^1\text{H}$  NMR (500 MHz,  $\text{CDCl}_3$ )  $\delta$  7.00 – 5.96 (br, 2H), 3.95 – 3.29 (br, 2H), 3.04 – 1.80 (br, 5H), 1.47 – 0.50 (br, 21H);  $^{13}\text{C}$  NMR (125 MHz,  $\text{CDCl}_3$ )  $\delta$  139.17, 123.27, 67.60, 38.30, 36.55, 18.22, 12.25.

### Characterization of dimers (3) and trimers (4)

The spectroscopic data of **3a**<sup>23</sup> and **3c**<sup>3</sup> were reported in the literature.

**4a**: <sup>1</sup>H NMR (500 MHz, CDCl<sub>3</sub>) δ 7.08 (d, *J* = 7.6 Hz, 2H), 6.96 (d, *J* = 10.3 Hz, 4H), 4.19 (q, *J* = 7.1 Hz, 8H), 4.08 (q, *J* = 7.1 Hz, 4H), 3.54 (d, *J* = 3.0 Hz, 8H), 3.15 (s, 4H), 1.25 (t, *J* = 7.1 Hz, 12H), 1.14 (t, *J* = 7.1 Hz, 6H); <sup>13</sup>C NMR (125 MHz, CDCl<sub>3</sub>) δ 171.76, 171.13, 140.16, 138.76, 135.22, 129.01, 126.08, 124.01, 61.82, 61.32, 60.61, 60.42, 40.55, 40.33, 39.17, 14.17, 14.03.; HRMS (ESI): *m/z* for C<sub>39</sub>H<sub>48</sub>NaO<sub>12</sub> [M+Na]<sup>+</sup>, calcd. 731.3038, found: 731.3040.

**3b**: <sup>1</sup>H NMR (500 MHz, CDCl<sub>3</sub>) δ 7.07 (d, *J* = 7.6 Hz, 1H), 6.99 (s, 1H), 6.94 (d, *J* = 7.7 Hz, 1H), 4.19 – 4.05 (m, 8H), 3.53 (s, 4H), 3.34 (s, 2H), 2.66 (d, *J* = 2.0 Hz, 2H), 2.12 (t, *J* = 2.2 Hz, 1H), 1.66 – 1.57 (m, 8H), 1.29 (d, *J* = 4.5 Hz, 24H), 0.88 (dd, *J* = 6.9, 2.2 Hz, 12H); <sup>13</sup>C NMR (125 MHz, CDCl<sub>3</sub>) δ 171.80, 169.87, 140.47, 139.10, 134.48, 128.69, 125.75, 124.23, 79.61, 72.22, 66.00, 60.71, 58.40, 40.58, 40.39, 37.28, 31.50, 28.57, 28.55, 25.65, 25.59, 22.67, 22.66, 22.30, 14.13; HRMS (ESI): *m/z* for C<sub>42</sub>H<sub>64</sub>NaO<sub>8</sub> [M+Na]<sup>+</sup>, calcd. 719.4493, found: 719.4490.

**4b**: <sup>1</sup>H NMR (500 MHz, CDCl<sub>3</sub>) δ 7.07 (d, *J* = 7.7 Hz, 2H), 6.98 – 6.92 (m, 4H), 4.12 (t, *J* = 6.7 Hz, 8H), 3.99 (t, *J* = 6.7 Hz, 4H), 3.53 (d, *J* = 3.1 Hz, 8H), 3.15 (s, 4H), 1.66 – 1.58 (m, 8H), 1.54 – 1.46 (m, 4H), 1.28 (m, 36H), 0.88 (m, 18H); <sup>13</sup>C NMR (125 MHz, CDCl<sub>3</sub>) δ 171.82, 171.20, 140.20, 138.77, 135.24, 129.00, 126.04, 124.01, 66.00, 65.55, 60.73, 60.52, 40.59, 40.38, 39.19, 31.54, 31.51, 28.58, 28.42, 25.71, 25.60, 22.66, 14.13; HRMS (ESI): *m/z* for C<sub>63</sub>H<sub>96</sub>NaO<sub>12</sub> [M+Na]<sup>+</sup>, calcd. 1067.6794, found: 1067.6761.

**3d**: <sup>1</sup>H NMR (500 MHz, CDCl<sub>3</sub>) δ 7.08 (d, *J* = 7.6 Hz, 1H), 7.01 – 6.94 (m, 2H), 4.08 (s, 4H), 3.97 (dd, *J* = 31.0, 11.2 Hz, 4H), 2.85 (d, *J* = 5.6 Hz, 4H), 2.75 (s, 2H), 2.17 (d, *J* = 2.5 Hz, 2H), 2.07 (d, *J* = 14.5 Hz, 12H); <sup>13</sup>C NMR (125 MHz, CDCl<sub>3</sub>) δ 171.16, 170.76, 141.30, 139.62, 134.27, 129.07, 126.86, 124.91, 79.82, 72.18, 66.87, 65.11, 46.63, 41.04, 38.86, 38.56, 36.81, 21.85, 20.99; HRMS (ESI): *m/z* for C<sub>26</sub>H<sub>32</sub>NaO<sub>8</sub> [M+Na]<sup>+</sup>, calcd. 495.1989, found: 495.1988.

**4d:**  $^1\text{H}$  NMR (500 MHz,  $\text{CDCl}_3$ )  $\delta$  7.06 (d,  $J$  = 7.4 Hz, 2H), 6.87 (d,  $J$  = 8.2 Hz, 4H), 4.08 (s, 8H), 3.83 (s, 4H), 2.84 (s, 8H), 2.72 (s, 4H), 2.11 (s, 6H), 2.06 (s, 12H);  $^{13}\text{C}$  NMR (125 MHz,  $\text{CDCl}_3$ )  $\delta$  171.18, 170.79, 141.18, 139.39, 135.17, 129.16, 126.98, 124.82, 66.89, 65.55, 46.62, 41.48, 39.19, 38.85, 38.58, 21.12, 21.01; HRMS (ESI):  $m/z$  for  $\text{C}_{39}\text{H}_{48}\text{NaO}_{12}$   $[\text{M}+\text{Na}]^+$ , calcd. 731.3038, found: 731.3036.

**3e:**  $^1\text{H}$  NMR (500 MHz,  $\text{CDCl}_3$ )  $\delta$  7.06 (dd,  $J$  = 13.0, 7.5 Hz, 1H), 7.02 – 6.91 (m, 2H), 3.52 – 3.36 (m, 6H), 3.31 – 3.10 (m, 3H), 3.07 – 2.85 (m, 6H), 2.83 – 2.76 (m, 1H), 2.59 – 2.52 (m, 1H), 2.40 – 2.33 (m, 1H), 1.98 – 1.96 (m, 1H), 1.22 (td,  $J$  = 7.1, 1.4 Hz, 3H), 1.13 (t,  $J$  = 7.1 Hz, 3H), 1.02 (q,  $J$  = 7.2 Hz, 3H), 0.94 (dt,  $J$  = 11.0, 7.2 Hz, 3H);  $^{13}\text{C}$  NMR ; HRMS (ESI):  $m/z$  for  $\text{C}_{24}\text{H}_{34}\text{N}_2\text{NaO}_2$   $[\text{M}+\text{Na}]^+$ , calcd. 405.2512, found: 405.2513.

**4e:**  $^1\text{H}$  NMR (500 MHz,  $\text{CDCl}_3$ )  $\delta$  7.05 (t,  $J$  = 7.7 Hz, 2H), 6.99 (s, 2H), 6.96 – 6.92 (m, 2H), 3.51 – 3.36 (m, 10H), 3.31 – 3.16 (m, 6H), 3.06 – 2.87 (m, 7H), 2.74 – 2.61 (m, 4H), 1.24 – 1.20 (m, 6H), 1.14 (t,  $J$  = 7.1 Hz, 6H), 0.97 – 0.90 (m, 3H), 0.62 – 0.55 (m, 3H);  $^{13}\text{C}$  NMR ; HRMS (ESI):  $m/z$  for  $\text{C}_{36}\text{H}_{51}\text{N}_3\text{NaO}_3$   $[\text{M}+\text{Na}]^+$ , calcd. 596.3823, found: 596.3822.

**3f:**  $^1\text{H}$  NMR (500 MHz,  $\text{CDCl}_3$ )  $\delta$  7.11 (d,  $J$  = 7.6 Hz, 1H), 7.03 (s, 1H), 6.97 (d,  $J$  = 7.6 Hz, 1H), 4.14 – 4.01 (m, 4H), 3.36 – 3.27 (m, 1H), 3.26 – 3.11 (m, 4H), 3.03 – 2.85 (m, 2H), 2.86 – 2.78 (m, 1H), 2.48 – 2.36 (m, 2H), 2.02 (t,  $J$  = 2.5 Hz, 1H), 1.68 – 1.52 (m, 4H), 1.26 (s, 28H), 0.88 (t,  $J$  = 6.6 Hz, 6H);  $^{13}\text{C}$  NMR (125 MHz,  $\text{CDCl}_3$ )  $\delta$  175.45, 173.90, 142.15, 140.10, 137.02, 127.56, 125.09, 124.39, 81.47, 70.38, 65.02, 46.52, 44.02, 36.83, 36.26, 36.04, 32.05, 29.69, 29.68, 29.67, 29.46, 29.40, 29.38, 28.81, 28.73, 26.07, 26.01, 22.83, 20.60, 14.26; HRMS (ESI):  $m/z$  for  $\text{C}_{36}\text{H}_{56}\text{NaO}_4$   $[\text{M}+\text{Na}]^+$ , calcd. 575.4071, found: 575.4073.

**4f:**  $^1\text{H}$  NMR (500 MHz,  $\text{CDCl}_3$ )  $\delta$  7.09 (d,  $J$  = 7.6 Hz, 2H), 6.99 (s, 2H), 6.94 (d,  $J$  = 7.6 Hz, 2H), 4.11 (t,  $J$  = 6.7 Hz, 4H), 3.90 (t,  $J$  = 6.6 Hz, 2H), 3.35 – 3.26 (m, 2H), 3.25 – 3.10 (m, 8H), 2.95 – 2.87 (m, 3H), 2.74 (d,  $J$  = 8.6 Hz, 2H), 1.68 – 1.60

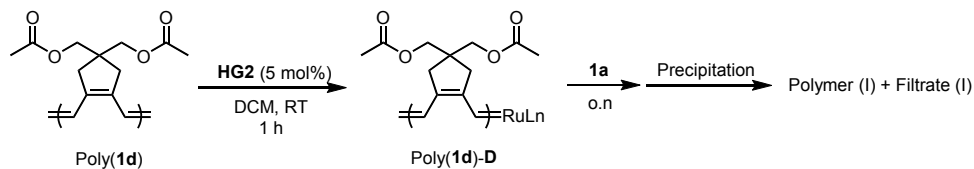


(m, 4H), 1.44 – 1.07 (m, 44H), 0.88 (t,  $J = 6.9$  Hz, 9H);  $^{13}\text{C}$  NMR (125 MHz,  $\text{CDCl}_3$ )  $\delta$  175.47, 175.20, 142.01, 139.81, 137.76, 127.44, 124.95, 124.27, 64.98, 64.55, 50.07, 44.03, 38.26, 36.25, 36.02, 32.04, 29.71, 29.67, 29.47, 29.45, 29.40, 28.80, 28.64, 26.06, 25.93, 22.83, 14.27; HRMS (ESI):  $m/z$  for  $\text{C}_{54}\text{H}_{84}\text{NaO}_6$   $[\text{M}+\text{Na}]^+$ , calcd. 851.6160, found: 851.6158.

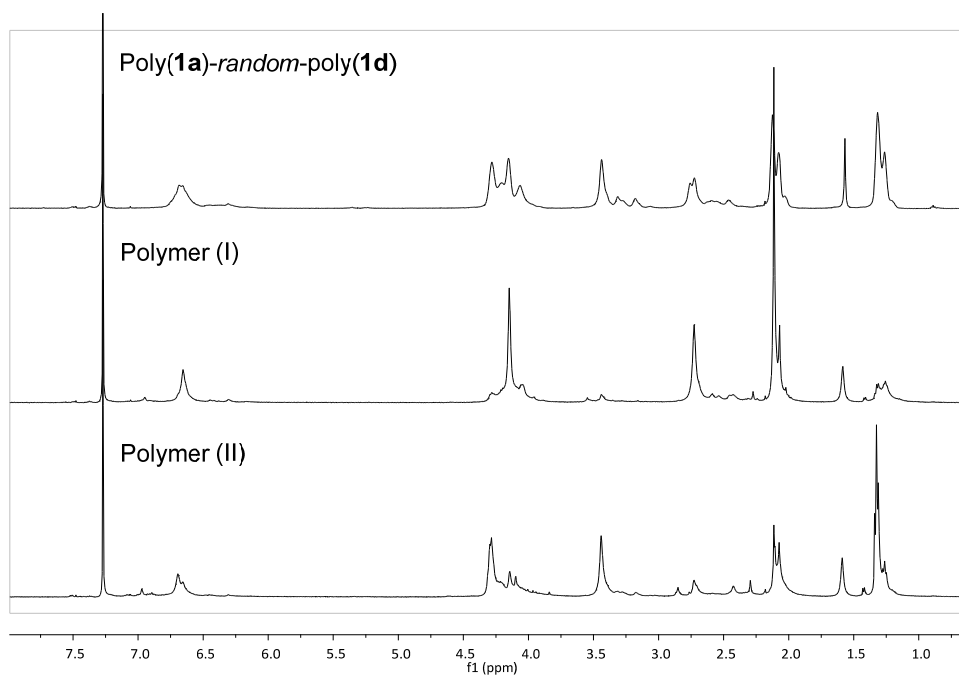
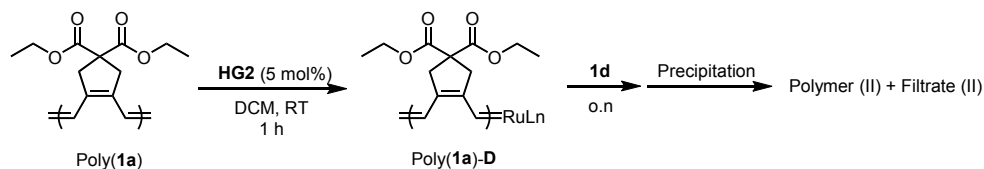
## 4.6. Supporting Information

### Cross-over experiments

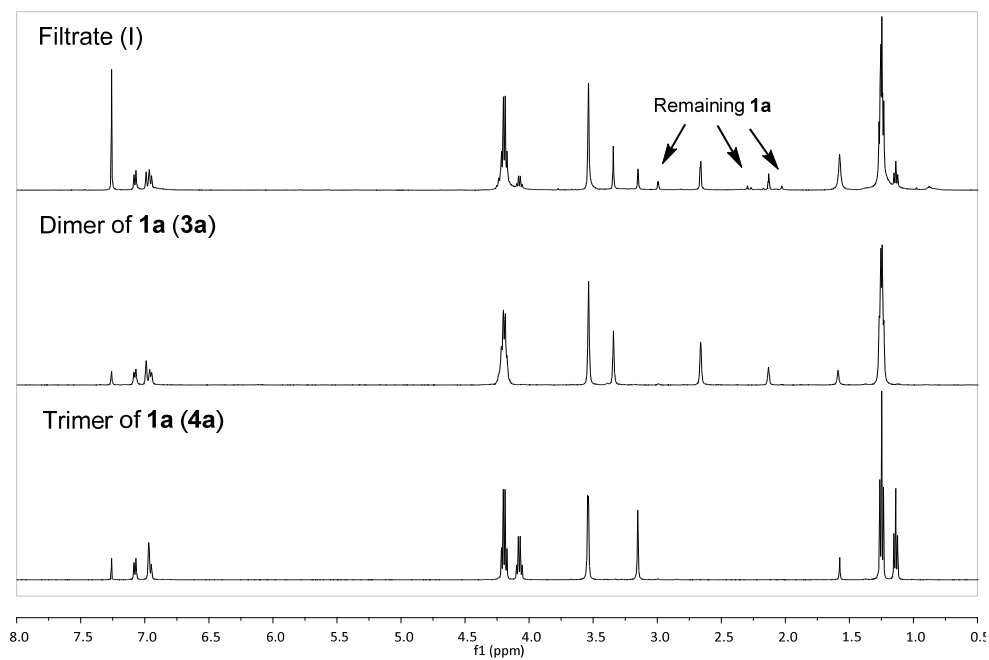
#### Reaction (I)



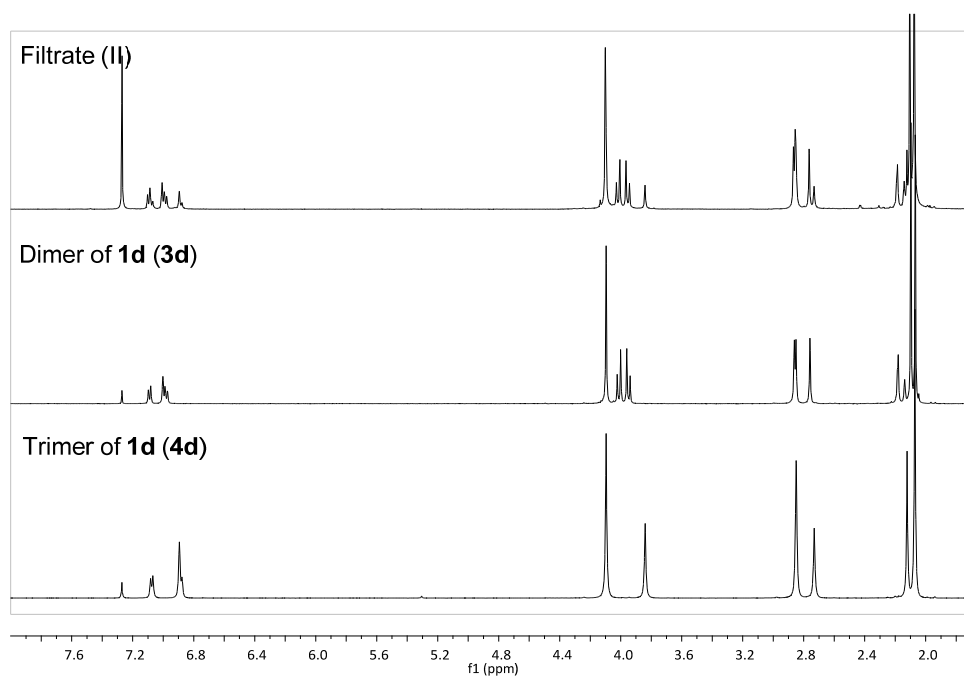
#### Reaction (II)



**Figure S4.1.** <sup>1</sup>H NMR spectra of copolymer (poly(**1a**)-*ran*-poly(**1d**)), polymer (I), and polymer (II).



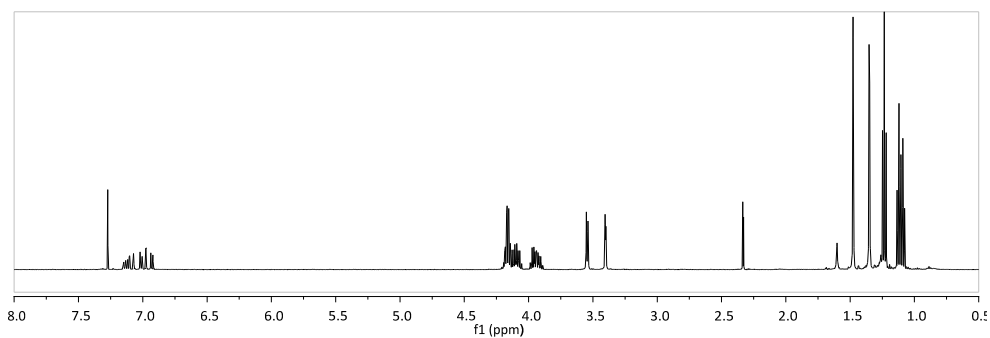
**Figure S4.2.**  $^1\text{H}$  NMR spectra of filtrate from reaction (I), **3a**, and **4a**.



**Figure S4.3.**  $^1\text{H}$  NMR spectra of filtrate from reaction (II), **3d**, and **4d**.

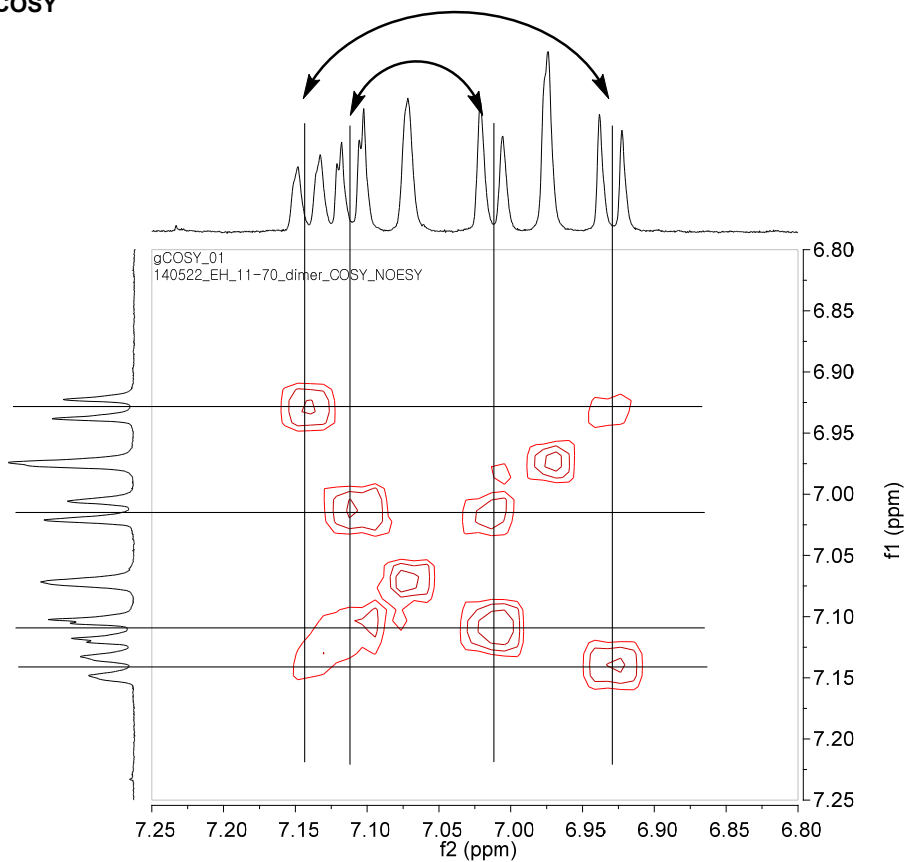
## Characterization of mixture of 3a'-i and 3a'-ii

### (1) $^1\text{H}$ and 2D NMR analysis



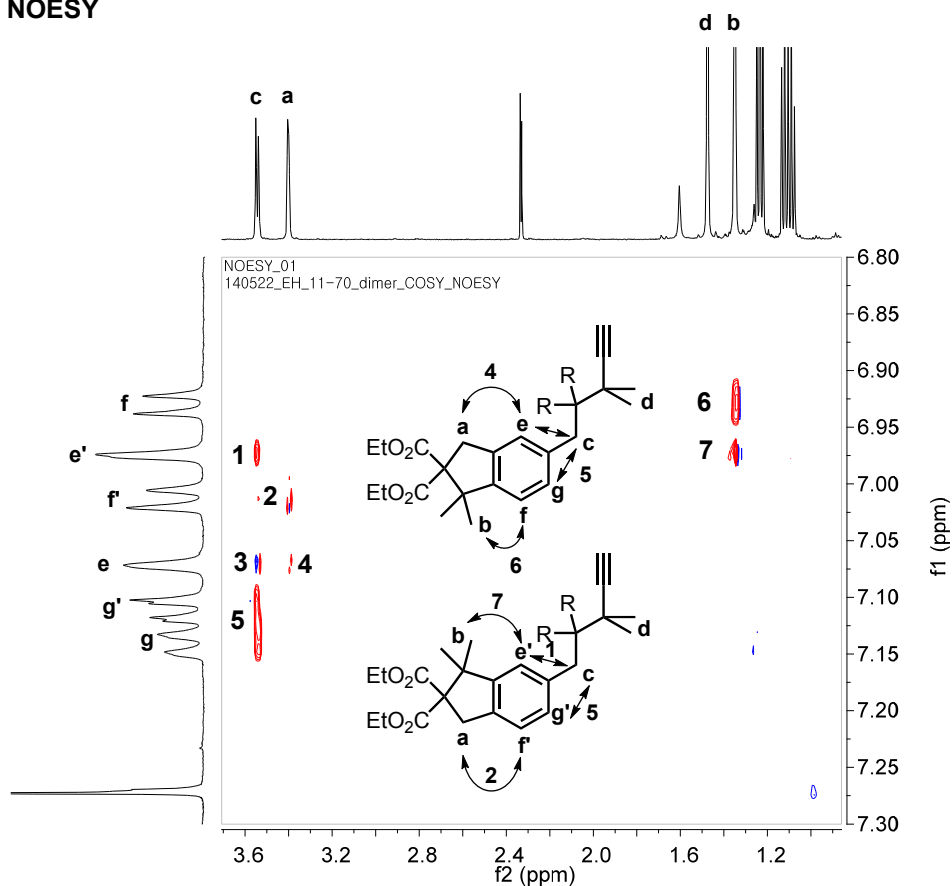
**Figure S4.4.**  $^1\text{H}$  NMR spectrum of the mixture of **3a'-i** and **3a'-ii**

### COSY



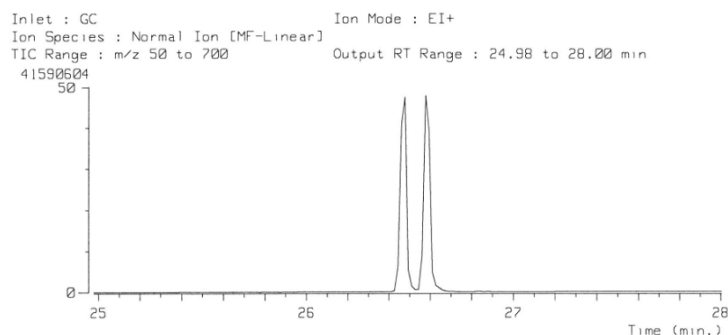
**Figure S4.5.** COSY of the mixture of **3a'-i** and **3a'-ii** (aromatic signals)

## NOESY



**Figure S4.6.** NOESY of the mixture of **3a'-i** and **3a'-ii**

## (2) GC/MS analysis



**Figure S4.7.** Gas chromatography of **3a'-i** and **3a'-ii** mixture.

For 26.46 min; HRMS (EI+): calcd. for  $\text{C}_{30}\text{H}_{40}\text{O}_8$ , 528.2723, found, 528.2717

For 26.58 min; HRMS (EI+): calcd. for  $\text{C}_{30}\text{H}_{40}\text{O}_8$ , 528.2723, found, 528.2720

## 4.7. References and Notes

- (1) Kang, E.-H.; Lee, I.-H.; Choi, T.-L. *ACS Macro Lett.* **2012**, *1*, 1098-1102.
- (2) Kumar, P. S.; Wurst, K.; Buchmeiser, M. R. *J. Am. Chem. Soc.* **2009**, *131*, 387-395.
- (3) Sudheendran, M.; Horecha, M.; Kiriy, A.; Gevorgyan, S. A.; Krebs, F. C.; Buchmeiser, M. R. *Polym. Chem.* **2013**, *4*, 1590-1599.
- (4) Kang, E.-H.; Choi, T.-L. *ACS Macro Lett.* **2013**, *2*, 780-784.
- (5) For [2+2+2] cycloadditions using **G2** or **HG2**; see:
  - (a) Mallagaray, A.; Medina, S.; Domínguez, G.; Pérez-Castells, J. *Synlett* **2010**, 2114-2118.
  - (b) Medina, S.; Domínguez, G.; Pérez-Castells, J. *Org. Lett.* **2012**, *14*, 4982-4985.
  - (c) Alvarez, S.; Medina, S.; Domínguez, G.; Pérez-Castells, J. *J. Org. Chem.* **2013**, *78*, 9995-10001.
  - (d) Alvarez, S.; Medina, S.; Domínguez, G.; Pérez-Castells, J. *J. Org. Chem.* **2015**, *80*, 2436-2442.
- (6) For reviews on [2+2+2] cycloaddition; see:
  - (a) Ken, T. *Transition-metal mediated aromatic ring construction*; John Wiley & Sons, Inc.: Hoboken, New Jersey, 2013.
  - (b) Saito, S.; Yamamoto, Y. *Chem. Rev.* **2000**, *100*, 2901-2915.
  - (c) Kotha, S.; Brahmachary, E.; Lahiri, K. *Eur. J. Org. Chem.* **2005**, 4741-4767.
  - (d) Chopade, P. R.; Louie, J. *Adv. Synth. Catal.* **2006**, *348*, 2307-2327.
  - (e) Domínguez, G.; Pérez-Castells, J. *Chem. Soc. Rev.* **2011**, *40*, 3430-3444.
- (7) For mechanistic studies on [2+2+2] cycloaddition; see:
  - (a) Hardesty, J. H.; Koerner, J. B.; Albright, T. A.; Lee, G.-Y. *J. Am. Chem. Soc.* **1999**, *121*, 6055-6067.
  - (b) Dazinger, G.; Torres-Rodrigues, M.; Kirchner, K.; Calhorda, M. J.; Costa, P. J. *J. Organomet. Chem.* **2006**, *691*, 4434-4445.
  - (c) Agenet, N.; Gandon, V.; Vollhardt, K. P. C.; Malacria, M.; Aubert, C. *J. Am. Chem. Soc.* **2007**, *129*, 8860-8871.
  - (d) Valera, J. A.; Saá, C. *J. Organomet. Chem.* **2009**, *694*, 143-149.
- (8) (a) Kirchner, K.; Calhorda, M. J.; Schmid, R.; Veiros, L. F. *J. Am. Chem.*

- Soc.* **2003**, *125*, 11721-11729. (b) Yamamoto, Y.; Aarakawa, T.; Ogawa, R.; Itoh, K. *J. Am. Chem. Soc.* **2003**, *125*, 12143-12160.
- (9) Peters, J.-U.; Blechert, S. *Chem. Commun.* **1997**, 1983-1984.
- (10) Witulski, B.; Stengel, T.; Fernández-Hernández, J. M. *Chem. Commun.* **2000**, 1965-1966.
- (11) Lee, I. S.; Kang, E.-H.; Park, H.; Choi, T.-L. *Chem. Sci.* **2012**, *3*, 761-765.
- (12) (a) Yamamoto, Y.; Nagata, A.; Itoh, K. *Tetrahedron Lett.* **1999**, *40*, 5035-5038. (b) Thiel, I.; Jiao, H.; Spannenberg, A.; Hapke, M. *Chem. Eur. J.* **2013**, *19*, 2548-2554.
- (13) 1,6-Heptadiyne was the simplest monomer giving the distinguished signals from other monomers, and also easy-to-remove due to low b.p.
- (14) (a) Sanford, M. S.; Love, J. A.; Grubbs, R. H. *J. Am. Chem. Soc.* **2001**, *123*, 6543-6554. (b) Nelson, D. J.; Manzini, S.; Urbina-Blanco, C. A.; Nolan, S. P. *Chem. Commun.* **2014**, *50*, 10355-10375.
- (15) **1f** was chosen rather than **1e**, because the low solubility of **2e** in THF or chloroform with high molecular weight limited further characterization.
- (16) Eglinton, G.; Galbraith, A. R. *J. Chem. Soc.* **1959**, 889.
- (17) Kim, S.-H.; Kim, Y.-H.; Cho, H.-N.; Kwon, S.-K.; Kim, H.-K.; Choi, S.-K. *Macromolecules* **1996**, *29*, 5422-5426.
- (18) Park, H.; Lee, H.-K.; Choi, T.-L. *Polym. Chem.* **2013**, *4*, 4676-4681.
- (19) Ungold, J.; Wang, D.; Frey, W.; Buchmeiser, M. R. *Polym. Chem.* **2013**, *4*, 4219-4233.
- (20) Atkinson, R. S.; Grimshire, M. J. *J. Chem. Soc. Perkin Trans. 1* **1986**, 1215-1224.
- (21) Carney, J. M.; Donoghue, P. J.; Wuest, W. M.; Wiest, O.; Helquist, P. *Org. Lett.* **2008**, *10*, 3903-3906.
- (22) Anders, U.; Wagner, M.; Nuyken, O.; Buchmeiser, M. R. *Macromolecules* **2003**, *36*, 2668-2673.
- (23) Saino, N.; Amemiya, F.; Tanabe, E.; Kase, K.; Okamoto, S. *Org. Lett.*

**2006**, 8, 1439-1442.



## **Chapter 5. Grafting-Through Synthesis of Dendronized Polymers and Brush Polymers by Cyclopolymerization of 1,6-Heptadiynes**

### **5.1. Abstract**

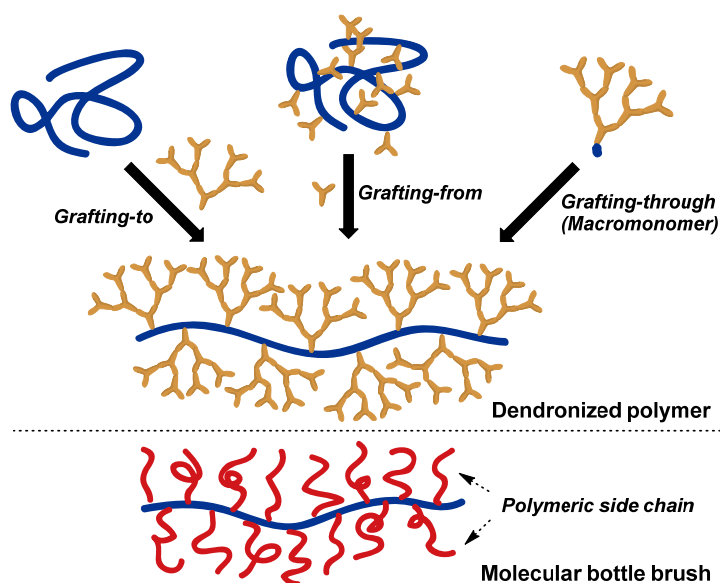
Through a grafting-through strategy, dendronized polymers and brush polymers containing semiconducting polyene backbones were efficiently synthesized by cyclopolymerization. Macromonomers with 2<sup>nd</sup>-G and 3<sup>rd</sup>-G ester-type dendrons polymerized in a living manner using the third generation Grubbs catalyst. For molecular brushes, macromonomers containing poly(L-lactide) and poly( $\epsilon$ -caprolactone), prepared by living ring-opening polymerization, were polymerized using the second generation Hoveyda-Grubbs catalyst to produce high molecular weight (> 500 kDa) brush polymers. In addition, the extended conformation of single chains of the dendronized and brush polymers was visualized by atomic force microscopy, which revealed the structure of a single molecular wire surrounded by insulating dendrons or polymers.

## 5.2. Introduction

Dendronized polymers and molecular brushes are a unique class of polymers containing densely grafted side chains, which control the polymer's conformation and physical properties via steric repulsion (Figure 5.1).<sup>1</sup> There are three general strategies for preparing those graft polymers: the grafting-from, grafting-onto, and grafting-through methods. Although the grafting-through approach (macromonomer approach) affords many advantages, such as well-defined grafting density and side-chain length, defect-free polymer structures, and even easy access to block copolymer synthesis, the polymerization of macromonomers is still challenging because of the severe steric hindrance between the propagating species and the monomers. For this reason, many brush polymers are preferentially prepared via the grafting-from approach.<sup>2</sup> Recently, ring-opening metathesis polymerization (ROMP) has become one of the most popular methods for the synthesis of dendronized<sup>3</sup> and brush polymers<sup>4</sup> by the grafting-through approach because the ROMP of norbornenyl macromonomers is highly efficient when a powerful third generation Grubbs catalyst is used.

The concept of brush polymers also has been employed in the synthesis of conjugated polymers to increase solubility, as well as to demonstrate unique optical properties and morphology control.<sup>5</sup> In particular, the insulated form of the organic nanowire has the advantage of preventing short circuits or crosstalk because of its insulating cover.<sup>6</sup> Dendronized or brush polymers containing conjugated backbone are desirable candidates for insulated molecular wires (IMWs). The behavior of insulated individual extended  $\pi$ -system is not much explored. Although various dendronized conjugated polymers have been investigated for the formation of IMWs, most were prepared by step-growth polymerization, which results in the formation of IMWs with broad PDIs and short polymer chains as a result of the large steric hindrance from high-generation dendrons. Nevertheless, there have been only a few examples of direct synthesis of conjugated polymers prepared by

the grafting-through approach<sup>7</sup> because of the synthetic difficulties arising from severe steric hindrance. One of the successful cases was the chain-growth polymerization using a Rh catalyst was adopted by the Percec group for the synthesis of substituted *cis*-polyacetylene to prepare dendronized conjugated polymers with controlled PDIs and DPs of up to 100.<sup>8</sup> However, these conjugated dendronized and brush polymers prepared via the grafting-through approach showed only wide band gap ( $E_g > 3.0$  eV), indicating that their conjugation lengths were quite short due to *cis*-olefin and steric hindrance.



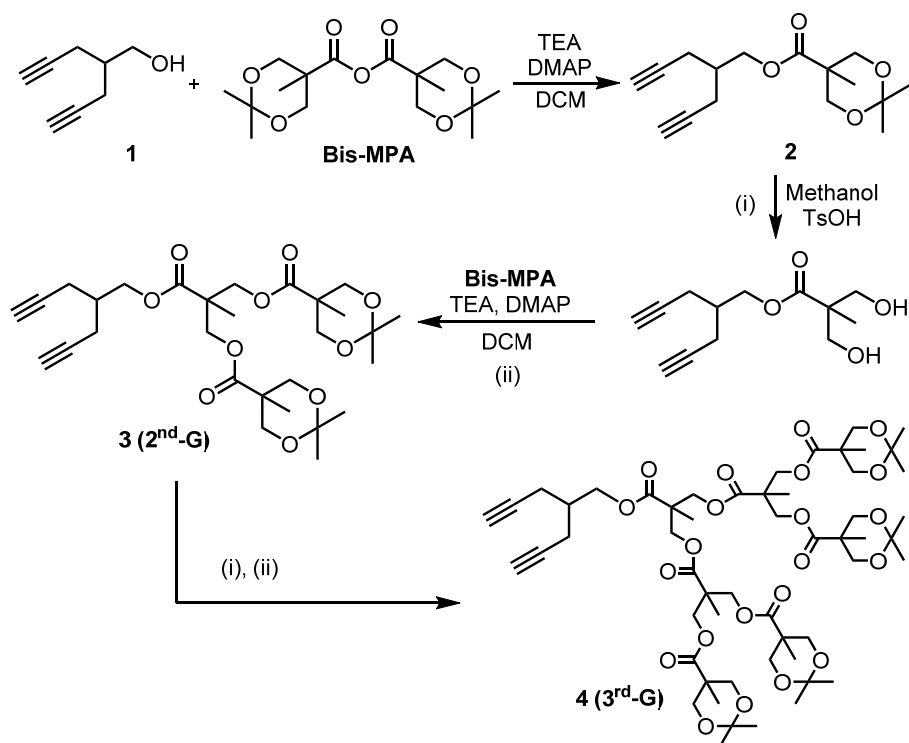
**Figure 5.1.** Synthetic schemes of dendronized and brush polymers.

To provide a solution to these challenges, the effective cyclopolymerization (CP) of 1,6-heptadiyne was chosen as a new candidate, because it soluble semiconducting polyenes with narrow polydispersity indices (PDIs). In this chapter, we report the synthesis of semiconducting conjugated dendronized polymers and brush polymers grafted by hydroxymethyl propionic acid-based (MPA) dendrimers, poly(L-lactide) (PLLA), and poly( $\epsilon$ -caprolactone) (PCL). Furthermore, the brush polymers underwent unique conformational changes, which were supported by characterization in both solution and solid states.

## 5.3. Results and Discussion

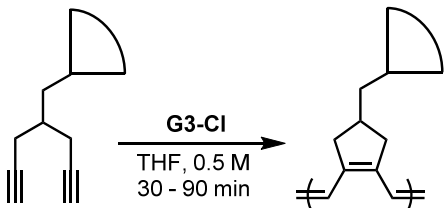
### 5.3.1. Synthesis of Dendronized Polymers

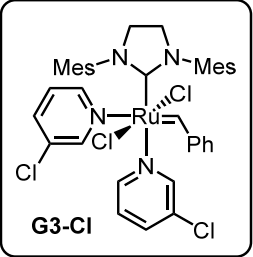
The successful polymerization of various monomers in Chapter 2 showed the possibility of synthesizing dendronized polymers by the macromonomer approach. Encouraged by the high activity of the third generation Grubbs catalyst (**G3-Cl**) toward CP of the mono-substituted monomers, we prepared macromonomers containing MPA-dendron<sup>9</sup>. **3** (second generation, **2<sup>nd</sup>-G**) and **4** (third generation, **3<sup>rd</sup>-G**) were synthesized from 4-hydroxymethyl-1,6-heptadiyne (**1**) and 2,2-bis(hydroxymethyl)propionic anhydride (**bis-MPA**) (Scheme 5.1). The polymerization condition of **3** and **4** using **G3-Cl** was optimized in THF at low temperature (−10 – 0 °C). Even with the bulky **3<sup>rd</sup>-G** dendron, the dendronized polymers were prepared in a living manner; the resulting polymers exhibited narrow PDIs (1.1–1.2) and excellent molecular weight control up to a high degree of polymerization (DP = 200) (Table 5.1 and Figure 5.2). The CP of 200 equiv of the bulky **4** was completed in 90 min at low temperature, reflecting the high activity of **G3-Cl**. More importantly, the chain transfer reaction seemed to be more suppressed, resulting in lower PDIs, because the large dendrons blocked the approach of the active metal carbene to the polyene backbone.



**Scheme 5.1.** Synthesis of macromonomers (**3** and **4**) for dendronized polymerization

**Table 5.1. CP of **3** and **4**<sup>a</sup> using G3-Cl**

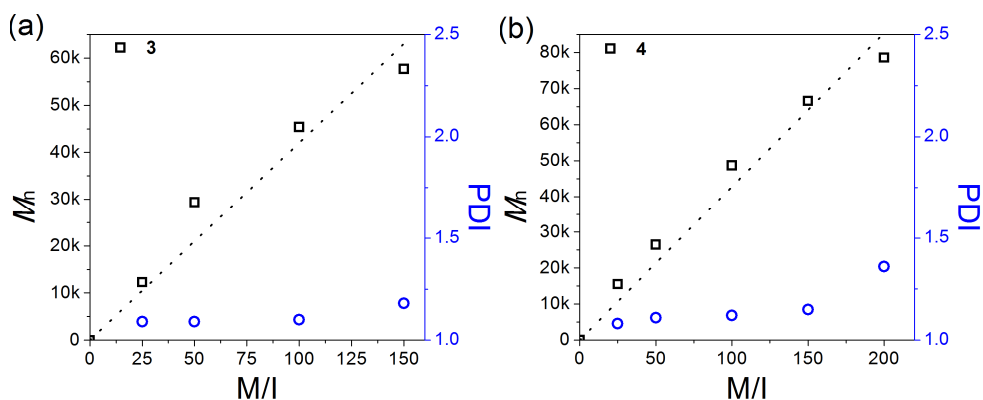




**G3-Cl**

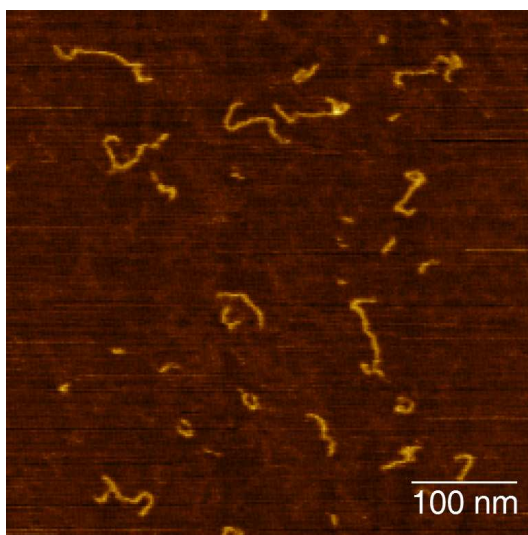
entry	monomer	M/I	temp (°C)	$M_n^b$ (kDa)	PDI <sup>b</sup>	yield <sup>c</sup> (%)
1	<b>3</b>	25	-10	12.3	1.09	88
2	<b>3</b>	50	-10	29.4	1.09	93
3	<b>3</b>	100	-10	45.4	1.10	78
4	<b>3</b>	150	-10	57.7	1.18	79
5	<b>4</b>	25	-12	15.5	1.08	92
6	<b>4</b>	50	-10	26.5	1.11	>99
7	<b>4</b>	100	0	48.7	1.12	82
8	<b>4</b>	150	-5	66.6	1.15	70
9	<b>4</b>	200	-5	78.6	1.36	86

<sup>a</sup>Polymerization conditions: 0.5 M THF within 1.5 h. <sup>b</sup>Determined by THF SEC calibrated using PS standards. <sup>c</sup>Isolated yields after purification. Monomer conversions were > 95%.



**Figure 5.2.** Plots of  $M_n$  vs. M/I and corresponding PDI values for (a) poly(**3**) and (b) poly(**4**).

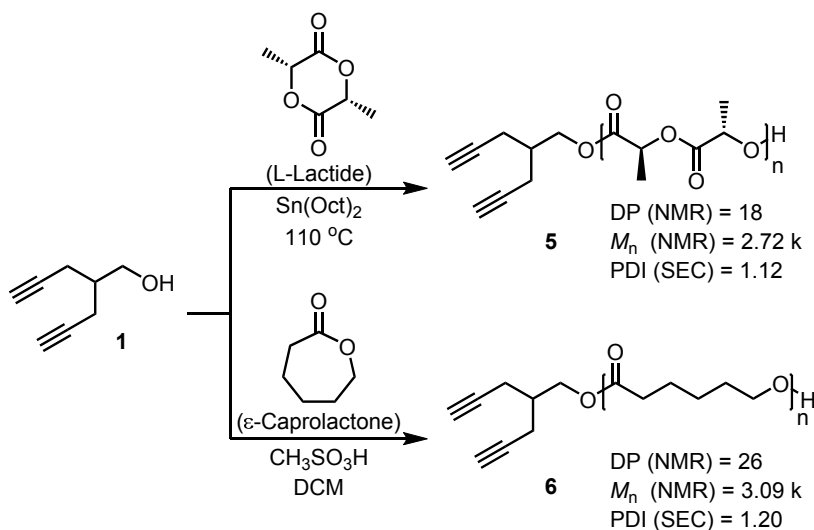
Individual molecules of dendronized polymers can be visualized by atomic force microscopy (AFM) because of their bulky substituents and an extended structure of the chains. The AFM image of poly(**4**) (Table 5.1, entry 9) provided vivid structural information on the single polymer chain; however, the AFM analysis of poly(**3**) failed because of the low height of the **2<sup>nd</sup>-G** dendron. As a result of the bulky dendrons, poly(**4**) showed an extended morphology resembling a rigid rod rather than a random coil (Figure 5.3). This provides a new route to the synthesis of IMWs with lengths of a few tens to hundreds of nanometers.



**Figure 5.3.** AFM image (height) of poly(**4**). Polymer solution in dichloromethane (1.25 mg/L) was spin-coated on mica. Average height is 0.4 nm.

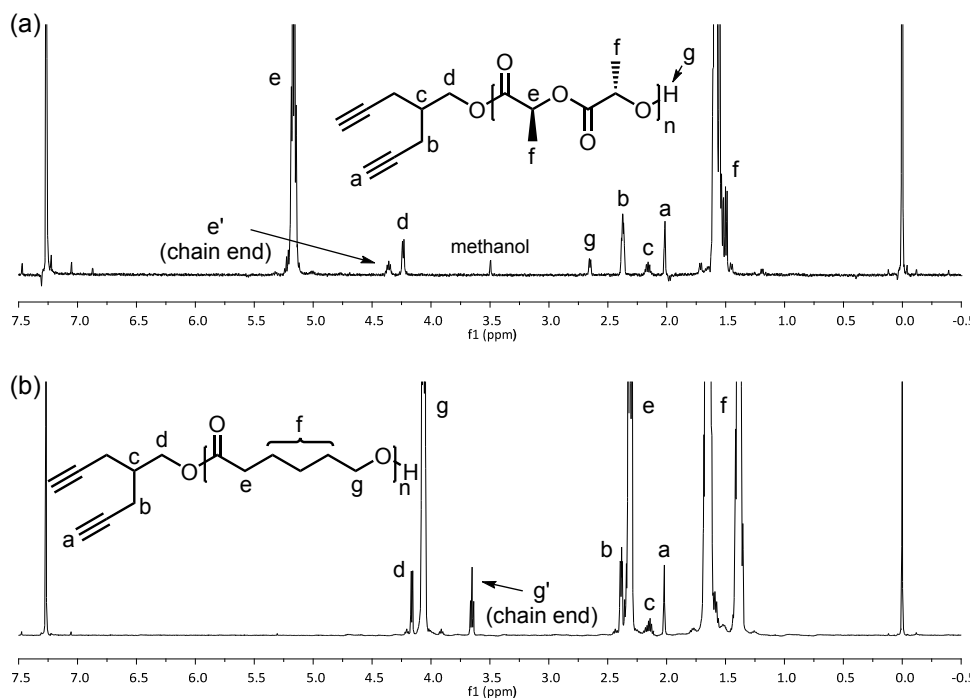
### 5.3.2. Synthesis of Brush Polymers

In contrast to the dendron-containing macromonomer, which is a well-defined single molecule, macromonomers for brush polymers are inevitably polydisperse because those are polymers. Therefore, it is essential to prepare macromonomers having polymeric side chains with narrow PDIs, which would allow the synthesis of final brush polymers having more precise nanostructures. In this point of view, living ring-opening polymerization (ROP) of cyclic esters was selected for the preparation method of polymeric macromonomers.<sup>10</sup> The hydroxyl group of **1** was used as an initiator for the ROP of PLLA and PCL. Owing to the orthogonal reactivity of alkynes and alcohols,  $\text{Sn}(\text{Oct})_2^{10a}$  and methanesulfonic acid catalysis<sup>11</sup> led to the convenient preparation of macromonomers **5** and **6** with narrow PDIs (Scheme 5.2). Molecular weights of the macromonomers **5** and **6** were determined by end group analysis by  $^1\text{H}$  NMR spectroscopy, based on the integration ratio of PLLA or PCL and heptadiyne signals (Figure 5.4). Most importantly, end group analysis by MALDI-TOF mass spectrometry confirmed that, even after ROP, both macromonomers retained the heptadiyne functionality that was essential for the next CP (Figure 5.5).



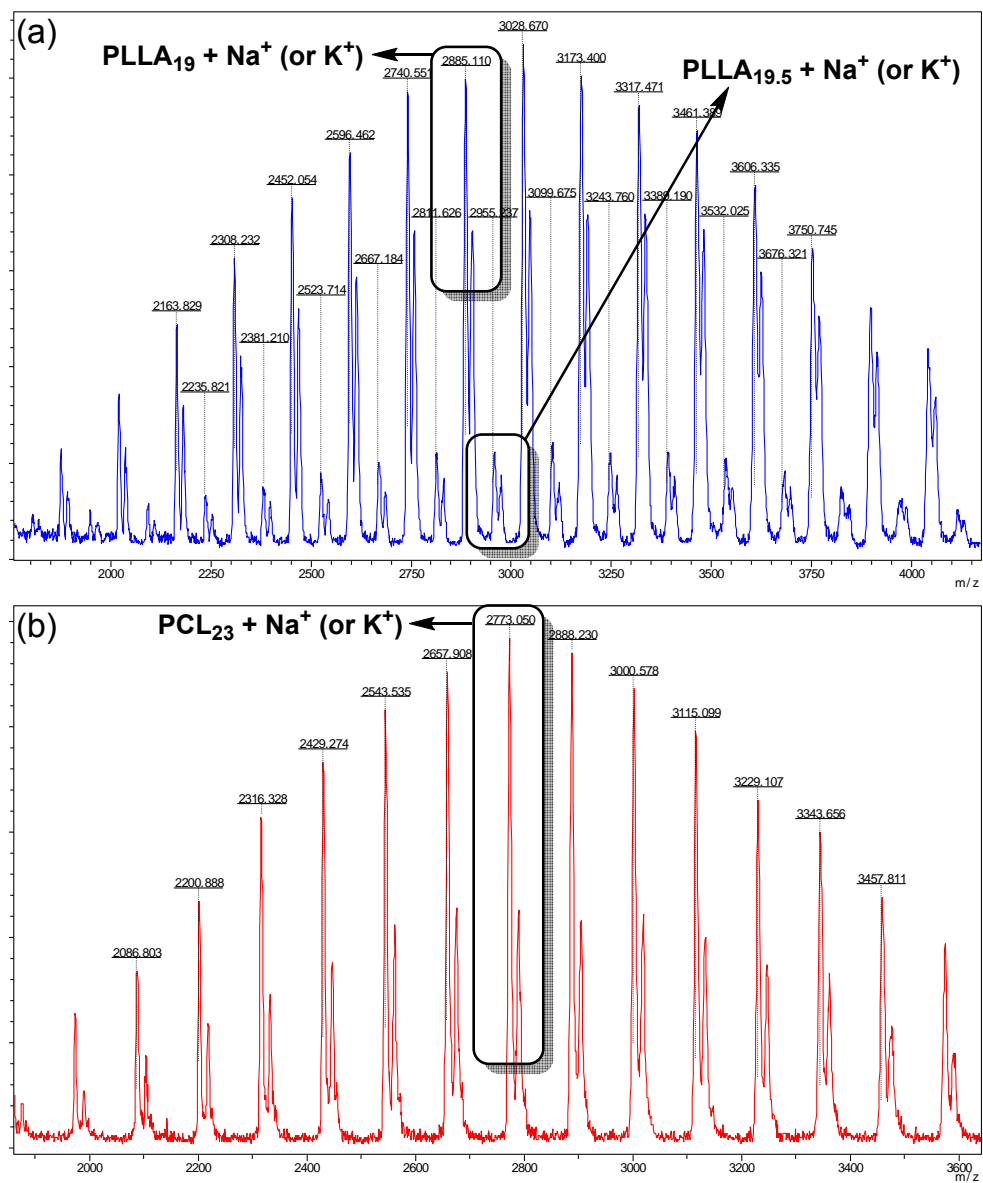
**Scheme 5.2.** Synthesis of polymer-substituted macromonomers (**5** and **6**)





**Figure 5.4.** (a)  $^1\text{H}$  NMR spectra of PLLA (**5**) and (b) PCL (**6**).  $M_n$  of **5** and **6** were calculated by the equation below :

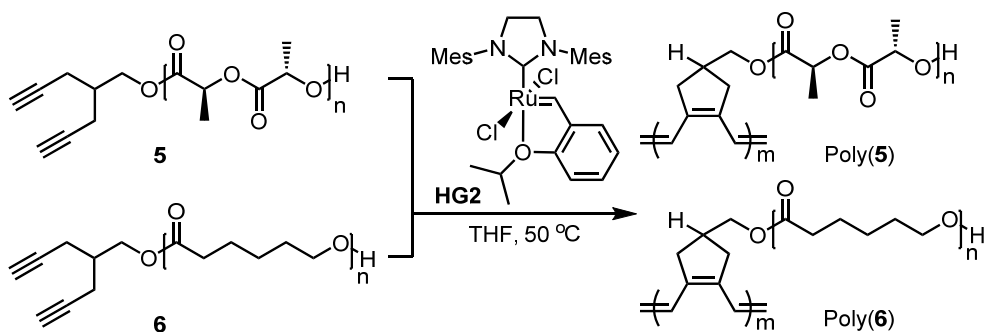
$[\text{MW of } \mathbf{5}] = \{(\text{MW of } \mathbf{1}) + (\text{MW of L-lactide}) * (\text{integration of } e) / 2\}$  when  $d$  was calibrated as 2.  $[\text{MW of } \mathbf{6}] = \{(\text{MW of } \mathbf{1}) + (\text{MW of } \epsilon\text{-caprolactone}) * (\text{integration of } g) / 2\}$  when  $d$  was calibrated as 2. Conversion of CP was calculated by the ratio of (integration of residual signal of  $d$ ) / (integration of  $e$  or  $g$ ).



**Figure 5.5.** MALDI-TOF spectra of (a) PLLA (**5**) and (b) PCL (**6**).

In each spectrum, there were Na<sup>+</sup>-bounded and K<sup>+</sup>-bounded signals for every peak, and the mass difference between each peak was exactly the mass of the monomers (L-lactide and  $\epsilon$ -caprolactone). **5** showed small peaks, which indicated the molecular weight of half of lactide, between two large peaks. For this, it was suggested that a small amount of chain transfer during the ROP occurred. However, no signal for the polymer initiated by water was found.

The cyclopolymerization of **5** and **6** was investigated using the second generation Hoveyda-Grubbs catalyst (**HG2**) in THF (Scheme 5.3). With a monomer-to-initiator ratio (M/I) of 100, 90% of **5** was converted into the brush polymer in 1 h at room temperature. The conversions of the macromonomers were confirmed from integration analysis on crude samples by  $^1\text{H}$  NMR spectroscopy or size-exclusion chromatography (SEC; Figure 5.6), and the absolute molecular weights of the brush polymers were obtained by multi-angle laser light scattering (MALLS) detection. After this initial success in CP, we changed the catalyst to **G3-Cl** to test if living CP would also be possible. Gratifyingly, **5** with M/I of 50 was cyclopolymerized at room temperature to give the brush polymer with  $M_n$  of 132 k (theoretical  $M_n$ : 135 k) and narrow PDI of 1.18. However, unfortunately, all attempts to achieve living polymerization failed with M/I of 100, and only brush polymers with broad PDIs ( $> 1.4$ ) similar to the initial case were obtained. Instead of aiming for living polymerization, thermally more stable **HG2** was used to maximize conversion by increasing temperature to 50 °C (99%, Table 5.2, entry 1). Under these conditions, CP with higher M/I of 200 and 300 was attempted to obtain high molecular weight brush polymers with much lower catalyst loading: the maximum average degree of polymerization (DP), up to 220, was obtained (Table 5.2, entries 2 and 3).

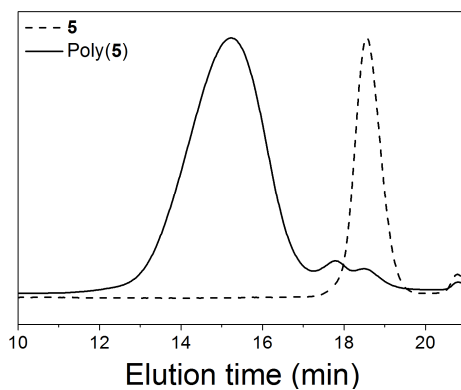


**Scheme 5.3.** Cyclopolymerization of macromonomers (**5** and **6**) using **HG2** for the synthesis of molecular brushes

**Table 5.2. CP of 5 and 6 by HG2 at 50 °C**

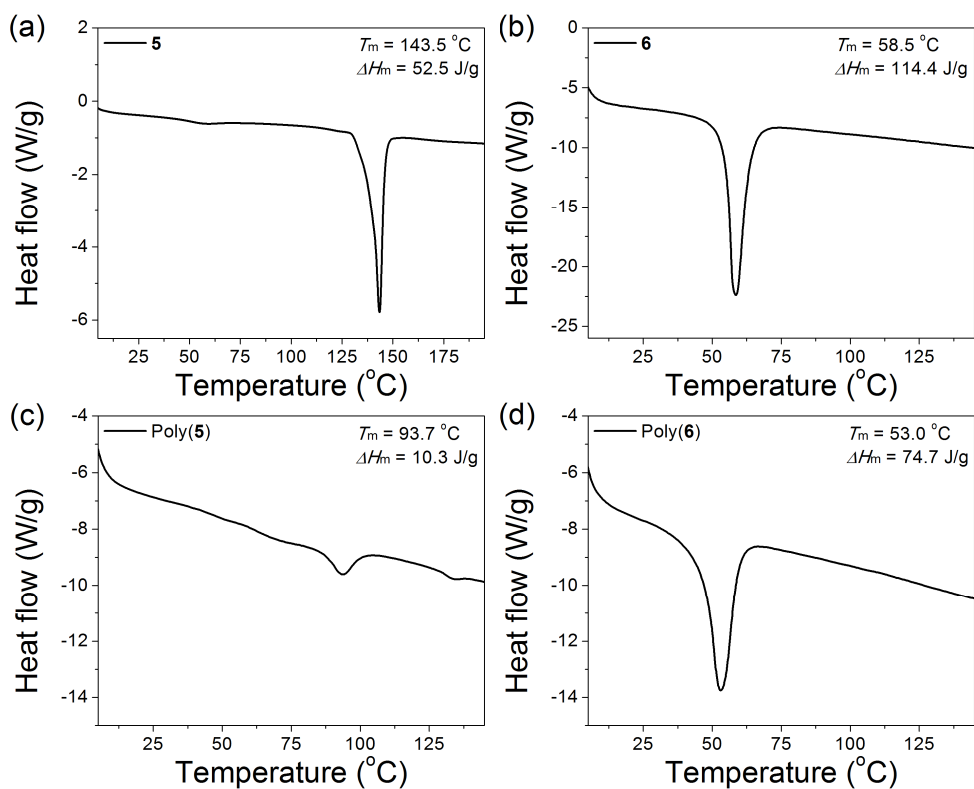
entry	monomer	M/I	time (h)	$M_n^a$ (kDa) (theor.)	$M_n^b$ (kDa)	PDI <sup>b</sup>	conv <sup>c</sup> (%)
1	<b>5</b>	100	1	269	424	1.47	99
2	<b>5</b>	200	2	511	453	1.51	94
3	<b>5</b>	300	6	604	583	1.42	74
4 <sup>d</sup>	<b>6</b>	100	1	346	209	1.63	99

<sup>a</sup>Calculated by this equation: ( $M_n$  of macromonomer)  $\times$  (M/I ratio)  $\times$  (monomer conversion). <sup>b</sup>Determined by THF SEC using MALLS detectors. <sup>c</sup>Calculated from the NMR spectral integration of monomers remained. <sup>d</sup>Determined by CHCl<sub>3</sub> SEC using light scattering detector.



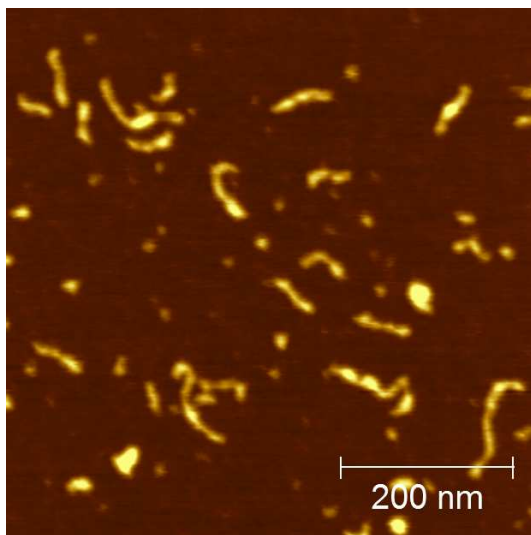
**Figure 5.6.** SEC traces of the macromonomer **5** (dashed) and crude sample of poly(**5**)<sub>90</sub> (solid).

Under the same conditions, the other macromonomer **6** also showed good reactivity toward CP; for  $M/I = 100$ , full conversion into the brush polymer was achieved within 1 h (Table 5.2, entry 4). However, the solubility of poly(**6**) in common organic solvents, such as chloroform and THF, was much poorer than poly(**5**), which made SEC analysis troublesome because it took 2 days to dissolve fully poly(**6**) in chloroform. Although both PLLA and PCL are crystalline polymers, they have different degrees of crystallinity and different physical properties,<sup>12</sup> and their polymer brushes may show different properties as well. Hence, to investigate the solubility issue in detail, differential scanning calorimetry (DSC) analyses on both macromonomers and brush polymers were performed (Figure 5.7). The crystallinities of the macromonomers were easily calculated as 56% (**5**) and 85% (**6**), by comparison with the reported enthalpy of fusion for the parent polymer crystal. Despite the high crystallinities for both macromonomers, DSC analysis on the brush polymers poly(**5**) and poly(**6**) showed different results. For poly(**6**), a melting temperature ( $T_m$ ) of 53.0 °C was very similar to that of the **6** (58.5 °C), and the enthalpy of fusion did not decrease significantly (114.4 J/g for **6** and 74.7 J/g for poly(**6**)). However, poly(**5**) showed a much smaller enthalpy of fusion (10.3 J/g) at much lower  $T_m$  (93.7 °C) than the values for **5** (52.5 J/g at 143.5 °C). From these DSC analyses, it was clear that poly(**5**) had low crystallinity, whereas poly(**6**) was significantly more crystalline, which might be reflected in the poorer solubility of poly(**6**) in common organic solvents.



**Figure 5.7.** DSC thermograms of macromonomers (**5** and **6**) and brush polymers (poly(**5**) and poly(**6**)). The crystallinity of each polymer was calculated by the given equation:  $x_c(\%) = 100 \times (\Delta H_f + \Delta H_c) / \Delta H_f^{\circ}$ , where  $x_c$  is crystallinity,  $\Delta H_f$  and  $\Delta H_c$  are the enthalpy fusion and crystallization, and  $\Delta H_f^{\circ}$  is the enthalpy of fusion of 100% polymer crystal (93 J/g for PLLA and 135 J/g for PCL).

The single chains of the brush polymer were vividly visualized by atomic force microscopy (AFM), as shown in Figure 5.8. While the imaging of a polymer single chain was more difficult from the just-prepared solution, the extended conformation of the individual brush was observed clearly on mica from the aged solution. Their heights ranged from 0.7 to 1.5 nm because the polymeric side chains were still polydisperse despite the living ROP (PDI of 1.2), and the maximum length was up to 200 nm. The broad dispersity with respect to the length was inevitable due to the large PDI of the brush polymer ( $> 1.4$ ). Some brighter (larger height) but short chains might be due to backbone cleavage in the brush as a result of surface adsorption-induced chain scission from the brush polymers<sup>13</sup> or the kinetically trapped brush polymers in coil conformation. Unfortunately, single chains of poly(**6**) could not be visualized in the same way, presumably because the high crystallinity and low solubility of poly(**6**) made AFM imaging very difficult.



**Figure 5.8.** AFM image (height) of poly(**5**).

## 5.4. Conclusion

In summary, the efficient grafting-through syntheses of high molecular weight dendronized and brush polymers having conjugated polyene backbones were demonstrated by CP using Grubbs catalysts. Remarkable reactivity of dendronized macromonomer achieved living CP by a fast-initiating third generation Grubbs catalyst. Sterically more challenging brush polymers were either successfully prepared from PLLA and PCL-based macromonomers by highly stable second generation Hoveyda-Grubbs catalyst. The markedly different solubility of the two brushes, PLLA and PCL, was noticed, and using DSC, a simple comparison of the crystallinity of the brushes provided an explanation for it. Finally, AFM imaging of single chains further confirmed the extended conformation of the dendronized and brush polymers. Potentially, those are expected as another example of insulated molecular wires.



## 5.5. Experimental Section

### Characterization

$^1\text{H}$  NMR and  $^{13}\text{C}$  NMR spectra were recorded by Varian/Oxford As-500 (500 MHz for  $^1\text{H}$  and 125 MHz for  $^{13}\text{C}$ ) spectrometer. The molecular mass of macromonomers was measured by Bruker Daltonics autoflex II TOF/TOF. Dithranol and Ag-TFA 1:1 mixture in THF was used as a matrix. THF-based size exclusion chromatography (SEC) for polymer analysis was carried out with Waters system (1515 pump, 2414 refractive index detector) and Shodex GPC LF-804 column. Samples were diluted in 0.001-0.003 wt% by THF (GPC grade, J. T. Baker<sup>®</sup>) and passed through a 0.20- $\mu\text{m}$  PTFE filter (Whatman<sup>®</sup>). Flow rate was 1.0 mL/min and temperature of the column was maintained at 35 °C. For the MALLS-VIS-RI analysis (including Mark-Houwink-Sakurada plot), Wyatt triple detector, Dawn 8+ / Viscostar<sup>®</sup> II / Optilab<sup>®</sup> T-rEX were used. The SEC data were analyzed using Breeze (for conventional mode) and Astra (for MALLS). DSC analysis was carried out on DSC 2910, TA Instruments. All of the polymer samples around 4 mg were heated from 0 °C to 150 or 200 °C at a rate of 10 °C/min. Multimode head and Nanoscope IV controller of Veeco Instrument were used on AFM imaging with E-type piezoelectric scanner. All images were operated on tapping mode using non-contact mode tip from Nanoworld (Pointprobe<sup>®</sup> tip, NCHR type) with spring constant of 42 N m<sup>-1</sup> and tip radius of  $\leq 8\text{nm}$ . Samples for imaging were prepared by spin-coating on freshly cleaved mica surface from 0.01 g/l chloroform solution. Elemental analyses were performed by the National Center for Inter-University Research Facility.

### Materials

All reactions were carried out under dry argon atmospheres using standard Schlenk-line techniques. All reagents which are commercially available, without

additional notes, were used without further purification. 4-Hydroxymethyl-1,6-heptadiyne (**1**) was prepared by reported literature.<sup>14</sup> Second generation Hoveyda-Grubbs catalyst was purchased from Sigma-Aldrich®. **G3-Cl** was prepared in the procedure in Chapter 2. L-Lactide was recrystallized from ethyl acetate three times after a preparation process as described below.  $\epsilon$ -Caprolactone (99%) was passed through a neutral alumina column and stored with 4 Å molecular sieve in argon. THF was distilled over sodium and benzophenone, and degassed by Ar bubbling for 10 minutes before using on polymerization. DCM was purified by solvent purification system using alumina column.

## Synthesis

### 2<sup>nd</sup>-G MPA dendronized 1,6-heptadiyne (**3**)

To a mixture solution of **1** (339.5 mg, 2.78 mmol), triethylamine (0.77 mL, 5.56 mmol), and DMAP (17.0 mg, 0.139 mmol) in dichloromethane (8 mL) was added **bis-MPA** (1.102 g, 3.33 mmol) and stirred for a few hours. Saturated NaHCO<sub>3</sub> aqueous solution was added to the mixture, followed by more stirring for 1 h. The mixture was washed with saturated NH<sub>4</sub>Cl solution then the organic layer was extracted with ethyl acetate (75 mL\*2). It was washed again with NaHCO<sub>3</sub> solution twice and extracted with ethyl acetate. The organic layer was dried over MgSO<sub>4</sub>, concentrated, and purified by flash column chromatography on silica gel (EtOAc:hexane = 1:5) to afford compound **2** as a colorless liquid (706.2 mg, 2.54 mmol, 99.4%). The acetal moiety of **2** was deprotected in excess methanol (20 mL \* 2) with a catalytic amount of *p*-toluenesulfonic acid (5 mol %). After evaporation of methanol and byproduct of deprotection, it was dried *in vacuo* to yield white solid. The mixture of the deprotected product (505 mg, 2.12 mmol), triethylamine (1.8 mL, 12.8 mmol), DMAP (25.9 mg, 0.212 mmol), and **bis-MPA** (2.10 g, 6.36 mmol) in dichloromethane (6 mL) was stirred overnight. Saturated NaHCO<sub>3</sub> aqueous solution was added to the mixture, followed by more stirring for 1 h. The

mixture was washed with saturated  $\text{NH}_4\text{Cl}$  solution then the organic layer was extracted with ethyl acetate (75 mL\*2). It was washed with  $\text{NaHCO}_3$  solution twice and extracted with ethyl acetate. The organic layer was dried over  $\text{MgSO}_4$  and purified by flash column chromatography on silica gel ( $\text{EtOAc}$ :hexane = 1:2) to afford compound **3** as a colorless liquid (1.14 g, 2.08 mmol, 98.1%).

$^1\text{H}$  NMR (500 MHz,  $\text{CDCl}_3$ ):  $\delta$  1.15 (s, 6 H), 1.31 (s, 3 H), 1.36 (s, 6 H), 1.41 (s, 6 H), 2.02 (t, 2 H), 2.17 (hept, 1 H), 2.38 (q, 4 H), 3.62 (d, 4 H,  $J = 12.25\text{Hz}$ ), 4.15 (d, 4 H,  $J = 12\text{ Hz}$ ), 4.22 (d, 2 H), 4.34 (d, 4 H);  $^{13}\text{C}$  NMR (125 MHz,  $\text{CDCl}_3$ ):  $\delta$  17.9, 18.7, 20.1, 22.2, 25.4, 36.3, 42.3, 47.1, 65.4, 66.2, 70.9, 80.8, 98.3, 172.6, 173.8; HRMS (FAB<sup>+</sup>): calcd. for  $\text{C}_{29}\text{H}_{43}\text{O}_{10}$ , 551.2856, found, 551.2859.

### 3<sup>rd</sup>-G MPA dendronized 1,6-heptadiyne (**4**)

The acetal group of **2** (821 mg, 1.49 mmol) was deprotected by excess methanol (20 mL \* 3) and a catalytic amount of *p*-toluenesulfonic acid (12.8 mg, 5 mol%). After evaporation of methanol and byproduct of deprotection, it was dried *in vacuo* to yield white solid. The mixture of the deprotected product, pyridine (1.2 mL, 15.2 mmol), DMAP (28.0 mg, 0.228 mmol), and **bis-MPA** (2.516 g, 7.62 mmol) in dichloromethane (5 mL) was stirred overnight. Saturated  $\text{NaHCO}_3$  aqueous solution was added to the mixture, followed by more stirring for 1 h. The mixture was washed with saturated  $\text{NH}_4\text{Cl}$  solution then the organic layer was extracted with ethyl acetate (75 mL\*2). It was washed again with  $\text{NaHCO}_3$  solution twice and extracted with ethyl acetate. The organic layer was dried over  $\text{MgSO}_4$  and purified by flash column chromatography on silica gel ( $\text{EtOAc}$ :hexane = 1:1) to afford compound **4** as a colorless sticky liquid (1.30 g, 1.19 mmol, 79.9%).

$^1\text{H}$  NMR (500MHz,  $\text{CDCl}_3$ ) :  $\delta$  1.15 (s, 12 H), 1.29 (s, 9 H), 1.36 (s, 12 H), 1.42 (s, 12 H), 2.05 (t, 2 H), 2.16 (hept, 1 H), 2.40 (q, 4 H), 3.62 (d, 8 H,  $J = 11.5\text{Hz}$ ), 4.15 (d, 8 H,  $J = 11.5\text{Hz}$ ), 4.22 (d, 2 H), 4.28 (d, 4 H,  $J = 13\text{Hz}$ ), 4.32 (s, 8 H);  $^{13}\text{C}$  NMR (125MHz,  $\text{CDCl}_3$ ) :  $\delta$  17.9, 18.7, 20.1, 22.2, 25.4, 36.3, 42.2, 47.0, 65.1, 66.1, 71.1, 80.8, 98.3, 172.1, 173.7; MS (MALDI-TOF):  $[\text{M}-\text{H}^+]$  calcd. for  $\text{C}_{55}\text{H}_{81}\text{O}_{22}$ , 1094.22,

found, 1094.66

### **L-Lactide preparation**

L-lactide was prepared by following literature<sup>15</sup>: L-lactic acid in Kugelrohr distillation apparatus was slowly heated from room temperature to 175 °C for 10 minutes with rotation (50 rpm), maintained for 7 h. Generated water was removed by evaporation from the container during the process. After cooling down to room temperature, 1 mol % of Sn(Oct)<sub>2</sub> relative to the amount of L-lactic acid was added to the resulting oligomer. The mixture was distilled at 200 °C under a pressure of 10–30 mbar for 1–2 h to obtain the solidified crude lactide mixture (GC-MS: DD,LL/meso=94/6). The crude mixture was recrystallized three times from ethyl acetate. White solid was obtained in 16% yield.

### **PLLA macromonomer (5)**

To a 10-mL Schlenk tube with a magnetic bar were added **1** (51.9 mg, 0.425 mmol), L-lactide (1.225 g, 8.50 mmol), and tin(II) 2-ethyl hexanoate (8.6 mg, 0.0212 mol). The tube was evacuated and backfilled with argon four times, then immersed in 110 °C oil bath. After stirring 1 h, the reaction mixture was cooled down to room temperature, diluted with dichloromethane, and precipitated into methanol. White solid was isolated with filter paper then dried *in vacuo* (1.152 g, 90.2%).  $M_n$  (NMR)= 2.72 kDa,  $M_w/M_n$  (SEC)= 1.12

<sup>1</sup>H NMR (500 MHz, CDCl<sub>3</sub>): δ 1.48-1.62 (m, 108 H), 2.02 (br s, 2 H), 2.16 (m, 1 H), 2.37 (m, 4 H), 2.65 (br, 1 H), 4.24 (d, 2 H), 4.36 (q, 1 H), 5.13-5.21 (m, 35 H); <sup>13</sup>C NMR (125 MHz, CDCl<sub>3</sub>): δ 16.9, δ 36.4, δ 40.9, δ 66.4, δ 66.9, δ 69.3, δ 70.9, δ 80.7, δ 169.8

### **PCL macromonomer (6)**

To a solution of **1** (61.1 mg, 0.500 mmol) in dichloromethane (10 mL) under argon, methanesulfonic acid (32.4 μL, 0.500 mmol) and ε-caprolactone (1.1 mL, 10.0 mmol) were added and immersed in 30 °C oil bath. After 2.5 h with stirring, the

reaction mixture was concentrated then precipitated into cold methanol. White solid was isolated with filter paper then dried *in vacuo* (657.3 mg).  $M_n$  (NMR)= 3.09 kDa,  $M_w/M_n$  (SEC)= 1.20

$^1\text{H}$  NMR (500 MHz,  $\text{CDCl}_3$ ):  $\delta$  1.39 (br, m, 52 H), 1.65 (br, m, 104 H), 2.02 (t, 2 H), 2.31 (t, 52 H), 2.39 (q, 4 H), 3.66 (t, 2 H), 4.07 (t, 50 H), 4.17 (d, 2 H);  $^{13}\text{C}$  NMR (100 MHz,  $\text{CDCl}_3$ ):  $\delta$  20.1,  $\delta$  24.8,  $\delta$  25.8,  $\delta$  28.5,  $\delta$  32.6  $\delta$  34.2,  $\delta$  36.5,  $\delta$  62.8,  $\delta$  64.3,  $\delta$  65.3,  $\delta$  70.7,  $\delta$  81.1,  $\delta$  173.8

### General procedure of cyclopolymerization

To a 4-mL vial with a PTFE-silicon septum cap were added macromonomer and a magnetic bar. The vial was purged with argon four times, and degassed dry THF was added ( $[\text{M}]_0 = 0.05\text{--}0.10\text{ M}$ ) to dissolve the macromonomer with stirring. After immersing the vial in the bath of proper temperature, the solution of initiator prepared from the inert atmosphere was added at once under vigorous stirring. The reaction was quenched by excess ethyl vinyl ether after desired reaction time, and precipitated in isopropanol/hexane mixture (for poly(**3**) and poly(**4**)), diethyl ether and acetone mixture (9:1) (for poly(**5**)), or only diethyl ether (for poly(**6**)). Obtained solid was filtered immediately to remove residual macromonomers then dried *in vacuo*.

### $^1\text{H}$ NMR and elemental analysis of dendronized and brush polymers

Poly(**3**):  $\delta$  1.13 (br m, 6 H), 1.25–1.33 (br m, 9 H), 1.39 (br m, 6 H), 2.30–3.00 (br m, 5 H), 3.61 (br m, 4 H), 3.90–4.20 (br m, 6 H), 3.34 (br m, 4 H), 6.30–6.75 (br m, 2 H)

Poly(**4**):  $\delta$  1.10–1.15 (br m, 12 H), 1.23–1.30 (br m, 9 H), 1.33 (br m, 12 H), 1.39 (br m, 12 H), 2.30–3.10 (br m, 5 H), 3.60 (br d, 8 H), 4.00–4.20 (br m, 10 H), 4.20–4.40 (br m, 12 H) 6.3–6.8 (br m, 2 H)

Elemental analysis calcd. (%) for  $C_{134}H_{178}O_{85}$  (unit of poly(**5**), DP of **5** = 20), C 51.140, H 5.700, found, C 51.089, H 5.695; calcd (%) for  $C_{302}H_{500}O_{99}$  (unit of poly(**6**), DP of **6** = 49), C 63.468, H 8.818, found, C 61.971, H 8.844

## 5.6. References and Notes

- <sup>†</sup> Portions of this chapter have been previously reported, see: (a) Kang, E.-H.; Lee, I. S.; Choi, T.-L. *J. Am. Chem. Soc.* **2011**, *133*, 11904-11907. (b) Kang, E.-H.; Lee, I.-H. ; Choi, T.-L. *ACS Macro Lett.* **2012**, *1*, 1098-1102.
- (1) For reviews on dendronized polymers, see:  
 (a) Zhang, A.; Shu, L.; Bo, Z.; Schlüter, A. D. *Macromol. Chem. Phys.* **2003**, *204*, 328-339. (b) Frauenrath, H. *Prog. Polym. Sci.* **2005**, *30*, 325-384. (c) Chen, Y.; Xiong, X. *Chem. Commun.* **2010**, *46*, 5049-5060.  
 For reviews on cylindrical molecular brushes, see:  
 (d) Sheiko, S. S.; Sumerlin, B. S.; Matyjaszewski, K. *Prog. Polym. Sci.* **2008**, *33*, 759-785. (e) Zhang, M.; Müller, A. H. E. *J. Polym. Sci., Part A: Polym. Chem.* **2005**, *43*, 3461-3481.
- (2) (a) Runge, M. B.; Bowden, N. B. *J. Am. Chem. Soc.* **2007**, *129*, 1055-1064. (b) Lee, H.; Jakubowski, W.; Matyjaszewski, K.; Yu, S.; Sheiko, S. *Macromolecules* **2006**, *39*, 4983-4989. (c) Cheng, G.; Böker, A.; Zhang, M.; Krausch, G.; Müller, A. H. E. *Macromolecules* **2001**, *34*, 6883-6888.
- (3) (a) Ball, Z. T.; Sivula, K.; Fréchet, J. M. J. *Macromolecules* **2006**, *39*, 70-72. (b) Nyström, A.; Malkoch, M.; Furó, I.; Nyström, D.; Unal, K.; Antoni, P.; Vamvounis, G.; Hawker, C. J.; Wooley, K.; Malmström, E.; Hult, A. *Macromolecules* **2006**, *39*, 7241-7249. (c) Rajaram, S.; Choi, T.-L.; Rolandi, M.; Fréchet, J. M. J. *J. Am. Chem. Soc.* **2007**, *129*, 9619-9621. (d) Jung, H.; Carberry, T. P.; Weck, M. *Macromolecules* **2011**, *44*, 9075-9083. (e) Kim, K. O.; Choi, T.-L. *ACS Macro Lett.* **2012**, *1*, 445-448.
- (4) (a) Li, A.; Li, Z.; Zhang, S.; Sun, G.; Policarpio, D. M.; Wooley, K. L. *ACS Macro Lett.* **2012**, *1*, 241-245. (b) Johnson, J. A.; Lu, Y. Y.; Burts, A. O.; Lim, Y.-H.; Finn, M. G.; Koberstein, J. T.; Turro, N. J.; Tirrell, D. A.; Grubbs, R. H. *J. Am. Chem. Soc.* **2011**, *133*, 559-566. (c) Li, Z.; Ma, J.; Cheng, C.; Zhang, K.; Wooley, K. L. *Macromolecules* **2010**, *43*, 1182-1184. (d) Xia, Y.; Olsen, B. D.; Kornfield, J. A.; Grubbs, R. H. *J. Am.*

- Chem. Soc.* **2009**, *131*, 18525-18532. (e) Xia, Y.; Kornfield, J. A.; Grubbs, R. H. *Macromolecules* **2009**, *42*, 3761-3766.
- (5) (a) Rugen-Penkalla, N.; Klapper, M.; Müllen, K. *Macromolecules* **2012**, *45*, 2301-2311. (b) Ding, L.; Huang, Y.; Zhang, Y.; Deng, J.; Yang, W. *Macromolecules* **2011**, *44*, 736-743. (c) Fruth, A.; Klapper, M.; Müllen, K. *Macromolecules* **2010**, *43*, 467-472. (d) Wang, M.; Zou, S.; Guerin, G.; Shen, L.; Deng, K.; Jones, M.; Walker, G. C.; Scholes, G. D.; Winnik, M. A. *Macromolecules* **2008**, *41*, 6993-7002. (e) Economopoulos, S. P.; Chochos, C. L.; Gregoriou, V. G.; Kallitsis, J. K.; Barrau, S.; Hadziioannou, G. *Macromolecules* **2007**, *40*, 921-927. (f) Breen, C. A.; Deng, T.; Breiner, T.; Thomas, E. L.; Swager, T. M. *J. Am. Chem. Soc.* **2003**, *125*, 9942-9943.
- (6) Frampton, M. J.; Anderson, H. L. *Angew. Chem., Int. Ed.* **2007**, *46*, 1028-1064.
- (7) (a) Maeda, K.; Wakasone, S.; Shimomura, K.; Ikai, T.; Kanoh, S. *Chem. Commun.* **2012**, *48*, 3342-3344. (b) Cheng, X.; Ma, J.; Zhi, J.; Yang, X.; Hu, A. *Macromolecules* **2010**, *43*, 909-913. (c) Yurteri, S.; Cianga, I.; Demirel, A. L.; Yagci, Y. *J. Polym. Sci., Part A: Polym. Chem.* **2005**, *43*, 879-896.
- (8) (a) Percec, V.; Rudick, J. G.; Wagner, M.; Obata, M.; Mitchell, C. M.; Cho, W.-D.; Magonov, S. N. *Macromolecules* **2006**, *39*, 7342-7351. (b) Percec, V.; Rudick, J. G.; Peterca, M.; Staley, S. R.; Wagner, M.; Obata, M.; Mitchell, C. M.; Cho, W.-D.; Balagurusamy, V. S. K.; Lowe, J. N.; Glodde, M.; Weichold, O.; Chung, K. J.; Ghionni, N.; Magonov, S. N.; Heiney, P. A. *Chem. Eur. J.* **2006**, *12*, 5731-5746.
- (9) (a) Ihre, H.; Hult, A. *Macromolecules* **1998**, *31*, 4061-4068. (b) Ihre, H.; De Jesús, O. L. P.; Fréchet, J. M. J. *J. Am. Chem. Soc.* **2001**, *123*, 5908-5917.
- (10) (a) Dechy-Cabaret, O.; Martin-Vaca, B.; Bourissou, D. *Chem. Rev.* **2004**,



- 104, 6147-6176. (b) Labet, M.; Thielemans, W. *Chem. Soc. Rev.* **2009**, 38, 3484-3504.
- (11) Gazeau-Bureau, S.; Delcroix, D.; Martín-Vaca, B.; Bourissou, D.; Navarro, C.; Magnet, S. *Macromolecules* **2008**, 41, 3782-3784.
- (12) Kim, J. K.; Park, D.-J.; Lee, M.-S.; Ihn, K. J. *Polymer* **2001**, 42, 7429-7441.
- (13) (a) Sheiko, S. S.; Sun, F. C.; Randall, A.; Shirvanyants, D.; Rubinstein, M.; Lee, H.; Matyjaszewski, K. *Nature* **2006**, 440, 191-194. (b) Lebedeva, N. V.; Sun, F. C.; Lee, H.; Matyjaszewski, K.; Sheiko, S. S. *J. Am. Chem. Soc.* **2008**, 130, 4228-4229.
- (14) Carney, J. M.; Donoghue, P. J.; Wuest, W. M.; Wiest, O.; Helquist, P. *Org. Lett.* **2008**, 10, 3903-3906.
- (15) Anderson, K. S.; Hillmyer, M. A. *Macromolecules* **2004**, 37, 1857-1862.

## Chapter 6. Coil-to-Rod Transition of Conjugated Polymers Prepared by Cyclopolymerization of 1,6-Heptadiynes

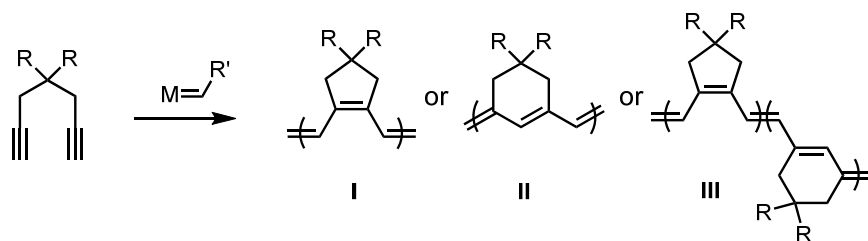
### 6.1. Abstract

The conformational change resulting from the coil-to-rod transition was investigated in conjugated polymers prepared by the cyclopolymerization (CP) of 1,6-heptadiyne derivatives (poly-(cyclopentenylene-vinylene), PCPV). First, a brush polymer prepared by CP showed a unique change in absorption spectra, with an appearance of a 0–0 vibronic peak during the aging of the polymer solution. It was revealed as a conformational change of coil-to-rod transition, which was supported by UV–vis analysis and Mark-Houwink-Sakurada shape parameter. Furthermore, aging of PCPV containing smaller substituent in solution state under various conditions resulted in same conformational change, showing the change of absorption spectra and shape parameter.  $^1\text{H}$  NMR analysis of PCPV backbone and various control experiments demonstrated that the coil-to-rod transformation resulted from the *cis*-to-*trans* isomerization of the conjugated olefins by a radical mechanism.

## 6.2. Introduction

The conformational behavior of conjugated polymers is understood to differ from the classic random-coil model, because of their longer persistence lengths derived from  $\pi$ -electron delocalization.<sup>1</sup> These studies of conjugated polymers have been of great interest to many physicists and chemists because the optical and electronic properties of conjugated polymers are affected by both the conformation of the single chains and the interaction between individual chains.<sup>2</sup> Many spectroscopic investigations have been carried out on well-known conjugated polymers such as poly(3-alkylthiophenes) (PATs)<sup>3</sup> and poly(phenylene-vinylenes) (PPVs) to elucidate structure–property relationships on the electronic transitions and energy transfer of the conjugated polymers.<sup>4</sup>

The cyclopolymerization (CP) of 1,6-heptadiyne derivatives produces cyclopentenylene-vinylene alternating repeat units (**I**), methylenecyclohexene repeat units (**II**), or a random mixture of the two units (**III**) (Scheme 6.1). During the past two decades, many efforts have been made to avoid the random structure seen in **III** by developing a regioselective polymerization to expand the scope of this polymerization.<sup>5</sup> The macromolecular conformation and optical properties of these poly(cyclopentenylene-vinylene)s (PCPVs, **I**) are still little understood; only a few studies on **II** or **III**, prepared from the CP of diethyl dipropargylmalonate (DEDPM), have been reported.<sup>6</sup> On the other hand, **I** exhibits an interesting absorption spectrum showing clear vibronic bands, which are absent in the spectra of **II** and **III**. These bands provide information on the conformational order of the more coplanar polymer backbone.<sup>7</sup> Unfortunately, little attention has been paid to investigating the conformational-spectroscopic correlation for PCPV systems.<sup>8</sup>



**Scheme 6.1.** Repeat unit structures produced by CP of 1,6-heptadiynes

In Chapter 5, we addressed the synthesis of dendronized polymers and brush polymers by CP to extend the PCPV backbone for single molecular wires. In this chapter, a unique change in the absorption spectrum of this brush polymer by simple aging in organic solvents is reported. With detailed analysis of UV-vis absorption spectroscopy (Huang-Rhys factor,  $S$ ) and Mark-Houwink-Sakurada plot (shape parameter,  $\alpha$ ), it was revealed that a spontaneous coil-to-rod conformational change of the brush polymer occurred. The origin of the coil-to-rod conformational change was further investigated on the simpler PCPV as a model system. Using NMR analysis and other measurements, we confirmed that simple aging under light caused *cis*-to-*trans* isomerization of the olefins of the polyenes. This isomerization to the more stretched *E*-olefins, in turn, led to the coil-to-rod transition. This analysis was quite meaningful because a theoretical prediction obtained from spectroscopy was confirmed by a chemical method using NMR spectroscopy and viscosity measurements.

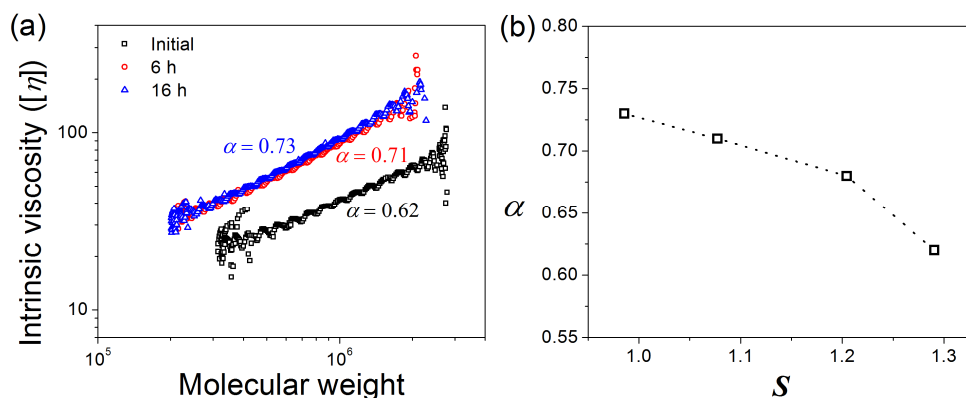
## 6.3. Results and Discussion

### 6.3.1. Coil-to-rod Conformational Transition of Brush Polymer

To obtain extended and rigid conjugated backbone as a candidate of single molecular wires, we prepared poly(L-lactide)-based brush polymer (poly(PLLA)) in Chapter 5 (Scheme 6.2). Since the CP produces the fully conjugated polymer structures, careful UV-vis analysis may provide additional information on the polymer conformation. The UV-vis spectrum for the poly(PLLA) dissolved in tetrahydrofuran (THF) revealed two distinct vibronic bands with  $E_g = 2.0$  eV, indicating that the microstructure of the polymer was regioregular polyenes consisting exclusively of five-membered ring structures (Figure 6.1).<sup>7</sup> This provided strong support for the uniform microstructure of the brush polymers prepared via selective  $\alpha$ -addition of the catalyst. Interestingly, a closer inspection revealed that the  $\lambda_{\max}$  and the relative intensities of the two vibronic bands changed with time. Compared to the UV-vis spectrum obtained immediately after the synthesis of poly(PLLA), the spectrum of an aged solution showed that  $\lambda_{\max}$  was not only red-shifted, but also that the intensity of the first vibronic band at 580 nm (0-0 transition) had significantly increased with aging time (Figure 6.1a). Since the growth of the intensity for the 0-0 band indicates more coplanar, extended, and stiffer conformations of the conjugated polymers<sup>4a,9</sup> (lower Huang-Rhys factor,  $S$ : relative intensity of 0-1 to 0-0 transitions obtained from optical spectra; Figure 6.1b), this observation implied that the conformation of the brush polymers might be undergoing a transformation to a more extended structure over time. This change was certainly not due to the aggregation of the poly(PLLA) because the steric hindrance of the polymeric side chains should prevent any possibility of intermolecular aggregation.

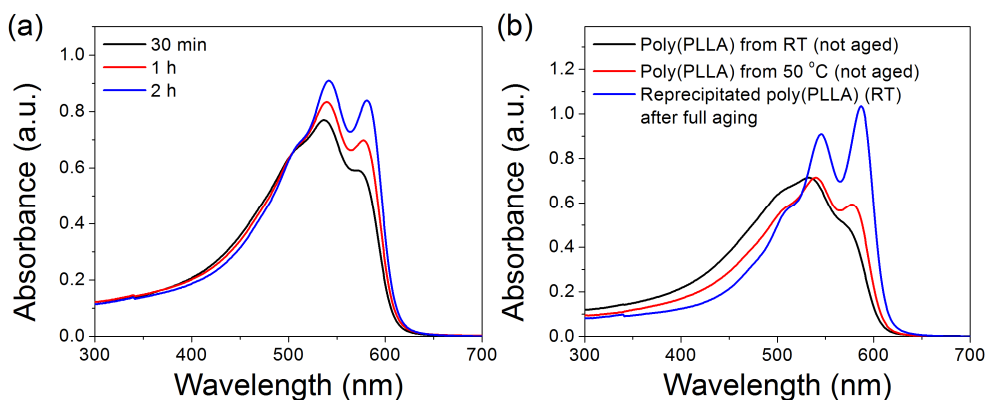


polymers at extremely low temperatures and in an aligned solid state, while the conformation of those polymers returned to the coil-like structure at room temperature because of entropic factors.<sup>4a</sup> However, the correlation of the theoretical  $S$ -value on the polymer conformation has not been supported by chemical methods yet because these extreme conditions were not suitable for typical chemical analysis in solution at ambient conditions. Fortunately, these brush polymers may now be suitable for chemical analysis because they seem to undergo the conformational transition at room temperature slowly enough so that reliable time-dependent analysis would be possible. To confirm this conformational change by a polymer chemistry method, we measured the time-dependent shape parameter  $\alpha$ , which was obtained by Mark–Houwink–Sakurada plots from SEC–viscometry analysis: a higher  $\alpha$ -value indicates a more extended or stiffer polymer chain. By comparing  $\alpha$  as a function of aging time, we realized that the  $\alpha$ -values increased from 0.62 (the initial state) up to 0.73 (after 16 h of aging), strongly suggesting that the brush polymers underwent conformational changes to form relatively more extended structures (Figure 6.2).<sup>12</sup> This coil-to-rod transition<sup>13</sup> on poly(PLLA) is evident because the interpretation of the changes in both the UV–vis spectra and the shape parameter  $\alpha$  leads to the same conclusion (Figure 6.2b).



**Figure 6.2.** (a) Time-dependent Mark–Houwink–Sakurada plots of poly(PLLA)<sub>190</sub> in THF (2.3 g/L) confirming the coil-to-rod transition. (b) Correlation between Huang–Rhys factor  $S$  and shape parameter  $\alpha$ .

We believe that the brush polymer with a relatively more extended conformation is thermodynamically more stable than the initial conformation, based on the following two observations. First, UV-vis spectra immediately obtained after the CP conducted at 50 °C with a longer reaction time showed a more intense 0–0 band than that obtained after a shorter reaction time (Figure 6.3a). Likewise, the polymer obtained by the CP at room temperature without aging showed the lowest 0–0 band (Figure 6.3b). In all conditions, molecular weights of poly(PLLA) were similar. These observations conclude that longer reaction time and higher temperature conditions facilitate the conformational change. Second, the changes in both the UV-vis spectra and the  $\alpha$ -values were irreversible. Even if the aged solution was reprecipitated as a solid and redissolved, the UV-vis spectra and  $\alpha$ -values remained unchanged ( $\alpha = 0.72$ , blue spectrum in Figure 6.3b). In short, these conformational analyses in solution revealed that the more coil-like kinetic conformation of poly(PLLA) transformed into the more extended rigid-rod-like conformation that was the thermodynamically favored state.

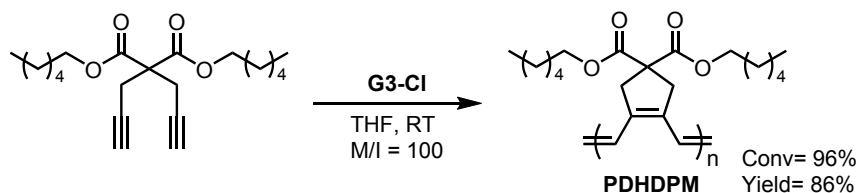


**Figure 6.3.** (a) UV-vis spectra of poly(PLLA) obtained from the polymerization with various reaction times (without aging) at 50 °C. (b) UV-vis spectra of poly(PLLA) of initial state obtained from the polymerization at room temperature (black) and 50 °C (red). Blue line indicates the spectrum from re-precipitated poly(PLLA) obtained from room temperature after aging and dilution ( $\sim 0.1$  g/l).



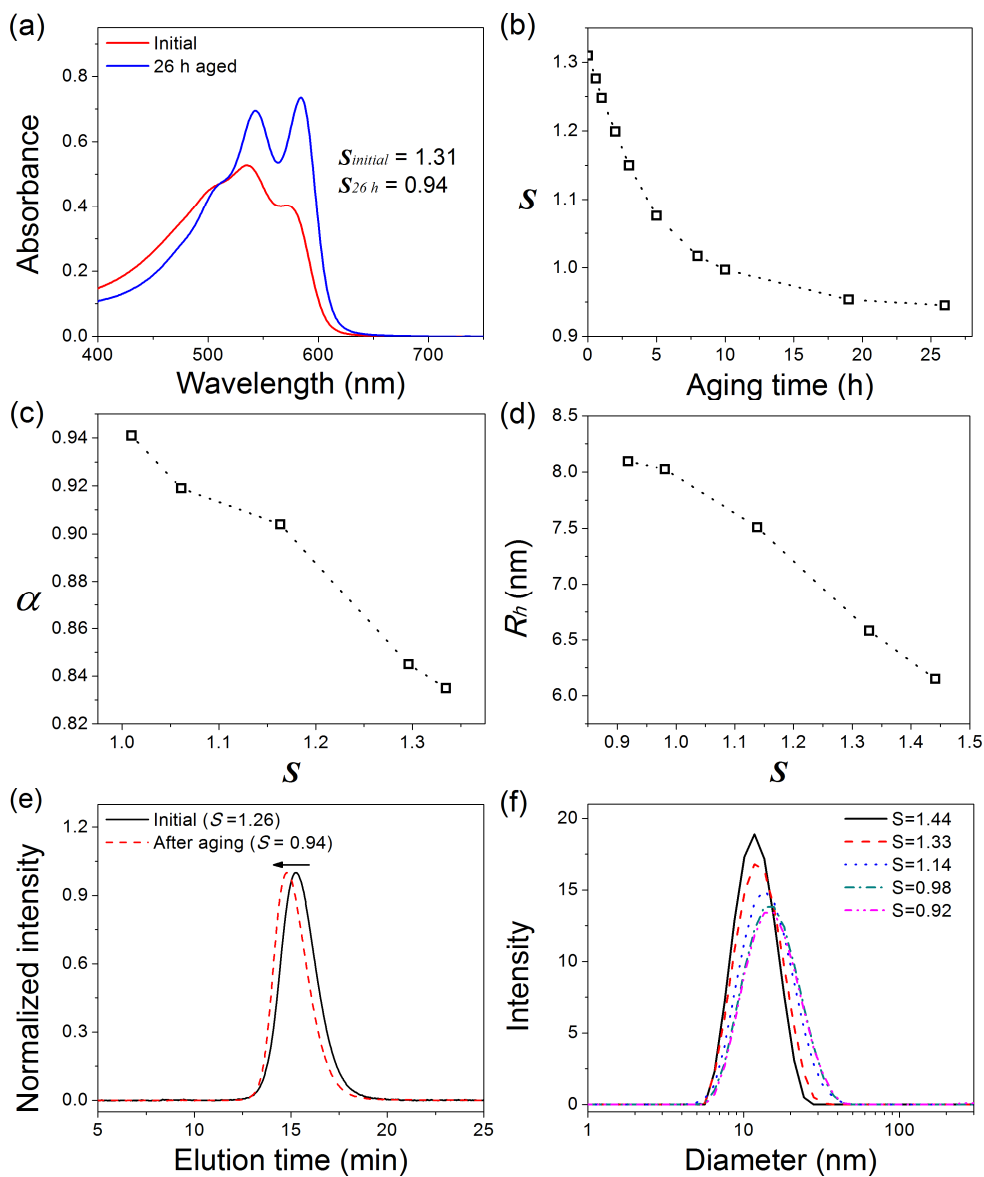
### 6.3.2. General Features on Conformational Change of PCPV

There was a question mark on the origin of the conformational change; because it was unclear whether the sterically demanding grafted side chain of poly(PLLA) induces this spontaneous transition, or it is a unique behavior of the PCPV backbone regardless of the substituent. To check the generality of the conformational change, we chose to examine poly(dihexyl dipropargylmalonate) (PDHDPM,  $M_n = 44.3$  kDa, PDI = 2.1, yield = 86%) as a model polymer and measured the absorption spectra at various aging times in THF (Scheme 6.3).<sup>14</sup> Similar to poly(PLLA), when a dilute solution of PDHDPM was aged,  $\lambda_{\max}$  of the 0–0 band was red-shifted (approximately 13 nm), and a gradual increase in the vibronic signal was observed with the aging time (Figure 6.4a).



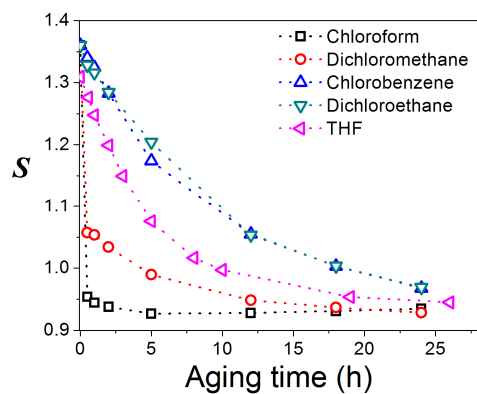
**Scheme 6.3.** Synthesis and chemical structure of PDHDPM

As shown in Figure 6.4b,  $S$  decreased from 1.31 to 0.94 over a period of 1 day in THF, demonstrating that the change to a more extended conformation was not limited to brush polymers. As another proof for the coil-to-rod transition, the  $\alpha$ -value gradually increased from 0.83 to 0.94 (Figure 6.4c). Moreover, the increase in hydrodynamic radius ( $R_h$ ) of the polymer measured by dynamic light scattering (DLS) with the decrease in  $S$  and the shift of SEC trace to the left after the aging further supported the conformation transition (Figure 6.4d–f). With an excellent correlation between  $S$  and  $\alpha$  for PDHDPM and other substituted PCPVs (Figure S6.1), we concluded that this coil-to-rod transformation was a general phenomenon for cyclopolymerized products containing five-membered rings.

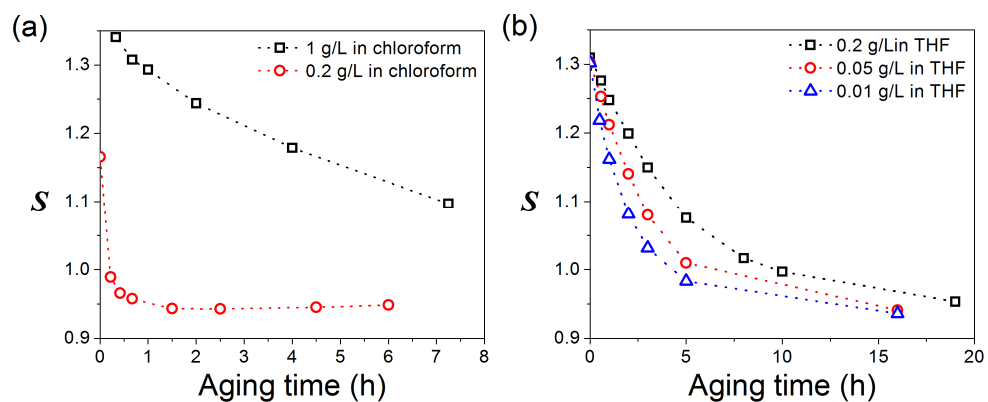


**Figure 6.4.** (a) Change in the absorption spectrum of PDHDPM and (b) time-dependent change of  $S$  by aging in THF (0.2 g/L). (c) Linear correlation between  $S$ – $\alpha$  and (d)  $S$ – $R_h$  during the aging process in THF (2 g/L for (c) and 1 g/L for (d)).<sup>15</sup> (e) SEC trace shift after aging, which indicates that the hydrodynamic volume of the polymer increased. (f) Hydrodynamic diameter change as  $S$  decreased.

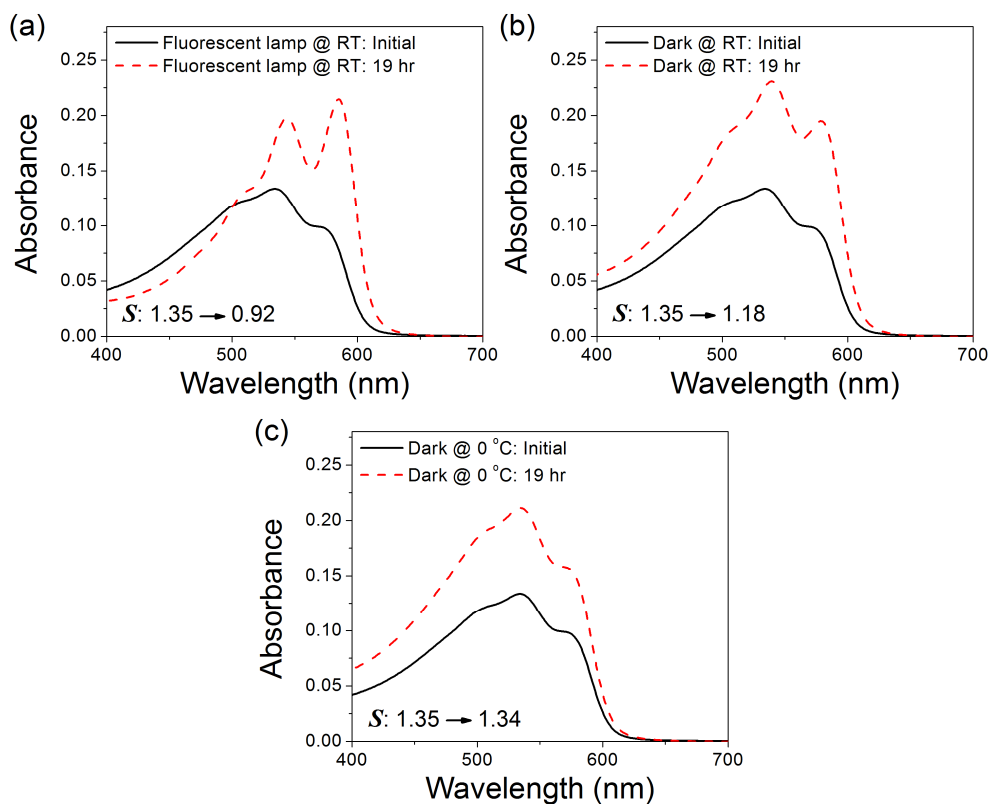
To obtain a better understanding of this coil-to-rod transition, we investigated how the transformation rate was affected by various changes in the aging conditions such as solvent, concentration, and light source. (i) Solvent: Among the many organic solvents tested, chloroform and dichloromethane (DCM) induced the fastest transition, which was completed in only a few minutes (monitored by UV-vis analysis), whereas other solvents (chlorobenzene, THF, etc.) showed much slower changes on the timescale of hours (Figure 6.5). This explains why the transition has not been observed by others; the changes are too rapid in chloroform and DCM, which are the most commonly used solvents to prepare and study these polyenes. This extreme solvent dependence implied a transformation based on chemical reactions rather than physical folding or aggregation, because all the tested solvents were good solvent to dissolve PDHDPM. (ii) Concentration: A lower concentration induced a faster conformational change (Figure 6.6). Therefore, the transition to the extended conformation was not caused by intermolecular aggregation of the polymers. (iii) Light source: The presence of light and the nature of the light source significantly affected the transition rate. The transition in the dark was much slower than that when the polymer solution was exposed to an ordinary fluorescent lamp (Figure 6.7). For the comparison of light effect in detail, the polymer solution in THF was exposed to blue and green LED with narrow wavelength ranges for aging. Irradiation by the blue LED provoked a faster change than did irradiation by the green LED, even though the absorption  $\lambda_{\text{max}}$  of PDHDPM matched well with the wavelength of the green LED (Figure 6.8). These results suggest that changes in the chemical structure of the conjugated backbone are responsible for the transition rather than changes in the electronic structure.



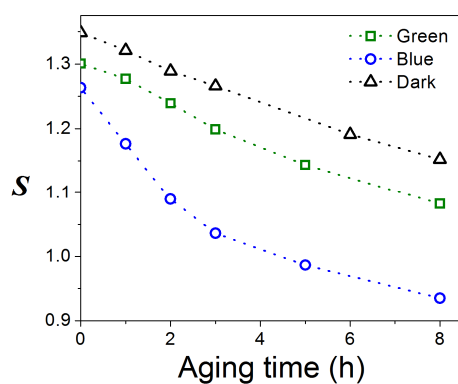
**Figure 6.5.** Time-dependent changes of Huang-Rhys factor  $S$  of PDHDPM in various organic solvents.



**Figure 6.6.** Time-dependent changes of  $S$  with different concentrations of PDHDPM solution in (a) chloroform and (b) THF.



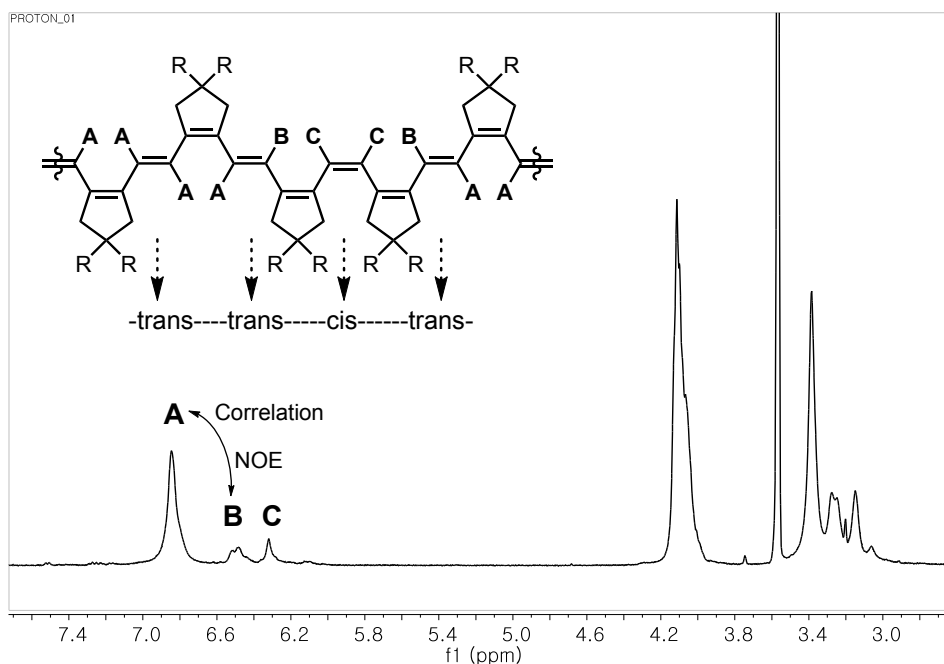
**Figure 6.7.** Changes in absorption spectra of PDHDPM solution in THF (0.1 g/l) (a) under fluorescent lighting and (b) dark at room temperature, and (c) dark at 0 °C.



**Figure 6.8.** Light source effect on the isomerization of PDHDPM in THF- $d_8$  (50 g/L).

### 6.3.3. Cis-to-trans isomerization of PCPV and Conformational Change

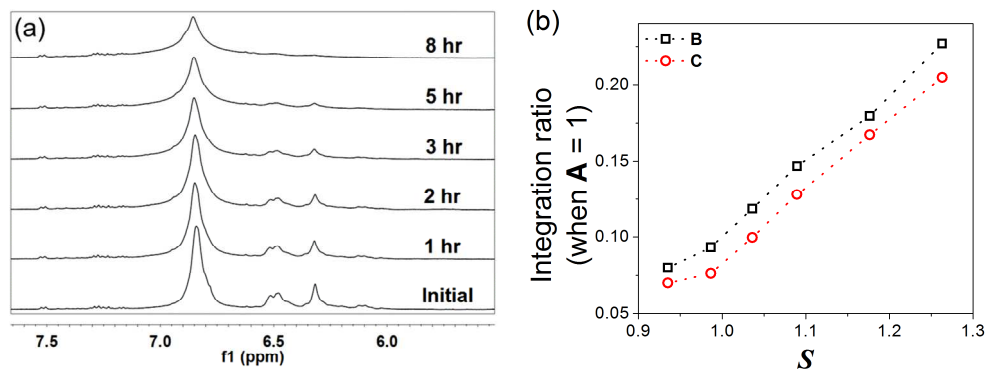
Based on all the factors that influenced the transition, we hypothesized that the conformational change was caused by *cis-to-trans* isomerization of the vinyl group in the conjugated backbone through a radical reaction, as the transition was accelerated in chlorinated solvents<sup>16</sup> and by exposure to light. If the transformation depended on the stereochemistry of the conjugated olefin, NMR spectroscopy would be a definitive tool for precise analysis. Unfortunately, the signals for the olefinic protons of the brush polymer (poly(PLLA)) were too weak in <sup>1</sup>H NMR spectra because of overwhelming signals from the polymeric side chains. Conversely, the <sup>1</sup>H NMR spectrum of PDHDPM showed clear signals for the conjugated olefinic protons. To suppress the transformation, we chose THF-*d*<sub>8</sub> as the optimal solvent for NMR analysis. Before aging, three different olefinic signals were initially observed (Figure 6.9), labeled as **A** (6.86 ppm), **B** (6.52 ppm), and **C** (6.33 ppm). Interestingly, other groups observed only a single olefinic signal at 6.8 ppm in CDCl<sub>3</sub>.<sup>17</sup> To fully characterize these peaks, we conducted two-dimensional (2D) NMR analysis, homonuclear correlation spectroscopy (COSY), and Nuclear Overhauser effect spectroscopy (NOESY; Figure S6.2 and Figure S6.3). First, singlet **A** was unambiguously assigned to the *E*-olefin proton. Definitive cross peak coupling between the **A** and **B** protons was observed in the COSY spectrum, confirming that **B** was also an *E*-olefin proton but located in a different environment than **A**. NOESY revealed a strong interaction between **B** and **C**, but COSY showed no through-bond interaction. Therefore, we assigned the **C** proton as belonging to the *Z*-olefins and **B** as the *E*-proton next to the *Z*-olefin, which brings **B** and **C** very close to each other in space. The integration values of **B** and **C** were nearly equal, supporting the assignment of a *trans-cis-trans* structure. From these results, the initial *E:Z* ratio was calculated as 5.4:1 (16% *cis*-olefin).



**Figure 6.9.**  $^1\text{H}$  NMR spectrum of PDHDPM in  $\text{THF-}d_8$  with the protons assigned by 2D NMR spectroscopy.

To understand the origin of the coil-to-rod transition, we monitored the changes in the *E:Z* ratio of the polymer with aging time. Indeed, as the aging proceeded, a gradual decrease in the signals for **B** and **C** was evident, and the initial *E:Z* ratio of 5.4 increased to 11.7 after 5 h. The signals from **B** and **C** disappeared completely after 8 h (Figure 6.10a). Moreover, the real-time changes in the *S*-values correlated well with the integration changes in the NMR spectra when the polymer solution was aged by blue LED light (Figure 6.10b). For example, the initial *E:Z* ratio in Figure 6.10a was 5.4:1 when *S* was 1.26, and after 5 h of aging, the *E:Z* ratio increased to 11.7:1 with a concomitant decrease of *S* to 0.99, confirming that the *cis*-to-*trans* isomerization caused the coil-to-rod transition. This isomerization extended the polymer conformation because the *cis*-geometry of the olefin imposes kinks in the polymer (more steric hindrance), resulting in a twist in the conjugated backbone and a lower coplanarity, while the *trans*-olefin experiences no such hindrance, thereby increasing the conjugation length and

stretching the polymer chain. In short, the conformational transformation by aging was caused by a change in the molecular structure, *cis*-to-*trans* isomerization, which led to a macroscopic change.

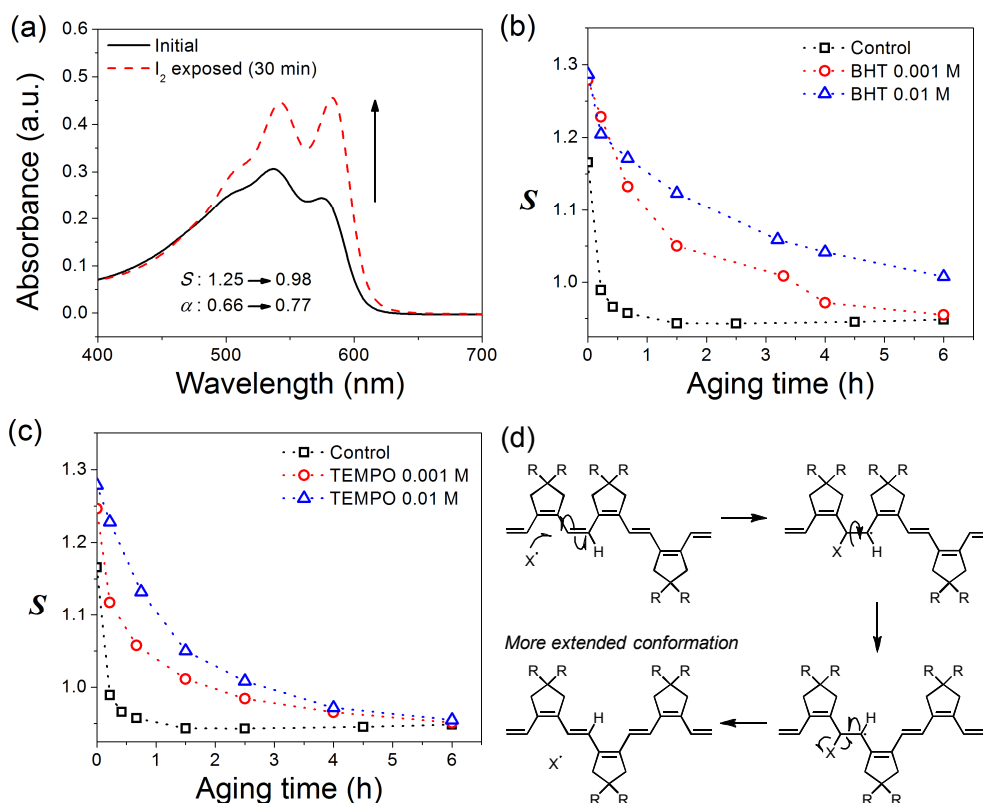


**Figure 6.10.** (a) Change in the  $^1\text{H}$  NMR spectrum for a PDHDPM solution in  $\text{THF-}d_8$  aged by blue LED light and (b) a plot of  $S$  and the corresponding integration ratios of **B** and **C** from  $^1\text{H}$  NMR spectra.

To provide further support for the *cis*-to-*trans* isomerization and to understand the mechanism, we designed two more experiments. (i)  $\text{I}_2$  addition: Iodine is a well-known reagent that isomerizes olefins including polyacetylene.<sup>18</sup> We prepared a PDHDPM film and exposed it to iodine vapors. The excess iodine was removed by vacuum, and subsequent absorption spectrum analysis and shape parameter analysis in THF revealed that the coil-to-rod transition occurred rapidly within 30 min (Figure 6.11a). The addition of iodine to the polymer solution induced the same rapid isomerization and transformation to the rod-like structure. (ii) Addition of a radical scavenger: Based on the observation that the isomerization was facilitated by light, a radical generator, we proposed that the isomerization proceed through a radical mechanism. To test this idea, a radical scavenger, butylated hydroxytoluene (BHT), was added to the polymer solution in chloroform to monitor the effect. Indeed, the solution exposed to 0.001 M BHT underwent a much slower transition compared to the control experiment without



BHT (Figure 6.11b). Furthermore, adding more BHT (0.01 M) retarded the transition even further. TEMPO, another radical scavenger, worked in a similar fashion to reduce the rate of isomerization by the same mechanism (Figure 6.11c). All the data supported the coil-to-rod transition due to *cis*-to-*trans* isomerization via a radical mechanism.



**Figure 6.11.** Change in the UV-vis spectra by (a) I<sub>2</sub> vapor and (b) BHT and (c) TEMPO addition in chloroform. (d) Isomerization by radical mechanism.

Even though the initial *cis*-vinylene content was relatively low (16%), the *cis*-component could behave as a “defect” to shorten the effective conjugation length, resulting in a more coil-like conformation. Therefore, the irreversible isomerization to *trans*-vinylene resulted in a dramatic spectral change. We can perceive this phenomenon as an extension of short polyene systems such as carotenoids, which show a similar behavior. For example, a similar change in the

vibronic peaks was observed in the absorption spectra for the mono-*cis* and all-*trans* isomers of  $\beta$ -carotene.<sup>19</sup> However, in the case of the polymer, the changes are more drastic, as they involved more than just a local molecular change, but a macroscopic conformational change in the nanostructure, as confirmed by the Mark–Houwink–Sakurada parameter.

Our conclusion can explain many observations in the literature. First, others could not notice this transition because DCM and chloroform were used, both of which promote rapid isomerization, and thus, only *E*-olefins were obtained. Second, a clean transformation to a rod-like structure was observed for the brush polymer, as confirmed by the viscosity and AFM analysis. This also explains why the isomerization for the brush polymer was much slower than that for PDHDPM, because the bulky polymeric side chains retarded the radical isomerization. The observation of well-resolved vibronic bands in solution even at room temperature is a unique characteristic of PCPV, which distinguishes it from many other conjugated polymers whose absorption spectra usually exhibit ill-defined and broadened electronic transitions. With numerous debates on the origins and contributions of the inhomogeneous line broadening of the optical spectra of PPVs,<sup>20</sup> the intense 0–0 vibronic transition of PCPVs containing only *E*-olefins may provide an interesting insight into the structure–property relationships of conjugated polymers<sup>6</sup> as well as their energy relaxation dynamics.<sup>21</sup>

## 6.4. Conclusion

It was demonstrated that PCPV, a product of CP, in organic solution showed unique coil-to-rod conformational changes over time. Parallel observation of the change in absorption spectra and Mark-Houwink-Sakurada plots proved that the brush polymer, poly(PLLA), underwent the coil-to-rod transition by simple aging in organic solvents. It was disclosed that this conformational transition is a general phenomenon of PCPV backbone, rather than a particular property of the brush polymer. From our detailed  $^1\text{H}$  NMR spectroscopic observations, we confirmed that the initial polymer containing 16% *cis*-olefin was isomerized to the final structure of all-*trans*-vinylene. This *cis*-to-*trans* isomerization resulted in a decrease in  $S$  and an increase in the shape factor  $\alpha$ , confirming the chain extension of PCPV leading to the coil-to-rod transition. A radical mechanism was proposed for the isomerization based on several control experiments (solvent, light, and the addition of iodine and radical scavengers). The linear relationships among  $S$ , the  $E:Z$  ratio, and  $\alpha$  showed a unique correlation of chemical, optical, and physical properties, supporting the changes in macroscopic structure. It is important to emphasize that all the transitions were slow enough in THF so that the analyses could be reliably conducted, whereas the transition in DCM or chloroform was too rapid to be detected.

## 6.5. Experimental Section

### Characterization

$^1\text{H}$  NMR and  $^{13}\text{C}$  NMR spectra were recorded by Varian/Oxford As-500 (500 MHz for  $^1\text{H}$  and  $^{13}\text{C}$ ) spectrometer and Agilent 400-MR (400 MHz for  $^1\text{H}$ ). UV-vis spectra were measured by Jasco Inc. UV/vis-Spectrometer V-550. Size exclusion chromatography (SEC) for the polymer analysis was carried out with Waters system (1515 pump, 2414 refractive index detector) and Shodex GPC LF-804 column on samples diluted in 0.001-0.003 wt% by THF (GPC grade, J. T. Baker<sup>®</sup>) and filtered through a 0.20- $\mu\text{m}$  PTFE filter. Flow rate was 1.0 mL/min and temperature of the column was maintained at 35 °C. For the MALLS-VIS-RI analysis (obtaining Mark-Houwink-Sakurada plot and shape parameter  $\alpha$ ), Wyatt triple detector, Dawn 8+ / Viscostar<sup>®</sup> II / Optilab<sup>®</sup> T-rEX were used. Dynamic Light Scattering (DLS) data were obtained in 1 g/L THF solution by Malvern Zetasizer Nano-S.

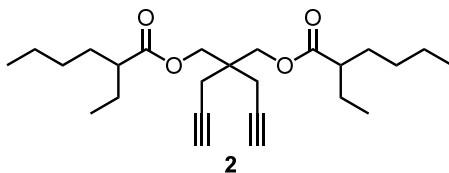
### Materials

All reagents which are commercially available from Sigma-Aldrich<sup>®</sup> and Alfa Aesar<sup>®</sup>, without additional notes, were used without further purification. All of the monomers and third generation Grubbs catalyst were prepared following the reported literature.<sup>7</sup> THF for the polymerization was distilled over sodium and benzophenone, and degassed by Ar bubbling for 10 minutes before using. For aging and GPC analysis, BHT-contained (104 ppm) GPC grade THF was purchased from J. T. Baker<sup>®</sup>. NMR solvent (THF- $d_8$ , 99.50% D, 0.75 mL) was purchased from euriso-top<sup>®</sup> and used without further purification.

## General polymerization procedure

To a 4-mL sized screw-cap vial with a septum were added monomer and a magnetic bar. The vial was purged with argon four times, and degassed THF was added ( $[M]_0$ : 0.05 M for poly(PLLA) and 0.5 M for others). The solution of initiator was added at once under vigorous stirring. The reaction was quenched by excess ethyl vinyl ether after desired reaction time, and precipitated in a poor solvent (diethyl ether and acetone mixture (9:1) for poly(PLLA), and methanol for others). Obtained solid was filtered and dried *in vacuo*. (Caution: Do not dissolve the polymer after precipitation, because the isomerization can occur.)

## Synthesis and characterization of **2**



To a mixture solution of 4,4-bis(hydroxymethyl)-1,6-heptadiyne<sup>6b</sup> (323.2 mg, 2.12 mmol), triethylamine (1.48 mL, 10.6 mmol) and 4-dimethylaminopyridine (DMAP) (13.0 mg, 0.106 mmol) in dichloromethane (6 mL), ethylhexanoyl chloride (0.80 mL, 4.67 mmol) was added dropwisly at 0 °C. The reaction mixture was stirred overnight at room temperature. The reaction was quenched by adding saturated NaHCO<sub>3</sub> aqueous solution and stirred for a few minutes. The mixture was washed with saturated NH<sub>4</sub>Cl solution and extracted by ethyl acetate (75 mL\*2). The organic layer was dried over MgSO<sub>4</sub> and concentrated to give a yellow colored liquid. It was purified by flash column chromatography on silica gel (ethyl acetate : hexane = 1 : 20,  $R_f$  = 0.24) to afford compound **2** as a pale yellow liquid (828.6 mg, 2.05 mmol, 96%). <sup>1</sup>H NMR (500 MHz, CDCl<sub>3</sub>):  $\delta$  0.88 (m, 12 H), 1.21-1.35 (m, 8 H), 1.43-1.66 (m, 8 H), 2.03 (t, 2 H), 2.29 (m, 2 H), 2.41 (d, 4 H), 4.11 (s, 4 H); <sup>13</sup>C NMR (125MHz, CDCl<sub>3</sub>) :  $\delta$  11.8, 13.9, 22.1, 22.6, 25.4, 29.5, 31.7, 40.0, 47.4, 64.5,

71.6, 78.7, 175.8; HRMS (EI+): calcd. for C<sub>25</sub>H<sub>40</sub>O<sub>4</sub>, 404.2926, found, 404.2925

**Poly(2):** <sup>1</sup>H NMR (500 MHz, CDCl<sub>3</sub>): δ 0.88 (br m, 6 H), 1.27 (br m, 8 H), 1.40-1.75 (br m, 8 H), 2.32 (br m, 2 H), 2.40-2.95 (br m, 4H), 3.80-4.40 (br m, 4 H), 6.10-6.80 (br m, 2 H); <sup>13</sup>C NMR (125MHz, CDCl<sub>3</sub>) : δ. 11.9, 14.0, 22.6, 25.5, 29.6, 31.6, 39.8, 43.0, 47.3, 66.9, 123.1, 137.6, 176.0

### **Aging procedure and UV–vis spectra measurement of polymer solutions**

After dissolving the polymers in various organic solvents (generally 0.2 g/l), it was left on the laboratory bench under fluorescent light. All of the UV–vis absorption spectra were obtained in THF with proper concentration.

To compare three data (<sup>1</sup>H NMR, Huang-Rhys factor *S*, shape parameter *α*) in real-time, we followed this special procedure: (a) Prepare PDHDPM in THF-*d*<sub>8</sub> following the polymerization procedure (0.1 mmol of DHDPM in 0.2 mL of THF-*d*<sub>8</sub>, M/I ratio=100). (b) After the monomer was fully converted to the polymer, dilute the solution (0.2 mL of reaction mixture + 0.5 mL of THF-*d*<sub>8</sub>) for NMR measurement, and transfer it into sealed NMR tube. (c) Obtain initial <sup>1</sup>H NMR spectrum, and take 30 μL of the solution from the NMR tube by using micro-syringe. The extract was dried *in vacuo*, and its *S* and *α* values were obtained from UV–vis absorption spectrum and viscosity analysis. (d) Age the remaining polymer solution under irradiation of LED (blue, green) on NMR tube, and repeat (c) after 1, 2, 3, 5, and 8 hours. A control experiment (dark) was performed in the same manner, but the NMR tube was stored in the dark.

## 6.6. Supporting Information

### Huang-Rhys factor calculation

Huang-Rhys factor (S) is defined by the equation below:

$$\frac{I_{0 \rightarrow n}}{\sum_{n=0}^{\infty} I_{0 \rightarrow n}} = \frac{S^n e^{-S}}{n!}$$

$$\text{when } n = 0, \frac{I_{0 \rightarrow 0}}{\sum_{n=0}^{\infty} I_{0 \rightarrow n}} = e^{-S}$$

$$\text{when } n = 1, \frac{I_{0 \rightarrow 1}}{\sum_{n=0}^{\infty} I_{0 \rightarrow n}} = S e^{-S}$$

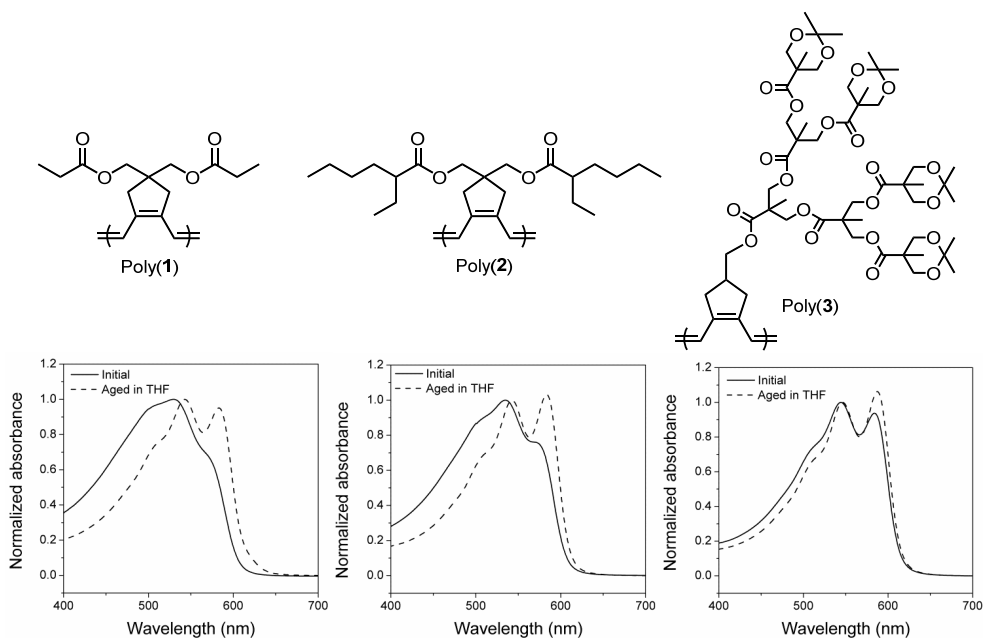
$$\therefore S = \frac{I}{e^{-S}} * \frac{I_{0 \rightarrow 1}}{\sum_{n=0}^{\infty} I_{0 \rightarrow n}} = \frac{\sum_{n=0}^{\infty} I_{0 \rightarrow n}}{I_{0 \rightarrow 0}} * \frac{I_{0 \rightarrow 1}}{\sum_{n=0}^{\infty} I_{0 \rightarrow n}} = \frac{I_{0 \rightarrow 1}}{I_{0 \rightarrow 0}}$$

( $I_{0 \rightarrow n}$  is an intensity of 0–n transition)

Therefore, S was calculated by the maximum intensity of each band (0–0 and 0–1).

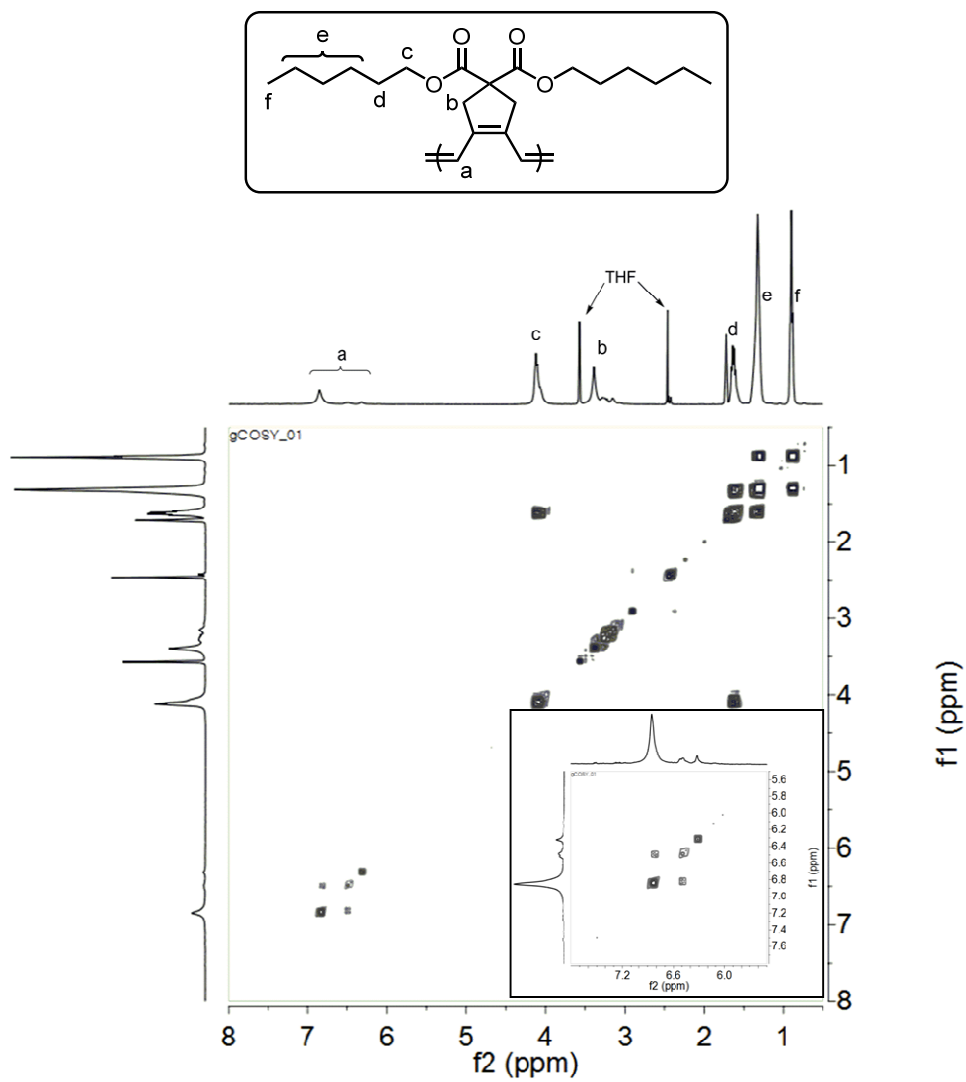
**Table S6.1. Characterization of PDHDPM prepared in THF- $d_8$  for the experiment of light irradiation**

Light source	$M_n$ (MALLS)	PDI (MALLS)
Blue LED	41.2 k	1.68
Green LED	47.8 k	1.42
Dark	37.3 k	1.81

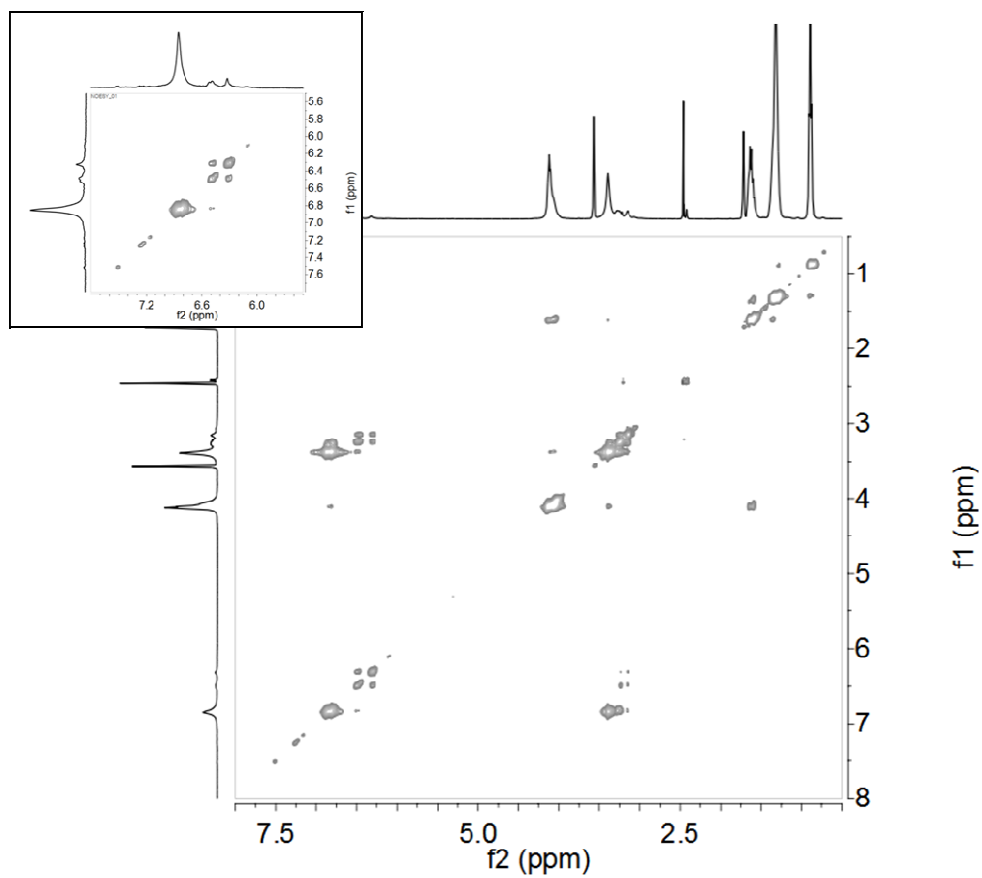


**Figure S6.1. Changes in absorption spectra of PCPV derivatives.**





**Figure S6.2.** COSY of PDHDPM (inset: conjugated olefin region)



**Figure S6.3.** NOESY of PDHDPM (inset: conjugated olefin region)

## 6.7. References and Notes

- <sup>†</sup> Portions of this chapter have been previously reported, see: (a) Kang, E.-H.; Lee, I.-H.; Choi, T.-L. *ACS Macro Lett.* **2012**, *1*, 1098-1102. (b) Kang, E.-H.; Choi, T.-L. *ACS Macro Lett.* **2013**, *2*, 780-784.
- (1) Spiegel, D.; Pincus, P.; Heeger, A. J. *Synthetic Metals* **1989**, *28*, C385-C391.
  - (2) Schwartz, B. J. *Annu. Rev. Phys. Chem.* **2003**, *54*, 141-172.
  - (3) (a) Daoust, G.; Leclerc, M. *Macromolecules* **1991**, *24*, 455. (b) Adachi, T.; Lakhwani, G.; Traub, M. C.; Ono, R. J.; Bielawski, C. W.; Barbara, P. F.; Vanden Bout, D. A. *J. Phys. Chem. B* **2012**, *116*, 9866-9872.
  - (4) (a) Hagler, T. W.; Pakbaz, K.; Voss, K. F.; Heeger, A. J. *Phys. Rev. B* **1991**, *44*, 8652-8666. (b) Yu, J.; Hu, D.; Barbara, P. F. *Science* **2000**, *289*, 1327-1330. (c) Huser, T.; Yan, M.; Rothberg, L. J. *Proc. Natl. Acad. Sci. USA* **2000**, *97*, 11187-11191.
  - (5) (a) Fox, H. H.; Schrock, R. R. *Organometallics* **1992**, *11*, 2763-2765. (b) Fox, H. H.; Wolf, M. O.; O'Dell, R.; Lin, B. L.; Schrock, R. R.; Wrighton, M. S. *J. Am. Chem. Soc.* **1994**, *116*, 2827-2843. (c) Schattenmann, F. J.; Schrock, R. R.; Davis, W. M. *J. Am. Chem. Soc.* **1996**, *118*, 3295-3296. (d) Anders, U.; Nuyken, O.; Buchmeiser, M. R.; Wurst, K. *Angew. Chem., Int. Ed.* **2002**, *41*, 4044-4047.
  - (6) (a) Ledoux, I.; Samuel, I. D. W.; Zyss, J.; Yaliraki, S. N.; Schattenmann, F. J.; Schrock, R. R.; Silbey, R. J. *Chem. Phys.* **1999**, *245*, 1-16. (b) Wood, P.; Samuel, I. D. W.; Schrock, R.; Christensen, R. L. *J. Chem. Phys.* **2001**, *115*, 10955-10963. (c) Christensen, R. L.; Faksh, A.; Meyers, J. A.; Samuel, I. D. W.; Wood, P.; Schrock, R. R.; Hultsch, K. C. *J. Phys. Chem. A* **2004**, *108*, 8229-8236.
  - (7) Anders, U.; Nuyken, O.; Buchmeiser, M. R. *Des. Monomers Polym.* **2003**, *6*, 135-143.
  - (8) Spectroscopic analysis of oligomer of **I**:

- (a) Scriban, C.; Amagai, B. S.; Stemmler, E. A.; Christensen, R. L.; Schrock, R. R. *J. Am. Chem. Soc.* **2009**, *131*, 13441-13452. (b) Christensen, R. L.; Enriquez, M. M.; Wagner, N. L.; Peacock-Villada, A. Y.; Scriban, C.; Schrock, R. R.; Polivka, T.; Frank, H. A.; Birge, R. R. *J. Phys. Chem. A* **2013**, *117*, 1449-1465.
- (9) Ohira, A.; Swager, T. M. *Macromolecules* **2007**, *40*, 19-25.
- (10) (a) Yu, J.; Hayashi, M.; Lin, S. H.; Liang, K.-K.; Hsu, J. H.; Fann, W. S.; Chao, C.-I.; Chuang, K.-R.; Chen, S.-A. *Synth. Met.* **1996**, *82*, 159-166. (b) Zeng, Q. G.; Ding, Z. J. *J. Phys.: Condens. Matter* **2004**, *16*, 5171-5178. (c) Quan, S.; Teng, F.; Xu, Z.; Qian, L.; Zhang, T.; Liu, D.; Hou, Y.; Wang, Y.; Xu, X. *J. Lumin.* **2007**, *124*, 81-84.
- (11) (a) Bassler, H.; Schweitzer, B. *Acc. Chem. Res.* **1999**, *32*, 173-182. (b) Heeger, A. J. *Chem. Soc. Rev.* **2010**, *39*, 2354-2371.
- (12) The  $\alpha$  value (0.73) is slightly lower than the theoretical value of the rigid-rod structure (0.8) because the polymeric side chains in brush polymers locally adopt random coil conformations, which lead to lower  $\alpha$  values. This is typically observed for the brush polymers, whereas the  $\alpha$  values for dendronized polymers containing more densely packed side chains are over 0.8. See: Kim, K. O.; Choi, T.-L. *ACS Macro Lett.* **2012**, *1*, 445-448.
- (13) (a) Patel, G. N.; Chance, R. R.; Witt, J. D. *J. Chem. Phys.* **1979**, *70*, 4387-4392. (b) Lim, K. C.; Fincher, C. R.; Heeger, A. J. *Phys. Rev. Lett.* **1983**, *50*, 1934-1937. (c) Taylor, M. A.; Odell, J. A.; Batchelder, D. N.; Campbell, A. J. *Polymer* **1990**, *31*, 1116-1121.
- (14) Commercially available SEC grade THF stabilized with butylated hydroxytoluene (104 ppm) was used, because without any stabilizer, the decomposition of the conjugated polymers occurred at faster rate, presumably due to peroxide radical generated from THF.
- (15) To measure Mark-Houwink-Sakurada parameter  $\alpha$  by SEC-viscometry analysis, and  $R_h$  by DLS, the higher concentration was required than

normal aging condition.

- (16) Chiefari, J.; Rizzardo, E. Control of Free Radical Polymerization by Chain Transfer Methods. In *Handbook of Radical Polymerization*; Matyjaszewski, K.; Davis, T. P., Eds.; John Wiley & Sons, Inc.: Hoboken, 2002.
- (17) Anders, U.; Nuyken, O.; Buchmeiser, M. R.; Wurst, K. *Macromolecules* **2002**, *35*, 9029-9038.
- (18) (a) Tanaka, K.; Yoshizawa, K.; Ohzeki, K.; Yamabe, T. *Solid State Commun.* **1983**, *45*, 391-393. (b) Ideses, R.; Shani, A. *J. Am. Oil. Chem. Soc.* **1989**, *66*, 948-952.
- (19) O'Neil, C. A.; Schwartz, S. J. *J. Chromatogr. A* **1992**, *624*, 235-252.
- (20) Hoffmann, S. T.; Bäessler, H.; Köhler, A. *J. Phys. Chem. B* **2010**, *114*, 17037-17048.
- (21) Antognazza, M. R.; Lüer, L.; Polli, D.; Christensen, R. L.; Schrock, R. R.; Lanzani, G.; Cerullo, G. *Chem. Phys.* **2010**, *373*, 115-121.

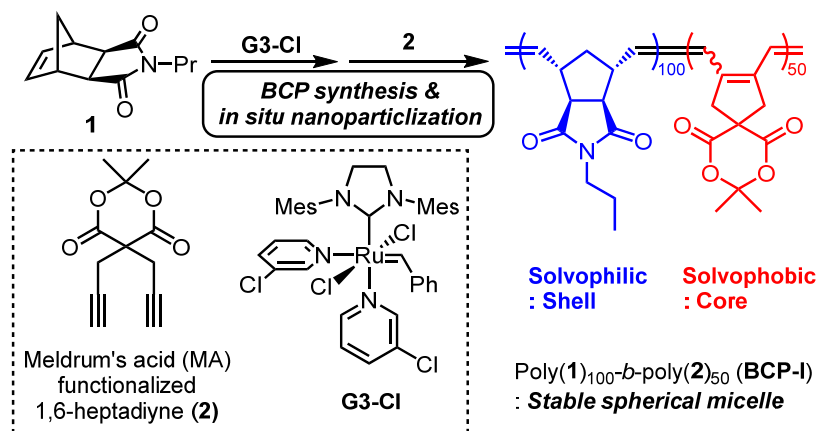
# Chapter 7. Light-driven Evolution of Nanostructures Prepared from Cyclopolymerization of 1,6-Heptadiynes

## 7.1. Abstract

For the spontaneous macroscopic evolution of the nanostructures obtained by in situ nanoparticlization of conjugated polymers (INCP), a new strategy utilizing a unique conformational change of poly(cyclopentenylene-vinylene) is studied. The combination of living ring-opening olefin metathesis polymerization (ROMP) and cyclopolymerization produced block and gradient copolymers through one-pot or one-shot polymerization, which initially formed 0D spheres via INCP. Then, the core block of the micelle stiffened through a coil-to-rod conformational change by simple aging in organic solvents because of *cis*-to-*trans* isomerization of the conjugated polymer under the light. Subsequently, this enhanced the  $\pi$ - $\pi$  interaction between the cores, and eventually promoted the hierarchical growth of stable nanostructures from 0D spheres to 1D nanocaterpillars or 2D sheet-like architectures. This time-dependent macroscopic evolution provides deeper insight into the production of a variety of kinetically fixed nano- and mesoscale structures through INCP.

## 7.2. Introduction

Conjugated polymers have become powerful candidates for the self-assembly of BCPs, not only because their crystallization provides a strong driving force for self-assembly, but also because of the interesting optoelectronic properties of the resulting nanomaterials.<sup>1</sup> For simple processes to produce self-assembled nanostructures from polymeric materials without post-modifications, a new strategy of spontaneous formation of nanostructures during polymerization, which was termed as *in situ* nanoparticlization of conjugated polymers (INCP) was developed.<sup>2-5</sup> Typically, conjugated polymers without side chains are insoluble in all solvents due to strong  $\pi$ - $\pi$  interactions; ironically, this became the crucial driving force for the self-assembly. Early investigations of *in situ* INCP started with the living ring-opening olefin metathesis polymerization (ROMP) of norbornene (NB) derivatives and cyclooctatetraene (COT), which spontaneously produced the core-forming polyacetylene (PA) block.<sup>2</sup> Based on this observation, the combination of ROMP and cyclopolymerization of 1,6-heptadiyne derivatives broadened the scope of INCP. It was reported the synthesis of a BCP using the product of the ROMP of an NB derivative (**1**) as the soluble block and the product of the cyclopolymerization of Meldrum's acid (MA)-substituted 1,6-heptadiyne (**2**) as the core block (Scheme 7.1).<sup>6</sup> As a result, the insoluble poly(cyclopentenylene-vinylene) (PCPV) backbone containing the MA moiety spontaneously formed spherical micelles via INCP process. Unfortunately, no higher dimensional structure was observed with **BCP-I**.



**Scheme 7.1.** Synthesis of block copolymer using living ROMP and cyclopolymerization

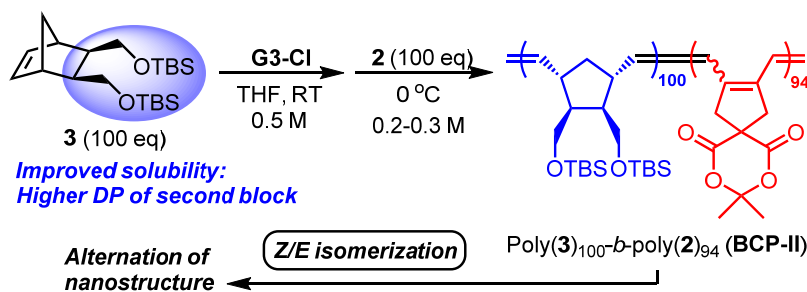
In Chapter 6, we described a coil-to-rod conformational change of PCPV by simple *cis*-to-*trans* olefin isomerization through evidence from a spectral change in UV–Vis absorption, and increases in hydrodynamic volume and shape parameter,  $\alpha$ , obtained from Mark-Houwink-Sakurada plots. This transition implied that the polymer backbone became more planar, rigid, and extended. Taking advantage of this unique transition of PCPV, we proposed that the original 0D nanospheres produced by INCP could spontaneously evolve into higher dimensional nanostructures by themselves during light-induced molecular level configurational change in the PCPV backbone, which would change the volume of the micelle core. In this chapter, we address a new INCP strategy to form multidimensional nanostructures using block and gradient copolymers prepared from living ROMP and cyclopolymerization in one-pot or one-shot procedures. Using this simple transition, even purified polymers in solution underwent spontaneous evolution from 0D to higher dimensional 1D or 2D nanostructures over time. Therefore, we could take real-time snapshots of the morphological changes of the nanostructures, revealing additional insights into the mechanism of hierarchical transformations such as INCP.



## 7.3. Results and Discussion

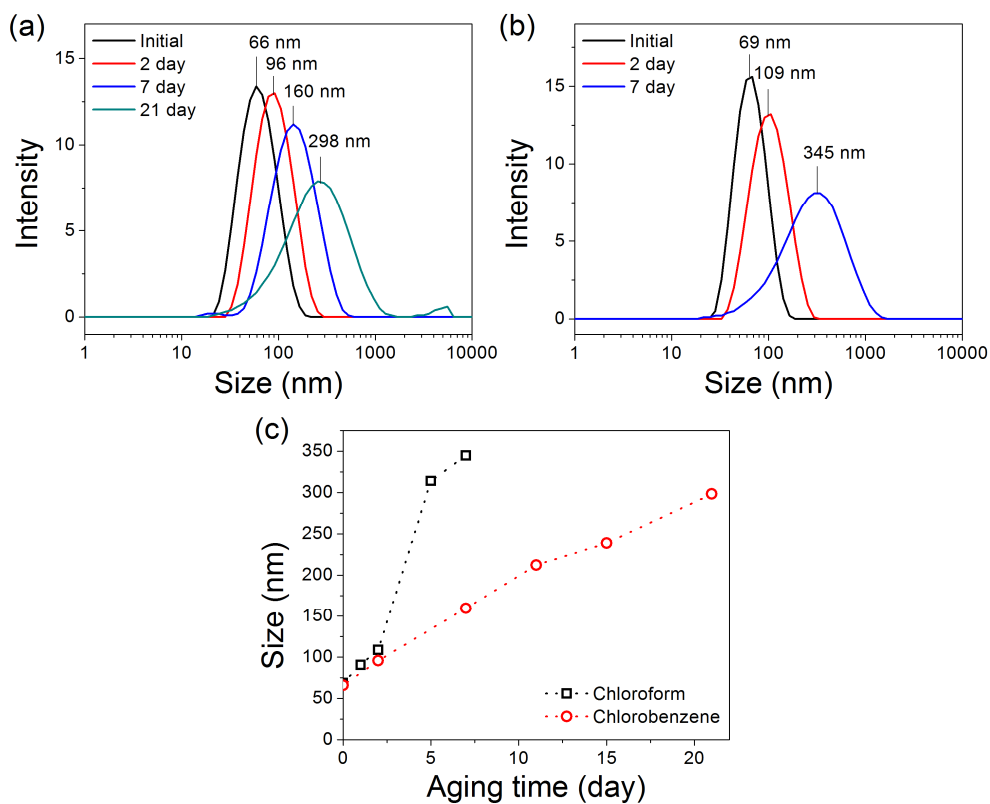
### 7.3.1. Structural Evolution of Poly(NB)-*b*-poly(MA-1,6-heptadiyne)

The third generation Grubbs catalyst (**G3-Cl**) (Scheme 7.1) was employed to synthesize BCPs by a combination of the living olefin metathesis polymerizations, ROMP and cyclopolymerization. Initially, we tested our hypothesis by monitoring the volume change in the previously reported poly(**1**)<sub>100</sub>-*b*-poly(**2**)<sub>50</sub> (**BCP-I**, Scheme 7.1). However, even with accelerated aging using a blue light-emitting diode (LED) for 11 h, the size of **BCP-I** increased only slightly from 64 to 83 nm (Figure S7.1). It seemed that the core exposure in **BCP-I** containing poly(**2**) with a low degree of polymerization (DP) (DP = 50) was not enough to induce intermicellar interactions. To achieve a more effective volume change in the core, incorporating poly(**2**) with a higher DP seemed essential; unfortunately, the DP was limited to only 50 because **BCP-I** containing poly(**2**) with a higher DP was insoluble and underwent precipitation. To synthesize a longer second block, a more soluble monomer, *exo*-2,3-bis((*tert*-butyldimethoxy)methyl)-5-norbornene (**3**), was introduced as the first block. Using **G3-Cl**, we prepared poly(**3**)-*b*-poly(**2**) (**BCP-II**) by living ROMP of **3** followed by living cyclopolymerization of **2**. Gratifyingly, this increased DP of the second block to almost 100 (Scheme 7.2). As expected, the new **BCP-II** spontaneously underwent INCP process to form the core-shell structure, which was confirmed by <sup>1</sup>H NMR spectroscopy, UV–Vis spectroscopy, and dynamic light scattering (DLS) analysis (Figure S7.2).

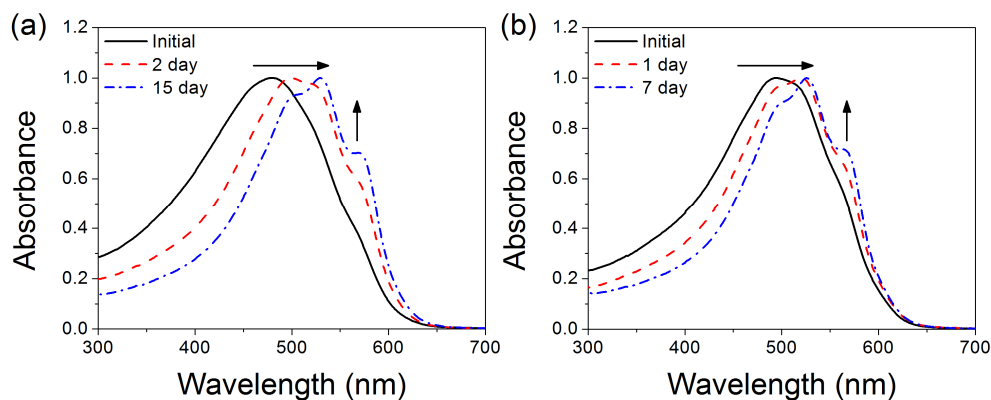


**Scheme 7.2.** Synthesis of block copolymer containing modified NB derivative (**3**) and MA-containing 1,6-heptadiyne (**2**)

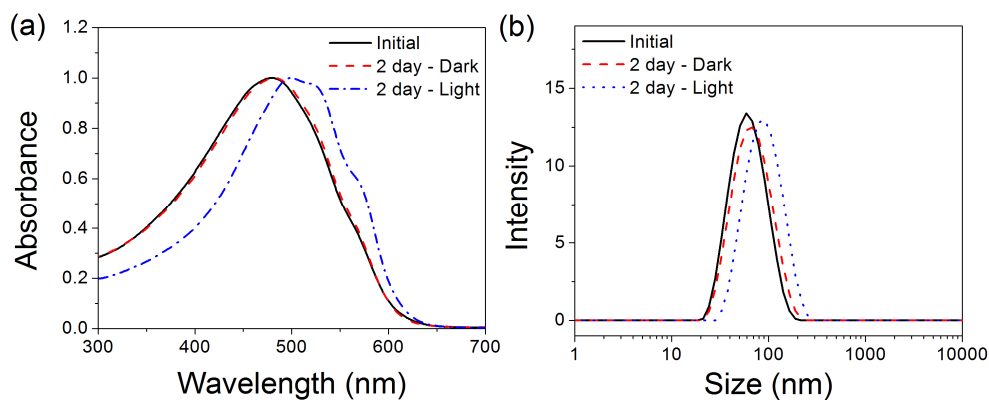
As an initial test of our hypothesis, purified solutions containing only **BCP-II**<sup>7</sup> were left on the workbench under conventional fluorescent lighting at room temperature for the olefin isomerization, and the size of the nanostructure in solution was monitored by DLS over time. Initially, the hydrodynamic diameter ( $D_h$ ) of the nanostructure from **BCP-II** was 66 nm, but the size indeed increased slowly up to 300 – 350 nm depending on aging time and solvents (chloroform and chlorobenzene) (Figure 7.1a and 7.1b). The rate of growth was much faster in chloroform with early saturation (5 days), whereas the growth of the nanostructure in chlorobenzene was slower but steady even after three weeks (Figure 7.1c). Clear changes in UV–Vis absorption provided an explanation for the size growing. Over the time, the  $\lambda_{\text{max}}$  values were red-shifted (in chlorobenzene: 480 nm  $\rightarrow$  530 nm, and in chloroform: 494 nm  $\rightarrow$  526 nm) and 0–0 vibronic bands increased accordingly (Figure 7.2), indicating successful *cis*-to-*trans* isomerization on the PCPV core. On the other hand, the control experiment under dark condition resulted in almost no changes in UV–Vis absorption spectrum and  $D_h$  (Figure 7.3). These observations suggested in favor of our hypothesis that the isomerization strategy might induce macroscopic evolution of the micelles.



**Figure 7.1.** DLS profiles of aged nanostructures (**BCP-II**) in (a) chlorobenzene (1 g/L) and (b) chloroform (1 g/L) at 20 °C. (c) Plot of size ( $D_h$ ) vs. aging time.



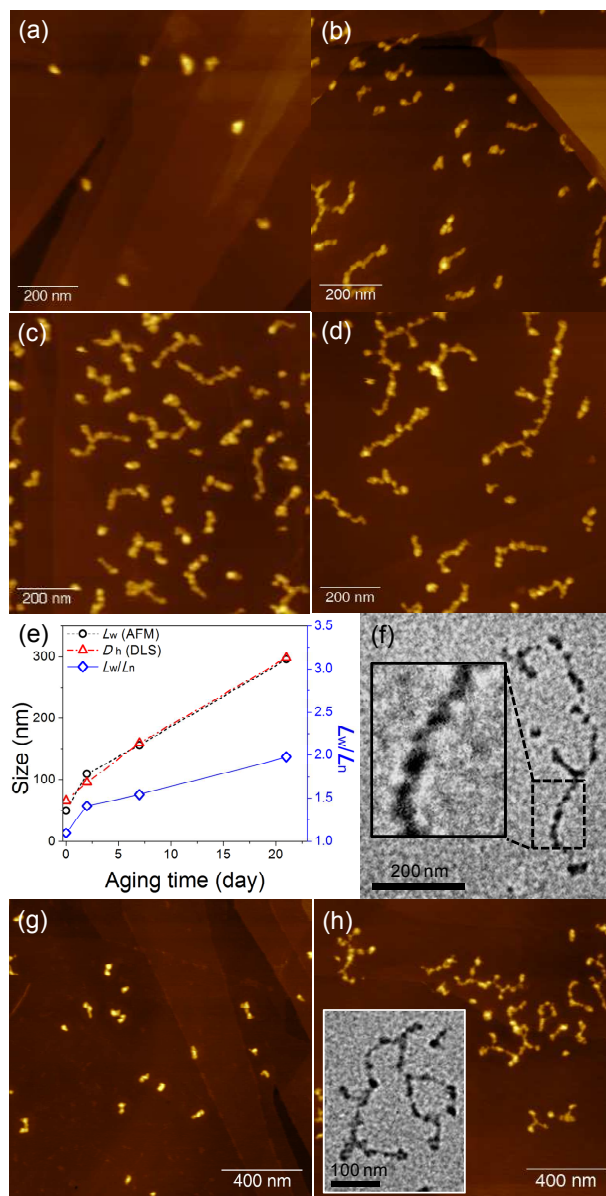
**Figure 7.2.** Changes in UV-vis absorption spectra of **BCP-II** by aging in (a) chlorobenzene and (b) chloroform.



**Figure 7.3.** Changes of (a) UV-vis absorption spectra and (b) DLS profiles of **BCP-II** by aging under the dark condition and light for 2 days in chlorobenzene.

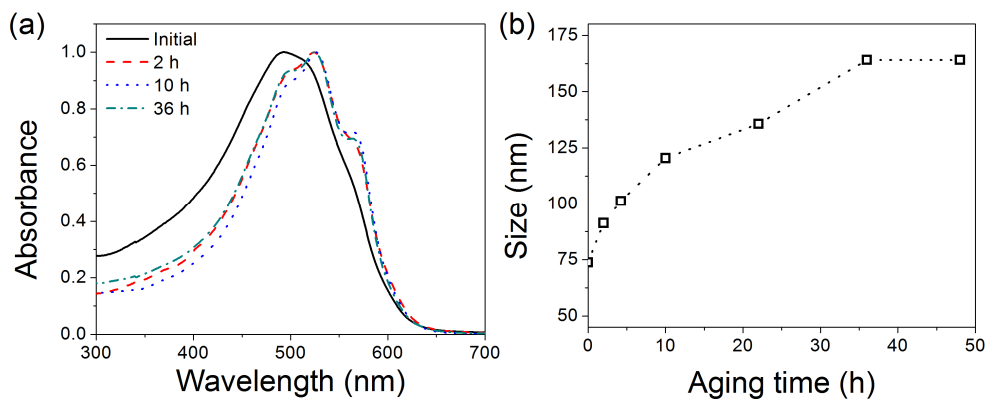
To visualize these evolutions, we imaged the nanostructures by atomic force microscopy (AFM) and transmission electron microscopy (TEM). First, the slowly growing micelle in chlorobenzene showed, over time, a transformation from spherical micelles to linear undulated caterpillar-like nanostructures. Time-dependent imaging of the nanostructures by AFM clearly illustrated the 1D elongation of caterpillars (Figure 7.4a-c) and even the generation of a few short-branched nanostructures (Figure 7.4d). Using AFM, the length of the nanostructures was determined at each stage of aging, and it was found that the increase in the weighted average length ( $L_w$ ) was in excellent agreement with the

$D_h$  obtained from intensity-based DLS measurements (Figure 7.4e). The length dispersity ( $L_w/L_n$ ) of the nanocaterpillars was broadened while aging (initial = 1.10; after 21 days = 1.98, Figure 7.4e and Figure S7.3). It implied that supramolecular growth occurred in a typical step-growth mechanism. TEM analysis, without any staining, provided insights on how aging of individual micelles evolved into larger 1D nanocaterpillars. TEM images showing only the core structure due to the much higher electron density on the conjugated PCPV block revealed that the nanocaterpillar structures were made from loosely interconnected individual spheres (Figure 7.4f). Therefore, one could conclude that the coil-to-rod transition, resulting from the *cis*-to-*trans* isomerization, caused the expansion and stiffening of the core, which led to the more favorable  $\pi$ - $\pi$  stacking of the PCPV conjugated backbones and eventually resulted in the macroscopic evolution toward 1D nanocaterpillars. The similar hierarchical growth of micelles was observed in the aging of **BCP-II** in chloroform where the isomerization and evolution of the nanostructure occurred more rapidly within 7 days (vs. 21 days in chlorobenzene). Due to the faster transformation in chloroform, more branched nanocaterpillars were observed by AFM and TEM (Figure 7.4g and 7.4h).

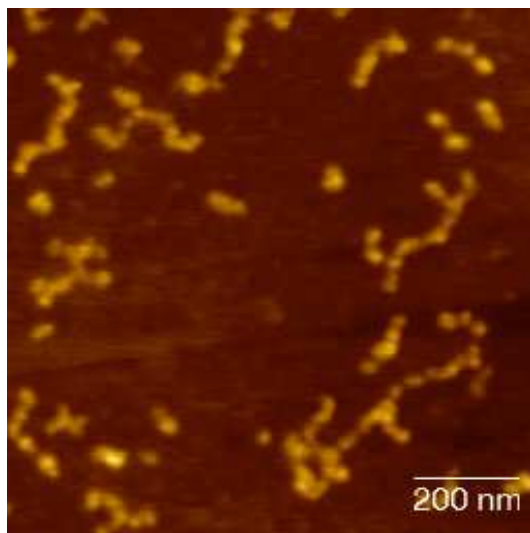


**Figure 7.4.** Growth of spherical micelles into 1D and branched structures. AFM height images from **BCP-II** (a) the initial and after (b) 2 days, (c) 7 days, and (d) 21 days of aging in chlorobenzene. (e) Plot showing the comparison between the weighted average length ( $L_w$ ), calculated from AFM (black, circle), and  $D_h$ , measured by DLS (red, triangle), and the change of in the length dispersity ( $L_w/L_n$ , right axis). (f) TEM image for the BCP after 21 days in chlorobenzene. AFM height images for **BCP-II** (g) before and (h) after 7 days of aging in chloroform (inset: a TEM image of the same sample).

Even though the macroscopic evolution occurred more rapidly in chloroform, it was still slower than the isomerization of a well-solvated homopolymer of a PCPV derivative. To accelerate the isomerization, a blue LED, the most efficient light source, was used to age the solution of **BCP-II** in chloroform (Figure 7.5a). As a result, the  $D_h$  of the micelle increased from 74 nm to more than 100 nm within 5 h, and the size became saturated at 164 nm after 1.5 days (Figure 7.5b). Just like the previous aging experiment under fluorescent light, the AFM results confirmed that the final product, after LED aging, showed linear and branched structures (Figure 7.6). Nevertheless, **BCP-II** did not show further evolution to higher dimensional nanostructures after aging. Consequently, we modified our strategy to changing the structure of the monomer of the first block to alter the core-shell interaction.<sup>2,3</sup>



**Figure 7.5.** (a) Change in UV-vis absorption spectra and (b) increase in  $D_h$  of **BCP-II** induced by aging in chloroform (1 mg/mL) under a blue LED.

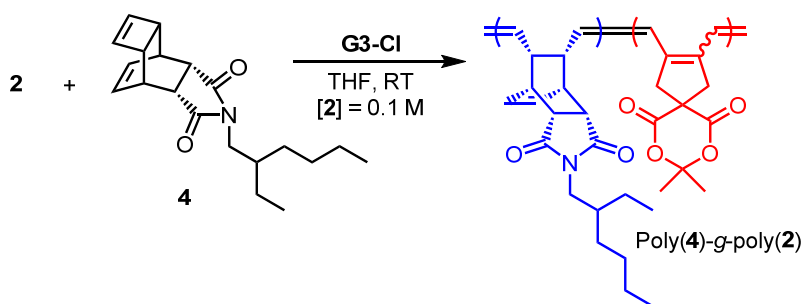


**Figure 7.6.** AFM image of **BCP-II** after 48 h of aging in chloroform under a blue LED.



### 7.3.2. One-shot Copolymerization of Poly(TD)-g-poly(MA-1,6-heptadiyne) and Structural Evolution

Recent reports suggested that the backbone of poly(*endo*-tricyclo[4.2.2.0]deca-3,6-diene) (PTD) was more rigid than that of PNB.<sup>7,8</sup> This affected the INCP behavior because BCPs containing the PTD shell and PA core allowed for enhanced  $\pi$ - $\pi$  interaction, resulting in the formation of 3D nanoaggregates.<sup>2,3</sup> By combining the effects of the rigid shell and the time-dependent expansion of the PCPV core, we designed and prepared another conjugated polymer that would also undergo spontaneous macroscopic evolution under the light by living ROMP and cyclopolymerization. Furthermore, the ROMP of *endo*-tricyclo[4.2.2.0]deca-3,6-diene (TD) derivatives has an advantage of allowing one-shot copolymerization to form gradient or block-like copolymers, because the catalyst preferentially reacts with the TD monomers.<sup>3,8,9</sup> Various feed ratios of **[2]**, **[4]**, and **[G3-Cl]** were screened for effective one-shot gradient or block-like copolymerization and INCP behavior (Scheme 7.3 and Table 7.1). A high **2:4** ratio (50:100, entry 1) required a very long reaction time of over 17 h. Therefore, the DP of **4** was fixed at 50 while that of **2** was varied from 10 to 50 for successful INCP. By simple one-shot reaction, copolymers having DP ratios of 50:30 and 50:50 clearly produced nanostructures with initial  $D_h$  of more than 100 nm (entries 3 and 4).



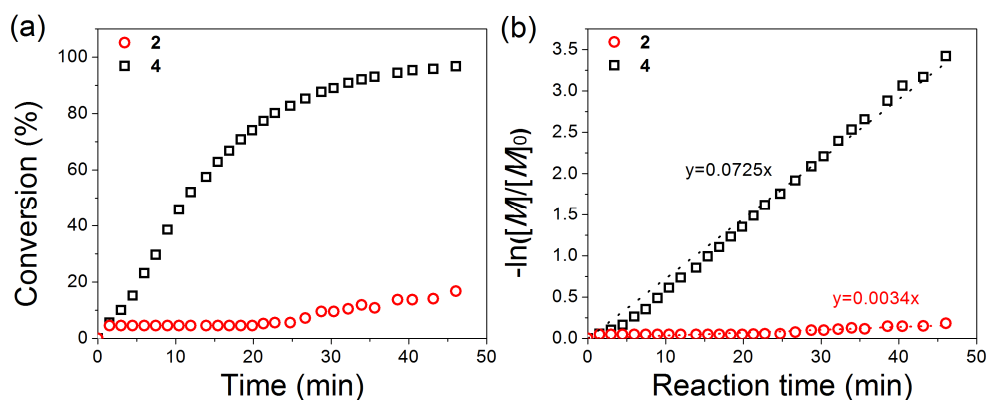
**Scheme 7.3.** One-shot gradient copolymerization of MA-1,6-heptadiyne (**2**) and TD derivative (**4**)

**Table 7.1. One-shot copolymerization of 2 and 4**

entry	4/2/G3-Cl	time (h)	conv (2) <sup>a</sup> (%)	D <sub>h</sub> (nm) <sup>b</sup>
1	100/50/1	17	95	106
2	50/10/1	1	93	36
3	50/30/1	2	Full	112
4	50/50/1	2.5	Full	146

<sup>a</sup>Calculated from <sup>1</sup>H NMR spectra. <sup>b</sup>DLS was measured using chloroform solutions (1 mg/mL).

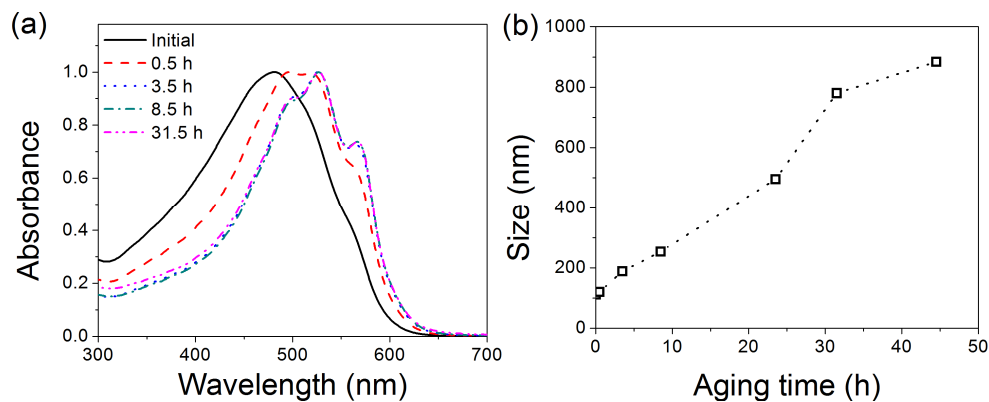
To examine the microstructure of these copolymers, the conversion of the two monomers during copolymerization was monitored by kinetic analysis using <sup>1</sup>H NMR spectroscopy (Figure 7.7a). In the early stage, the ROMP of **4** preferentially occurred with almost no conversion of **2**. Overall, the ROMP of **4** was 21 times faster than the cyclopolymerization of **2** ( $k_{p,4}/k_{p,2} = 0.0725/0.0034$ , Figure 7.7b), and this was similar to the rate difference during the one-shot copolymerization of the NB derivative and COT.<sup>3</sup> Thus, we concluded that the one-shot copolymerization produced a gradient copolymer (GCP), which spontaneously underwent INCP process.



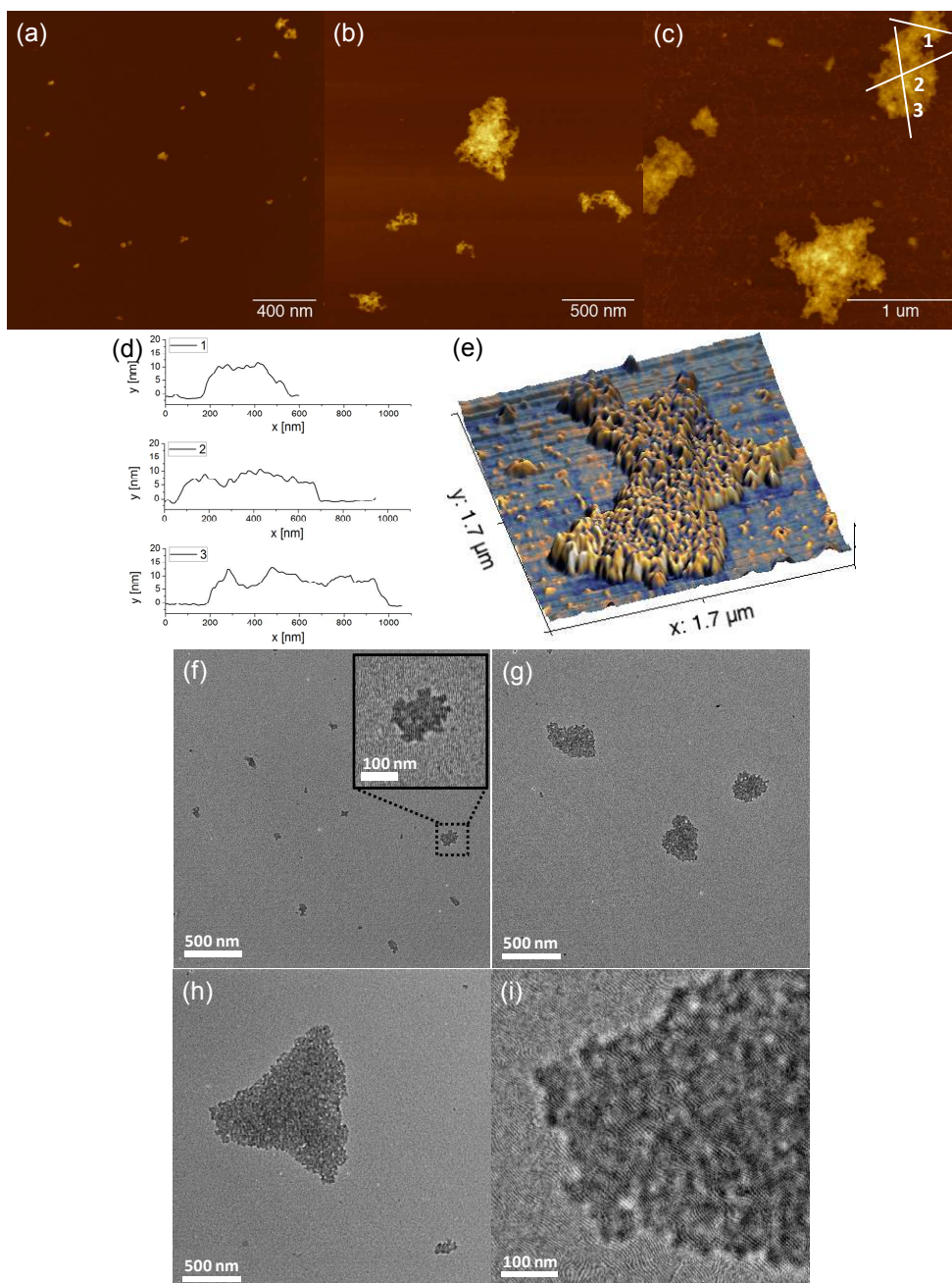
**Figure 7.7.** Plots of (a) monomer conversion vs. time and (b)  $-\ln([M]/[M]_0)$  vs. time for one-shot copolymerization at room temperature ( $[4]:[2]:[G3-Cl] = 50:30:1$ ,  $[2] = 0.1$  M).

Like the previous case with **BCP-II**, we monitored how the conformational changes in the core affected the evolution of nanostructures from the purified poly(**4**)<sub>50</sub>-*g*-poly(**2**)<sub>30</sub> (**GCP-50-30**) in chloroform under blue LED exposure. As expected, the  $\lambda_{\text{max}}$  from UV–Vis spectral analysis shifted from 480 nm to 527 nm and the 0–0 vibronic band grew stronger, confirming the facile *cis*-to-*trans* isomerization of the PCPV core (Figure 7.8a). According to DLS analysis, this led to a gradual increase in  $D_h$  from 112 to 884 nm (Figure 7.8b). So far, the growth mechanism, or pattern, appeared similar to that for **BCP-II**, but the change in magnitude was much larger for **GCP-50-30**. As a result, a more interesting macroscopic evolution was observed in the AFM and TEM images obtained during LED aging. The AFM images showed that the initial nanostructure was small spherical aggregates with a  $D_h$  of approximately 100 nm and variable height between 5 and 7 nm. Again, just like the DLS analysis, a gradual increase in size was observed by AFM and TEM (Figure 7.9a-c and f-h), and the nanostructures eventually grew to almost 1  $\mu\text{m}$  size after 44.5 h. However, the heights only increased to 10–15 nm and no aggregate with height over 20 nm was found (Figure 7.9d). This was a significant difference from the previously reported INCP of PTD-*b*-PA copolymers, in which 3D microaggregates with 100 nm height were produced.<sup>2</sup> Another difference was that no 1D nanostructures of **GCP-50-30** were found during evolution, whereas the previous 3D aggregates formed from the secondary assembly of 1D nanocaterpillars. This implies that **GCP-50-30** grew in the horizontal direction to give 2D sheet or island-like nanostructures having a mono-to-bilayer arrangement. More details were obtained by TEM imaging without staining. A size increase similar to that seen in AFM and DLS analysis confirmed the evolution of nanostructures by simple aging (Figure 7.9f-h). Looking in detail at the core structure, we noticed that small individual spheres were closely packed to form a 2D sheet-like morphology (Figure 7.9i). Notably, the distribution of contrast from the electron density was relatively uniform, while that of the 3D aggregates produced by the previously reported INCP of PTD-*b*-PA was much

more irregular.<sup>2</sup> These images confirmed that the 0D nanoparticles evolved to micron-size 2D sheets or islands through lateral growth instead of axial growth (Figure 7.4 vs. Figure 7.9).



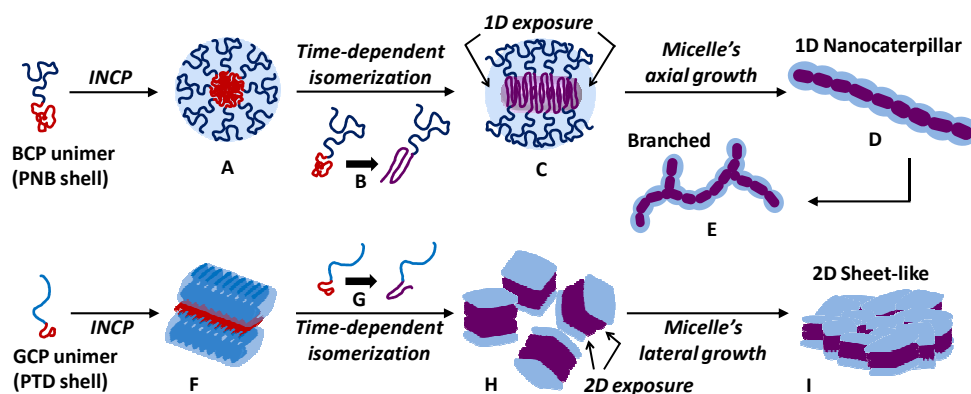
**Figure 7.8.** (a) Time-dependent increase in  $D_h$  by aging **GCP-50-30** in chloroform (1 mg/mL) under a blue LED and (b) change in the UV–Vis spectra.



**Figure 7.9.** AFM height images of **GCP-50-30** (a) before and after (b) 8.5 h and (c) 44.5 h of aging in chloroform. (d) Height profile of the final nanostructure in (c). (e) 3D phase overlaid topography of phase image after 31.5 h of aging. TEM images of **GCP-50-30** (f) before and after (g) 8.5 h and (h) 31.5 h. (i) Magnified image of (i).

Time-dependent aging studies of nanostructures having the PCPV core enabled to obtain real-time snapshots of the macroscopic evolution and provided deeper insights and evidence to support the previously proposed INCP mechanism (Figure 7.10). Initially, both BCP and GCP spontaneously formed spherical nanoparticles (**A** and **F**) via conventional INCP. Subsequently, light-triggered *cis*-to-*trans* isomerization on the core PCPV block led to a coil-to-rod transition and stiffening (**B** and **G**). This expanded the core volume and enhanced  $\pi$ - $\pi$  interaction between the cores, thereby promoting macroscopic evolution to higher dimensional nanostructures. For **BCP-II**, the flexible shell based on the PNB block provided effective stabilization of the core (**C**), resulting in alignment of 1D or lightly branched nanocaterpillars alignment (**D** and **E**). On the other hand, the rigid PTD shell (**GPC-50-30**) was less efficient for solvating the PCPV core (**H**). Thus, instead of axial growth, the micelles grew in the lateral direction to form 2D sheet- or island-like structures (**I**). Several interesting comparisons can be made between this work and the previous INCP results. Firstly, the simple configurational change in molecular structure, initiated by *cis*-to-*trans* isomerization, drove the entire macroscopic evolution process. This seemingly minor conformational change promoted the microscopic rearrangement of the core, which then led to the final macroscopic evolution. Secondly, the evolution occurred with no external inputs such as the addition of additives or monomers, or changes in temperature or solvent composition; only light was required to trigger this spontaneous evolution. Thirdly, it is notable that the micelles obtained from GCP directly formed 2D-sheet- or island-like morphologies, unlike the previous cases where the 0D micelles initially formed 1D structures before evolving into higher dimensional structures.<sup>3</sup> Finally, this is the first example of 2D sheet formation by INCP. It is supposed that the relatively slow isomerization and aging made it possible, where the gradual changes in molecular structure propagated to changes on the macroscopic level. Therefore, the evolution described in this work occurred under thermodynamic control, whereas, in previous cases, the evolution was triggered by the actual

ROMP of COT, wherein the INCP was much faster and under kinetic control.



**Figure 7.10.** Schematic illustration for the spontaneous macroscopic evolution of nanostructures by aging.

## 7.4. Conclusion

The combination of living ROMP and cyclopolymerization broadened the scope of INCP by utilizing the insoluble PCPV block as the driving force for in situ self-assembly. The light-driven coil-to-rod transition of PCPV, occurring because of *cis*-to-*trans* isomerization, led to various interesting macroscopic evolutions through volume expansion and enhanced  $\pi$ - $\pi$  interaction among the cores. As a result, small spherical micelles in solution transformed into larger, higher dimensional architectures by simple aging in solution under the light. The structure of the solubilizing shell block was crucial in determining the final dimensions of the self-assembled structures. (i) The PNB shell initially formed spherical micelles by INCP, which then grew into 1D nanocaterpillars or branched nanostructures. (ii) The more rigid PTD shell formed densely packed 2D sheet-like structures. Notably, the synthesis of GCP-containing PTD shell was simplified to a step-economical one-shot copolymerization. The evolution of nanostructures formed by INCP is distinct from the conventional transformation of the morphology of dynamic micelles, in terms of illustrating the hierarchical growth of kinetically fixed and stable micelles. This time-dependent light-driven hierarchical growth might give us better insights into new strategies for precisely controlled INCP and the preparation of more complex mesophase structures.



## 7.5. Experimental Section

### Characterization

$^1\text{H}$  NMR and  $^{13}\text{C}$  NMR spectra were recorded by Varian/Oxford As-500 (500 MHz for  $^1\text{H}$  and 125 MHz for  $^{13}\text{C}$ ) spectrometer and Agilent 400-MR (400 MHz for  $^1\text{H}$ ). High resolution mass spectroscopy (HRMS) analysis was performed by the National Center for Inter-University Research Facility. UV-vis spectra were obtained by a Jasco Inc. UV/vis spectrometer V-630, and dynamic light scattering (DLS) data were obtained by a Malvern Zetasizer Nano ZS. Multimode 8 and Nanoscope V controller (Veeco Instrument) were used for AFM imaging. All images were obtained on tapping mode using noncontact mode tip from Nanoworld (Pointprobe<sup>®</sup> tip, NCHR type) with a spring constant of 42 N m<sup>-1</sup> and tip radius of  $\leq 10$  nm. Transmission electron microscopy (TEM) analysis was performed on JEM-2100 operating at 200 kV and 120 kV accelerating voltage, using the images acquired with Orius SC600 and Orius SC1000 CCD camera (Gatan, Inc.)

### Materials

All reactions were carried out under dry argon atmospheres using standard Schlenk-line techniques. All reagents which are commercially available from Sigma-Aldrich<sup>®</sup>, Tokyo Chemical Industry Co. Ltd., Acros Organics, and Alfa Aesar<sup>®</sup>, without additional notes, were used without further purification. **1**<sup>10</sup>, **2**<sup>5</sup>, and **4**<sup>2</sup> were prepared in the same method from previous literature. Tetrahydrofuran (THF) for the polymerization was distilled from sodium and benzophenone and degassed further by Ar bubbling for 10 minutes before performing reactions. Thin-layer chromatography (TLC) was carried out on MERCK TLC silica gel 60 F254 and flash column chromatography was performed using MERCK silica gel 60 (0.040~0.063 mm).  $\text{CDCl}_3$  (99.50% D) and  $\text{THF-}d_8$  (99.50% D, 0.75 mL) were purchased from Euriso-top<sup>®</sup> and used without further purification.

## Synthesis

### ***exo*-2,3-bis((*tert*-butyldimethyloxy)methyl)-5-norbornene (3)**

*exo*-2,3-Dihydroxymethyl-5-norbornene<sup>11</sup> (1.90 g, 12.6 mmol), triethylamine (11.4 mL, 82.1 mmol) and 4-dimethylaminopyridine (154 mg, 1.26 mmol) was placed into a 100 mL round-bottom flask with 60 mL of DCM. The mixture was cooled to 0 °C, and the addition of *tert*-butyldimethylsilyl chloride (4.95 g, 32.8 mmol) was followed. After the reaction temperature had been elevated to the room temperature, the mixture was stirred overnight. The reaction was quenched with saturated NH<sub>4</sub>Cl aqueous solution then diluted by excess EtOAc. The organic phase was sequentially washed with saturated NaHCO<sub>3</sub> and NH<sub>4</sub>Cl aqueous solutions. The separated organic phase was dried over MgSO<sub>4</sub>, concentrated, and purified by silica flash column chromatography (EtOAc: hexane = 1:30) to afford **3** (4.30 g, 11.3 mmol, 90%) as a colorless oil. <sup>1</sup>H NMR (500 MHz, CDCl<sub>3</sub>): δ 6.14 (t, 2 H), 3.82 (m, 2 H), 3.51 (m, 2 H), 2.73 (s, 2 H), 1.63 (m, 2 H), 1.51 (d, 1 H), 1.22 (d, 1 H), 0.90 (s, 18 H), 0.04 (d, 12 H); <sup>13</sup>C NMR (125 MHz, CDCl<sub>3</sub>): δ 137.7, 64.4, 44.7, 43.3, 42.7, 26.1, 18.4, -5.1; HRMS (FAB+): calcd. for C<sub>21</sub>H<sub>43</sub>O<sub>2</sub>Si<sub>2</sub>, 383.2802, found, 383.2808.

### **General procedure for block copolymers**

To a flame-dried 4-mL vial with a cap containing PTFE-silicon septum were added the first monomer (**1** or **3**) and a magnetic bar. The vial was purged with argon four times, and degassed dry THF was added. The solution of **G3-Cl** prepared under inert atmosphere was rapidly injected into the solution of the first monomer at room temperature under vigorous stirring. The reaction vial was cooled to 0 °C after 15–20 minutes, then, the solution of **2** was added. The reaction was quenched by excess ethyl vinyl ether after 1.5 hours and the reaction mixture was precipitated in methanol. Obtained solid was washed with methanol, filtered, and dried *in vacuo*.

### General procedure for one-shot gradient copolymers.

To a flame-dried 4-mL vial with a cap containing PTFE-silicon septum were added **2**, **4**, and a magnetic bar. The vial was purged with argon four times, and degassed dry THF was added. The solution of **G3-Cl** prepared under inert atmosphere was rapidly injected into the monomer solution at room temperature under vigorous stirring. After the desired time, the reaction was quenched by excess ethyl vinyl ether and precipitated in methanol. Obtained solid was washed with methanol, filtered, and dried *in vacuo*.

### Characterization of copolymers

Poly(**3**)-*b*-poly(**2**). <sup>1</sup>H NMR (500 MHz, CDCl<sub>3</sub>): δ 5.36–5.08 (m, 2 H), 3.79–3.49 (m, 4 H), 2.82–2.26 (m, 2 H), 2.16–1.77 (m, 3 H), 1.23–0.98 (m, 1 H), 0.98–0.79 (bs, 18 H), 0.05–0 (bs, 12 H); <sup>13</sup>C NMR (125 MHz, CDCl<sub>3</sub>): δ 134.1 (br), 62.7 (br), 50.5 – 49.0, 44.6, 41.1 – 40.1, 26.2, 18.3, 5.1.

Poly(**4**)-*g*-poly(**2**). <sup>1</sup>H NMR (500 MHz, CDCl<sub>3</sub>): δ 6.32 (s, 1H), 5.09 (s, 1H), 3.20–2.70 (br, 7H), 1.68 (s, 1H), 1.59 (s, 1H), 1.25–1.16 (br, 8H) 1.00–0.81 (br, 6H); <sup>13</sup>C NMR (125 MHz, CDCl<sub>3</sub>): δ 178.7, 132.4, 131.3 44.0 (br), 42.7, 40.8, 38.6 (br), 37.5, 30.6, 28.7, 23.7, 23.3, 14.3, 10.4.

### General procedure for aging and characterization.

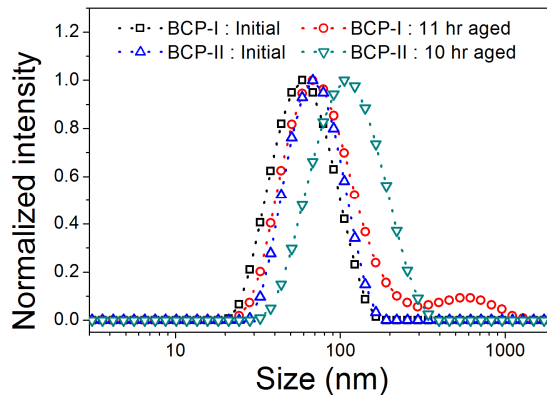
The copolymer was fully dissolved by 30 minutes – 1 hour of bath sonication in organic solvents (chloroform or chlorobenzene, 1 g/L). The solution was filtered by 1 μm PTFE syringe filter (Whatman®), transferred to a vial, and left on the workbench under the fluorescent light. (For rapid aging, the vial was left in the blue LED-containing bath with water to suppress the elevation of temperature.) The portion of the aged solution was taken on each time, and the size of nanoparticle was measured by DLS. After diluting it 10-20 times (0.1 – 0.05 g/L,

chlorobenzene), the film for AFM imaging was prepared by spin-coating on HOPG (spin rate = 3000 rpm, 120 sec). The samples for TEM were prepared by drop-casting 10  $\mu$ L of aliquots of the diluted solution (0.005 g/L) onto a carbon coated copper grid which was placed on a piece of paper to get rid of excess solvent. This thin polymer film was dried *in vacuo* for 2 h.

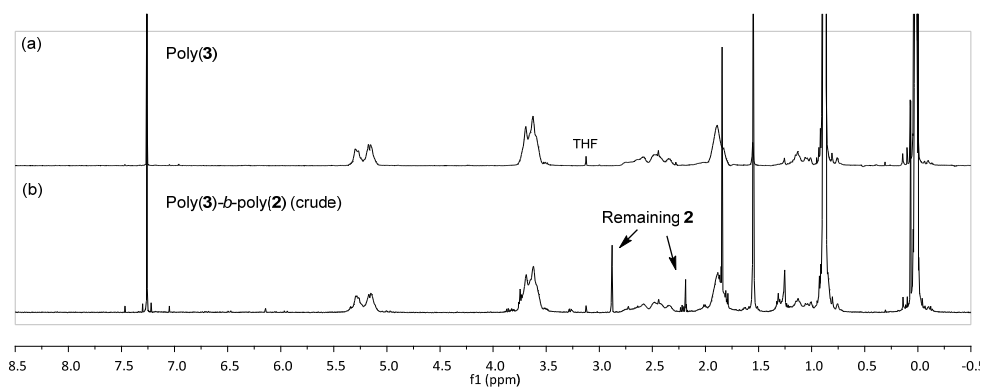
### **In situ $^1\text{H}$ NMR analysis for monitoring the consumption of **2** and **4****

To a screw-cap NMR tube (Wilmad-Labglass, screw-cap tube, 500 MHz, 5 mm) were added **2** (0.085 mmol, 50 eq) and **4** (0.051 mmol, 30 eq). THF- $d_8$  (400  $\mu$ L) was added after the tube was purged with argon. **G3-Cl** (0.0017 mmol, 1 eq) was dissolved in THF- $d_8$  (100  $\mu$ L) under argon, and it was injected into the monomer-containing NMR tube.  $^1\text{H}$  NMR spectra of this mixture were recorded over time. The monomer conversion was calculated using a specific signal of the monomer as the internal standard.

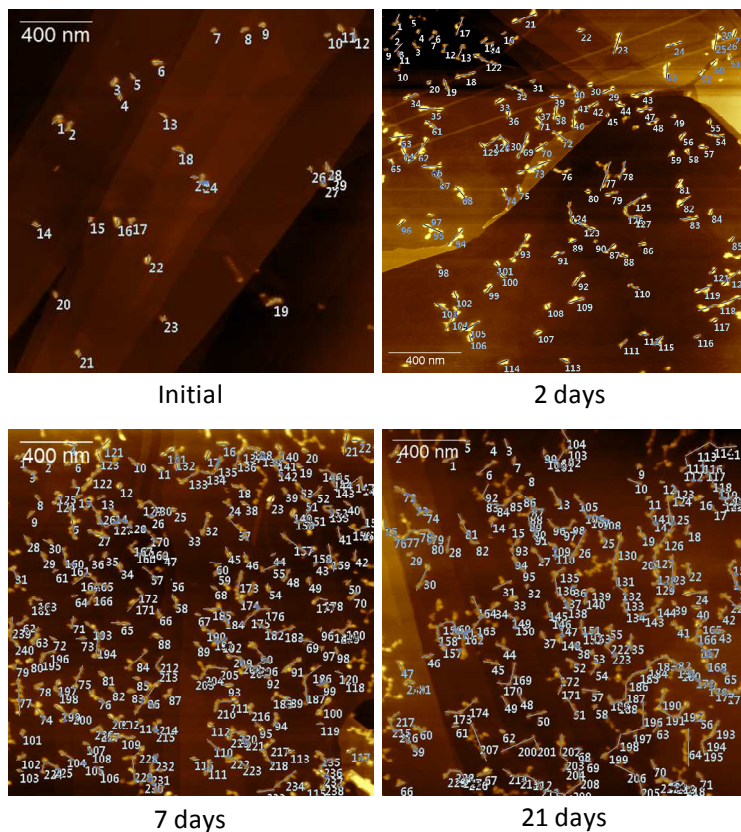
## 7.6. Supporting Information



**Figure S7.1.** DLS profiles ( $D_h$ ) of **BCP-I** and **BCP-II** after blue LED aging in chloroform (1 g/L).



**Figure S7.2.** Identical  $^1\text{H}$  NMR spectra of (a) poly(**3**) homopolymer and (b) the crude of poly(**3**)-*b*-poly(**2**) (**BCP-II**). Invisible conjugated backbone on 6–7 ppm indicates the micelle formation.



	Initial	2 day	7 day	21 day
$L_n$	45.3 nm	78.0 nm	101.8 nm	149.0 nm
$L_w$	49.9 nm	109.7 nm	156.2 nm	295.6 nm
$L_w/L_n$	1.10	1.41	1.54	1.98

**Figure S7.3.** Statistics of the length distribution of **BCP-II** aged in chlorobenzene under the fluorescent light.

## 7.7. References and Notes

- (1) (a) Jenekhe, S. A.; Chen, X. L. *Science* **1998**, 279, 1903-1907. (b) Leclère, P.; Calderone, A.; Marsitzky, D.; Francke, V.; Geerts, Y.; Müllen, K.; Brédas, J. L.; Lazzaroni, R. *Adv. Mater.* **2000**, 12, 1042-1046. (c) Wang, H.; Wang, H. H.; Urban, V. S.; Littrell, K. C.; Thiyagarajan, P.; Yu, L. *J. Am. Chem. Soc.* **2000**, 122, 6855-6861. (d) Liu, J.; Sheina, E.; Kowalewski, T.; McCullough, R. D. *Angew. Chem., Int. Ed.* **2002**, 41, 329-332. (e) Kong, X.; Jenekhe, S. A. *Macromolecules* **2004**, 37, 8180-8183. (f) Schenning, A. P. H.; Meijer, E. W. *Chem. Commun.* **2005**, 3245-3258. (g) Patra, S. K.; Ahmed, R.; Whittell, G. R.; Lunn, D. J.; Dunphy, E. L.; Winnik, M. A.; Manners, I. *J. Am. Chem. Soc.* **2011**, 133, 8842-8845.
- (2) (a) Yoon, K.-Y.; Lee, I.-H.; Kim, K. O.; Jang, J.; Lee, E.; Choi, T.-L. *J. Am. Chem. Soc.* **2012**, 134, 14291-14294. (b) Yoon, K.-Y.; Lee, I.-H.; Choi, T.-L. *RSC Adv.* **2014**, 4, 49180-49185.
- (3) Yoon, K.-Y.; Shin, S.; Kim, Y.-J.; Kim, I.; Lee, E.; Choi, T.-L. *Macromol. Rapid Commun.* **2015**, 36, 1069-1074.
- (4) Shin, S.; Yoon, K.-Y.; Choi, T.-L. *Macromolecules* **2015**, 48, 1390-1397.
- (5) (a) Lee, I.-H.; Amaladass, P.; Yoon, K.-Y.; Shin, S.; Kim, Y.-J.; Kim, I.; Lee, E.; Choi, T.-L. *J. Am. Chem. Soc.* **2013**, 135, 17695-17698. (b) Lee, I.-H.; Amaladass, P.; Choi, T.-L. *Chem. Commun.* **2014**, 50, 7945-7948.
- (6) Kim, J.; Kang, E.-H.; Choi, T.-L. *ACS Macro Lett.* **2012**, 1, 1090-1093.
- (6) After the purification of polymers, solutions were prepared by 30 minutes – 1 hour of bath sonication.
- (7) (a) Charvet, R.; Novak, B. M. *Macromolecules* **2001**, 34, 7680-7685. (b) Charvet, R.; Acharya, S.; Hill, J. P.; Akada, M.; Liao, M.; Seki, S.; Honsho, Y.; Saeki, A.; Ariga, K. *J. Am. Chem. Soc.* **2009**, 131, 18030-18031.
- (8) Kim, K. O.; Choi, T.-L. *Macromolecules* **2013**, 46, 5905-5914.
- (9) Kim, K. O.; Shin, S.; Kim, J.; Choi, T.-L. *Macromolecules* **2014**, 47,

1351-1359.

- (10) Meijer, A.; Otto, S.; Engbert, Jan B. F. N. *J. Org. Chem.* **1998**, *63*, 8989-8994.
- (11) Long, T. R.; Maity, P. K.; Samarakoon, T. B.; Hanson, P. R. *Org. Lett.* **2010**, *12*, 2904-2907.



## 국문 초록

올레핀 복분해 반응을 기반으로 하는 1,6-헵타다이아인의 고리화 중합은 전도성 고분자로 알려진 폴리아세틸렌의 유도체를 손쉽게 합성한다. 고리화 중합으로 합성된 공액 고분자는 일반적인 폴리아세틸렌에 비해 공기 중에서 안정하고, 용해도를 자유롭게 조절할 수 있어 전도성 고분자의 연구 대상으로서 활용 방안이 매우 높을 것으로 기대되어왔다. 그러나 고분자의 구조 및 분자량을 정확히 조절할 수 있는 촉매가 매우 제한적이고, 촉매의 선택성 및 안정성 역시 낮아 여러 연구 분야에서 쉽게 접근하기 어려웠다.

본 연구에서는 반응의 선택성이 좋고 공기 중에서도 안정하게 사용할 수 있는 루테튬 기반의 그럽스 촉매를 고리화 중합에 활용할 수 있도록 시스템을 개발하고 여러 분야에 중합을 응용하였다. 루테튬 촉매는 다이아인의 고리화 중합을 매개하기에는 반응성이 부족한 것으로 알려졌으나, 적절한 반응 조건, 특히 금속 촉매에 배위할 수 있는 용매를 사용할 때 중합 효율이 매우 증가하는 점을 발견하였다. 이러한 사실은 그 동안 그럽스 촉매가 고리화 중합에 이용될 수 없었던 이유를 분석하는데 바탕이 되어, 약한 배위 결합을 할 수 있는 리간드의 존재가 중합을 지속시키는데 매우 중요하다는 결과를 도출하였다. 용매 또는 리간드의 존재는 중합이 이루어지는 사슬 끝의 활성 촉매가 반응성을 잃지 않고 유지하는데 매우 중요한 역할을 한다. 같은 이유로 낮은 반응 온도나 입체 효과 등 역시 촉매 활성 유지에 도움을 주고 중합 효율을 증진시킬 수 있다. 반대로 리간드가 존재하지 않을 경우 고분자 중합 대신 1,6-헵타다이아인의 이합체나 삼합체가 생성된다. 이 부반응은 약한 배위 결합을 할 수 있는

용매나 리간드가 없을 때 카빈 활성을 잃은 루테튬 촉매가 새롭게 매개하는 반응이며, 중합 효율을 낮추게 된다. 이러한 반응성에 대한 전반적인 이해를 토대로 빠른 개시 촉매에 의한 리빙 중합이 구현되었다.

그럽스 촉매를 이용하여 공액 고분자를 높은 효율로 리빙 중합할 수 있게 되면서, 절연된 단일 분자 와이어나 블록 공중합체 합성을 기반으로 하는 자기조립 연구 등 응용 분야를 확대할 수 있었다. 먼저 나노 크기의 소자로 사용될 수 있는 단일 분자 와이어를 목표로 하여 텐드리머화 고분자 및 고분자 브러쉬를 결합 없이 합성할 수 있었다. 이러한 거대 분자들의 구조가 특이한 변화 양상을 보여 구조 변화에 대한 메커니즘 연구를 진행하였다. 고리화 중합으로 합성된 공액 고분자 사슬에서 일어나는 시스-트랜스 이성질화 반응은 고분자의 전체 구조를 더 펼쳐진 막대 구조로 변형시키며, 길게 펼쳐진 고분자 사슬은 원자간력 현미경 (AFM)으로 이미징되었다. 또한 고리개환복분해중합 (ROMP)과 고리화 중합의 연계 반응을 통해 제작된 블록 공중합체는 반응 과정에서 자기조립에 의한 구형 마이셀을 형성하는데, 앞서 발견된 고분자의 구조 변화는 구형 마이셀의 구조 변화 및 마이셀 간의 결합을 유도하여 고차원 나노 구조를 제작할 수 있게 하였다.

주요어: 고리화 중합, 리빙 중합, 폴리아세틸렌, 루테튬 촉매, 단일 거대분자, 고분자 구조, 자기 조립

학번: 2010-20262